UNIVERSITY OF CATANIA

Department of Chemical Sciences

INTERNATIONAL DOCTORATE IN CHEMICAL SCIENCES

XXXVI CYCLE

Claudia Sciacca

From natural polyphenols to synthetic bioactive analogues

Ph.D. thesis

Tutor **Coordinator**

Prof. Vera Muccilli *Prof. S. Sortino*

Academic years 2020-2023

Preface

My three-year Ph.D. course in International Chemical Sciences at the Department of Chemical Sciences of the University of Catania started in November 2020 under the supervision of Prof. Vera Muccilli. During the second year of my Ph.D., I moved to the Institut des Sciences Moléculares (ISM) at the University of Bordeaux (France) for a six-month research period.

My research activity was focused on three neolignans, magnolol, honokiol, obovatol, and related oligomers present in the *Magnolia* species. This thesis reports on the synthesis of their bioinspired analogues and the evaluation of the inhibitory activity towards target enzymes for obesity and hypoglycemic management (pancreatic lipase, α-glucosidase, and α-amylase).

The Introduction Section (**Chapter 1**) of this thesis reports a general overview of the natural compounds and, more specific, of neolignans. The synthetic strategies that might be used to obtain the structures inspired by these scaffolds are also reported. In addition, this section summarizes plant natural compounds that have already been studied as metabolic enzyme inhibitors.

The Results and Discussion Section comprises the development of new synthetic compounds inspired by magnolol, honokiol, obovatol, and their related oligomers (**Chapter 3**). Different synthetic strategies are described here to obtain the following compound libraries:

i) magnolol and honokiol inspired analogues were obtained through Suzuki-Miyaura cross-coupling reaction, allylation reaction, and Claisen rearrangement (**Chapter 3.1**);

ii) obovatol and its biaryl ether analogs were achieved by an allylation reaction, Claisen-Cope rearrangement, methylation reaction, Ullmann coupling, and demethylation reaction. In addition, a *one-pot* strategy involving phenol oxidation and Michael-type addition was employed to give new thioether analogues (**Chapter 3.2**);

iii) magnolol and honokiol oligomeric compounds were obtained through biomimetic reaction with chemical catalyst and green chemistry approaches involving safer reaction conditions and enzyme as catalyst (**Chapter 3.3**).

The synthesized compounds were evaluated for their inhibitory activities towards metabolic enzyme inhibitions using *in vitro* biochemical assays, kinetic analysis, fluorescence spectroscopy, circular dichroism experiments, and *in silico* study (**Chapter 3.4 – 3.7**).

Table of contents

List of abbreviations

$(CD_3)_2$ CO	Acetone -d6
^{13}C NMR	Carbon nuclear magnetic resonance
^{1}H NMR	Proton nuclear magnetic resonance
2D	Bidimensional
2D NMR	Bidimensional nuclear magnetic resonance
3D	Tridimensional
ABTS	2,2'- azino-bis(3-ethylbenzothiazoline-6-sulfonic acid)diamminium salts
ADME	Absorption, distribution, metabolism, and excretion
Ag_2O	Silver (I) oxide
BBr_3	Boron tribromide
BF_3*$O(Et)_2$	Boron trifluoride diethyl etherate
BOG	β-octylglucoside
CAN	Ceric ammonium nitrate
CD	Circular dichroism spectroscopy
$CDCl_3$	Chloroform-d1
CH_2Cl_2	dichloromethane
CH_3CN	Acetonitrile
CH_3I	Iodomethane
$CHCl_3$	Chloroform
COX2	Cyclooxygenase 2
Cs_2CO_3	Cesium carbonate
$CuCl_2$	Copper (II) chloride
CuI	Copper (I) iodide
DCM	Dichloromethane
DMA	*N, N*- dimethylacetamide
DMF	Dimethylformamide
DMSO	Dimethyl sulfoxide

DNS	3,5-dinitro salicylic acid
dppf	1,1'-bis(biphenylphosphino)ferrocene
EI	Enzyme- inhibitor complex
ERK	Extracellular kinase regulared
ESI	Enzyme- substrate- inibitor complex
ESI	Electro Spray Ionization
ET_2AlCl	Diethyl aluminum chloride
FDA	Food and Drug Administration
$FeCl_2$	Iron (II) chloride
$FeCl_3$	Iron (III) chloride
GABA	γ- aminobutyric acid
gCOSY	Gradient correlation spectroscopy
GDM	Gestational diabetes mellitus
gHMBC	Gradient heteronuclear multiple-bond correlation adiabatic
gHSQC	Gradient heteronuclear single quantum coherence adiabatic
$H_3PMo_{12}O_{40}$	Phosphomolybdic acid
HBT	1-hydroxybenzotriazole
HPLC	High Performance Liquid Chromatography
HRMS	High-resolution mass spectra
HRP	Horseradish peroxidase
IBA	2-iodobenzoic acid
IBX	2-iodoxybenzoin
IC_{50}	Concertation inhibiting of the 50 % of enzyme activity
*i*NOS	Inducible nitric oxide synthase
IR	Infrared spectroscopy
K_2CO_3	Potassium carbonate
Ka	Binding constant
Kq	Biomolecule quenching rate
Ksv	Stern-Volmer quenching constant

L-B	Lineweaver-Burk plot
LC	Liquid chromatography
LTV	Laccase from Trametes versicolor
MAPK	Mitogen-activated protein kinase
$Mn(OAc)_3$	Manganese (III) acetate
MUP	Methoxy undecyl phosphonic acid
n	Number of binding sites
NADPH	Nicotinamide adenine dinucleotide phosphate
NAH	Sodium hydride
$NAHCO_3$	Sodium bicarbonate
NF-kB	Nuclear factor k-light-chain-enhancer of activated B cell
NPs	Natural products
OD	Optical density
$OPLS_3$	Optimized potential liquid simulation
P450	Cytochrome
PAF	Platelet – activating factor antagonist
PAINS	Pan assays interference compounds
$Pd(OAc)_2$	Palladium acetate (II)
$Pd(PPh3)_4$	Palladium tetrakis- triphenylphosphine
pin_2B_2	Bis(pinacolato)diboron
PL	Pancreatic lipase
p-NP- α-G	*p*-nitrophenyl α-D-glucopyranoside
p-NPB	*p*-nitrophenyl butyrate
RNS	Reactive nitrogen species
ROS	Reactive oxygen species
SAR	Structure – activity relationship
SD	Standard deviation
SIBX	Stabilized IBX
SM	Suzuki-Miyaura cross coupling reaction

SNAr	Nucleophilic aromatic substitution reactions
SPhos	Dicyclohexyl(2′,6′-dimethoxy[1,1′-biphenyl]-2-yl)phosphine
SPO	Soybean peroxidase
T1DM	Type 1 diabetes
T2DM	Type 2 diabetes
TEMPO	(2,2,6,6-tetramethylpiperidin-1-yl)oxyl radical
THF	tetrahydrofuran
TLC	Thin-layer chromatography
TLR4	Toll-like receptor 4
TTFA	Thallium (III) trifluoroacetate
TTN	Thallium (III) nitrate
UV	Ultraviolet
UV-vis	Ultraviolet visible
α-Amy	α-Amylase
α-Glu	α-Glucosidase

Abstract

Obesity is a complex disease characterized by an excessive body fat. It is considered a risk factor for chronic disorders and cardiovascular diseases, cancer, osteoarthritis, and hypertension. The incidence of obesity is frequently linked to the incidence of type 2 diabetes, a metabolic disease characterized by dysfunctional insulin hormone and high blood glucose levels. It is also noteworthy that hyperglycemia associated with type 2 diabetes is characterized by increased production of reactive oxygen species, causing oxidative tissue damage.

Some therapeutic approaches to the management of obesity and type 2 diabetes are related to the inhibition of metabolic enzymes: pancreatic lipase, the enzyme responsible for the hydrolysis of free fatty acid from triglycerides; α-amylase and α-glucosidase, carbohydrate hydrolyzing enzymes, whose inhibition is a well-established strategy to manage hyperglycemia. Approved anti-obesity and hypoglycemic drugs are, respectively, orlistat and acarbose, showing, however, some side effects. Hence, increasing interest has turned to natural products and their analogues to find new and safe enzyme inhibitors with low or without side effects.

This thesis reports on phenolic compounds and their inspired analogues as new potential inhibitors of metabolic enzymes.

Magnolia species contain several compounds with different structures and biological activities. The neolignans magnolol and honokiol have been extensively investigated for their wide biological effects. Consequently, nowadays there is an increasing interest in synthesizing new analogues inspired by the two neolignans to enhance their biological effects. Thus, the first phase of this research aimed to synthesize nitrogenated analogues inspired by magnolol and honokiol as potential lipase inhibitors.

Obovatol, a lesser-studied biphenyl ether compound isolated from the bark and leaves of *Magnolia obovata,* exhibits promising biological activities, even if its low bioavailability hinders extensive research. For this reason, the research activity was focused on developing a convenient access to obovatol and its analogues by total chemical synthesis and to evaluate their inhibitory activity towards carbohydrate hydrolyzing enzymes.

In addition to biphenyl and biaryl ether compounds, *Magnolia* species also contain oligomeric compounds. Among them, honokiol dimer houpulin B has been reported with 0.003% yield extraction from the roots of *M. officinalis* and consequently, few studies have been carried out to evaluate its biological activity. For this reason, the main challenge was developing and carrying out a chemical synthesis. Thus, the research project was devoted to the optimization and biomimetic synthesis of houpulin B and two new dimers not naturally occurred: magnolol dimer and honokiol-magnolol dimer.

The evaluation of the inhibitory activity towards pancreatic lipase, α-glucosidase and α-amylase of the three natural products and their bioinspired compounds (nitrogenated magnolol and honokiol analogues, biaryl or thiol ether compounds, and oligomeric products) was performed with *in vitro* biochemical assays, kinetic analysis, fluorescence spectroscopy, circular dichroism experiments and *in silico* analysis.

This research contributes to identify key structural features in the search for more suitable candidates for metabolic enzyme inhibitors, thus considering these natural compounds and their analogues as interesting scaffolds for future studies.

Chapter 1

Introduction

Natural compounds

The use of natural extracts as the only remedy for treating several diseases and disorders affecting man dates back to ancient times. Traditional medicine has been developed over the millennia and specialized in the treatment of a wide variety of diseases clinics as well as gastrointestinal disorders, asthma, anxiety, allergies, cardiovascular diseases, antimicrobial and antiviral, inflammation and other autoimmune response-related disorders and many more [1, 2]. An example is the "Saiboku-to", a natural extract obtained from the barks of *Magnolia spp*. plants and used as a remedy to treat depression, anxiety, asthma, and stroke [3, 4]. The use of this and other extracts obtained from different species of *Magnolia* dates back from 1083 BC in some traditional Chinese medicine documents. Some old remedies are still quite widespread in Chinese and Japanese popular culture.

Extracts from natural sources have been used exclusively according to accumulated experience and not based on scientific knowledge [5]. In recent years, several natural products (**NPs**) have been identified and isolated following the development of sophisticated methodologies of investigation and analysis. Many bioactive compounds were thus identified, and in many cases, now constitute the active ingredients of the therapeutic activity recognized to a natural source. For example, the main bioactive compounds in the above "Saiboku-to" are phenolic compounds belonging to the class of neolignans such as magnolol and honokiol (see further) [5].

These findings led to a growing interest in the study of bioactive natural products to identify potential lead compounds for the research and development of new drugs. Generally, bioactive natural products derive from primary metabolites that originate from the metabolic processes of living organisms such as plants, animals, and microorganisms. These compounds, which can be defined

as secondary metabolites, differ from the primary ones due to their lack of ubiquity; in fact, secondary metabolites are an individual characteristic of one species over another. Secondary metabolites can be divided into large families based on the biogenetic pathway they derive from i) isoprenoids, derived from the biosynthetic pathway of mevalonate; ii) polyketides originating from the acetate pathway; iii) alkaloids, derived from a mixed biosynthesis and iv) polyphenols, coming from the biosynthetic pathway of shikimate [6-9]. Among the various families of natural products, phenolic compounds, and polyphenols have recently received increasing attention. The increased interest in compounds biologically isolated from natural sources is mainly characteristic of low toxicity and high and complete biodegradability [10]. A renewed attention to bioactive natural products has arisen from the observation that their structural diversity (also called "chemo-diversity") is far superior to the compounds obtainable by synthetic methods, including combinatorial synthesis [11, 12].

One further reason is the awareness that many natural products are rich source of several "*lead compounds*" for the development of new drugs [13, 14]. However, they exhibit significant limitations, such as low yields, unknown biological targets, and precise mechanisms of action. Furthermore, some difficulties in structural modifications and total synthesis have been highlighted for synthetic compounds based on the pharmacopeia of natural product. An updated study highlighted the high contribution (53.1%) of **NPs** to the total amount of small molecules approved as drugs in the nearly forty years (accounting data from 1981 to 2019) to treat of human diseases [15] or under investigation at preclinical and clinical trial levels [16]. Focusing on the "small-molecules approved drugs" (n, number of molecules = 1211), it is noteworthy that compounds from natural sources, their synthetic or semi-synthetic derivatives, or those showing a "natural-product pharmacophore" highly contributed to the total amount of approved drugs (n = 791, representing the 65%) (**Figure 1**). Nowadays, a big challenge for the discovery of new bioactive compounds is to reconsider

natural products as a source of inspiration and starting point for the synthesis of novel drugs. The development of these "*natural leads*" has been exploited in drug discovery: modifying and optimizing key features of selected natural compounds can improve their biological activity, bioavailability, mode of administration, etc.

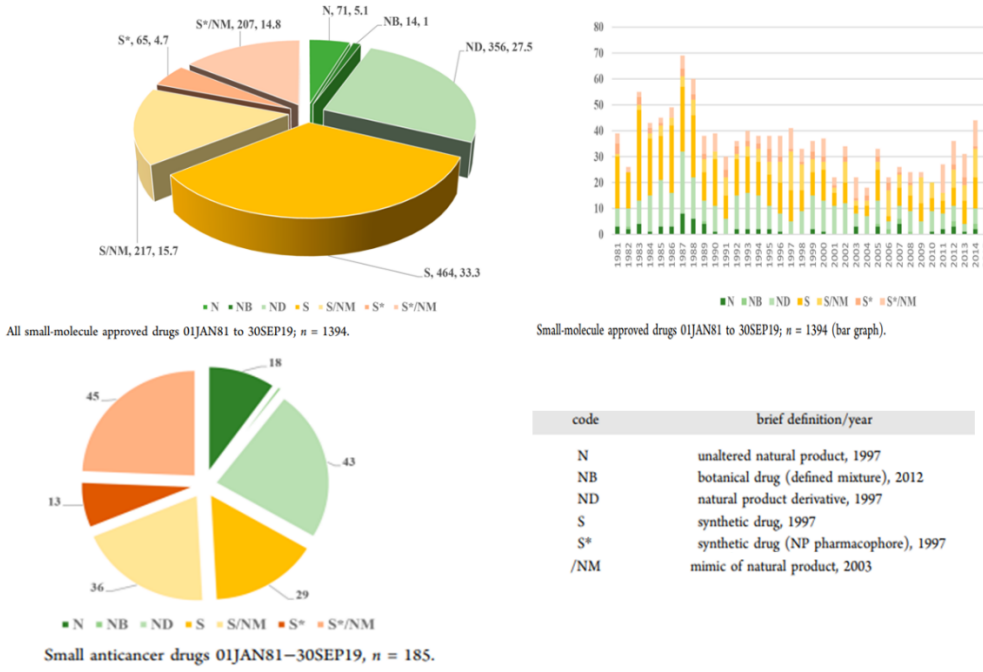

Figure 1. Statistical data related to the impact of **NPs** on the "small-molecules approved drugs" [15].

Polyphenols

The term "polyphenols" was originally used as synonym for "vegetable tannins" (compounds with a rather complex structure and rich in phenolic functions [17]) to refer to plant substances able to convert animal skin into leather. This term has taken on a more collective note to identify compounds containing a polyphenolic structures and molecules with a single phenolic ring, such as phenolic acids and phenolic alcohols [18, 19]. They are a class of secondary plant metabolites that play an essential role in reproduction and protection against agents in several plants. These metabolites are characterized by a broad and diverse range of bioactive properties, making them highly valued for their beneficial effects on human health [20]. Polyphenols are generally divided into large families: flavonoids, stilbenoids, phenylpropanoids, tannins, and lignans. All polyphenol subfamilies of polyphenols are originated from the shikimate biosynthetic pathway, whose name derives from the intermediate formed: shikimic acid. Although it has not an aromatic structure, it is considered a precursor of various polyphenols families listed above. **Figure 2** shows a summary of the products obtained by the shikimate biosynthetic pathway o starting from shikimic acid.

Great attention to polyphenols has arisen thanks to their antioxidant activity. They are defined as radical scavengers: that is, chemical molecules capable of inhibiting or slowing down reactions to free radical chains, donating a hydrogen atom to reactive oxygen species (ROS) or nitrogen (RNS) by oxidizing them instead of other substrates present in the cell and thus avoiding oxidative damage. This results in more stable phenoxy radicals forming due to the resonance structures reported in **Figure 3.**

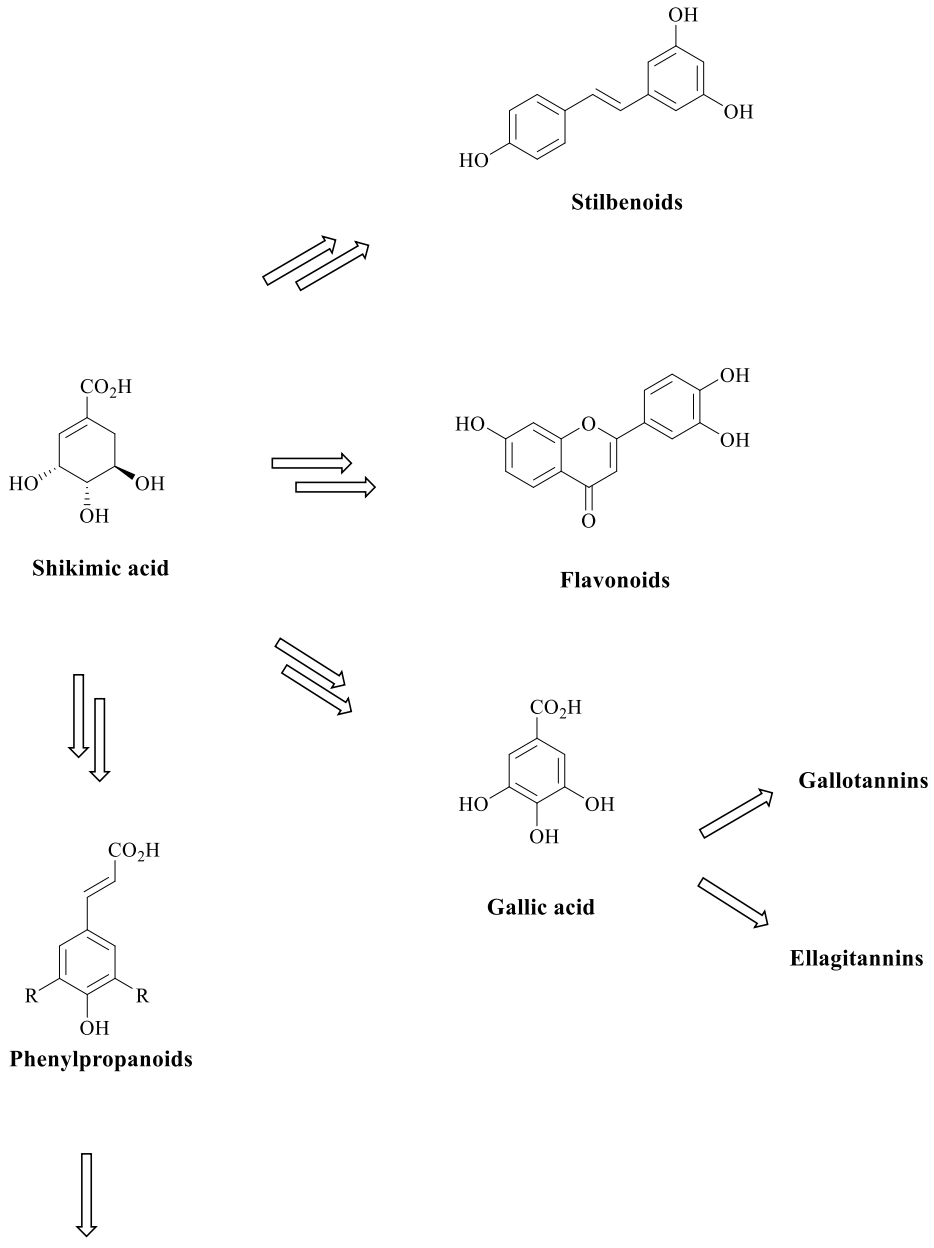

Figure 2. Summary mechanism of derivatives of the biosynthetic pathway of shikimate.

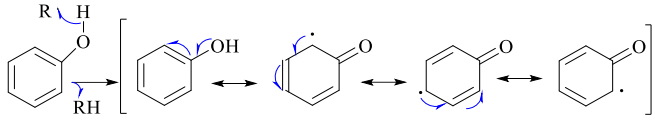

Figure 3. Mechanism of action of a radical scavenger.

The interest originated from their known antioxidant properties and their role in preventing various diseases associated with oxidative stress, such as cardiovascular, neurodegenerative, and cancer [21]. Moreover, numerous studies have shown that polyphenols also own anti-inflammatory, antiviral, and chemo-protective activity against neurodegenerative diseases such as Alzheimer's disease [21, 22]. Among polyphenols, the subfamily of lignans and neolignans is known for numerous components studied for multiple biological properties.

Lignans and neolignans

Lignans and neolignans represent a large class of natural compounds originating from the biosynthesis of phenylpropanoids. Most lignans are present in plants, and some coexist with sugars to form glycosides in wood and plant resin [23]. They are also known for their numerous pharmacological activities such as antitumor activity, hepatoprotective, platelet-activating factor antagonist (PAF), insecticide and estrogenic, antifungal, antihypertensive, soothing, and antioxidant activity. For example, some are employed as drugs in approved therapies, while others are considered lead structures for developing new drugs [24].

These compounds display dimeric structures formed by β-β' bonds between two phenylpropanoid units (C_6C_3) with a different degree of oxidation in the side chains and different aromatic rings' substitutions. According to the IUPAC nomenclature, if the coupling between the two C_6C_3 units takes place in position 8-8', the dimeric compound that is formed is called "lignan"; in the absence of the C-8 to C-8' bond, the dimer formed from the two C_6C_3 units takes

place is called "neolignan"; compounds in which an ether oxygen atom provides the linkage between the two C_6C_3 units are also classified under neolignans and are called "oxyneolignans" [25-27]. The general structures of lignans and neolignans are indicated in **Figure 4.**

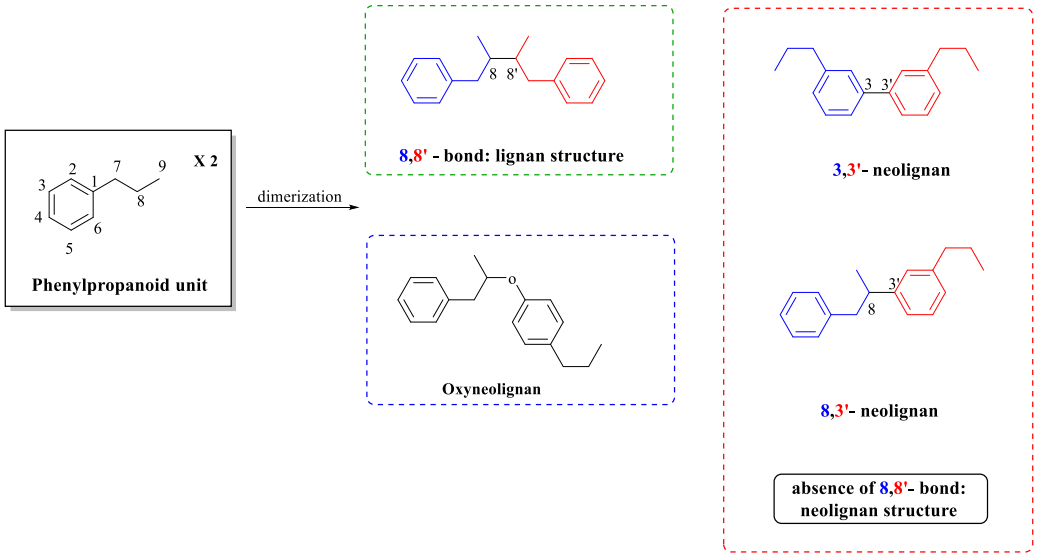

Figure 4. Representative structures of lignan and neolignans dimeric compounds.

According to Teponno *et al.* [23], lignans are classified into eight groups based on their skeletons and structural patterns, including their carbon skeletons, the way in which oxygen is incorporated into the skeletons, and the cyclization pattern. This classification is reported in **Figure 5**.

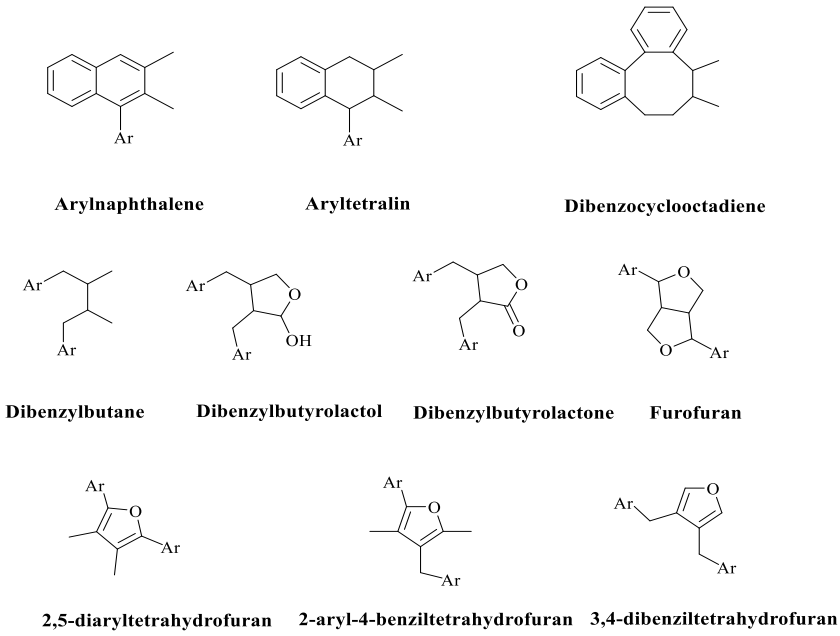

Figure 5. Classification of lignans according to Teponno *et al*. [23].

According to Teponno *et al.* [23], neolignans are classified into fifteen groups to which name has been assigned. Therefore, they are designated by the letters "NL" and increasing wording from NL1 to NL15, and no special names have been assigned to them. This classification is shown in **Figure 6**.

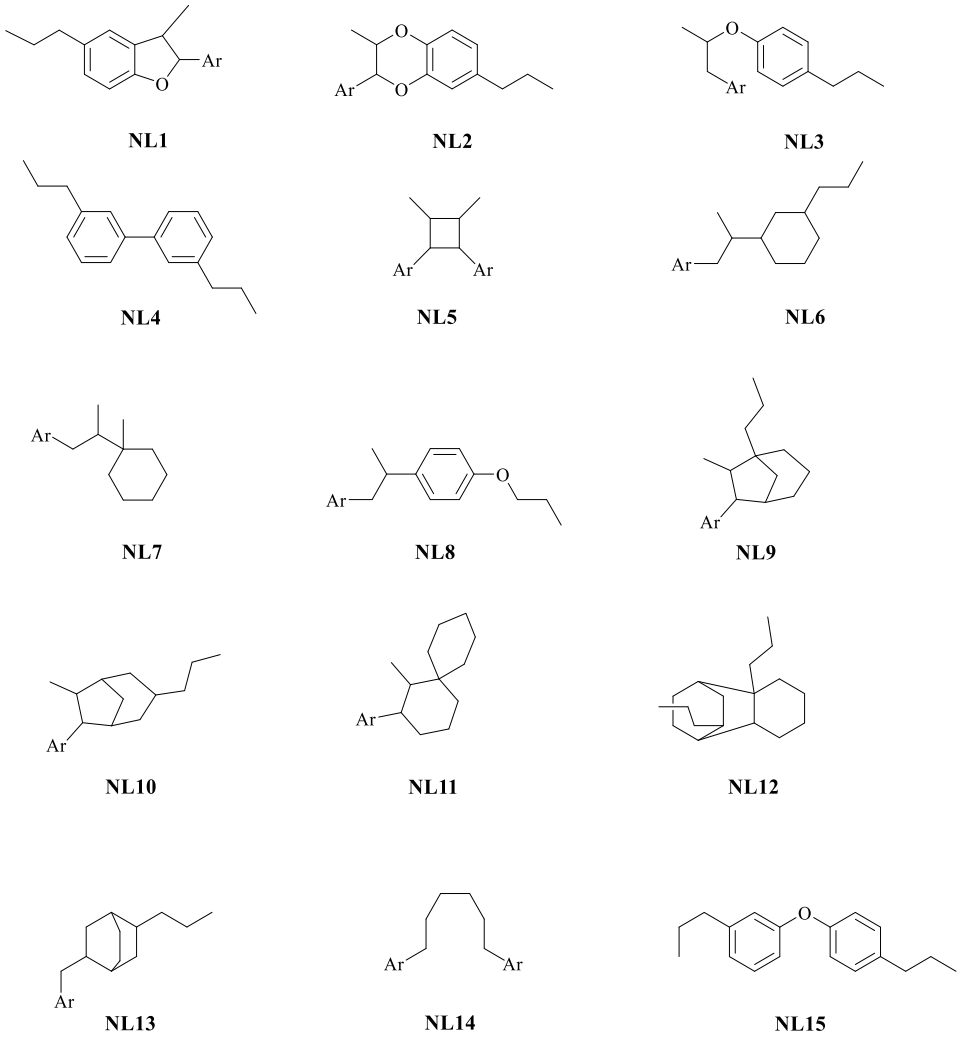

Figure 6. Classification of neolignans according to Teponno *et al.* [23].

Neolignans from Magnolia spp.

Plants of the family *Magnoliaceae* have been used since ancient times as the traditional herbal medicine in many oriental countries (China, South Korea, and Japan) because they contain a variety of natural substances with potential biological activity. The genus *Magnolia* is representative of the ancient family of *Magnoliaceae,* and, among them, the stem bark, root bark and seeds of *Magnolia officinalis* and *Magnolia obovata* have been used to treat several diseases such as headache, stroke, diarrhea, gastrointestinal discomfort, allergies and anxiety [28]. The use of extracts from *Magnolia* is also documented in other civilizations: Native Americans used these extracts for relief pains due to stomach cramps or toothache, against rheumatism and malarial fever. Thanks to their properties, these natural remedies were qualified as real medicines and registered in the American Pharmacopoeia from 1787 to 1900 [29-31].

The studies on the genus *Magnolia spp*. have shown a few phenolic compounds with different structures showing a wide range of biological activities such as antioxidants, antimicrobial and anti-inflammatory properties [5, 32]. The main metabolites are lignans, neolignans, phenylpropanoids, terpenes, and some alkaloids [33]. In particular, major components isolated from *Magnolia spp*., are magnolol (**1**), honokiol (**2**), obovatol (**3**). **Figure 7** reports the structure of the three natural compounds.

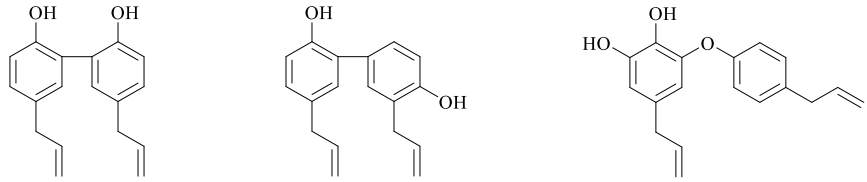

1 **2** **3**

Figure 7. Structure of magnolol (**1**), honokiol (**2**), and obovatol (**3**).

Magnolol and honokiol are two phenyl propanoic compounds belonging to the NL4 neolignan class (**Figure 6**). The molecular structure consists of two phenyl rings linked together by a C-C bond in the 1-1' positions, two allyl chains at the 5-3' position, and two hydroxyl groups, respectively, at the 2-2' position for magnolol and the 2-4' position for honokiol. The content of magnolol in *Magnolia* bark is generally in the range of 2-10%, while honokiol is naturally occurring at 1-5% in the dried bark [34]. They are, without any question, the pharmacologically most meaningful constituents of *Magnolia* bark [35], and despite their rigid structure, they establish a fair number of interactions with numerous biological targets. The two neolignans have been the subject of several studies aimed at evaluating their biological properties.

Magnolol has been reported to exert various properties, including endothelial cell protection [36], antitumor [37], antioxidant [38], and anti-inflammatory activities [32, 39]. It also has been reported to exert neuroprotective effects in intracerebral hemorrhage [37], stroke [40], Alzheimer's [41], and Parkinson's [42] diseases. Magnolol was evaluated as a potential antidepressant [36], and it showed beneficial effects on gastrointestinal disorders [43], atherosclerosis, and re-stenosis [44]. Other studies have shown that magnolol exhibits pharmacological effects, including antidiabetic [39], anti-obesity [45], cardiovascular [46] and antimicrobial activity [34, 47]. Different therapeutic applications of magnolol are reported in **Table 1**.

Honokiol, as well as magnolol [48], is a molecule that manages to cross the blood-brain barrier and can intervene against the development of neurodegenerative disorders [49, 50]. It also shows antioxidant activity, anxiolytic action and cytotoxicity activity against various cancer cell lines as colon, breast, gastric and carcinoma cancer [51]; it impacts cell signaling of neuroinflammation [52]. Recent studies have highlighted that honokiol exhibits anticancer properties with inhibition of cell proliferation by differentiation and apoptosis [53], thus contrasting the development of metastases [54]. This neolignan is known for its

ability to reduce free radicals generated by ultraviolet (UV) irradiation and for inhibiting the mutation induced by UV rays in *Salmonella* [55]. The *in vitro* analysis on different cell cultures has pointed out that honokiol is also a promising inhibitor of xanthine oxidase [55], a good protector of the enzyme of the mitochondrial respiratory chain, a reducer of the activation of the extracellular kinase regulated by signals (ERK), a suppressor of protein kinase and NADPH oxidase, resulting in inhibition of respiratory explosion by neutrophils and cellular protection [56]. Honokiol is considered a bioactive pleiotropic neolignan with various pharmacological effects [47], including antidiabetic, antidiarrheal, anti-obesity, anti-inflammatory [57], antistress, antithrombotic, cardio and neuroprotective [57], antimicrobial activity. Mainly, it owns an effective antimicrobial activity against *Actinobacillus asctinomycetemcomirans, Porphyromonas gingivalis, Prevotella intermedia, Micrococcus luteus,* and *Bacillus subtillis*, while showing little activity against *Shigella flexneii*, *Staphylococcus epidermidis, Enterobacter aerogenes*, *Proteus vulgaris Escherichia coli*, and *Pseudomonas aeruginosa* [47]. Other studies have shown that honokiol, although showing an antimicrobial activity lower than the antibiotics today in trade, it is particularly effective against periodontal pathogens [47]. The absence of toxicity *in vitro*, *in vivo*, and in humans has been demonstrated, and therefore this molecule is marketed as a dietary supplement to reduce stress [58]. It is also believed that honokiol behaves like a positive allosteric modulator on the GABA receptor, allowing the entry of chloride ions and increased cell polarization, which results in antidepressant [59] relaxing and anxiolytic properties[60, 61]. The high combination of biological activities makes this molecule potentially employable for different therapeutic applications (**Table 1**).

Table1. Summary of most relevant studies on magnolol, honokiol and obovatol activities.

Health perspectives	Results	Reference
Magnolol		
Antidepressant	Adjusting the hypothalamic–pituitary–adrenal	[36]
Antitumor	Inhibition of the growth of various cancers originating from different organs such as brain, breast, cervical, colon, liver, lung, prostate, skin	[37]
Antioxidant	Protection against cellular oxidative stress	[38]
Anti - inflammatory	Inhibition of lipopolysaccharide (LPS)-induced production of nitric oxide and beneficial effects on atherosclerosis and re-stenosis	[32, 39, 44]
Neuroprotective	Protection of endothelial cell, beneficial effects on Alzheimer and Parkinson, intracerebral hemorrhage and stroke and manages to cross the blood-brain barriers	[44]
Gastrointestinal protection	Inhibition of diarrhea. Nausea and abdominal pain	[43]
Antidiabetic	Inhibition of α-glucosidase and promotion glucose uptake by regulating insulin signaling pathway	[39, 46]
Anti - obesity	Inhibition of pancreatic lipase and protective role against insulin resistance	[45]
Antimicrobial	Inhibition effect exerted by microbes	[34, 46]
Cardioprotective	Reduction of the proportion of myocardial ischemic necrosis	[46]
Honokiol		
Anticancer	Inhibition of cell proliferation by differentiation and apoptosis	[51, 53, 54]
Antioxidant	Decreasing of oxidative stress-induced neurotoxicity	[57]
Neuroprotective	Protection brain against ischemia and cross the blood brain barrier and neuroblastoma apoptosis Inhibition of the inflammatory reaction during cerebral ischemia reperfusion	[49, 57]
Antidiabetic	Inhibition of α-glucosidase and promotion glucose uptake by regulating insulin signaling pathway	[47]
Anti - obesity	Inhibition of pancreatic lipase and protective role against insulin resistance	[47]
Cardioprotective	Inhibition of xanthine oxidase and protection of the mitochondrial respiratory chain	[54]
Antimicrobial	Inhibition effect exerted by microbes especially periodontal pathogens	[47]
Antidepressant	Improvement of depression-like behavior caused by inflammation and action on the mouse lipopolysaccharide depression model	[59]
Anti - inflammatory	inhibition the inflammatory response of LPS-induced dendritic cells	[57]
Obovatol		
Antioxidant	Attenuation of oxidative stress-induced inflammation	[62]
Antiproliferative	Treatment of prostate, leukemia, colon and carcinoma cancer	[63, 64]
Anti - inflammatory	Inhibition of vascular muscle cell proliferation	[65]
Antibacterial	Inhibition of Salmonella type II secretion system	[66]

Neuroprotective	Protection against microglia-mediated neurotoxicity	[67]
Anxiolytic	Inhibition of nitric oxide production and activation of kinases in lipopolysaccharide cells	[68]
Cardiovascular	Improvement cardiac dysfunction as arterial thrombosis and collagen induced platelet aggregation	[69]

Studies on the structure-activity relationship (SAR) have shown that the various properties of honokiol and magnolol are attributable to the presence of hydroxyl and allyl groups on a biphenyl base structure [70]. Considering the above, numerous scientific publications report the synthesis of structural analogues and molecules related to both neolignans. Chemical modifications are generally performed to increase chemical features such as solubility, attractive biological properties, and bioavailability of the molecules. Some examples of synthesis of their derivatives and evaluation of their biological activities are reported in the literature [51, 61, 71-77].

While considerable progress in the study of biological activities has been achieved regarding magnolol and honokiol, obovatol (**3**) has attracted little attention. Obovatol is a phenylpropanoid dimer belonging to the neolignan class NL15 (**Figure 6**). The molecular structure consists of a unique biphenyl ether skeleton containing a catechol, appended with two allyl groups. Obovatol has been extracted from *Magnolia obovata* (yield < 1%): in the dried bark of *M. obovata,* the content of obovatol has been reported to be 0.26%; a study of the content in the leaves reports a rate of 0.76% [78]. Previous studies have shown different biological properties of obovatol. So far, it has shown several biological properties, including antioxidant [62], antiproliferative [63], antibacterial [66], neuroprotective [67], anti-inflammatory and antithrombotic activities [65]. Most of these biological activities have been shown to be through the inhibition of nuclear factor k-light-chain-enhancer of activated B cell (NF-kB) and mitogen-activated protein kinase (MAPK)[68]. Obovatol reduces inflammatory responses in macrophages and microglia by inhibiting the expression of inducible nitric oxide synthase (iNOS) and cyclooxygenase 2 (COX2), as well as the differential

response signaling pathways of myeloid and toll-like receptor 4 (TLR4) [68]. Little is known about its effects in the central nervous system and recently, anxiolytic effects mediated by GABA-benzodiazepine receptors has been reported [60]. Thus, it has been proposed as a therapeutic phytochemical for the treatment of neuronal and cardiovascular disease [69] and different tumors as prostate, acute myeloid leukemia, colon and carcinoma cancer [28, 79-81]. Furthermore, obovatol induces apoptotic cell death without exerting any cytotoxic activity in normal cells (up to 50 μM) [82] and shows inhibitory effects on either collagen or arachidonic acid-induced platelet aggregation and other biological effects, such as antiproliferative activity for vascular smooth muscle cells and cancer cells [64, 83].

Moreover, the effects of the biphenyl on brain inflammation or microglia have been investigated using cultured cells and a mouse model of neuroinflammation. The results have shown that obovatol inhibits inflammatory activation of microglia *in vitro* and neuroinflammation *in vivo*, and exerts protective effects against microglia-mediated neurotoxicity [62]. Other studies have highlighted that the neolignan **3** acts as an anti-inflammatory agent on the expression of inflammatory cytokines tested in macrophages [82]. The man health applications of obovatol are summarized in **Table 1**.

Magnolia species also contain oligomeric compounds in addition to biphenyl and biaryl ether compounds. These compounds have been identified and isolated from various *Magnolia* trees, although their extraction yields are quite low and require several purification steps. **Figure 8** reports some examples of isolated oligomers. For instance, bishonokiol A was extracted from the seeds of *Magnolia grandiflora* with a 0.013% yied [84]. The compound garrettilignan A was isolated from the leaves of *Magnolia Garretti* [85] with a yield of 0.003%, while from the leaves of *Magnolia chevalieri* [86], chevalierinol A was extracted with a yield of 0.009%. Two oligomers with different structures were isolated from the leaves of *Magnolia officinalis var. biloba* [87]: officinalignan A with 0.002% yield and

houpulignan H with 0.001% yield. Additionally, from the roots of *Magnolia officinalis* [88] four oligomers were extracted: houpulin B (0.003%), houpulin C (0.0004%), houpulin D (0.001%) and houpulin K (0.005 %).

The oligomers below reported show different structures linked through aromatic rings, including *ortho, ortho* (*o*,*o*)-linked dimers, *ortho, para*-linked dimers (*o*,*p*) and (*o*,*o*)-linked trimers, dimers and trimers with an *o*,*o*-linkage, and *o*,*o*-/*o*,*p*-linked trimer[88]. As an example, houpulin K is an (*o*,*o*)-linked dimer involving an *o,o*-linkage, houpulin H is formed by two moieties of obovatol and one of magnolol while officininalignan A is a obovatol dimers bearing the benzodihydropyran and 2,3- dihydrobenzofuran skeleton. Moreover, the neolignans isolated from *Magnolia officinalis* (houpulin B, C and D) are respectively a dimer of honokiol and two derivatives of magnolol. These oligomers have novel carbon scaffold that can be biosynthesized by the three or four C_6C_3 subunits coupling.

Recent studies have been dedicated to evaluating the biological activities of the dimers. Some studies have highlighted the anti-inflammatory [87, 88] activity of houpulin K, houpulin C and D; the antioxidant activity [86, 87] of houpulignan H, officinalignan A and chevalierinol A; the antitumor[89] and the α-glucosidase inhibitory [90] activity of various dimer and trimers of honokiol. Additionally, bishonokiol A has also demonstrated antiproliferative activity and induces apoptosis [84].

Few studies have been conducted to evaluating the houpulin B biological effects. It has shown promising antitumor activity and effects as inhibitor of superoxide anion generation and elastase release [91]. Research studies on these compounds are still ongoing and the main challenge is developing and carrying out a total chemical synthesis to increase the biological studies.

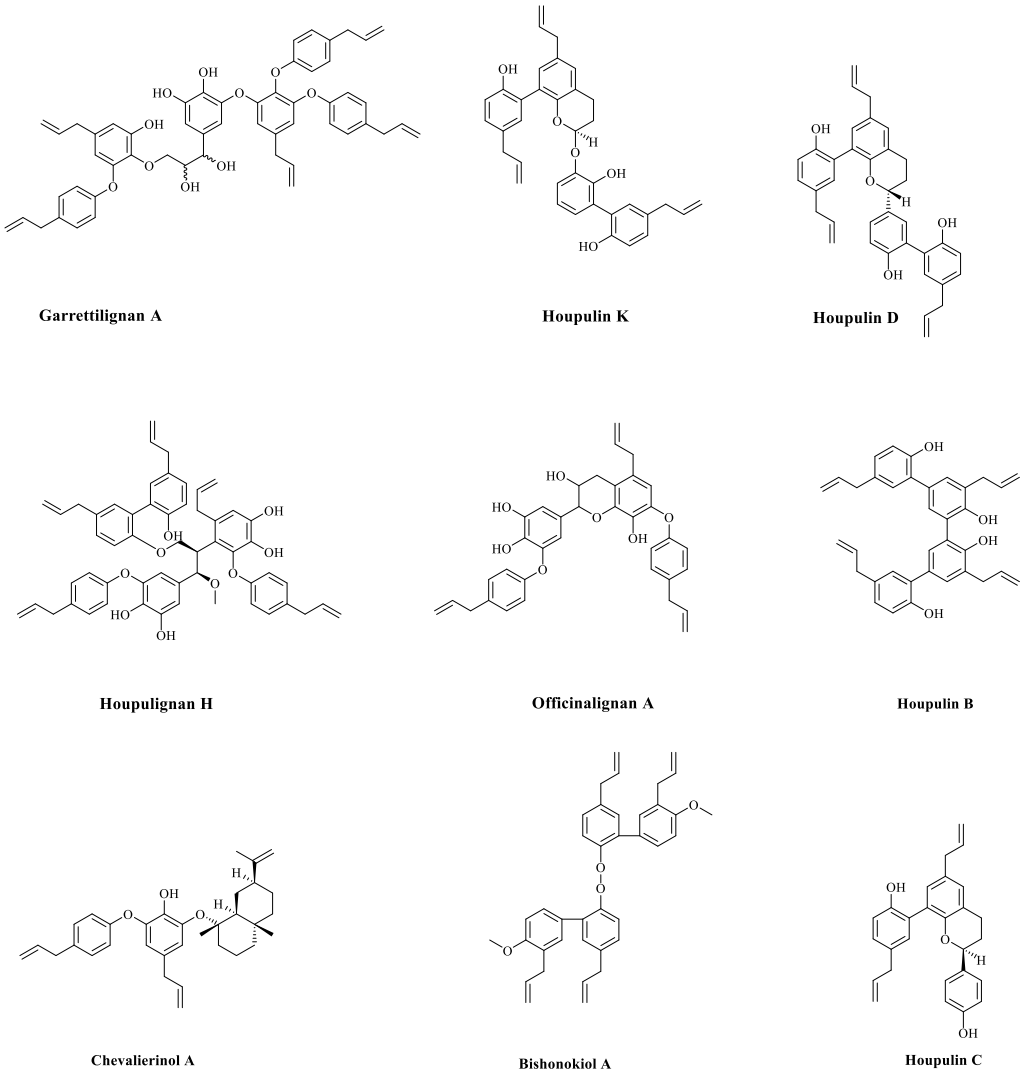

Figure 8. Structure of some oligomeric compounds.

Synthetic approaches for the synthesis of neolignans inspired by magnolol, honokiol and obovatol

The molecular backbone of neolignans consists typically of a phenylpropanoid (C_6C_3) building block: structural differences are mainly due to their biosynthetic mechanism, based on radical oxidative coupling reactions mediated in nature by peroxidases, laccases enzymes, or cytochrome P450 [72, 92]. It is known that oxidases intervene only in the first phase of the reaction, that is the radical formation. The stereochemical control of the reaction is exerted by a protein named "dirigent protein" [93]. In the absence of this protein, a mixture of products characterized by different structures would be obtained due to the radical species' unequal reactivity. Instead, in the case of neolignans biosynthesis, the enzyme leads to the oxidation of two phenolic units with the formation of a biphenyl bond. This process is described by Aldemir *et al*. [92] and the mechanism is reported in **Scheme 1**.

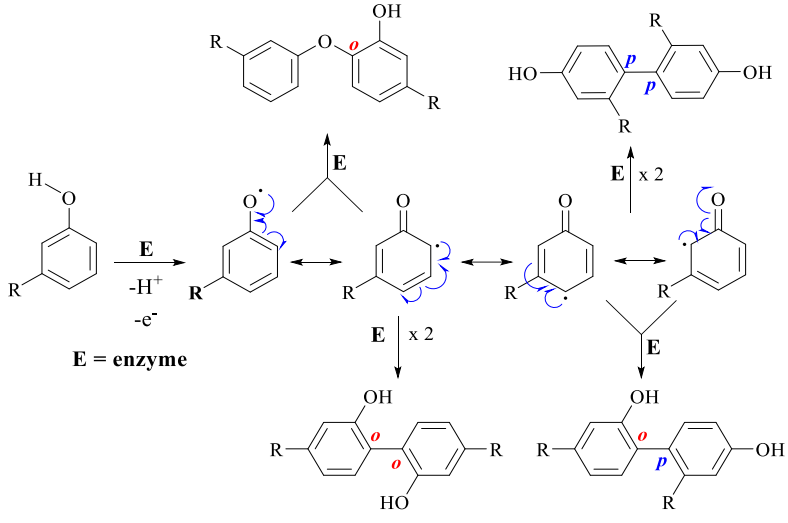

Scheme 1. Mechanism of biosynthesis of bisphenolic neolignans [92].

Scheme 1 demonstrates how the enzyme generates a phenoxydic radical by removing a proton and an electron (or a hydrogen radical). The spin density related to the radical is located on the oxygen atom and the *ortho* and *para* positions. So, through the coupling of two radicals occurring in different positions, a variety of products with C-C and/or C-O-C bond are obtained.

Synthetic strategies for biphenyls structures

In a laboratory scale the biphenylic structures related to magnolol and honokiol can be obtained through reactions involving the use of oxidizing agents (Ag_2O, $FeCl_3$, $CuCl_2$, or $Mn(OAc)_3$). However, the reactions conducted with enzymes such as peroxidase, laccase and cytochrome P450, have the advantage of being more environmentally sustainable than those involving the use of metals. Still, both processes do not show regioselectivity; in some cases, they provide a mixture of products with different dimeric structures [94]. Below, an overview of the coupling reaction is reported.

An arylation method that does not involve metal catalysis was described by Dichiarante *et al*. [95]. In this method, phenyl cations generated by photo-heterolysis of the aryl halides or esters with an electron-donating substituent undergo selective addition to π nucleophiles with no interference by the solvent even when it is a nucleophile (**Scheme 2a**). The mild reaction conditions distinguish the reaction, which looks like an excellent strategy for obtaining biphenyl compounds.

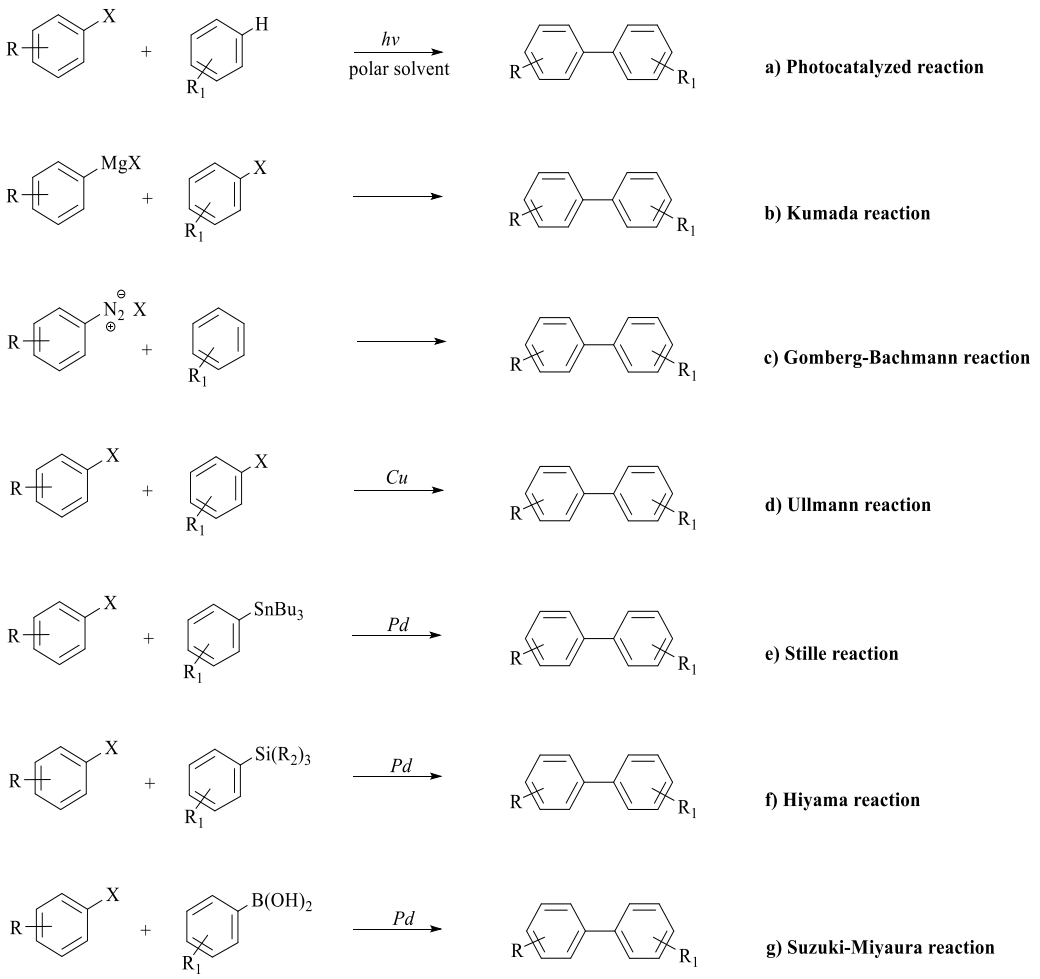

Scheme 2. Summary of some synthetic methods to achieve biphenyl compounds.

The synthesis of substituted biphenyl was also achieved by the Kumada coupling reaction, which involves the addition of Grignard aromatic reagents with aryl halide in the presence of nickel-phosphine catalysts (**Scheme 2b**) [96]. Other synthetic strategies are the Gomberg-Bachman reaction (**Scheme 2c**) and the Ullmann reaction (**Scheme 2d**). The first involves using aromatic derivatives such as diazonium salts [97]; the second allows to obtain biphenyl compounds following reductive coupling between two aryl halides in the presence of a copper catalyst in harsh reaction conditions such as high temperature [98]. Finally, other coupling methods to synthesize aryl biphenyl in less harsh conditions and the

presence of different complexes based on palladium are mentioned here: the Stille reaction (**Scheme 2e**), occurring between an aryl halide and an organotin; Hiyama reaction (**Scheme 2f**), between an aryl halide and an organosilane derivative; Suzuki-Miyaura (SM) reaction (**Scheme 2g**), between aryl halide and organoborane compound.

Scheme 3 reports the catalytic cycle of SM reaction. In particular, the commonly used palladium catalyst is Pd^0. In many cases, Pd^{2+} complexes are used, such as palladium acetate $Pd(OAc)_2$ which are reduced *in situ* by the presence of phosphine ligands as well as 1,1'-bis(biphenylphosphino)ferrocene (dppf) or dicyclohexyl(2′,6′-dimethoxy[1,1′-biphenyl]-2-yl)phosphine (SPhos). The main steps of the catalytic cycle are as follows: i) oxidative addition, in which Pd^0 binds to the aryl halide to form Pd-aryl complex; ii) displacement of the halide from the Pd-aryl complex to generate a more reactive hydroxylaryl-palladium complex, facilitated by the use of a base that promotes the subsequent iii) slow step of the transmetalation with boronic acid; iv) and the reductive elimination which allows the formation of a new C-C bond between the two aromatic rings and the reduction of the Pd^{2+} complex to Pd^0, making it available for a new catalytic cycle [99].

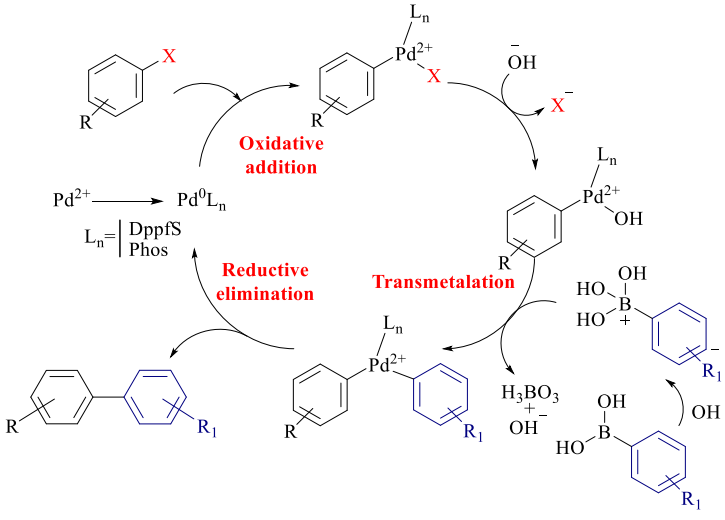

Scheme 3. Catalytic cycle of Suzuki-Miyaura cross-coupling.

Furthermore, the analysis of chemical reactions used in the last three decades (from 1984 to 2014) in medicinal chemistry pointed out the Suzuki-Miyaura reaction among the three most frequently used reactions to synthesize bioactive compounds [100]. Significantly, magnolol and honokiol were synthesized through the Suzuki-Miyaura cross-coupling reaction [101].

Synthetic strategies for dimeric and oligomeric polyphenols by enzymatic reactions

The synthesis of dimeric polyphenols often involves a "biomimetic" approach with enzyme-mediated processes used to mimic the biosynthetic coupling pathways. These reactions are preferably facilitated by oxidase enzymes [102]. The most prevalent enzymes employed for oxidative dimerization reactions are peroxidases. Among them, horseradish peroxidase is an eme-protein that generates phenoxy radicals and reduces hydrogen peroxide to water [103]. These enzymes have been used to catalyze the oxidation of low molecular weight organic compounds with a wide range of naturally attainable structures [104]. Laccase features consist of four copper ions, able to catalyze the oxidation of several organic compounds, including substituted phenols, diphenols, and polyphenols. [104]. Laccase features consist of four copper ions, able to catalyze the oxidation of several organic compounds including substituted phenols, diphenols and polyphenols. This enzyme converts the oxidizing agent, the atmospheric oxygen into water while facilitating the one-electron oxidation of four reducing substrate molecules, thereby achieving a four-electron reduction of molecular oxygen to water [105, 106]. The structures of the enzymatic site of peroxidase and laccase and the mechanism of reaction are reported in **Figure 9**.

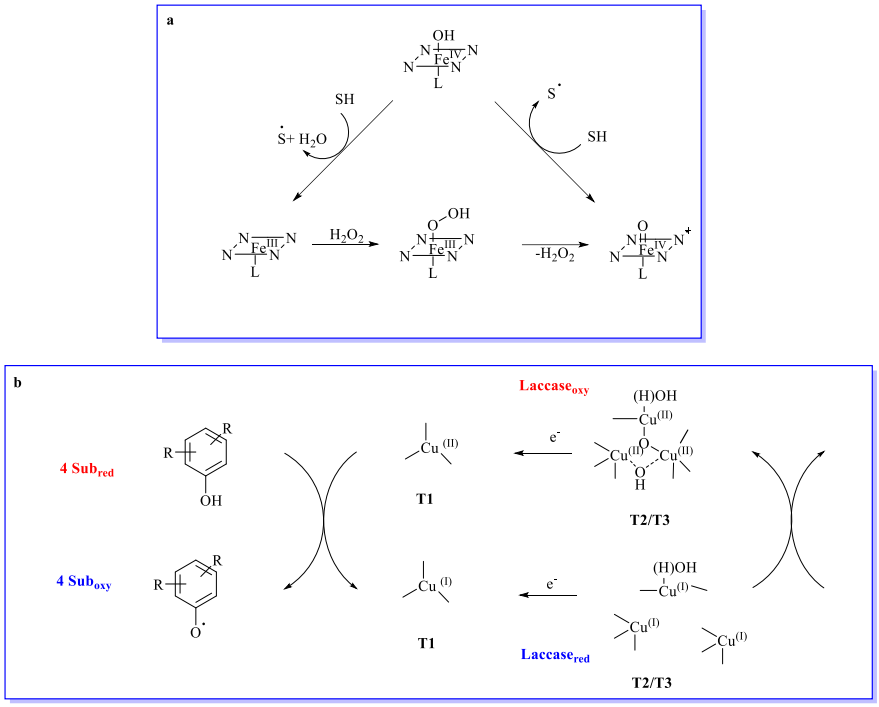

Figure 9. Proposed catalytic pathways of a) horseradish peroxidase (HRP) and b) laccase.

Generally, phenolic compounds are oxidized to radical and/or quinone intermediates which react to achieve dimeric products. Because these dimers could still contain phenolic functions, it is possible that they can produce dimeric radicals thus obtaining oligomers and/or polymers by self/cross-coupling [107].

On a laboratory scale, the oxidase enzymes have been employed in radical coupling reaction of several phenols to yield dimerization products as well as oligomeric compounds [108, 109]. It is known that the dimer synthesis occurs with the same mechanism through which plants produce natural products such as neolignans in presence of oxidase enzyme or other oxidative agents. Thus these synthetic reactions mimic the natural ones [108].

Laccase-catalyzed reactions can also be replicated in laboratory using chemical mediators such as (2,2,6,6-tetramethylpiperidin-1-yl)oxyl radical (TEMPO), 1-hydroxybenzotriazole (HBT), and 2,2'-azino-bis(3-ethylbenzothiazoline-6-sulfonic acid)diammonium salts (ABTS). These mediators

are commonly employed to enhance the enzyme efficiency allowing laccases to oxide a wide range of substrates in addition to phenolic compounds. They also contribute to improved stability and catalytic activity of laccase, and they can be employed when the direct oxidation is not possible to achieve due to the incompatibility of redox potential. Finally, the chemical mediators reduce the reaction time [107]. **Figure 10** reports the structure of the common chemical mediators.

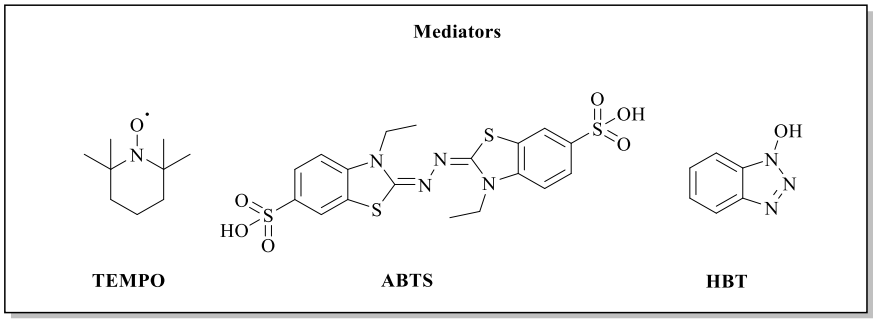

Figure 10. Structure of the common chemical mediators.

Synthetic strategies for biphenylic ether structure

Obovatol (**3**) bears a biphenyl ether skeleton and not a biaryl structure; for this reason, the previously synthetic approaches cannot synthesize it. Still, it is possible to take advantage of some reactions reported below.

The formation of carbon-heteroatom (C-X) bond is a strategy for the production of numerous scaffolds with biological and pharmaceutical applications [110]. A representative example is the selective ether bond linkage between two aryl scaffold, an important motif widely distributed in various natural products, synthetic pharmaceuticals, agrochemicals, and other chemical materials [111]. As a consequence, the development of synthetic methods to preparate or improve existing ones is an active research topic. From the retrosynthetic point of view, a biaryl ether can be synthesized by connecting two aryl moieties or by building up

the absent aryl ring from a suitable aryl alkyl ether. However, the first strategy is applied almost exclusively to the synthesis of natural biaryl ethers.

Three main groups of synthetic approaches for scaffold construction have been developed: nucleophilic aromatic substitution reactions (SNAr), oxidative coupling of phenols, and metal-mediated arylation of phenol [112].

SNAr occurs between aryl halide substituted with one or more strongly electron-withdrawing groups and phenoxides without the addition of a catalyst (**Scheme 4a**). The reactivity depends on the halide (F >> Br> Cl); the presence of an *ortho*-nitro group provides the ring activation. These features allow an efficient coupling reaction at room temperature, provided by solvents with high dielectric constants such as DMF or DMSO.

The biaryl ether scaffold can also be achieved by selective phenol oxidative coupling performed by cytochrome P450 [113], peroxidases, and thallium(III)nitrate (TTN) or thallium(III)trifluoroacetate (TTFA) as oxidizing agents (**Scheme 4b**) [112]. Bis-*ortho*-halogenated phenol serves as an essential substrate, as this synthetic methodology is ineffective even when one phenolic *ortho* position is left unsubstituted. Excess of thallium (III) salts are usually used as one-electron oxidants. However, due to the salt's high toxicity, the use of enzymes (H_2O_2-peroxidase, horseradish peroxidase (HRP), soybean peroxidase (SPO)) is recommended. Alternatively, reagents such as ceric ammonium nitrate (CAN**)** or electrochemical process more recently, anodic oxidation, are preferred even if the reaction yields are lower in many cases [112].

The arylation of phenol by aryl halides in the presence of copper powder or copper salts (Ullmann biaryl ether condensation) is another synthetic approach for the construction of biaryl ethers (**Scheme 4c**) [114]. Fair to good yields of biaryl ethers are obtained when electron-rich phenols and electron-poor aryl halides are employed. This synthetic method is explained in detail below.

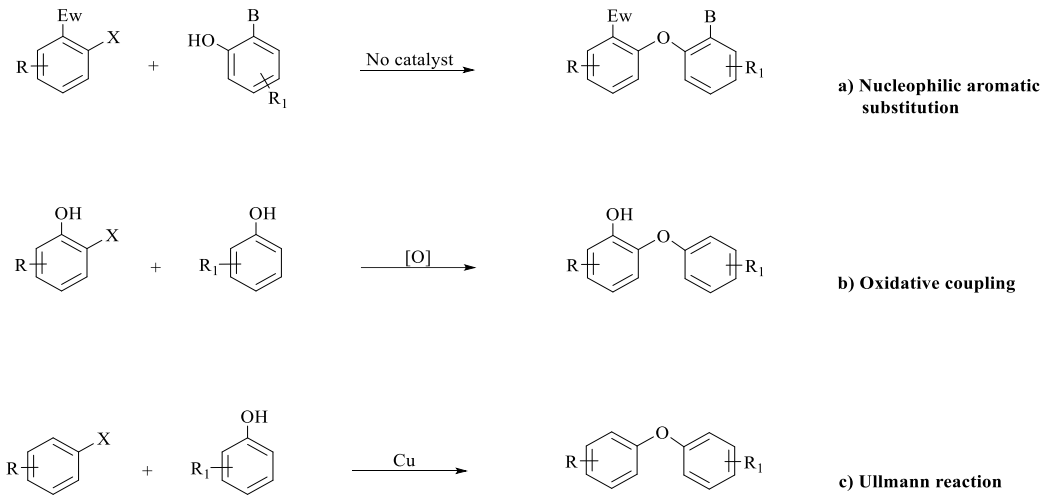

Scheme 4. Summary of some synthetic methods to achieve biaryl ethers compounds.

The Ullmann biaryl ether synthesis, or, more commonly, Ullmann condensation, has been extensively used to form biaryl ethers.

The original protocol for the coupling reaction required the use of stoichiometric or more significant amounts of the copper salts together with high reaction temperature (≥200°C), long reaction times, and a strong base [115]. These disadvantages associated with the low yields observed when using inactivated aryl halides have severely limited the synthetic applications of this reaction [114]. However, the search of cost-effective and sustainable reactions has stimulated researchers to explore to copper-mediated cross-coupling reactions. The successful development of improved catalytic versions has caused an interest in what is now referred to as the "modified Ullmann reaction" [116].

The key advancement in the new reaction procedure lies in the addition of ligands to the copper catalyst to improve the solubility and stability [117] of the copper precursors. This results in milder reaction conditions, lower reaction temperature, reduced reaction time, and a decrease in the catalyst loading (0.25 to 2.5 mol%). Additionally, nonpolar solvent like toluene are used while cesium carbonate, employed as a base, eliminates the need to form the phenoxide anion before the reaction [118]. The copper (pre-) catalyst is generally prepared *in situ*

by mixing a copper salt with a suitable, often bidentate, chelator such as diamine, amino acids, or other nitrogen- and oxygen-containing ligands. These developments have proven highly successful that the modified Ullmann reaction being applied in large-scale production. It is evident that this technology is much more cost-effective compared to the widely used palladium-catalyzed variants [116].

Only a few studies were dedicated to mechanistic investigation of the actual role of the ligand on a possible catalytic cycle. In an early publication concerning the synthesis of biaryl ethers, Buchwals observed that stoichiometric quantities of carboxylic acids facilitated the coupling of less reactive phenols with aryl bromides and iodides [118]. More recently, Taillefer and co-workers conducted a structure/activity relationship study on the biaryl ether formation catalyzed by CuI with *N,N*-chelating ligands [119]. The authors explained the results using a cycle involving an oxidative addition/reductive elimination mechanism (**Scheme 5**).

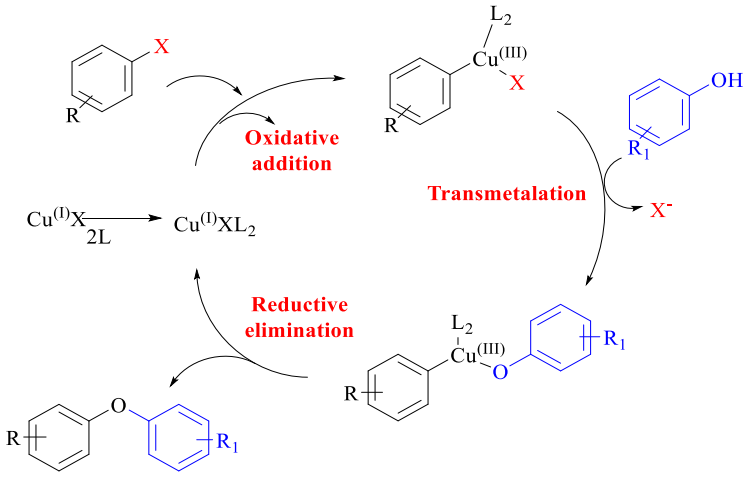

Scheme 5. Mechanistic proposal for the synthesis of biaryl ethers.

Scheme 5 illustrates the general catalytic cycle of an Ullmann coupling ether condensation. In particular, Cu (I) is prepared *in situ* by the presence of *N,N*-

chelating ligands in order to initiate the catalytic cycle. The main steps of the cycle are: i) the oxidative addition, in which Cu(I) binds to the aryl halide forming a Cu-aryl complex; ii) the subsequent transmetalation step with a phenol; iii) the reductive elimination, which allows the formation of a C-O bond between aryl halide and phenol and iv) the regeneration of the catalyst, thus available for a new catalytic cycle.

The general features of the Ullmann reaction can be summarized as follows:

a) aryl iodides, bromides, and chlorides are all good substrates with an opposite trend compared to uncatalyzed SNAr reactions (I > Br > Cl >> F) [112].
b) the introduction of several aryloxy groups is possible in a stepwise manner and the aromatic halide can contain many different substituents. Reactive functional groups such as. OH, NH_2, CHO do not require protection during the Ullmann biaryl coupling.
c) electron-withdrawing substituents (e.g., NO_2, CO_2R, COO^-) in the *ortho* and *para* positions of phenol significantly activate the reaction, leading to excellent yields, while electron-donating substituents anywhere on the aromatic ring do not significantly decrease the reactivity of the aryl halide compared to the unsubstituted aryl halide [120].
d) the required temperature ranges from 100 to 300 °C in the presence of copper metal, or a copper-derived catalyst [121];
e) a wide variety of solvents work well, and most of them contain a heteroatom with a lone pair of electrons (dioxane, pyridine, quinoline, DMSO, DMA, DMF, THF). The solvent serves to solubilize the catalytically active copper species by way of complexation.
f) the phenol component can be introduced in the form of free phenols or phenolate salts. When they are used, a base (e.x. K_2CO_3) is generally added to the reaction mixture. Other salts such as ammonium chloride, sodium chloride, lithium bromide and potassium bromide have proved to be ineffective.

g) if Cu_2O or CuO is used instead of copper, no base is required, since these substances serve as bases.
h) Finally, since phenols and phenolates are sensitive to oxidation, the use of an inert atmosphere is often required.

Metabolic disorder

Metabolism disorders are pathologic conditions that affect the body's metabolism. They are characterized by the inability to properly use and/or store energy at the cellular level [122]. Metabolic diseases affect the ability of the cells to perform critical biochemical reactions involving the processing or transport of proteins, carbohydrates, or lipids. Metabolic disorders include insulin resistance, abdominal obesity, hypertension, and hyperglycemia. These are also risk factors for cardiovascular disease, type 2 diabetes, stroke, chronic kidney illness, and cancer [123]. The burdens of metabolic disorders, such as obesity or diabetes, are believed to arise through a complex interplay between genetics and epigenetics predisposition, environment, and nutrition [122]. Therefore, several studied have been devoted to discovering novel methods to counteract both metabolic disorders.

Obesity

Obesity is one of the world's leading health problems. It is considered a risk factor for major chronic diseases and disabilities, like coronary heart disease, hypertension, heart failure, type 2 diabetes, cancer, and the reproductive system and gastrointestinal tract [124, 125]. Obesity is a condition characterized in most cases (95%) by an excessive accumulation of body fat caused by an incorrect lifestyle with a high-calorie diet often associated with reduced calorie consumption. Therefore, it would be a condition preventable by a healthy lifestyle. In the remaining number of cases (5%), obesity is related to identifiable organic causes of endocrine nature (cortisol, hypersecretion, hypothyroidism, hyperinsulinism), hypergenetic-malformative nature (due to the action of certain drugs), neurological and neoplastic origins [125].

Nevertheless, this condition represents one of the main public health problems worldwide, given the alarming speed with which cases are growing not only in Western countries but especially in developing countries [126]. Despite

the significant number of research reported in the literature, obesity remains an unsolved problem, and the discovery of drugs that aim to counteract obesity is growing strongly. Until today, several strategies are known to prevent and counteract the accumulation of fats. The two main ones involve the use of drugs to increase energy waste or reduce calorie count by reducing hunger or slowing down and/or inhibiting fats absorption [127]. In the latter cases, the therapy works on the enzymes involved in the digestion and absorption of fats, such as lipase enzymes.

The human lipases are the pre-duodenal (lingual and gastric) and the extra-duodenal (pancreatic, hepatic, lipoprotein, and the endothelial) lipase. Pancreatic lipase (triacylglycerol acyl hydrolase; PL), the principal lipolytic enzyme synthesized and secreted by the pancreas, plays a key role in digesting triglycerides [128]. It hydrolyzes fatty acids from the α and α' position of dietary triglycerides, yielding β- monoglycerides. (**Figure 11**)

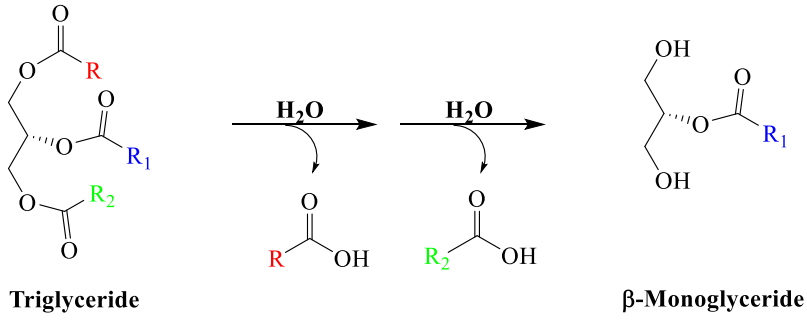

Figure 11. The hydrolysis reaction of triglyceride catalyzed by lipase.

PL is responsible for the hydrolysis of 50–70 % of total dietary fats, and **Figure 12** depicts the physiological role of the enzyme in lipid absorption.

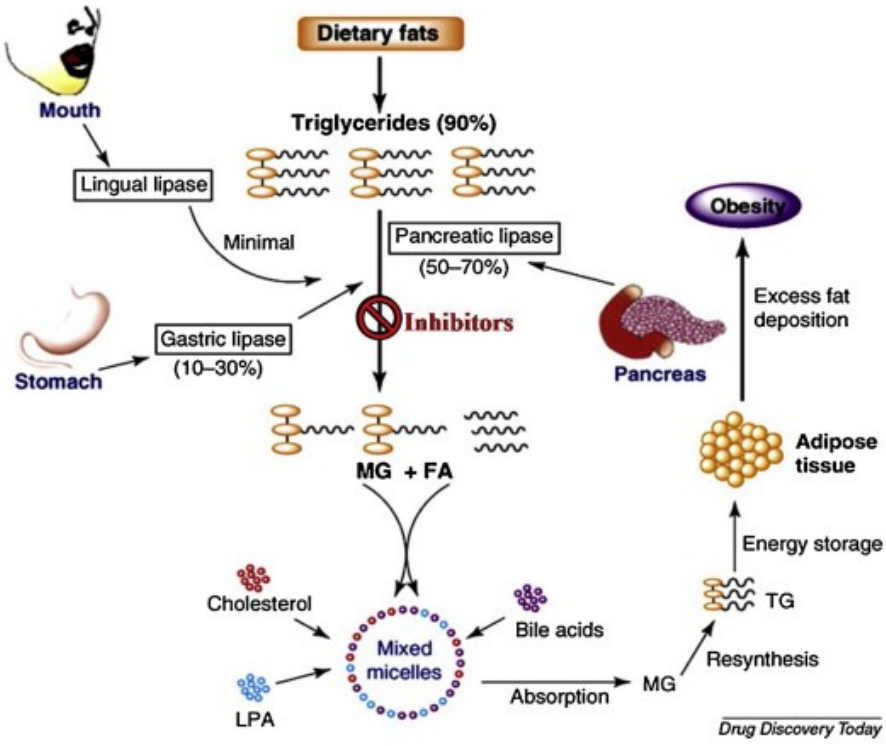

Figure 12. The physiological role of pancreatic lipase in lipid absorption.

Thanks to the knowledge on the hydrolysis process of fats, the pharmacological effects of the molecules able to inhibit the lipase activity have been studied to reduce and /or slow down the hydrolysis process and consequently decrease the accumulation of fats in the adipose cell of an obese person. These lipase inhibitors are used as drugs with strong anti-obesity action. Among these, orlistat, a potent and selective pancreatic lipase inhibitor [129], is the saturated derivative of lipstatin, a natural PL inhibitor isolated from the bacterium *Streptomyces toxytricini* [130, 131] (**Figure 13**). In addition to its activity as an anti-obesity agent, orlistat modestly decreases blood pressure and counteracts the onset of type 2 diabetes. It was approved by the Food and Drug Administration (FDA) in 1998 in the USA, and it is considered the only effective drug to control obesity.

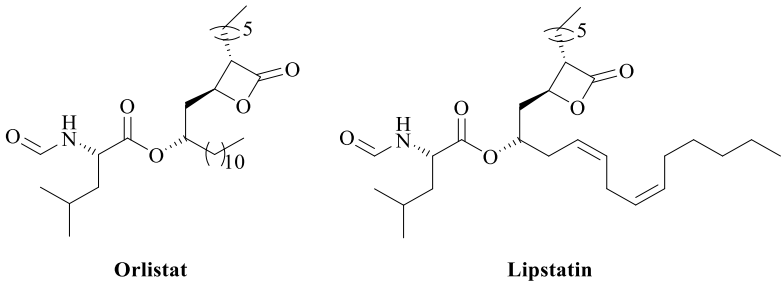

Figure 13. Structure of pancreatic lipase inhibitors.

The mechanism of lipase inhibition by orlistat is via covalent bonding formation with a serine present in the lipase's active site. Unfortunately, this drug shows several side effects, including abdominal cramps, incontinence, and other disorders [132]. For this reason, active research is aimed at discovering new and effective anti-obesity drugs with special attention devoted to compounds and/or natural extracts with negligible undesirable side effects.

Diabetes

Diabetes mellitus, commonly known as diabetes, is the general term to indicate a heterogeneous metabolism disturbance. The main finding is chronic hyperglycemia (high blood sugar), resulting from defects in insulin secretion, insulin action, or both. Chronic hyperglycemia of diabetes is associated with long-term damage, dysfunction, and failure of different organs such as the eyes, heart, kidneys, nerves and blood vessels [133, 134]. Most cases of diabetes fall into two broad etiopathogenetic categories[133, 135, 136]. The cause of type 1 diabetes (T1DM) is an absolute deficiency of insulin secretion. It is an autoimmune disease, where the immune system attacks and destroys cells in the pancreas, where insulin is made up. About 10% of people suffer from T1DM [137]. The second category is much more prevalent concerning the previous, and it's called type 2 diabetes

(T2DM). The cause is a combination of insulin action resistance, and inadequate compensatory insulin secretory response. In this category, hyperglycemia is sufficient to cause pathologic and functional changes in various target tissues. However, without clinical symptoms, it may be present for a long period before diabetes is detected. Type 2 diabetes develops in adulthood and is primary associated with incorrect lifestyles (sedentary life), consumption of industrially sourced food, and some chronic degenerative diseases. Other type of diabetes is prediabetes, which occurs in less than 1 % of the people with diabetes when your sugar is higher than usual but it's not high enough for a diagnosis of T2DM; gestational diabetes mellitus (GDM) which affects about 5-6% of pregnant women and in most instances is an early form of T2DM.

Hyperglycaemia causes the onset of other diseases (polyuria, polydipsia, weight loss, blurred vision, etc.). Retinopathy with a potential loss of vision, nephropathy leading to renal failure, peripheral neuropathy with risk of foot ulcers, amputations, autonomic neuropathy causing gastrointestinal, hypertension, cardiovascular symptoms, and sexual dysfunction, and an increase in the production of reactive radical species, with consequent oxidative damage to the involved tissues are long-term complications related to diabetes. Patients with diabetes also have an increased incidence of atherosclerotic cardiovascular, peripheral arterial, and cerebrovascular [138]. In 2019, diabetes was included in the top 10 global causes of death; thus, there is an urgent need to search for antidiabetic drugs to prevent and counteract sugar accumulation. Carbohydrates are among the main nutritious components of the human diet. Usually, after a meal, the blood sugar level responds highly to the digestion of carbohydrates, mainly starch. **Figure 14** depicts the digestion of carbohydrates thanks to two enzymes [139]: pancreatic α-amylase (α-1,4- glucan-4-glucanohydrolase; α-Amy), an endoglycosidase delivered into the intestinal lumen as a constituent of pancreatic juices and it catalyzes the hydrolysis of starch to maltose and

maltotriose; α-Glucosidase (α-Glu), a membrane-bound enzyme located in the epithelium of the small intestine, catalyzes the cleavage of glycosidic bonds and releases of glucose from disaccharides and oligosaccharides.

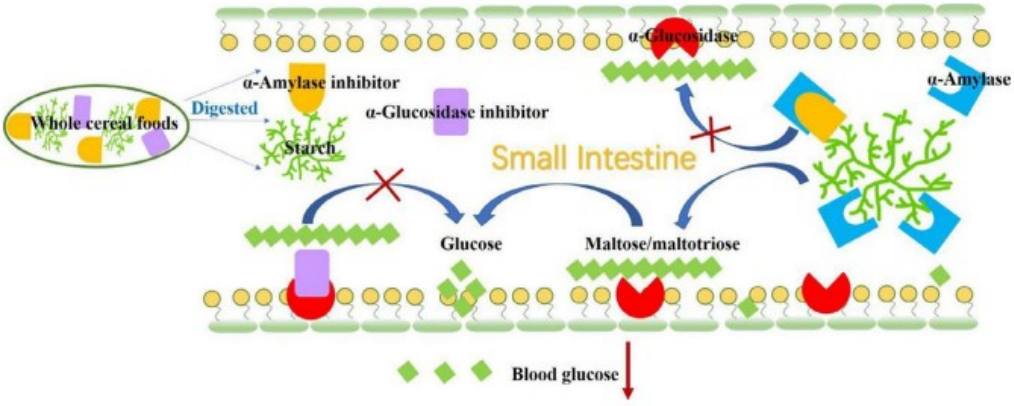

Figure 14. Biological mechanism of carbohydrate digestion.

Carbohydrates are initially hydrolyzed by salivary and pancreatic α-amylase to reduce into oligosaccharides. Then, the reducing sugars are digested by pancreatic α-glucosidase to glucose that enters blood circulation. Therefore, retarding starch digestion by inhibiting the activity of essential hydrolyzing enzymes, is beneficial to health as it alleviates the stimulation of pancreatic islet β cells.

One of the strategies in treating diabetes includes the development of absorption inhibitors [140]. The inhibition of digestive enzymes is one of the most widely studied mechanisms used to determine the potential efficacy of natural products as hypoglycaemic agents. Commercially available antidiabetic drugs are Bayer's acarbose [141], produced by microbial fermentation made with strains of the genus *Actinoplane*s, and the synthetic agents miglitol and voglibose (**Figure 15**). Different side effects are commonly associated with these drugs, including flatulence, diarrhea, abdominal distention and nausea [142]. These effects have prompted the search of new and effective hypoglycemic agents, with special attention given to natural or biocompatible compounds and natural extracts. The

aim is to discover alternatives with less or without undesirable side effect to counteract diabetes.

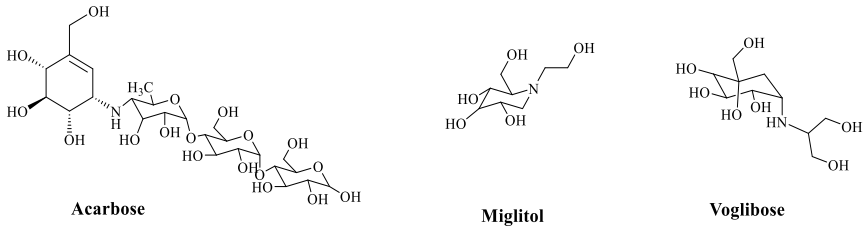

Figure 15. Structure of hypoglycemic agents.

Natural products as inhibitors of metabolic enzymes

The discovery of natural products derived from traditional medicinal plants continuously offers promising benefits for the advancement of new metabolic disease treatments. Over the years, many natural compounds have been demonstrated in clinical trials [128].

Recent research has been devoted to understanding and explore potential therapies for obesity with particular interest on the use of natural products. They offer a wide range of pancreatic lipase inhibitors to counteract obesity. One such example is saponins which effectively inhibit pancreatic lipase and may serve as a possible treatment for obesity and related disorders. Interestingly, the platycodin D, isolated from fresh root of *Platycodim grandiflorum*, showed even stronger lipase inhibitory activity [128]. Polyphenol compounds also exhibit lipase inhibitory activity due to their interactions with a variety of enzyme proteins. Various polyphenols including flavonols, tannins and chalcones have been shown to have activity towards pancreatic lipase [128]. Among these, (-)-epigallocatechin 3,5-O-gallate, a commonly flavonoid of *Camellia sinensis*, showed strong inhibitory activity with a IC_{50} value of 0.0098 μM [143]. In addition, alkaloids extracted from the leaves of *Murraya koenigii*, have been identified as attractive

natural compounds. One of them mahanimbine showed pancreatic lipase inhibitory effects with an IC_{50} value of 17.9 μM [143]. In the terpene family, carnosic acid isolated from the leaves of *Salvia officinalis* has been identified as a promising anti - obesity inhibitor with IC_{50} value of 36 μM [143]. These results highlight the promising potential of natural products in the development of new lipase-targeted inhibitors.

Similarly, several studies have been conducted to identify natural compounds which inhibit enzymes responsible for diabetes. Nature provides a wide range of natural products that offer the potential for development of new hypoglycaemic drugs. One of them, galargine has been derived from *Galega officinalis* plant and bears a similar to the antidiabetic drug metformin [144]. Natural products with hypoglycemic effects are categorized into various groups including terpenoids, alkaloids, flavonoid and others [145]. Recent researchers have been particularly interested in ginsenosides found in *Panax ginseng*, as they demonstrate significant hypoglycemic effects. Besides ginseng, several other traditional herbs rich in terpenoids have been studies as well as oleanolic acid isolate from the whole herb of *Swertia mileensis* and from the fruit of *Ligustrum lucidum* [145]. Moreover, polyphenol-rich diets have also shown benefits in improving glucose metabolism. As an example, naringin and hesperidin, two flavanones found in fruits and vegetables, exhibit anti-diabetic effects and promote glycogen synthesis [146]. Phenolic acids, found in various fruits, vegetable, spices, berries and grains, such as chlorogenic acid, ferulic acid, *p*-coumaric acid and cinnamic acid have been shown to improve hyperglycaemia, insulin resistance and reduce glucose absorption [146]. For example, chlorogenic acid exhibit a low α-glucosidase inhibitory effect an IC_{50} value of 45.5 μM [147]. Finally, the isoquinoline alkaloid derived from *Coptis chinensis Franch* has been traditionally used in Chinese medicine to manage diabetes [146]. These natural compounds hold promise as potential sources for developing new and effective inhibitors to treat diabetes.

Figure 16 reports the structure of some anti-obesity and hypoglycaemic natural inhibitors.

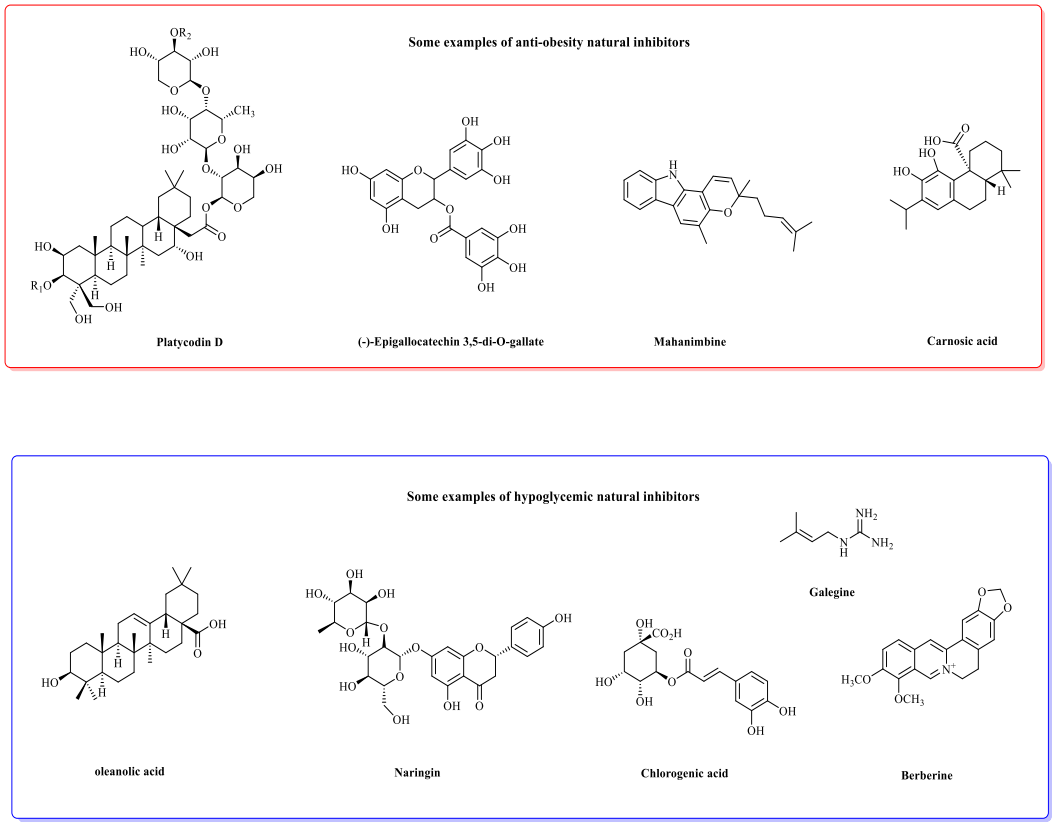

Figure 16. Examples of natural products as potential metabolic enzyme inhibitors.

Chapter 2

Aim of the work

Natural products from traditional medicinal plants and microbial origin are important sources of novel drug leads. Traditional Chinese medicinal herbs are a rich source of lead compounds and potential drug candidates. The two neolignans, magnolol (**1**) and honokiol (**2**), extracted from the bark and leaves of *Magnolia ssp*., are examples of biphenolic compounds with a wide array of biological properties, as formerly reported. Conversely, a limited number of studies are focused on the biaryl ether scaffold of obovatol (**3**) due to its low extraction yield and the low commercial availability.

The evaluation of new structures inspired by natural products is one of the main subjects for synthetic organic chemistry in light of developing new drugs. Biphenyl and biaryl ether scaffolds are essential intermediates in organic chemistry and constitute the structural moiety of a wide range of natural and pharmacologically active products [111, 148]. Consequently, in the last years, an increasing number of studies have been devoted to the synthesis of new compounds inspired by the three neolignans, although for obovatol, the limitations previously reported restrict the number of applications.

The discovery of new molecular entities as metabolic enzyme inhibitors, such as α-glucosidase and α-amylase for treating type 2 diabetes, and lipase for obesity, is an evolving research field, given the growing increase in subjects suffering from these pathologies. To date, only a few data are reported for magnolol as an α-glucosidase and α-amylase inhibitor, and some of its derivatives have also been synthesized and evaluated [72, 149]. Conversely, no data are reported in the evaluation of obovatol as a potential metabolic enzyme inhibitor, and only one study reports honokiol as a potential pancreatic lipase inhibitor [150].

In light of these considerations, this Ph.D. study aims to synthesize new libraries of derivatives inspired by the three neolignans and to evaluate them as

potential α-glucosidase, α-amylase, and lipase inhibitors. Moreover, a in deep evaluation of the inhibition activity of the natural compounds (**1** – **3**) through *in vitro* biochemical assays, kinetic analysis, fluorescence spectroscopy, and *in silico* analysis will be reported for the first time.

The first library proposed here is based on biphenyl structures related to magnolol (**1**) and honokiol (**2**), synthesized as potential pancreatic lipase inhibitors. An efficient synthetic procedure based on the employment of the Susuki-Miyaura (SM) cross-coupling reaction is proposed. The neolignans were designed to be structurally similar to the natural products by inserting amino or nitro groups. The choice to incorporate these functional groups, in addition to the hydroxyl group, is based on previous results on bioactive compounds containing amino or nitro groups, which were found to be potent lipase inhibitors [151].

The biaryl ether scaffold of obovatol (**3**) has inspired the second library. The new analogues were designed to include various functional groups (methoxy, brome, carboxy, and formyl groups) and moiety (ether and thioether derivatives). These compounds were synthesized to investigate the specific role of structural modifications performed on the obovatol scaffold in α-glucosidase and α-amylase inhibition in light of previous results. [152-155]. This thesis describes a total synthesis of obovatol involving the construction of the basic skeleton of the target molecule by the Ullman coupling reaction, and, for the first time, its evaluation as α-glucosidase and α-amylase inhibitor.

The last efforts were dedicated to the synthesis of oligomeric compounds inspired by the biphenyl compounds **1** and **2**. This thesis reports the optimization of the dimerization reaction conditions of honokiol to achieve houpulin B, an oligomeric compound of **2** with potential high biological activities. Still, only some studies are reported due to its low extraction yield [91]. Different synthetic approaches (chemical and enzymatic) are proposed, and the synthesis of two new oligomeric compounds based on magnolol-magnolol and magnolol-honokiol is

presented. The evaluation of the inhibition activities toward the digestive enzymes is also reported.

Chapter 3

Results and discussion

3.1 Synthesis of nitrogenated analogues inspired by magnolol and honokiol.

The synthesis of analogues of new compounds inspired by magnolol (**1**) and honokiol (**2**) (**Figure 7**) is an ongoing research activity of the Laboratory of Bioactive Natural Products. Different compounds have been synthesized and evaluated as promising α-glucosidase inhibitors [72] antioxidants [156] [157], anticancer activity as tankyrase inhibitors, [158]and, tumor cells growth [61]. In addition, ongoing evaluations are as promising agents against multi-drug resistance through down-regulation of ATP-binding cassette transporters (ABCG2) expression levels and prostate cancer therapeutics. This work aimed to optimize the synthetic strategy to obtain new neolignans with high yields and evaluate them as metabolic enzyme inhibitors (**Chapter 3**, **paragraph 3.5**).

For this reason, a library of nitrogenated biphenyls inspired by magnolol and honokiol was planned through Suzuki-Miyaura (SM) cross-coupling reaction. Obtaining high-yielding biphenyl structures inspired by natural products is one of the key topics for synthetic chemistry; moreover, up to date, few structures bearing amino and nitro groups have been reported with a biphenyl scaffold, while some previous findings on bioactive compounds bearing those functional groups which were potent lipase inhibitors [151].

Scheme 6 shows the synthetic strategy designed to yield new nitrogenated neolignans. The synthetic strategy is based on four steps. Specifically, the first step involves the borylation of phenol to synthesize arylboronate; the second, the use of SM cross-coupling reaction to afford new biphenyl compounds; the subsequent two steps, to insert the allyl chain onto the biphenyl core through allylation reaction, followed by a Claisen rearrangement.

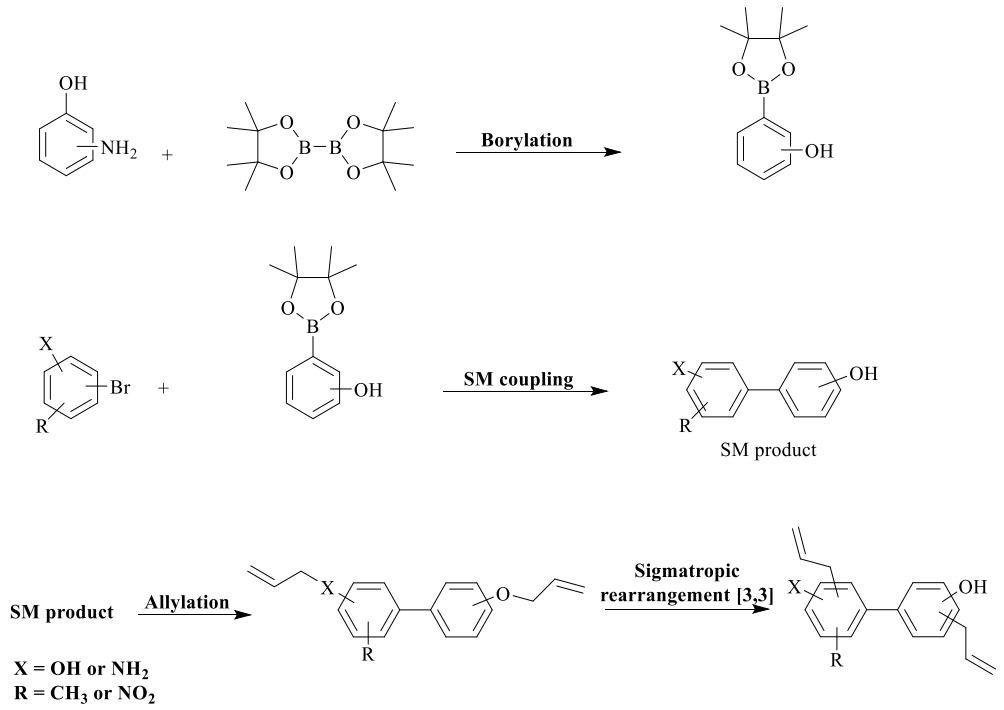

Scheme 6. Synthetic strategy proposed to achieve biphenyl inspired by **1** and **2**.

Borylation reaction

The first step of the procedure reported here is the borylation of arylamines to get pinacol boronic esters. Aryl boronic acids and boronates are useful building blocks in transition-metal-catalyzed cross-coupling reactions due to their low toxicity and high stability. In 2014, Wang *et al.* [159] reported a Sandmeyer-type borylation of arylamines by direct conversion of the amino group of aniline derivatives into the boronate group. The reaction occurs at room temperature with sodium nitrite and hydrochloric acid as diazotization agent, and the subsequent addition of bis(pinacolato)diboron (pin_2B_2), affording pinacol boronic esters with high yields. The two steps of the borylation reaction are reported in **Scheme 7**.

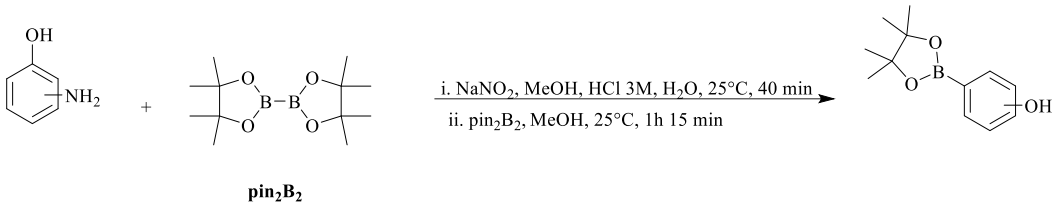

Scheme 7. Borylation reaction of aminophenol

Two pinacol boronic esters compounds were synthesized (**Figure 17**): 4 -(4,4,5,5-tetramethyl-1,3,2-dioxaborolan-2-yl) phenol (**4a**) and 2 -(4,4,5,5-tetramethyl-1,3,2-dioxaborolan-2-yl) phenol (**4b**). An overview of the experimental conditions and the spectroscopic characterization by mass spectrometry and ^{1}HNMR are reported in the **Chapter 5** (**paragraph 5.2**). Experimental data are reported in Supplementary materials (**Figure S1 - 4)** at the following link:
https://drive.google.com/file/d/1OxXuw5qQ0mIGLRJQivSZsiDnba253SV7/view?usp=sharing

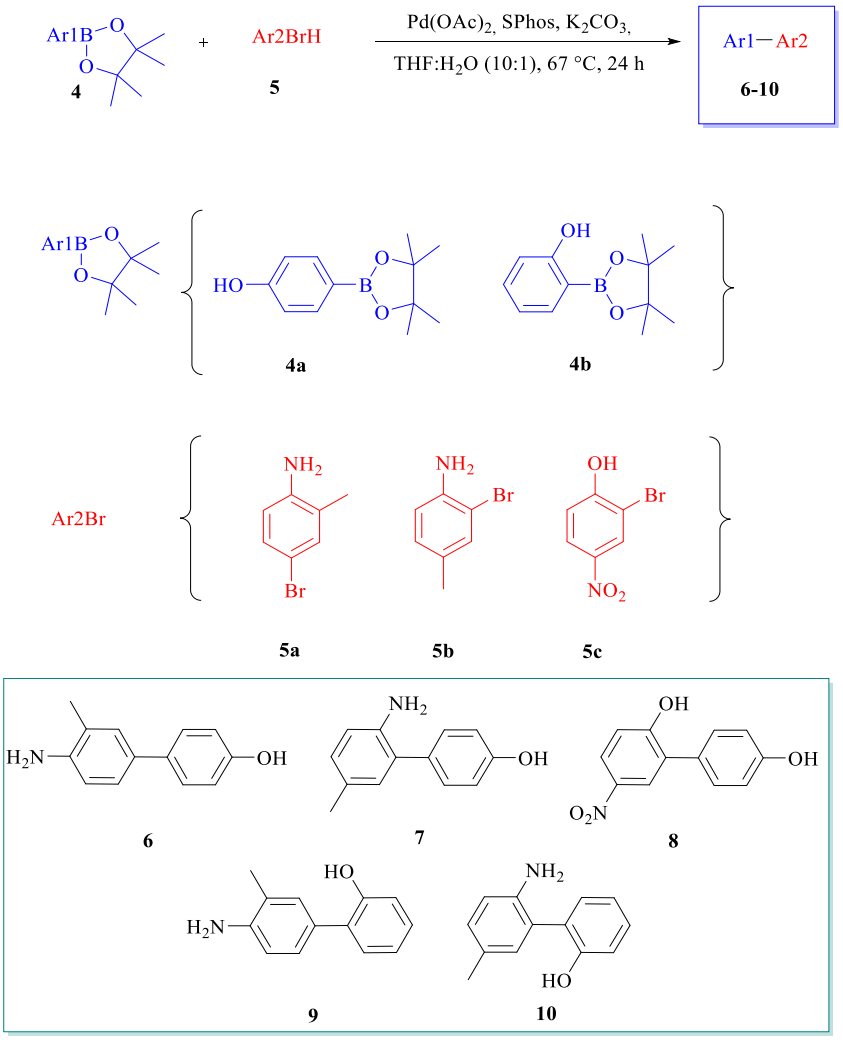

Figure 17. Synthesis of biphenyls **6** − **10**.

Suzuki-Miyaura cross-coupling reaction

The Suzuki-Miyaura coupling is a well-established and powerful tool for the construction of biaryl scaffolds [160] due to its efficiency and the innocuous character of the boron derivatives that are environmentally safer than other organometallic reagents. This is a reaction between aryl boronate and aryl halide

(substrate) in the presence of a catalyst, usually a palladium complex, a ligand, and a base.

Selected experiments for SM reaction were performed to optimize the reaction conditions employing 4- bromo- 2- methylaniline (**5a**) and pinacol boronic ester (**4a**) as model compounds using a Pd-based catalyst with several ligands and solvents reported in **Table 2**. $Pd(PPh_3)_4$ was used as a catalyst, and $Pd(OAc)_2$ as a precatalyst with 1'-bis(biphenylphosphino)ferrocene (Dppf) or 2 dicyclohexyl(2′,6′-dimethoxy[1,1′-biphenyl]-2-yl)phosphine (SPhos) as ligands to obtain the active form *in situ*. As reported in **Table 2,** the amount of catalyst and ligand varied respect to the molar percentage of aryl halide, using the ligand in molar percentage twice the catalyst. Based on the finding, traditional SM reaction conditions, including the use of $Pd(PPh_3)_4$ or $Pd(OAc)_2$ /Dppf, yielded unsatisfactory outcomes when applied to **5a**. Compound **6** was achieved with only 10% yield under the reaction condition reported in entry 3 (see **Table 2**). These findings suggest that this ligand-catalyst system, commonly used with aryl halides and boronic acids, may not be efficient when substituted aryl halide reacts with boronic acid pinacol esters, as indicated by Reizman *et al.* [161]. On the contrary, using SPhos combined with palladium precatalyst proved to be more effective in the synthesis of **6**. Compound **6** was thus achieved with yields from 25.2% and 33.6% (entries 5 and 7, **Table 2**) when the reaction was conducted in THF rather than toluene. Moreover, the yield was significantly improved from 33.6 to 98% (entries 7 and 8, **Table 2**) when a mixture of THF and H_2O (10:1) was employed. According to Altman *et al*. [162], SPhos generates a highly active and stable catalyst system, justifying the results. The SPhos-based catalyst promotes the reaction of electron-rich aryl halides with excellent yield (>90%) and enables the synthesis of highly hindered biaryl with *ortho*, *ortho*'- substituents [163]. Other experiments were performed to decrease the amount of precatalyst and ligand (see entries 9 and 10, **Table 2**). The reduction of the catalyst amount does not negatively impact reaction yield, providing the biphenyl with almost a quantitative

yield, even if with a longer reaction time. Based on these data, the reaction conditions reported in the entry 10 were used to synthesized other compounds modifying the aryl bromide (**5a** – **5c**) and arylboronate (**4a** and **4b**), favoring longer reaction times over higher catalyst loading. The new biphenyls **6** – **9** were obtained with a 70–97% yield, while the biphenyl **10**, previously reported in the literature by Cho *et al.* [164] was achieved herein with a yield of 65%. The synthesized neolignans are reported in **Figure 18**. An overview of the experimental conditions and the spectroscopic characterization by mass spectrometry, ^{1}H NMR, ^{13}C NMR and 2D NMR are reported in the **Chapter 5** (**paragraph 5.2**). Experimental data are reported in Supplementary materials (**Figure S5 - 30)** at the following link:
https://drive.google.com/file/d/1OxXuw5qQ0mIGLRJQivSZsiDnba253SV7/view?usp=sharing

Table 2. Substrate scope of SM cross-coupling of **4a** with **5a**.

Entry	Cat	mol%[a]	L	mol%[a]	Solvent	T (°C)	Time	%yield[b]
1	$Pd(PPh_3)_4$	8	-	-	THF	67	24h	0
2	$Pd(OAc)_2$	5	Dppf	15	THF-H_2O[e]	67	24h	0
3	$Pd(OAc)_2$	10	Dppf	30	THF-H_2O[e]	67	24h	10*c*
4	$Pd(OAc)_2$	1	SPhos	2	Toluene[d]	80	22h	8
5	$Pd(OAc)_2$	1	SPhos	2	THF	67	22h	25.2
6	$Pd(OAc)_2$	10	SPhos	20	Toluene[d]	80	22h	15
7	$Pd(OAc)_2$	10	SPhos	20	THF	67	22h	33.6
8	$Pd(OAc)_2$	10	SPhos	20	THF-H_2O[e]	67	3h	98
9	$Pd(OAc)_2$	5	SPhos	10	THF-H_2O[e]	67	5h	96.4
10	$Pd(OAc)_2$	1	SPhos	2	THF-H_2O[e]	67	24h	98.7

[a] referred to aryl halide **5a**; [b] determined by HPLC-UV quantification (see experimental section); [c]determined after column chromatography (see experimental section); [d] toluene dry; [e] THF-H_2O (10:1). Cat: catalyst, L: Ligand.

Allylation reaction

The various properties of honokiol and magnolol are attributable to hydroxyl and allyl groups on the biphenyl-based structure [73, 165-167]. The synthesized biphenyl analogues (**6** – **10**) were functionalized through a nucleophilic substitution to insert the allyl chains (**Scheme 8**). The reaction occurs in the presence of allyl bromide and base at 56°C temperature.

Allyl derivatives with one or two chains bound to the nitrogen were obtained from the allylation reaction as a result of the high reactivity of the amino group. Ten allylated derivatives (**11a** – **15**) were obtained with 9.2 to 82.6% yield (**Scheme 8**). An overview of the experimental conditions and the spectroscopic characterization by mass spectrometry, ^{1}H NMR, ^{13}C NMR, and 2D NMR are reported in **Chapter 5** (**paragraph 5.2**). Experimental data are reported in Supplementary materials (**Figure S31 - 90)** at the following link: https://drive.google.com/file/d/1OxXuw5qQ0mIGLRJQivSZsiDnba253SV7/view?usp=sharing

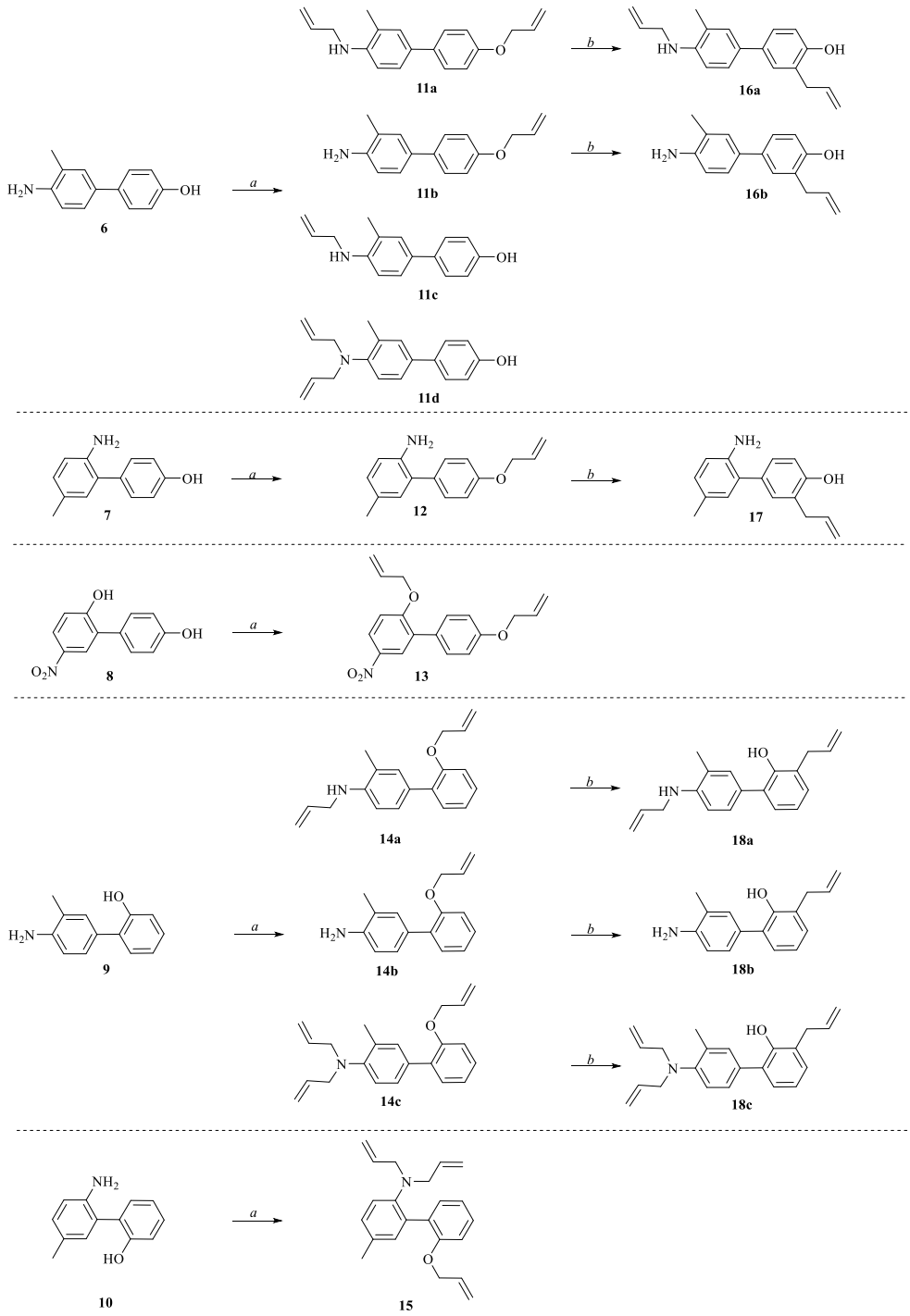

Scheme 8. Synthesis of biphenyls **11a** – **18c**. *a)* dry acetone, K_2CO_3, allyl bromide, 56 °C. *b*) dry CH_2Cl_2, 1M $(Et)_2AlCl$ (in dry *n*-hexane), room temperature.

Claisen rearrangement reaction

The last step of the synthetic route consists of a Claisen reaction to rearrange the allyl chains on the two rings in the *ortho* position to the hydroxyl group. This reaction occurred in mild reaction conditions with diethyl aluminum chloride as Lewis's acid to allow a complex ether-aluminum to speed up the reaction, promote the rearrangement and work at room temperature to avoid the high temperature commonly used [168]. These conditions efficiently rearranged the *O*-allyl chains of allyl derivatives except for compounds **13** and **15** and all *N*-allyl chains. A total of six derivatives (**16a** – **18c**) were obtained with yield of 25-72% (**Scheme 8**). An overview of the experimental conditions and the spectroscopic characterization by mass spectrometry, ^{1}H NMR, ^{13}C NMR and 2D NMR are reported in the **Chapter 5** (**paragraph 5.2**). Experimental data are reported in Supplementary materials (**Figure S91 - 126)** at the following link: https://drive.google.com/file/d/1OxXuw5qQ0mIGLRJQivSZsiDnba253SV7/view?usp=sharing

Commonly described reaction conditions for the Aza-Cope rearrangement of *N*-allyl anilines [169-171] were employed on the *N*-allyl derivative **11c**. The reaction scheme (**Scheme 9**) outlines the different reaction conditions employed, and an overview of the experimental conditions is reported in the **Chapter 5** (**paragraph 5.2**).

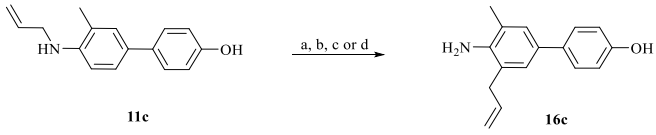

11c **16c**

Scheme 9. Synthesis of **16c**. *a)* dry CH_2Cl_2, 1M Et_2AlCl (*n*-hexane; 2 eq.), room temperature, 24h. *b*) dry CH_2Cl_2, 1M Et_2AlCl (*n*-hexane; 2 eq), 40°C, 24h. *c*) xylene, BF_3*$O(Et)_2$ (≥ 46.5%, 1 eq.), room temperature, 24 h. *d*) dry THF or dry CH_3CN or dry CH_2Cl_2, $H_3PMo_{12}O_{40}$ (20%mol), room temperature, 24 h.

However, the Aza-Cope rearrangement proved unsuccessful. Moreover, the approach of introducing *C*-allyl chains through the SM reaction before achieving the biphenyl scaffold was discarded due to palladium-induced isomerization of the double bond, resulting in the formation of a difficult-to-purify complex mixture of *cis* and *trans* isomers [172].

By employing this optimized synthetic strategy, it was possible to synthesize twenty-one nitrogenated analogues inspired by the natural product **1** and **2**, of which only one is reported in the literature. The evaluation of their inhibitory activity towards metabolic enzyme is reported in **Section 3.5**.

3.2 Synthesis of obovatol and its analogues

The synthesis of obovatol (**3**) and its analogues was successfully conducted at the Institut des Sciences Moléculaires at the University of Bordeaux during my visiting period.

*First retrosynthetic approach of **3**.*

The first attempt to obtain **3** was based on a retrosynthesis (**Scheme 10**) developed from the commercially available pyrogallol (**19**). The key precursor **24** serves as a pretarget molecule and could be prepared through Ullmann coupling reaction of aryl halide **23** and phenol **22**. Phenolic building block **22** could be obtained from the commercially available pyrogallol **19** through several steps: allylation reaction, Claisen-Cope rearrangement, followed by methylation reaction.

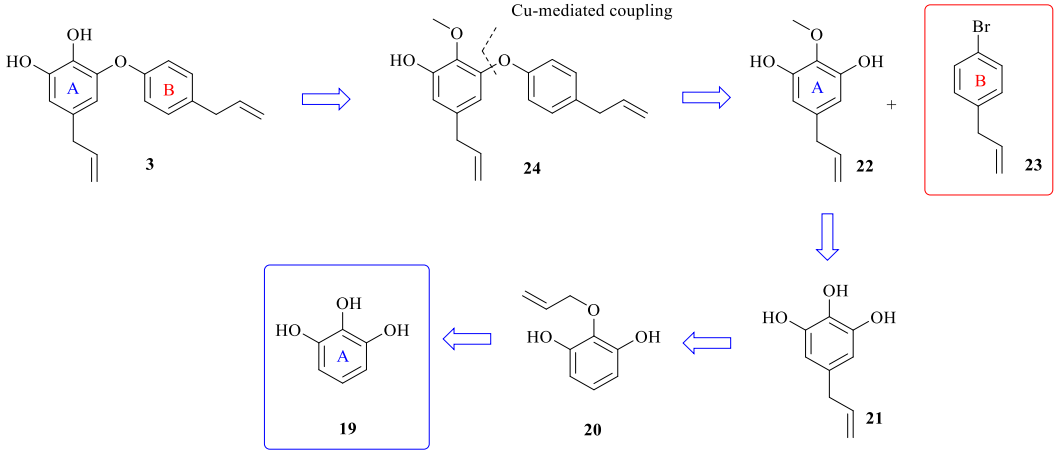

Scheme 10. First retrosynthetic analysis of obovatol.

To that purpose, the synthesis of **3** was achieved in five steps: i) allylation reaction to insert the allyl chain onto the biaryl ether scaffold; ii) Claisen rearrangement; iii) methylation reaction; iv) the Ullmann coupling reaction to

construct biaryl ether core; iv) demethylation reaction to give the desired molecule.

Allylation reaction

The synthesis begins with the preparation of the requisite *O*-allyl derivative through a nucleophilic substitution employing the commercially available pyrogallol (**19**) as the starting material. This reaction occurs in the presence of allyl bromide and base at 56°C. Preliminary experiments for allylation reactions have been performed to optimize the reaction yield by modifying the base and allyl bromide. **Table 3** describes the different reaction conditions evaluated. In detail, the mole of base and allyl bromide was varied respectively from 2 equivalents to 1, and from 1 equivalent to 1.4, with respect to pyrogallol to achieve an increase from 25 to 65% yield. The reaction detail is reported in **Scheme 11**.

Table 3. Optimization of reaction conditions for allylation reaction.

Entry	K_2CO_3(eq.)	Allylbromide(eq.)	Time	%Yield (5)
1	2	1	3h	25
2	1	1	2h	53
3	0.5 + 0.5 *	1	4h	35
4	1	1.25	6h	63
5	1	1.4	6h	65

*The second addition was carried out after 2 h due to the presence of unreacted pyrogallol

The most promising reaction condition is reported in the entry 5 where the use of an excess of allyl bromide and one equivalent of the base allows to obtain the desired 2 -(allyloxy) benzene-1,3-diol (**20**) with a higher yield in a shorter time. An overview of the experimental conditions is reported in the **Chapter 5** (**paragraph 5.3**).

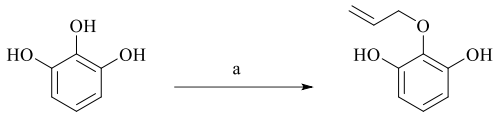

19 **20**

Scheme 11. Synthesis of **19**. *a)* dry acetone, K_2CO_3 (1 eq.), allyl bromide (1.4 eq.), 6h, 56 °C.

Claisen-Cope rearrangement

The synthesized *O*-allyl derivative **20** was subjected to a [3,3] sigmatropic reaction to rearrange the allyl chain on the aromatic ring. The thermal [3,3] sigmatropic reaction, involving the Claisen rearrangement of a substituted allyl aryl ether, typically yields an *ortho*-dienone species, which can then easily enolized to give an *ortho*-allylphenol system. However, when the rearrangement process occurs at an *ortho* position already bearing a substituent, a concomitant Cope rearrangement process can take place when it is followed by an enolization leading to a formation of a *para*-allylphenol species [173]. **Scheme 12** reports an example of Claisen rearrangement processes for allyl aryl ethers.

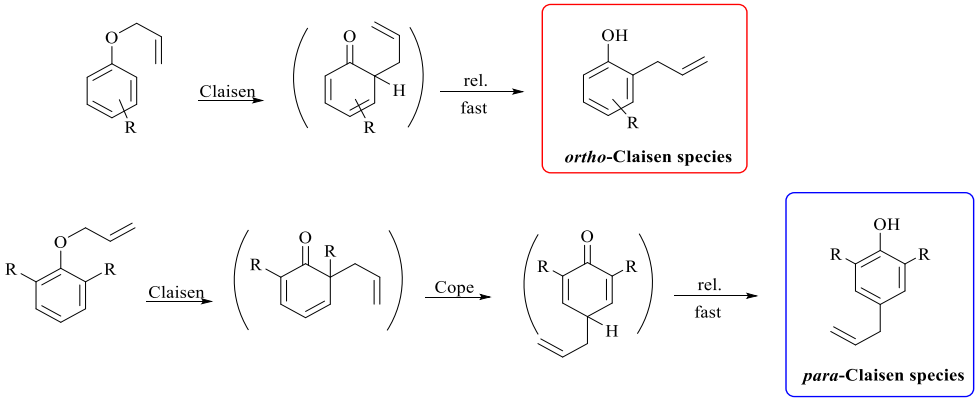

Scheme 12. Claisen-Cope rearrangement reaction.

The synthesized compound (**20**) presents a substituent (hydroxyl group) in *ortho,* thus leading to a Claisen-Cope reaction with a rearrangement of the allyl chain in *para* position. **Scheme 13** reports the Claisen-Cope rearrangement reaction detail.

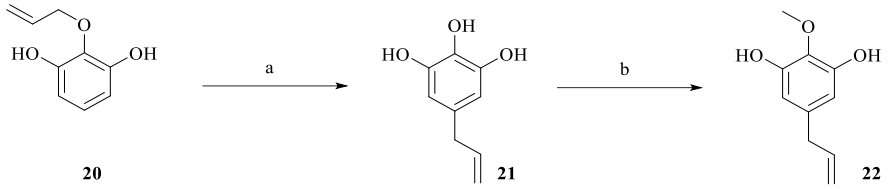

20 **21** **22**

Scheme 13. Synthesis of **21** and **22**. *a)* dry CH_2Cl_2, 1M $(Et)_2AlCl$ (in dry *n*-hexane, 2 eq.), 3h, room temperature. *b*) DMF, K_2CO_3 (2 eq.), CH_3I (1.5 eq.), 4h, room temperature.

An overview of the experimental conditions is reported in the **Chapter 5** (**paragraph 5.3**).

Methylation reaction

The synthesis of any phenol-containing product requires the protection of the hydroxyl group to prevent reaction with oxidizing agents and electrophiles or reaction of the nucleophilic phenoxide ion with even mild alkylating and acylating agents. Ethers are the most widely used phenol protective groups [174, 175]. This third step of the synthetic strategy is the protection of the hydroxyl group in *para* position with respect to the allylic chain. This was achieved thanks to the higher reactivity of OH in *para* position than the other two in *ortho* and using 1.5 equivalent of iodomethane. This reaction occurs in the presence of dimethylformamide as a solvent and potassium carbonate as a base at room temperature. **Scheme 13** reports the methylation reaction detail. An overview of the experimental conditions is reported in the **Chapter 5** (**paragraph 5.3**).

Ullmann coupling reaction

Copper-catalyzed arylation of nucleophiles, known as Ullmann condensation, is well known as one the most useful and practical methods in the formation of aryl ether block. This reaction has been carried out in the presence of an efficient copper/ligand systems allowing the use of catalytic amounts of metal under mild conditions. In detail, the coupling reaction took place using copper (I) iodide as a catalyst, *N, N*- dimethylglycine hydrochloride as ligand, 1-allyl-4 bromobenzene as aryl halide (**23**), phenol **22** and in the presence of base and solvent. **Scheme 14** reports the Ullmann coupling reaction. **Table 4** reports the different reaction conditions used to synthesize the desired coupling product varying the solvent, the temperature and the %mol of catalyst and ligand.

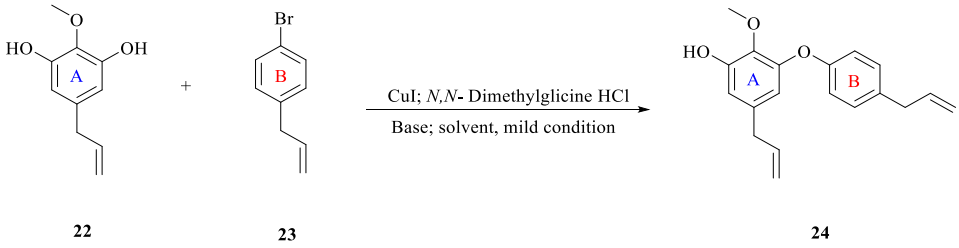

22 **23** **24**

Scheme 14. The Ullmann condensation of compounds **22** and **23** for the synthesis of **24**.

Table 4. Reaction conditions evaluated for the coupling reaction.

Entry	Catalyst	%mol	Ligand	%mol	Solvent	T (°C)	Time (h)	% Yield
1	CuI	5	*N, N*-Dimethylglycine hydrochloride	15	DMA	90	48	0
2	CuI	1.5	*N, N*-Dimethylglycine hydrochloride	5	DMF	135	24	0
3	CuI	10	*N, N*-Dimethylglycine hydrochloride	30	Dioxane	90	48	0
4	CuI	20	*N, N*-Dimethylglycine hydrochloride	60	Dioxane	90	48	0

Unfortunately, no attempts allowed the synthesis of aryl ether skeleton. Despite a careful study of the literature, it was impossible to obtain the desired product.

*Second retrosynthetic approach of **3**.*

For this reason, the synthetic strategy was revised, modifying the starting substrate of ring A and thus employing the commercial 3-bromobenezene-1,2 diol (**25**) as starting material. The retrosynthetic approach based on the previously described five steps, starting from **25**, is reported in **Scheme 15**.

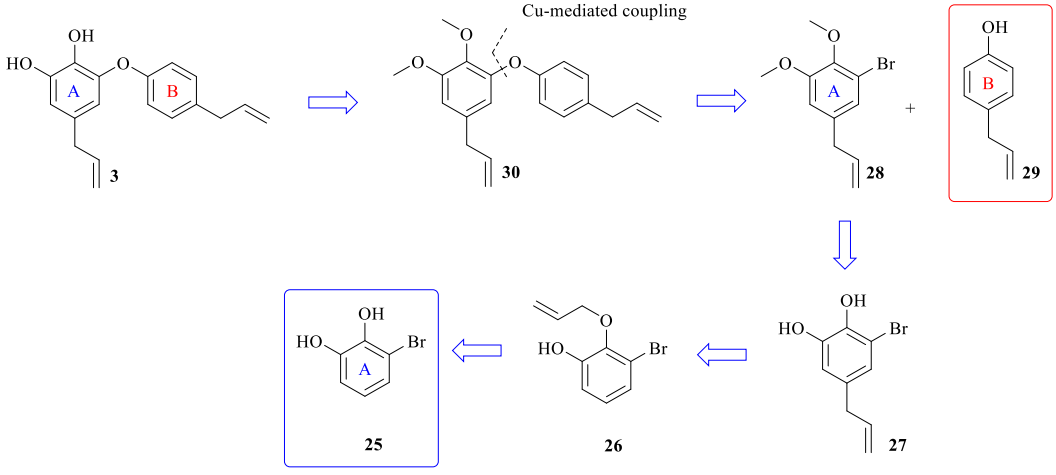

Scheme 15. Second retrosynthetic analysis of obovatol.

To that purpose, the synthesis of **3** was achieved by employing the optimized reaction condition previously reported, in the presence of allyl bromine. The desired *O*-allyl derivative (**26**) was achieved with a 65% yield, and subsequently, it was subjected to a Claisen-Cope reaction. The desired Claisen-Cope product (**27**) was obtained with 80% yield. An overview of the experimental conditions and the spectroscopic characterization by mass spectrometry, ^{1}H NMR ^{13}C NMR, and 2D NMR, are reported in the **Chapter 5** (**paragraph 5.3**). Experimental data are reported in Supplementary materials (**Figure S137 - 141)** at the following link:
https://drive.google.com/file/d/1OxXuw5qQ0mIGLRJQivSZsiDnba253SV7/view?usp=sharing

The third step is the methylation reaction on **27** to afford the required precursor **28** for the subsequent biaryl ether coupling. The reaction occurs in the presence of iodomethane, dimethylformamide as a solvent, and potassium carbonate as a base at room temperature. Compared to the experimental conditions previously reported, a different amount (3 equivalent) of iodomethane was used and **28** was achieved with 70% yield. **Scheme 16** reports, in detail, the three-step reaction.

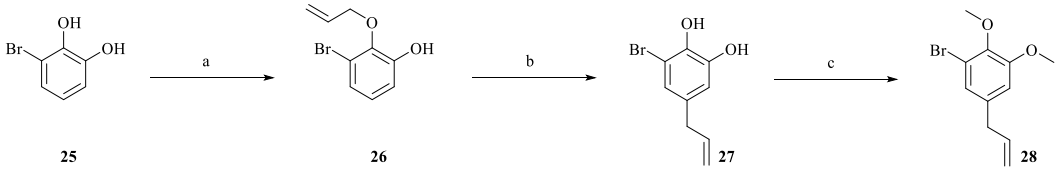

Scheme 16. Synthesis of **26**, **27**, and **28**. *a)* dry acetone, K_2CO_3 (1 eq.), allyl bromide (1.4 eq.), 6h, 56 °C. *b*) dry CH_2Cl_2, 1M $(Et)_2AlCl$ (in dry *n*-hexane, 2 eq.), 3h, room temperature. *c*) DMF, K_2CO_3 (2 eq.), CH_3I (3 eq.), 4h, room temperature.

An overview of the experimental conditions and the spectroscopic characterization by mass, ^{1}H NMR, and ^{13}C NMR are reported in the **Chapter 5**

(**paragraph 5.3**). Experimental data are reported in Supplementary materials (**Figure S142 - 143)** at the following link: https://drive.google.com/file/d/1OxXuw5qQ0mIGLRJQivSZsiDnba253SV7/view?usp=sharing

The key precursor **30** was prepared through the Ullmann coupling reaction of aryl halide **28** and *para*-allyl phenol **29**. The reaction was conducted following the reaction conditions reported in entry 3 of **Table 4**. The coupling product **30**, obtained with 52% yield, was subjected to deprotection of phenol groups to achieve to achieve the expected natural product **3**. Precisely, the demethylation reaction occurred with boron tribromide BBr_3 with an 84% yield. The total synthesis of **3** was achieved with an overall 15% yield. **Scheme 17** reports, in detail, the Ullman coupling and demethylation reaction.

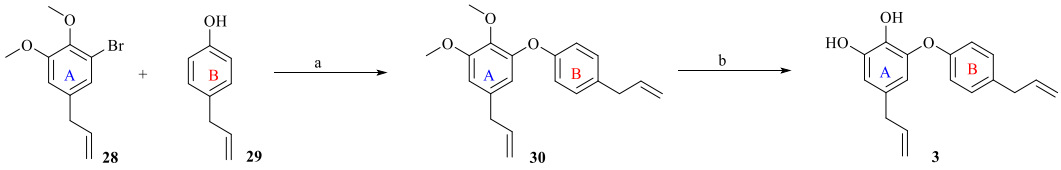

Scheme 17. Synthesis of **30** and **3**. *a)* dioxane, Cs_2CO_3 (2 eq.), *para*-allyl phenol (1.5 eq.), CuI (10 mol%), *N*, *N*-dimethylglycine HCl (30 mol%), 52h, 90 °C. *b*) dry CH_2Cl_2, BBr_3 (1M in DCM, 2 eq.), 3h, -78 °C.

An overview of the experimental conditions and the spectroscopic characterization by, ^{1}H NMR, and ^{13}C NMR and IR are reported in the **Chapter 5** (**paragraph 5.3**). Experimental data are reported in Supplementary materials (**Figure S144 - 147)** at the following link: https://drive.google.com/file/d/1OxXuw5qQ0mIGLRJQivSZsiDnba253SV7/view?usp=sharing

*Third retrosynthetic approach of **3***

Further, synthetic attempts were employed to increase the reaction yield, decrease the number of steps and reagents. A new route was planned to allow the total synthesis of the desired natural product **3** (**Scheme 18**).

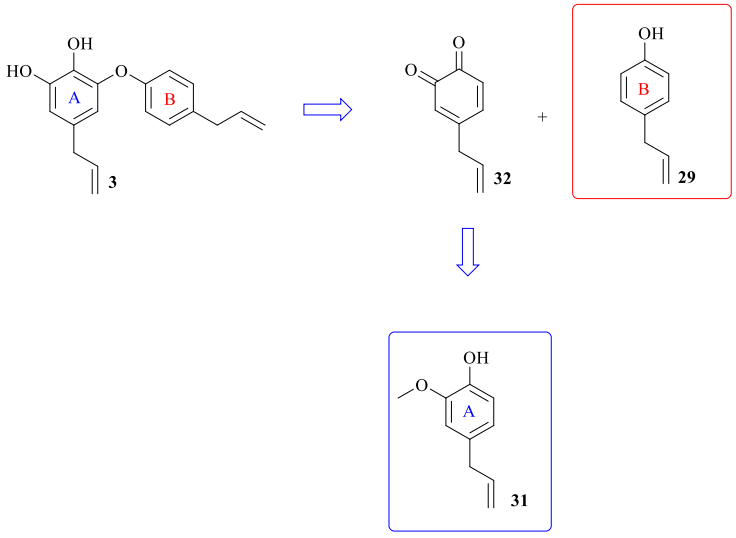

Scheme 18. *One-pot* retrosynthetic analysis of obovatol.

The synthesis of intermediate **32** was achieved by the reaction of commercially available eugenol (**31**) with a "stabilized" form of 2-iodoxybenzoin (SIBX), a nonexplosive oxidant that is more sustainable and safer than IBX [176]. The SIBX is a white-powder formulation composed of a mixture of benzoic acid (22%), isophthalic acid (29%), and o-iodoxybenzoic acid (49%). The structures are reported in **Figure 18**.

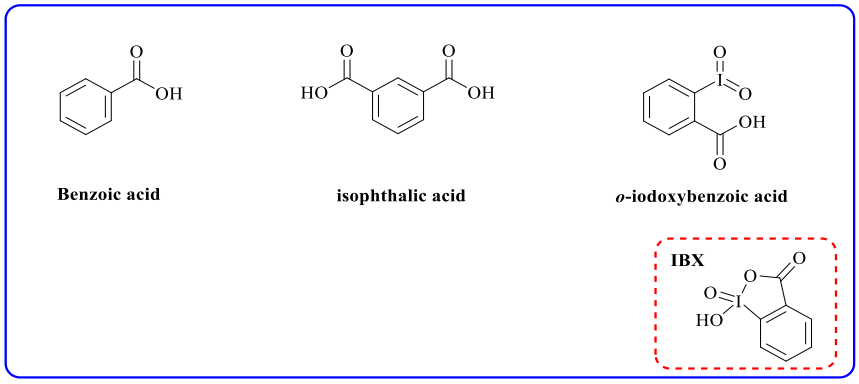

Figure 18. SIBX component's structure.

Scheme 19 reports the mechanism for the IBX-mediated regioselective hydroxylation of eugenol. According to the literature, **31** adds to the iodine(V) center of IBX to form a λ5 - iodanil intermediate, subsequently leading to a more stable λ3 -iodanil intermediate, for which the tautomeric form is hydrolyzed to give the ortho-quinone and 2-iodobenzoic acid (IBA). The final reductive step affords catechol **33** [176].

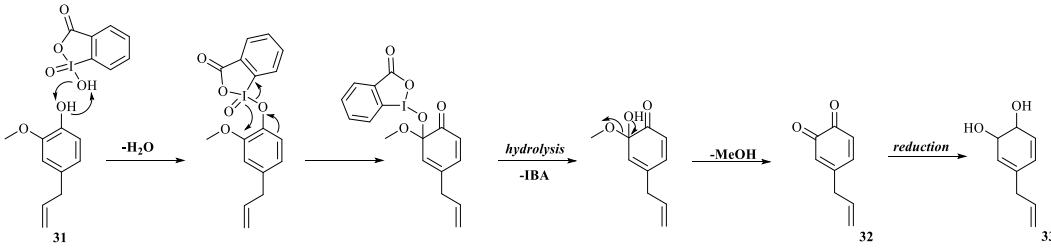

Scheme 19. Mechanistic description of IBX-mediated demethylation of eugenol.

The synthesized intermediate o*rtho*-quinone **33** was involved *in situ* in 1,6 a Michael-type addition of *para*-allyl phenol **29** in order to synthesize the biaryl ether skeleton. **Scheme 20** reports the *one-pot* reaction conditions for the synthesis of **3**. The reaction occurred with two equivalents of SIBX in THF at room temperature for 16 hours, followed by the addition of **29**. Unfortunately, it was

impossible to achieve obovatol due to the low nucleophilicity of *para*-allylphenol. Several attempts were thus evaluated for *one-pot* synthesis of **3**:

a) presence of $NaHCO_3$ (6 eq.) to quench the carboxyl group of the benzoic acid and isophthalic acid present in SIBX.

b) phenate ion generated separately using NaH (1.2 eq.) in THF at 0°C.

c) phenate ion generated separately using a mixture of NaH (1.2 eq.) and corona ether 15/5 (1 eq.) under the same reaction condition.

Unfortunately, all the synthetic approaches were unsuccessful. However, the *one-pot* strategy was exploited to synthesize new obovatol analogues using a benzenethiol, a nucleophile stronger than phenol (compounds **47** and **48**, see below).

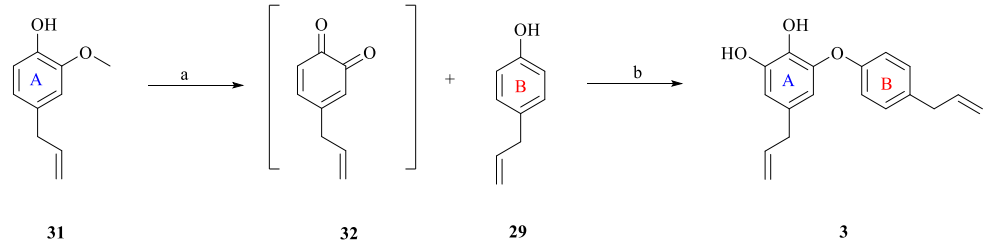

Scheme 20. Synthesis of analogues **3**. *a)* dry THF, SIBX (2.15 eq.), 16h, room temperature. *b)* *para*-allylphenol (3 eq,), dry 1-2h, room temperature.

Synthesis of obovatol analogues

The synthetic strategy reported has contributed to developing analogues. Two new analogues (**34** and **35**) were achieved by modifying the condition of the demethylation reaction. Compound **34** was obtained from **30**, decreasing the equivalents of BBr_3 (1 eq. solution 1M in CH_2Cl_2.) with an overall 18% yield. Conversely, the **35** was obtained by employing a single equivalent of BBr_3 (solution 1M in CH_2Cl_2) and stirring the reaction mixture for 30 min at -78° C, then allowing the reaction mixture to warm at room temperature and stirring for

2h. Compound **35** was achieved with 10% overall yield. **Scheme 21** reports, in detail, the new demethylation reaction conditions.

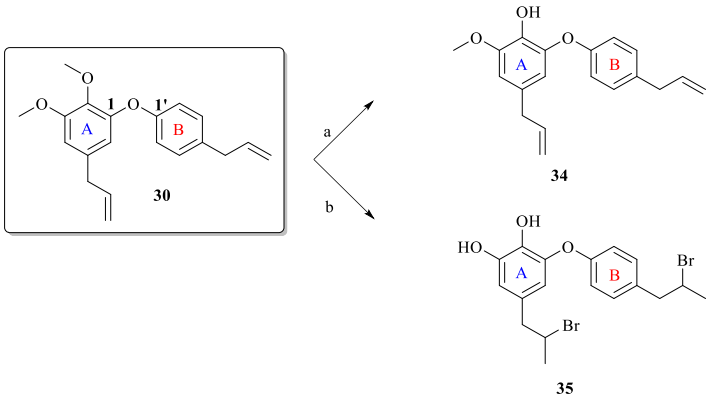

Scheme 21. Synthesis of analogues **34** - **35**. *a)* dry CH_2Cl_2, BBr_3 (1M in DCM, 1 eq.), 2h, -78 °C. *b)* dry CH_2Cl_2, BBr_3 (1M in DCM, 1 eq.), 30 min, -78 °C, room temperature, 2h.

An overview of the experimental conditions the spectroscopic characterization by, ^{1}H NMR, ^{13}C NMR and 2DNMR and IR are reported in the **Chapter 5** (**paragraph 5.3**). Experimental data are reported in Supplementary materials (**Figure S148 - 152)** at the following link: https://drive.google.com/file/d/1OxXuw5qQ0mIGLRJQivSZsiDnba253SV7/view?usp=sharing

The Ullmann coupling reaction and the subsequent demethylation reaction were also employed to obtain a variety of obovatol analogues. As depicted in **Scheme 22**, Ullmann condensation of eugenol (**31**) with 1-allyl-4-bromobenzene (**23**), 2-bromo-4-methoxyphenyl acetic acid (**38**) and 4-bromobenzoylchloride (**40**) gave obovatol analogues **36**, **39** and **41**, respectively with 94, 40 and 20% yield. The commercially available 5-bromo-2-methoxybenbenaldehyde (**42**) has been initially subjected to a methylation reaction to obtain the corresponding methylated compound (**43**) [177]. *Para*-allyl phenol (**29**) reacted with **43** to give **44** with 52% yield. Finally, demethylation of **36** afforded the analogue **37**

quantitatively. An overview of the experimental conditions and the spectroscopic characterization by mass, ^{1}H NMR, and ^{13}C NMR and IR are reported in the **Chapter 5** (**paragraph 5.3**). Experimental data are reported in Supplementary materials (**Figure S153 - 163)** at the following link: https://drive.google.com/file/d/1OxXuw5qQ0mIGLRJQivSZsiDnba253SV7/view?usp=sharing

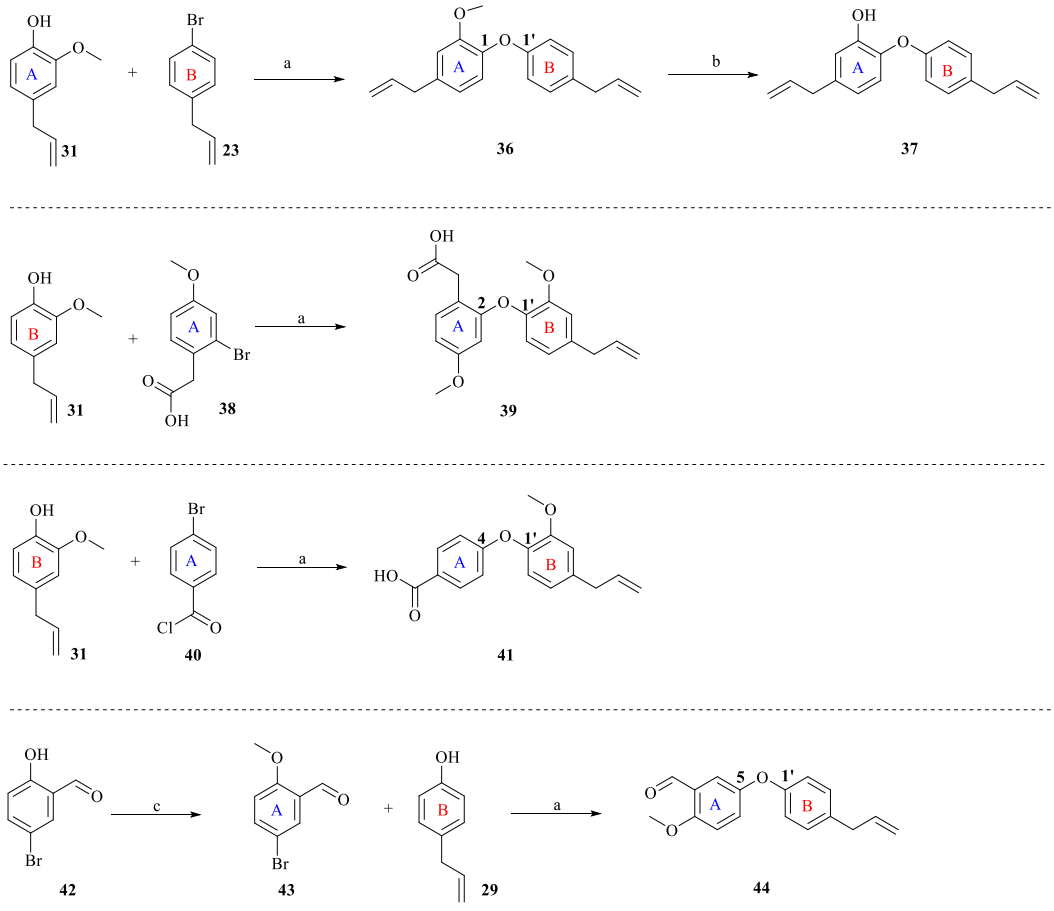

Scheme 22. Synthesis of analogues **36**, **37**, **39**, **41** and **44**. *a)* dioxane, Cs_2CO_3 (2 eq.), phenol (1.5 eq.), CuI (10 mol%), *N*, *N*-dimethylglycine HCl (30 mol%), 24h, 90 °C. *b)* dry CH_2Cl_2, BBr_3 (1M in DCM, 1 eq.), 3h, -78 °C. *c*) DMF, K_2CO_3 (3 eq.), CH_3I (3 eq.), overnight, room temperature.

The *one-pot* approach previously described was applied to synthesize two novel thioether analogues. **Scheme 23** reports, in detail, the *one-pot* reaction conditions for the synthesis of thioether analogues, using the IBX reaction to give the o*rtho*-quinone **32** that was involved *in situ* in 1,6 a Michael-type addition of benzenethiols **45** and **46** to give respectively **47** and **48** with 45 and 35% yield. An overview of the experimental conditions and the spectroscopic characterization by mass, ^{1}H NMR and, ^{13}C NMR and IR are reported in the **Chapter 5** (**paragraph 5.3**). Experimental data are reported in Supplementary materials (**Figure S164 - 167)** at the following link:
https://drive.google.com/file/d/1OxXuw5qQ0mIGLRJQivSZsiDnba253SV7/view?usp=sharing

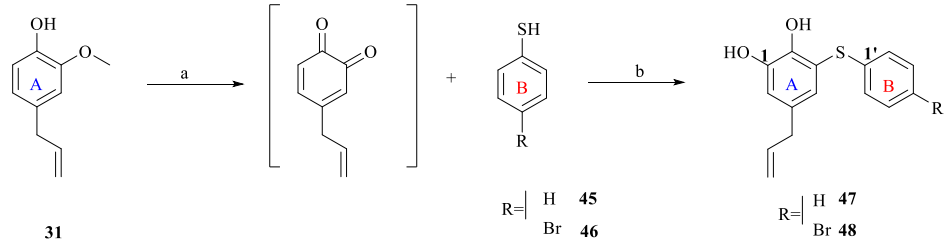

Scheme 23. Synthesis of analogues **47 - 48**. *a)* dry THF, SIBX (2.15 eq.), 16h, room temperature. *b)* thiol (3 eq,), dry 1-2h, room temperature.

It was also interesting to synthesize the corresponding obovatol sulfide (**50**), using compound **48** as an intermediate. The planned synthetic route involved inserting an allyl chain in the aromatic ring B through a Suzuki-Miyaura cross-coupling reaction. The SM reaction was performed employing compounds **48** and allyl boronic acid pinacol ester (**49**) as starting materials, in the presence of palladium acetate as a catalyst and either SPhos or dppf as ligands (see **Table 1**, entries 3 and 10). In detail, **Scheme 24** reports the Suzuki-Miyaura reaction conditions for the synthesis of obovatol sulfide. However, all attempts to achieve

the desired product **50** were unsuccessful. An overview of the experimental conditions is reported in the **Chapter 5** (**paragraph 5.3**)

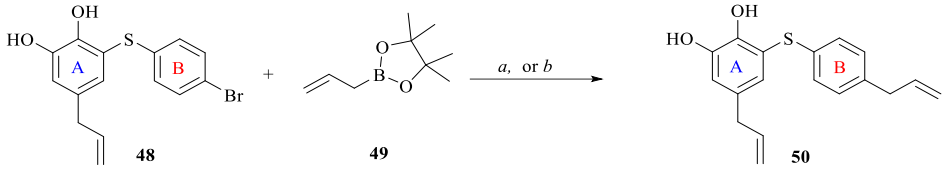

Scheme 24. Synthesis of analogues **50**. *a)* $Pd(OAc)_2$ (10%mol), dppf (30%mol), K_2CO_3 (5 eq), allyl boronic acid pinacol ester (1.5 eq.), THF:H_2O (10:1), 67°C, 24h.*b)* $Pd(OAc)_2$ (1%mol), SPhos(2%mol), K_2CO_3 (2 eq), allyl boronic acid pinacol ester (1.5 eq.), THF:H_2O (10:1), 67°C, 24h.

3.3 Synthesis of oligomeric compounds

Magnolia species also contain oligomeric compounds in addition to biphenyl and biaryl ether compounds (**Figure 8**). Their extraction yields are quite low and require several purification steps. Recent studies have been dedicated to evaluating the biological activities of some oligomers and today, the main challenge is developing synthetic strategy to increase their biological studies.

Thus, the optimization of the dimerization reaction conditions of honokiol to synthesize houpulin B, an oligomeric compound of **2**, was achieved following different synthetic approaches. Moreover, the synthesis of two new oligomeric compounds based on magnolol-magnolol and magnolol-honokiol was proposed as well. The evaluation of the inhibition activities toward the metabolic enzymes is also reported in **Chapter 3** (**paragraph 3.7**).

The strategy employed for the synthesis of houpulin B (**52**) was based on retrosynthesis reported in **Scheme 25**. The key precursor **51** serves as a pretarget molecule and could be prepared through phenol oxidation. The intermediate **51** could be subjected to free radical coupling to achieve the desired natural product.

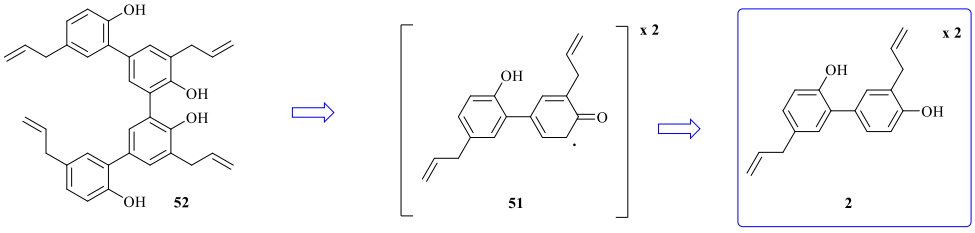

Scheme 25. Retrosynthetic analysis of houpulin B (**52**).

In plants, houpulin B is naturally achieved through a possible radical coupling reaction mediated by an enzyme, and the possible mechanism is described in **Scheme 26**. The process involves the dehydrogenation of honokiol, to produce a radical intermediate which can be located either at the phenolic

hydroxy group or at the *ortho*-position to the hydroxy group. The radical **51** is then subjected to free radical coupling, producing a new carbon-carbon bond and forming the natural product.

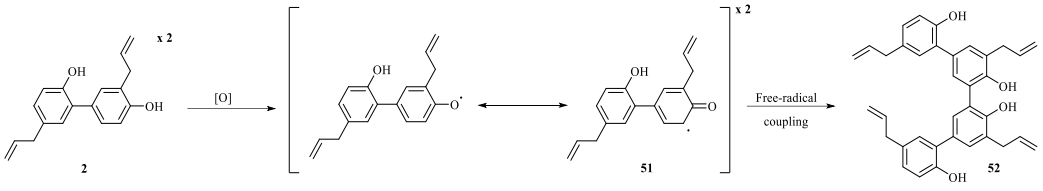

Scheme 26. Possible mechanism for the synthesis of **52**.

On a laboratory scale, biomimetic coupling reactions can provide natural products through a radical mechanism of phenolic oxidative coupling that mimic the natural biosynthetic process. Therefore, in principle, it is possible to exploit phenolic radical coupling reaction mediated by metals and enzymes. In this regard, the first part of the work was dedicated to optimizing the reaction conditions for obtaining the natural product **52** from honokiol (**2**).

At first, the focus was on using metal-catalyst ($FeCl_2$, Ag_2O) that had already been employed in literature for the dimerization reactions of phenolic compounds [102, 178]. Several experiments were conducted, varying the catalyst, solvent, and experimental conditions such as temperature, reaction time, and the employment of ultrasounds. These reaction conditions were evaluated according to the literature [102, 178]. **Table 5** describes the different reaction conditions evaluated.

Table 5. Reaction conditions evaluated for biomimetic synthesis of **52**.

Entry	Catalyst	Eq.[a]	Solvent	T (°C)	T (h)	%yield[b]
1	$FeCl_2$ [c]	0.02	Buffer phosphate [d]	25	24	0
2	$FeCl_2$ [c]	0.02	Buffer phosphate [d]	25	24 [e]	0
3	Ag_2O	1	$CHCl_3$	25	5	32

[a] referred to honokiol; [b] determined by HPLC-UV quantification (see experimental section); [c] reaction in presence of H_2O_2; [d] Buffer phosphate 0.1 M pH = 6; [e] using ultrasounds.

The most promising reaction condition is reported in the entry 3 where the use of Ag_2O as catalyst and chloroform as solvent in mild reaction conditions allows to obtain the desired compound with a 32% yield in a short time. Several attempts have been performed varying the catalyst's equivalents, but it was not possible to achieve the desired product. An overview of the experimental conditions and the spectroscopic characterization by mass spectrometry, ^{1}H NMR, ^{13}C NMR and 2D NMR are reported in the **Chapter 5** (**paragraph 5.4**). Experimental data are reported in Supplementary materials (**Figure S182 - 186)** at the following link:
https://drive.google.com/file/d/1OxXuw5qQ0mIGLRJQivSZsiDnba253SV7/view?usp=sharing

Once the desired molecule was obtained, the objective was to achieve the same molecule using eco-friendly reaction conditions, as biotransformation is considered an efficient and eco-friendly technology for the synthesis of natural compounds and derivatives [90]. For this reason, the focus shifted towards the use of enzymes [72, 179] as catalyst instead of metal-catalyst, aiming to reduce and/or remove the use and production of harmful and hazardous substances.
The synthesis of houpulin B is reported in the literature by employing peroxidase from bitter gourd (*Momordica charantia*) with a 3.1% yield [90]. Several attempts were performed, varying the enzyme (horseradish peroxidase or laccase from *Trametes versicolor*) and the solvents.

The two investigated enzymes belong to the oxidase enzyme family: horseradish peroxidase is an eme-protein extracted from the roots of horseradish plants and used to catalyze the oxidation of a wide range of substrates by hydrogen peroxide. At the same time, Laccase from *Trametes versicolor* is a multicopper oxidase enzyme found in fungi, and it catalyzes the oxidation of a wide range of substrates by using molecular oxygen as co-substrate. The reaction conditions were chosen based on the different reaction conditions reported in the literature.

Reactions were carried out in organic solvents (acetone, methanol, and dioxane), biphasic solvent reactions, or exclusively in aqueous solvents like acetate or phosphate buffer [108]. Furthermore, the use of chemical mediators such as acid 2,2'-azino-bis(3-etilbenzotiazolin-6-solfonico) or (2,2,6,6-Tetramethylpiperidin-1-yl)oxyl, reported in the literature for dimerization reactions [107, 180], was also considered. All the reactions were conducted at room temperature. The reaction conditions that allowed the product's synthesis were achieved using laccase as an enzyme, without organic solvent but only phosphate buffer and without any chemical mediator at room temperature (**Table 6** entry 16). Compared to the previous reaction conditions (see **Table 5** entry 3), compound **52** was achieved with a lower yield, approximately 13.4%, and a longer reaction time. However, the desired molecule was obtained without the employment of an organic solvent and a metal catalyst. **Table 6** summarizes all the reaction conditions evaluated.

Table 6. Reaction conditions evaluated for enzymatic synthesis of **52**.

Entry	Enzyme	Mediator	Solvent	Buffer	Time	%yield[a]
1	HRP[b]	-	Acetone	Acetate[c]	24 h	0
2	HRP[b]	-	Methanol	Acetate[c]	24 h	0
3	HRP[b]	-	Acetone	Acetate[c]	24 h	0
4	HRP[b]	-	-	Phospate[d]	24 h	0
5	LTV	-	-	Acetate[c]	4 gg	0
6	LTV	-	Dioxane	Acetate[c]	4 gg	0
7	LTV	TEMPO	-	Acetate[c]	4 gg	0
8	LTV	TEMPO	Dioxane	Acetate[b]	4 gg	0
9	LTV	ABTS	-	Acetate[c]	4 gg	0
10	LTV	ABTS	Dioxane	Acetate[b]	4 gg	4.0
12	LTV	TEMPO	-	Phosphate[d]	4 gg	0
11	LTV	TEMPO	Dioxane	Phosphate[d]	4 gg	0
13	LTV	ABTS	-	Phosphate[d]	4 gg	0
14	LTV	ABTS	Dioxane	Phosphate[d]	4 gg	0
15	LTV	-	Dioxane	Phosphate[d]	4 gg	2.4
16	LTV	-	-	Phosphate[d]	4 gg	13.4

[a] determined by HPLC-UV quantification (see experimental section); [b] reaction in presence of H_2O_2; [c] acetate buffer 0.1 M pH = 5; [d] phosphate buffer 0.1 M pH = 6; HRP: horseradish peroxidase; LTV: laccase from *Trametes versicolor;* TEMPO: (2,2,6,6-Tetramethylpiperidin-1-yl)oxyl; ABTS: acid 2,2'-azino-bis(3-etilbenzotiazolin-6-solfonico. All the reaction were performed at room temperature.

The two optimized reaction conditions for honokiol dimer synthesis were subsequently employed for the synthesis of novel oligomeric compounds. Specifically, the first dimer was obtained by modifying the natural product and using magnolol as the starting material. The dimer **53** was obtained with the same reaction yield as houpulin B, 33% using the Ag_2O-mediated reaction and 13% using the enzymatic reaction. Another dimer was synthesized using both magnolol and honokiol as starting materials. Dimer **54** is, therefore, a dimer inspired by magnolol and honokiol, and it was obtained with a yield of 30% using the Ag_2O-mediated reaction and 10% with the enzymatic reaction. **Scheme 27** provides, in

detail, the biomimetic reaction conditions for the synthesis of oligomeric compounds.

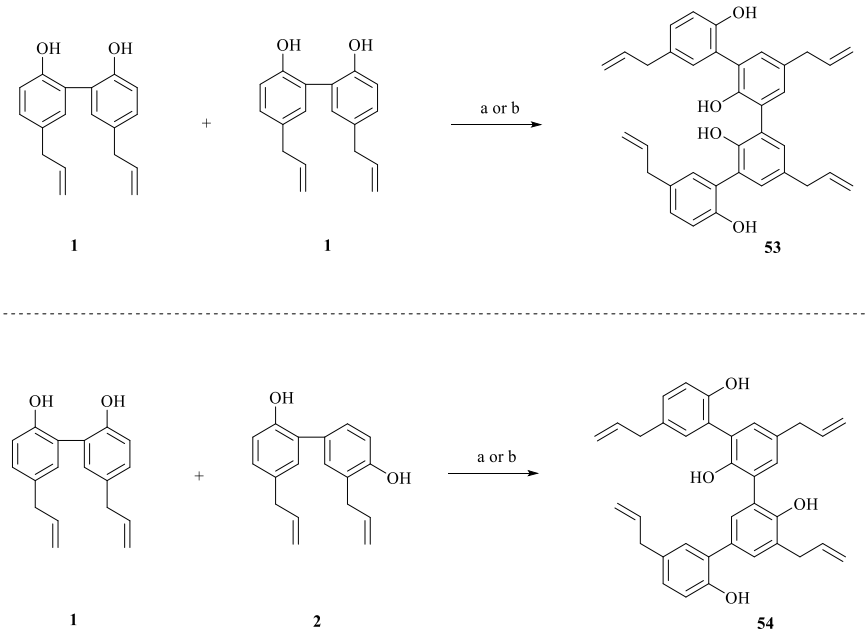

Scheme 27. Synthesis of oligomeric compounds **53- 54**. *a)* $CHCl_3$, Ag_2O (catalyst, 1 eq.), 5h, room temperature. *b)* LTV (catalyst), phosphate buffer 0.1 M pH = 6, 4 days, room temperature.

An overview of the experimental conditions and the spectroscopic characterization by mass spectrometry, ^{1}H NMR, ^{13}C NMR and 2D NMR are reported in the **Chapter 5** (**paragraph 5.4**). Experimental data are reported in Supplementary materials (**Figure S187 - 196)** at the following link: https://drive.google.com/file/d/1OxXuw5qQ0mIGLRJQivSZsiDnba253SV7/view?usp=sharing

3.4 Inhibition of metabolic enzymes

Magnolol (**1**), honokiol (**2**), and obovatol (**3**) have been reported to possess a wide range of biological effects. However, few studies investigate their potential as inhibitors of metabolic enzymes such as α-amylase, α-glucosidase, and pancreatic lipase. For this reason, a deep evaluation of the inhibitory activity of the three natural compounds towards these enzymes was conducted through *in vitro* assays, kinetic analysis, fluorescence spectroscopy, where possible, and molecular docking study. In addition, the assessment of their synthetic analogues' inhibitory activities is also reported.

In vitro inhibitory activity of natural compounds

The inhibition of the pancreatic lipase (PL) enzyme was assessed employing an established spectrophotometric methodology previously described [181]. The PL activity was measured using *p*-nitrophenyl butyrate (*p*-NPB) as substrate and the anti-obesity drug orlistat as a positive control. At the same time, the inhibitory activity towards α-glucosidase from *Saccharomyces cerevisiae* (α-Glu) and α-amylase from porcine pancreas (α-Amy) were established according to the previously described spectrophotometric methods [182] using *p*-nitrophenyl α-D-glucopyranoside (*p*-NP- α-G) as α-Glu substrate, and starch as substrate and 3,5-dinitro salicylic acid (DNS) as reagent for α-Amy assay. The inhibitory activity was expressed as the concertation inhibiting of the 50% of enzyme activity (IC_{50}), and a lower IC_{50} value indicates the higher inhibitory activity. The inhibition percentage of enzyme activity at increasing inhibitor concentration was related to the absorption intensity by the equation:

$$\%\ inhibition = \frac{OD_{control} - OD_{sample}}{OD_{control}} * 100$$

Here, $OD_{control}$ represents the measured optical density for the enzyme-substrate mixture in the absence of an inhibitor, and OD_{sample} represents the optical density of the reaction mixture in the presence of an inhibitor. The calculated inhibition rates at different concentrations for each inhibitor were developed using the linear regression method, calculating the concentration (μM) that inhibits 50% of enzymatic activity (IC_{50}).

The obtained IC_{50} values are reported in **Table 7**. The results are compared to the IC_{50} values of orlistat, the anti-obesity drug, and acarbose, the antidiabetic drug, used respectively as a positive control in PL assay and α-Glu and α-Amy assay. The experimental details are reported in **Chapter 5** (**Paragraphs 5.5 - 5.7**), and the enzyme inhibition graph of **1**, **2,** and **3** obtained by the linear regression method are reported in the supplementary material.
https://drive.google.com/file/d/1OxXuw5qQ0mIGLRJQivSZsiDnba253SV7/view?usp=sharing

Table 7. Inhibitory activity (IC_{50}) of natural products **1**, **2** and **3** towards PL, α-Amy, and α-Glu.

ID	PL	α-Amy	α-Glu
	[a] **IC_{50} ± SD**	[a] **IC_{50} ± SD**	[a] **IC_{50} ± SD**
1	158.7 ± 5.1	24.0 ± 2.7	47.1 ± 2.9
2	115.5 ± 9.0	44.3 ± 3.9	121.3 ± 5.5
3	270.0 ± 15.0	23.6 ± 2.0	124.6 ± 5.0
orlistat	0.9 ± 0.1	-	-
acarbose	-	34.6 ± 0.9	248.3 ± 2.3

[a] Results are expressed in μM. IC_{50} is the concentration required to inhibit 50% of enzyme activity. The IC_{50} values are mean ± SD (n = 3).

According to the results, magnolol was a slightly better α-Amy inhibitor (**1**: 24.0 μM) than acarbose (34.6 μM) and five times more active as an α-Glu inhibitor (**1**: 47.1 μM) than the hypoglycemic drug (248.3 μM). Honokiol and obovatol showed similar behavior, being twice as active as an α-Glu inhibitor (**2**: 121.3 μM; **3**: 124.6 μM) than acarbose. Obovatol was a slightly better α-Amy inhibitor (24.6 μM) than acarbose, while honokiol showed an IC_{50} value of 44.3

μM. All three natural neolignans were weak lipase inhibitors compared to the anti-obesity drugs according to IC_{50} value.

Except for magnolol and honokiol, whose IC_{50} values against α-Glu are reported in the literature [72, 149, 183, 184], and magnolol, for which the inhibition kinetics is reported [185], there are no detailed studies on their inhibitory activities toward the other enzymes. The three neolignans were also subjected to an *in silico* absorption, distribution, metabolism, and excretion (ADME) study on the SwissADME web platform [186]. The results are reported in Supplementary materials (**Figure S170, 200 - 201)** at the following link: https://drive.google.com/file/d/1OxXuw5qQ0mIGLRJQivSZsiDnba253SV7/view?usp=sharing

The neolignans exhibited suitable physiochemical properties concerning oral bioavailability [187] as lipophilicity values less than 5 (**1**: 4.22; **2**: 4.22; **3**:4.35). They also showed topological polar surface area (TPSA) less than 140 Angstroms squared [$Å^2$] (**1**: 40.46 $Å^2$; **2**: 40.46 $Å^2$; **3**:49.69 $Å^2$), thus demonstrating good gastrointestinal absorption and blood-brain barrier. **1**, **2,** and **3** also showed moderate water solubility and satisfied all Lipinski's rules [188].

3.5 Lipase inhibitory activity of nitrogenated analogues inspired by magnolol and honokiol.

Magnolol and honokiol are poor inhibitors of PL if compared with the currently employed anti-obesity drug orlistat. However, honokiol is considered a promising inhibitor in screening the component of various Chinese medicinal herbs [150]. For this reason, this compound was evaluated, considering its encouraging IC_{50} value. The study was extended to magnolol, as other biological investigations have observed different activities between the two isomeric neolignans [70, 189]. In light of these considerations and considering the lack of information, a detailed PL inhibitory study was performed.

Moreover, although the two neolignans are not potent lipase inhibitors, their structure was considered a promising scaffold. In general, several optimization steps have to be performed before a natural compound leads to the synthesis of a more effective analogues. Moreover, studying these natural compounds as lipase inhibitors may be relevant as obesity is connected to other metabolic disorders. Thus, the honokiol and magnolol may be interesting as they are also studied as inhibitors of other enzymes (i.e., α-Glu and α-Amy).

In addition, according to the inhibition results on other nitrogenated compounds [151], the synthesized nitrogenated analogues (**6** – **18c**; **Paragraph 3.1**) inspired by magnolol and honokiol (**Figure 7**) have been evaluated for their inhibitory activity towards PL.

The studies were conducted through *in vitro* assays, kinetic, and molecular docking analyses.

In vitro lipase inhibitory activity

The inhibition of the pancreatic lipase enzyme was assessed using established spectrophotometric methodologies previously described in the

literature [181] and before reported in **Paragraph 3.4**. The obtained IC_{50} values are reported in **Table 8**. The results were compared to the IC_{50} values of the anti-obesity drug orlistat used as a positive control in PL assay and compared to the two natural compounds **1** and **2**.

Based on the findings, all biphenyl compounds achieved by SM cross-coupling (**6** – **10**) exhibited either inactivity (>300 μM) or weak inhibitory activity (100-300 μM) on the PL. Whereas the *O*- and/or *N*-allyl derivatives (**11a** – **15**) and the products of Claisen rearrangement (**16a** – **18c**) demonstrated enhanced inhibitory activity. Compounds with free NH_2 and OH groups exhibited the highest PL inhibitory activity, and the potency of inhibition increased from SM products to the corresponding *O*-allyl derivatives with free NH_2 and further to the *C*-allyl derivatives with both free NH_2 and OH. As an example, the inhibitory activity increased as follows: **6** (225.5 μM) < **11b** (46.9 μM) ≤ **16b** (41.7 μM); **7** (180.0 μM) < **12** (106.1 μM) < **17** (42.6 μM); **9** (>300 μM,) < **14b** (82.6 μM) < **18b** (44.4 μM). An overview of the inhibition results highlighted the potential of neolignans **16b**, **17,** and **18b** as promising PL inhibitors (IC_{50} values < 45 μM). These compounds possessed an allyl chain in the *ortho* position to the hydroxyl group, a scaffold similar to the honokiol. Additionally, the IC_{50} of the three synthesized neolignans were lower than those of natural compounds **1** and **2** (158.7 μM and 115.5 μM) and poor compared to the anti-obesity drugs orlistat (0.9 μM). Furthermore, their scaffolds could be attributed to significant interest in developing novel anti-obesity drugs.

Table 8. Inhibition data of **1**, **2** and synthesized analogues (IC_{50}) towards PL enzyme.

ID	PL [a] IC_{50} ± SD
1	158.7± 5.1
2	115.5 ± 9.0
6	225.5 ± 11.0
7	180.0 ± 13.0
8	113.2 ± 1.7
9	>300
10	103.6 ± 19
11a	53.7 ± 0.2
11b	46.9 ± 1.4
11c	76.6 ± 7.0
11d	45.6 ± 5.0
12	106.1 ± 7.8
13	47.8 ± 2.1
14a	119.0 ± 6.9
14b	82.6 ± 2.9
14c	93.2 ± 9.4
15	57.0 ± 2.3
16a	54.0 ± 1.3
16b	41.7 ± 1.5
17	42.6 ± 2.0
18a	53.5 ±6.4
18b	44.4 ± 1.4
18c	93.2 ± 13.5
orlistat	0.9 ± 0.1

[a] Results are expressed in µM. IC_{50} is the concentration required to inhibit 50% of enzyme activity. The IC_{50} values are mean ± SD (n = 3).

The neolignans **16b**, **17,** and **18b** were also subjected to an *in silico* absorption, distribution, metabolism, and excretion (ADME) study on the SwissADME web platform [186]. The results are reported in Supplementary materials (**Figure S128 - 130)** at the following link:

https://drive.google.com/file/d/1OxXuw5qQ0mIGLRJQivSZsiDnba253SV7/view?usp=sharing

They exhibited good physicochemical properties, including lipophilicity and TSPA [188]. The synthesized biphenyl also showed poor/low water solubility, good bioavailability score [187], a good drug-likeness profile without Lipinski, Veber, and Ghose violation rules, and low skin permeation but high gastrointestinal absorption [188]. In addition, none of the selected compounds has been identified as pan assays interference compounds (PAINS) [186, 190]. Finally, adding functional groups like NH_2 and NO_2 could enhance ADME properties if they are irrelevant to the PL inhibitory activity.

Molecular docking analysis

The molecular docking studies were conducted thanks to a collaboration with Dr. Luana Pulvirenti of the ICB-CNR of Catania to understand the inhibition mechanism better, investigating the affinity for the PL catalytic site of magnolol, honokiol, and the biphenyls **6 – 18c**.

The key interacting residues in the binding site of PL include Ser152, Phe215, Arg256, His263, Leu264, Asp176, and Tyr114 [181].

All the ligands are well accommodated into the binding pocket, occupying almost the same spatial portion. The calculated binding energies (Kcal/mol) listed in **Table 9** suggested a good affinity for nitrogenated inhibitors. The list of molecular interactions for each analysed compound, obtained by the visual inspection of docked conformation, is reported in **Table 9**.

Table 9. Binding Energies (ΔG_{bind}) and Interacting Residues of magnolol (**1**), honokiol (**2**), and bisphenols **6** – **18c** with PL Catalytic Site. [a]

Ligands	[a] Autodock Vina calcd ΔG_{bind}	[a] Glide calcd ΔG_{bind}	Interacting residues	Interaction	Binding Glide distance (Å)
1					
A-ring	-8.7	-5.55	His263	π – π /π - cation	-
2					
B-ring	-8.6	-6.62	Phe77,	π – π	-
O2' (B-ring)			Phe77,	H-donor	2.0
B-ring			Phe215	π – π	-
6					
O4' (B-ring)	-7.4	-5.15	Gly76,	H-acceptor	2.6
O4' (B-ring)			His151,	H-acceptor	2.1
O4' (B-ring)			Asp79,	H-donor	1.8
B-ring			His263	π - π	-
7					
O4' (B-ring)	-7.7	-5.23	His151,	H-acceptor	2.7
O4' (B-ring)			Gly76,	H-acceptor	2.1
O4' (B-ring)			Asp79,	H-donor	1.8
B-ring			His263,	π – π/ π - cation	-
A-ring			Phe215	π - π	-
8					
O4' (B-ring)	-7.6	-5.18	Gly76,	H-acceptor	2.6
O4' (B-ring)			His151,	H-acceptor	2.1
O4' (B-ring)			Asp79	H-donor	1.8
9					
O2' (B-ring)	-8.1	-6.16	Ser152,	H-donor	1.8
B-ring			Phe77,	π - π	-
NH (A-ring			Asp79	H-donor	2.8
10					
B-ring	-8.2	-5.38	His263	π - π	-
B-ring			His263	π - cation	-
11a					
A-ring	-7.6	-3.39	His263,	π - π	-
N_2 (A-ring)			Ser152	H-donor	2.2
11b					
B-ring	-7.7	-5.19	His263	π – π/ π - cation	-
11c					
A-ring	-7.8	-4.95	His263	π – π/ π - cation	-
11d					
B-ring	-7.3	-3.98	His263	π – π	-
12					
B-ring	-8.1	-5.48	His263	π – π/ π - cation	-
13					
O4' (B-ring)	-7.6	-4.47	Arg256,	π - cation	-
A-ring			His151	salt bridge	-
14a	-7.1	-3.89			

A-ring			His263	π – π/ π – cation	-
14b					
A-ring	-7.3	-4.92	His263	π – π/ π - cation	-
14c					
B-ring	-7.0	-5.30	Phe77	π – π	-
15					
B-ring	-6.5	-4.45	-	-	-
16a					
A-ring	-8.4	-3.88	His263	π – π/ π - cation	-
16b					
A-ring	-8.4	-5.51	Phe77,	π – π	-
B-ring			His263,	π – π/ π - cation	-
O4' (B-ring)			Asp79	H-donor	2.0
17					
A-ring	-8.5	-5.70	Phe77,	π – π	-
B-ring			His263	π – π/ π - cation	-
O4' (B-ring)			Asp79	H-donor	2.4
18a					
O2' (B-ring)	-7.8	-4.77	Phe77,	H-donor	2.3
B-ring			His263	π - cation	-
18b					
O2' (B-ring)	-8.0	-6.71	Phe77,	H-donor	1.8
A/B-ring			Phe215,	π – π	-
A-ring			His263	π – π	-
N4 (A-ring)			Tyr114	H-donor	2.5
18c					
B-ring	-7.7	-6.58	Phe77,	π – π	-
O2' (B-ring)			Ser152	H-donor	2.1
orlistat	-6.6	-3.45	His263	H-acceptor	2.6

[a] The ΔG_{bind} values were calculated with Autodock Vina and Glide and are expressed as Kcal/mol. Otherwise indicated in **Figure 19**, the A-ring brings amino or nitro group, B-ring is the phenolic ring.

The analysis of docked poses showed the main interacting residues that can stabilize the complex between each compound and the enzyme. Non-covalent interactions are established with His263, His151, Ser152, Asp79, Gly76, Phe215, Arg256 and Phe77. This study suggests that His263 could play a key role in the interactions with this class of inhibitors, together with Phe77 and Phe215.

Some considerations concerning the interactions can be inferred:

- the B-ring bearing the free hydroxyl group in C-2' or C-4' position is involved in interactions with the residues in the binding cavity;
- the A-ring, bringing an amino or nitro group, was less involved and allowed to establish only weak interaction with the protein counterpart when bearing more

bulky substituents, probably due to the conformation geometry of the ligand into the cavity.

The biphenyl derivatives **6 – 10**, despite the promising interactions calculated and collected in **Table 9**, show scarce *in vitro* results towards PL, as explained by their lack of the right lipophilicity. The B-ring of **6** − **10**, lacking the allyl chain of the natural analogues **1** and **2**, remains wholly exposed to the solvent, not generating stabilizing interactions. Moreover, the functionalization of OH and NH_2 with allyl groups is not an excellent strategy to improve the affinity with the enzyme, as evidenced by the docking outcomes obtained for the allyl analogues **11a-d**, **12**, **13, 14a-c,** and **15**. The derivatization of NH_2 with an allylic chain at the A-ring changes the orientation into the cavity, worsening the interaction with PL (see the comparison between **16a** and **16b**). Also, a comparison between **17a** and **17c,** mono and bis *N*-allyl analogues, respectively, with **17b**, clearly shows a worsening in terms of interactions with PL. In particular, the interaction involving the A-ring is entirely lost, while the interaction pattern for the B-ring remains good. Compounds **16b**, **17,** and **18b** showed the best fitting for intermolecular interactions with PL with the A-ring (containing the amino group) surrounded by the hydrophobic residues (**Figure 19**).

Conversely, the B-ring (the phenolic ring) of **18b** is in a positively charged portion, whereas that of **16b** and **17** is in a negatively charged area. The docking analyses grouped the compounds **16b** and **17** with magnolol and **18b** with honokiol, in agreement with kinetic results. The results suggest the importance of free OH in the B-ring, mainly when this is in the C-2' position as for one of the most promising compounds, **18b**. Moreover, the allyl chain in *ortho* to the OH would seem necessary, as it mimics the natural distribution of the substituents of the natural compound **2**. The 2D interaction diagrams are reported in **Figure 19**.

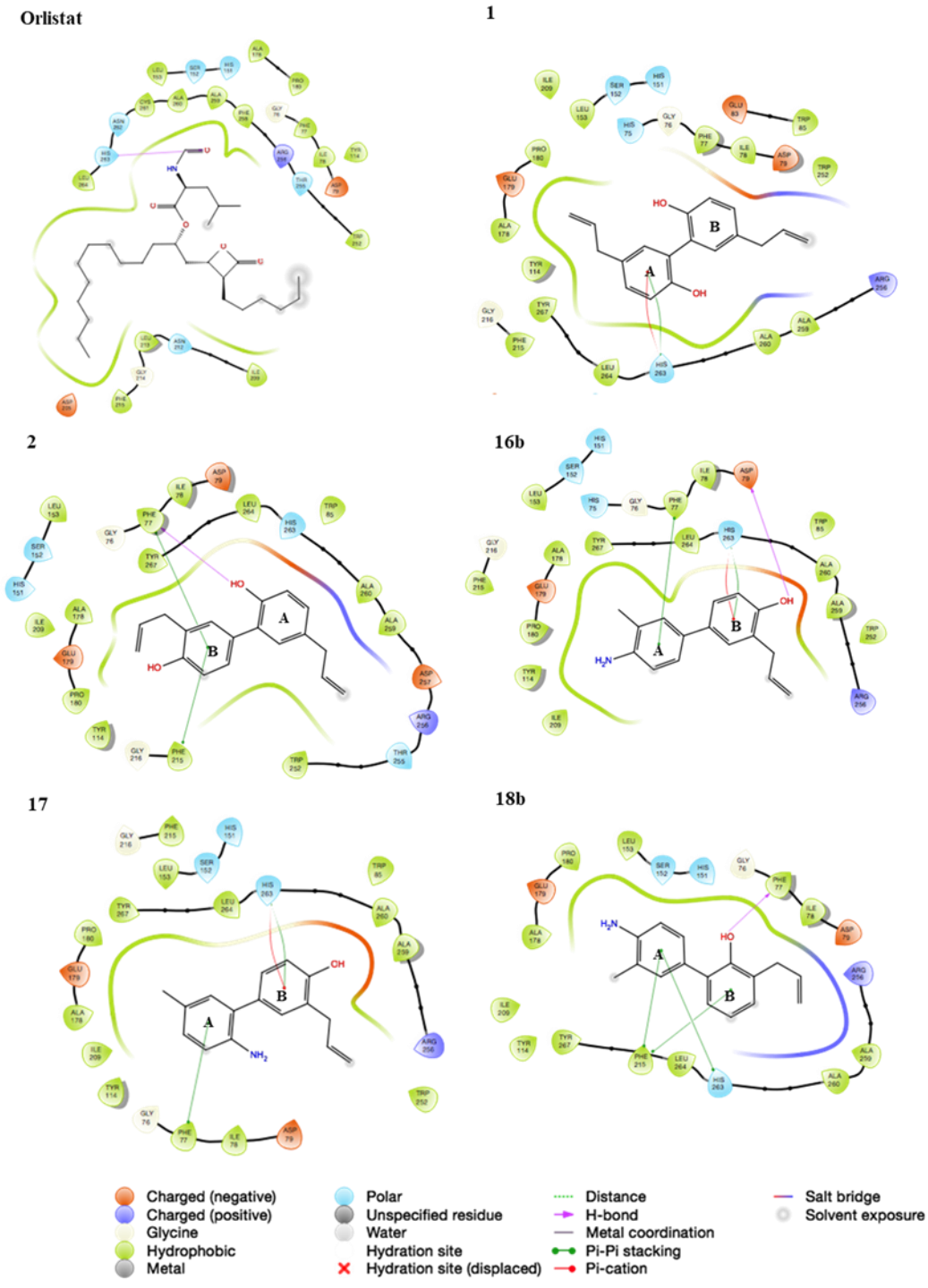

Figure 19. 2D interaction diagrams of **orlistat**, **1**, **2**, **16b**, **17,** and **18b** with PL.

Kinetic of inhibition

The inhibition of PL of the most promising inhibitors **16b**, **17,** and **18b** and of the magnolol (**1**) and honokiol (**2**) were determined using the enzyme kinetic study [181, 191]. The mode of inhibition on PL was determined through the Lineweaver-Burk (L-B) graph by plotting the reciprocal of initial velocity (v_0) and the reciprocal of the concentration of substrate concentration (NPB). The details are reported in **Chapter 5** (**Paragraphs 5.8)**, while the kinetic results are reported in **Table 10**.

Despite their similar structure, magnolol and honokiol act as PL inhibitors with different modes of inhibitions. Honokiol behaved as a competitive inhibitor, as data lines on the L-B plot crossing the y-axis indicated. This suggests the inhibitor did not influence the maximum reaction rate (v_{max}). The constant K_i: 674.8 µM, related to the formation of the enzyme-inhibitor complex (EI), was determined by plotting the slope of L-B plot lines and the inhibitor concentration. The secondary plots are reported in Supplementary materials (**Figure S132)** at the following link:
https://drive.google.com/file/d/1OxXuw5qQ0mIGLRJQivSZsiDnba253SV7/view?usp=sharing

Conversely, magnolol exhibited a mixed-type inhibition mode with the L-B plot lines intersecting in the third quadrant. This behaviour can be attributed to an intermediate mechanism between non-competitive and uncompetitive inhibition [147]. In this case, two constants were calculated: K_i the inhibitor constant for the formation of EI complex, and K'_i the inhibitor constant related to the formation of ESI complex. In particular, the K'_i should be less than K_i (K_i: 614.3 µM; K'_i: 176.2 µM), as confirmed by the secondary plots of the L-B plot. The secondary plots are reported in Supplementary materials (**Figure S132)** at the following link:

https://drive.google.com/file/d/1OxXuw5qQ0mIGLRJQivSZsiDnba253SV7/view?usp=sharing

The L-B plot of PL inhibition in the presence of **1** and **2** is reported in **Figure 20.**

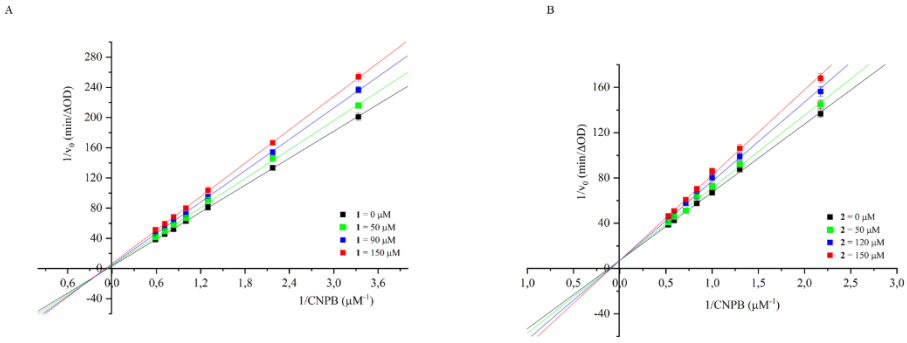

Figure 20. Lineweaver-Burk plots of pancreatic lipase inhibition in the presence of: A) **1**; B) **2**.

The synthetic biphenyls **16b** and **17** exhibited a mixed-type inhibition mode as for magnolol (**Figure 20 A**,). The two neolignans showed an intermediate behaviour between non-competitive and uncompetitive mode with $K'_i < K_i$ as described in the secondary plot (**Table 10**). The two synthetic neolignans also gave lower dissociation constants than the natural product **1**. The most promising inhibitor with a high affinity for ES complex was compound **17,** as confirmed by the low value of K'_i (6.4 μM). Conversely, compound **18b** acted with a competitive inhibition mode, as showed for honokiol (**Figure 20 B**). The kinetic constant (K_i = 249 μM) was determined by plotting the slope of the L-B plot line and the concentration of the inhibitor. The kinetic results are reported in **Table 10**, the L-B graph in **Figure 21,** and the secondary plot are reported in Supplementary materials (**Figure S132)** at the following link:

https://drive.google.com/file/d/1OxXuw5qQ0mIGLRJQivSZsiDnba253SV7/view?usp=sharing

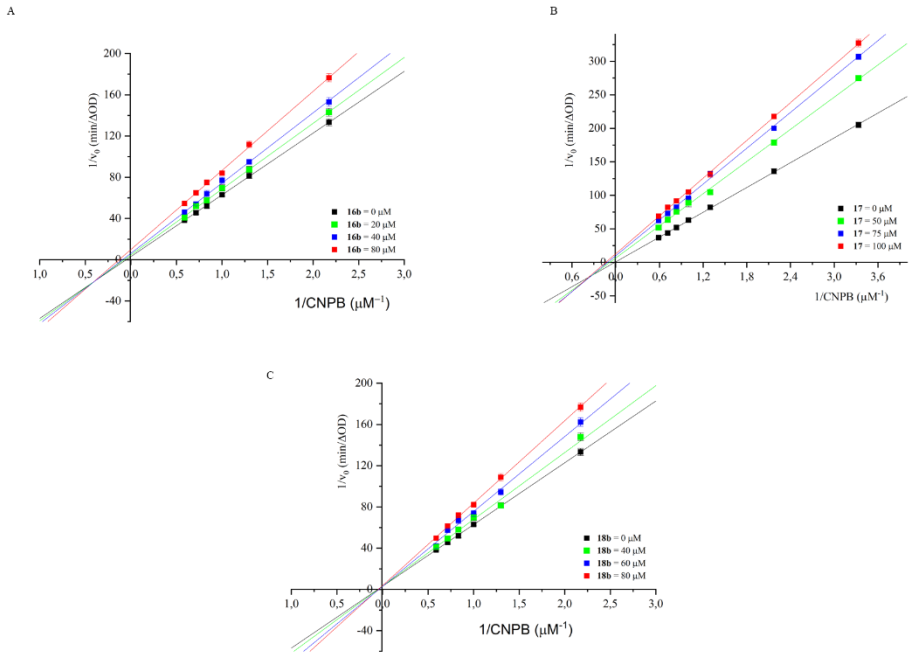

Figure 21. Lineweaver-Burk plots of A) **16b**, B) **17**, and C) **18b** with PL.

Table 10. Kinetic parameters for pancreatic lipase inhibition with **1**, **2**, **16b**, **17** and **18b**.[a]

ID	PL		
	Type of inhibition	**K_i ± SD (μM)**	**K_i' ± SD (μM)**
1	Mixed-type	614.3 ± 19.1	140.9 ± 8.6
2	Competitive	674.8 ± 43.1	-
16b	Mixed-type	286.4 ± 20.5	36.6 ± 2.3-
17	Mixed-type	176.2 ± 13.8	6.4 ± 1.4
18b	Competitive	249.0 ± 34.6	

[a]K_i refers to the constants for the formation EI complex; K'_i refers to the constants for the formation ESI complex.

Fluorescence quenching.

For an in-depth understanding of enzymatic inhibition, fluorescence quenching studies for backbone changes of enzymes in the presence of a ligand

are frequently performed. Unfortunately, the peculiar structure of the biphenyls has an intense fluorescence emission at 300-500 nm, which results in the overlapping of the fluorescence emission band of the biphenyl over the band of the enzyme (350 nm). Consequently, as the concentration of the inhibitor increases, the intensity of the biphenyl band increases; therefore, it is impossible to measure the decrease in the fluorescence of the enzyme. All the data for the fluorescence analysis of LP with **1**, **2**, **16b**, **17**, and **18b** are reported in the Supplementary material (**Figure S135** – **136**) in the following link: https://drive.google.com/file/d/1OxXuw5qQ0mIGLRJQivSZsiDnba253SV7/view?usp=sharing

3.6 α-glucosidase and α-amylase inhibitory activity of obovatol analogues

The small library of novel neolignans inspired by obovatol (**30**, **34** – **37**, **39**, **41**, **44** and **47** – **48**; **Paragraph 3.2**), exhibited different functional groups (methoxy, brome, carboxy, and formyl groups) and moieties (ether and thioether derivatives). These compounds were synthesized to investigate the specific role of structural modifications performed on the obovatol scaffold in α-glucosidase and α-amylase inhibition in light of previous results [152-155]. Obovatol and the new compounds have been evaluated for their inhibitory activity through *in vitro* assays, kinetic analysis, fluorescence quenching measurements, molecular docking and circular dichroism analyses.

In vitro α-glucosidase and α-amylase inhibitory activity

The inhibition of the α-glucosidase and α-amylase enzymes was assessed using established spectrophotometric methodologies previously described in the literature [182] and before reported in **Paragraph 3.4**. The obtained IC_{50} values are reported in **Table 11**. The results were compared to the IC_{50} values of the hypoglycaemic drug acarbose, used as a positive control, and to the natural compounds **3**. Based on the outcomes, the majority of the novel neolignan compounds were more active inhibitors towards α-Glu enzyme (39.6 – 97.7 μM) than obovatol (124.6 μM) and more effective than acarbose (248.3 μM). The synthesized analogues also showed α-Amy inhibitory activity with IC_{50} value between 6.2 and 43.6 μM. Significantly, compounds **35**, **41,** and **48** (IC_{50}: 6.2-17.6 μM) exhibited higher activity than both **3** (24.6 μM) and acarbose (34.6 μM).

Table 11. Inhibitory activity (IC_{50}) of **3** and synthesized analogues towards α-Amy and α-Glu.

ID	α-Amy [a] IC_{50} ± SD	α-Glu [a] IC_{50} ± SD
3	23.6 ± 2	124.6 ± 3
30	43.6 ± 3.5	198.0 ± 15.6
34	38.8 ± 2.9	167.5 ± 5.6
35	12.7 ± 0.9	111.0 ± 7.3
36	36.1 ± 2.8	177.7 ± 2.9
37	24.5 ± 2.1	127.7 ± 5.8
39	20.1 ± 0.4	97.7 ± 2.0
41	17.6 ± 1.6	119.4 ± 4.5
44	27.0 ± 2.3	65.6 ± 2.1
47	35.4 ± 1.2	56.1 ± 2.4
48	6.2 ± 1.0	39.8 ± 2.4
acarbose	34.6 ± 0.9	248.3 ± 2.3

[a] Results are expressed in μM. IC_{50} is the concentration required to inhibit 50% of enzyme activity. The IC_{50} values are mean ± SD (n = 3).

Some structure–activity relationship hypotheses can be formulated considering the functional groups and moieties linked in the biaryl ether scaffold. According to previous findings, the compounds featuring free hydroxyl groups exhibited relevant inhibitory activity [147, 192]. Consequently, methylated compounds displayed less inhibitory activity than their related compounds: neolignans **30** and **34** were less active than natural product **3**, while compound **36** showed less inhibitory activity than **37**.

Of particular interest was compound **35**, a neolignan bearing two free hydroxyl groups as the natural compounds and displaying an IC_{50} value of 111.0 μM for α-Glu inhibition and 12.7 μM for α-Amy inhibition. This enhanced inhibitory effect could be attributed to 2-bromo-propyl chains instead of allyl groups. The addition of bromine groups to aromatic or aliphatic moieties has been reported in the literature [152, 193, 194]. The "Br" group established hydrophobic interactions with specific active residues, thereby increasing the α-glucosidase inhibitory effects [194]. According to the inhibition data reported in **Table 11**,

bromine might also play a role in enhancing α-amylase inhibition. The combination of free hydroxyl groups and bromine in the scaffold also contributed to the overall inhibitory effects of thioether derivative **48** with IC_{50} values of 39.8 µM for α-Glu inhibition and 6.2 µM for α-Amy inhibition. Similarly, the thioether derivative **47** showed a higher α-glucosidase inhibitory activity (IC_{50} 56.1 µM). The enhanced activity of sulfide analogues can also be attributed to specific interactions established with specific residues of the α-glucosidase binding site as previously documented for α-Glu [154] but not for α-Amy.

Compounds **37**, **39**, **41**, and **44**, bearing the ring B moiety of obovatol but different functional groups on the A ring without an allyl chain, were active as **3** or more effective α-Glu inhibitors. Specifically, compound **37** exhibited a comparable inhibitory effect. In contrast, compounds **39** and **41**, bearing a carboxyl function on the A ring instead of an allyl chain, demonstrated either equivalent or slightly superior inhibitory activity than **3** towards both enzymes. Notably, neolignan **44**, featuring a 1-allyl-4-phenoxy moiety and a formyl group on the A ring, was a more potent α-glucosidase inhibitor than obovatol and related compounds. These findings indicated that an allyl chain on the biaryl ether scaffold might not be relevant to inhibitory activity. A summary of the structure-activity relationship is reported in **Figure 22**.

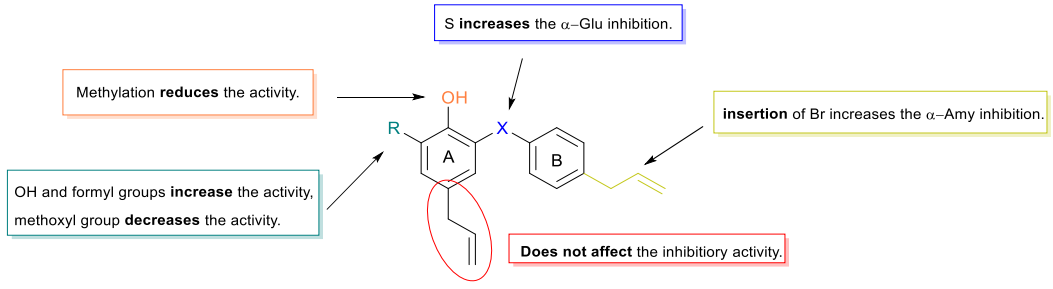

Figure 22. Structural features affecting the α-Amy and α-Glu inhibitory activity of obovatol analogues.

The neolignans **35**, **44**, **47,** and **48** were also subjected to an *in silico* absorption, distribution, metabolism, and excretion (ADME) study on the SwissADME web platform [186]. The results are reported in Supplementary materials (**Figure S171 - 174)** at the following link:

https://drive.google.com/file/d/1OxXuw5qQ0mIGLRJQivSZsiDnba253SV7/view?usp=sharing

Compounds **44**, **47,** and **48** exhibited suitable physicochemical properties, including oral bioavailability with lipophilicity values less than 5, while compound **35** showed a lipophilicity of 5.65. All tested compounds displayed a computational TPSA of less than 140 Angstroms squared [$Å^2$], between 35.53 and 65.76 [$Å^2$], thus showing computational good intestinal absorption. Compounds **3**, **44**, and **47** showed moderate water solubility and satisfied all of Lipinski's rules, whereas **48** violated one of Lipinski's rules. The neolignan **35** showed poor solubility and violated one of Lipinski's rules.

Molecular docking analysis

The molecular docking studies were conducted thanks to a collaboration with Dr. Luana Pulvirenti of the ICB-CNR of Catania.

To rationalize the *in vitro* inhibitory outcomes, obovatol and its analogues were *in silico* evaluated for their affinity for the α-glucosidase and α-amylase catalytic sites, and the output poses were carefully analyzed. The composition of the α-Glu binding site includes the following interacting residues: Asp68, Ser156, Phe157, Phe177, Asp214, His239, Asn241, His245, Glu276, Ala278, Phe300, Glu304, Thr307, Ser308, Pro309, Arg312, Gln222, Asp349, Gln350, and Asp408; whereas for α-Amy are Trp58, Trp59, Tyr62, Val98, His101, Tyr151, Leu162, Thr163, Leu165, Arg195, Ala198, Lys200, His201, Glu233, Glu240, Ile235, His299 and Asp300 [195].

The *in silico* data for α-Glu and α-Amy are listed in **Tables 12** and **13**; these values suggest a good interaction of obovatol and its analogues with both enzymes. In good agreement with the *in vitro* inhibition results (**Paragraph 3.6**), all the synthetic analogues, except **34**, **36**, and **37** showed lower binding energies toward both the enzyme catalytic sites (-4.14 to -5.52 α-Glu, and -4.83 to -5.60 Kcal/mol α-Amy) than obovatol (-3.69 α-Glu; and -4.48 Kcal/mol α-Amy). In general, a careful analysis of the pose outcomes allows to observe that all the ligands are compatible with the hydrophobic pocket of both enzymes, suggesting that they could be promising inhibitory agents.

The docking analysis of obovatol (**3**) shows a stabilization into the hydrophobic pocket of α-Glu originated by the formation of a hydrogen bond between the OH at C-3 and Asp408, a π-cation interaction between the A-ring and Arg312, and a π-π interaction between the B-ring and Phe300. Furthermore, the ligand would appear to be stabilized by a hydrophobic portion (Ala278, Val277, Ala21, Gly217, and Leu218) near the allylic chain of the B-ring. When the OH at C-3 is methylated, as in compound **34**, the ligand changes its orientation into the binding pocket, thus favoring the formation of a hydrogen bond between the OH at C-2 and Glu304 but maintaining the π-cation interaction with Arg312. These interactions worsen overall stabilization (-3.35 Kcal/mol) than the obovatol (**3**) as the ligand is more exposed to the solvent (see **Figure S1** in Supporting material). This finding agrees with the higher IC_{50} value determined for **34** (167.5 μM), with respect to that observed for **3** (124.6 μM). In the case of **30** in which both OH at C-2 and C-3 are methylated, the ligand is capable of forming two π-π interactions between B-ring and A-ring and α-Glu Phe177 and Phe300, respectively, thus favoring greater incorporation into the hydrophobic cavity. As far as α-Amy is concerned, the trend is the same, as the methylation of the C-2 and C-3 positions of the obovatol (**3**) does not represent an advantageous structural modification (see **Table 13** for more details).

If the methylation of the phenolic OH did not seem beneficial for the biological activity, the bromination of both allyl chains would appear to be. Indeed, ligand **35** shows better binding energies for both enzymes (-5.04 and -4.83 Kcal/mol, respectively); the data obtained for α-Glu and α-Amy are also confirmed by the IC_{50} values (111 μM and 12.7 μM, see section 2.2). Taking a look at the docking pose of **35** into α-Glu (**Figure 23**), it seems that the flexibility of the aliphatic chains associated with the hydrophobic effect of Br surrounded by a hydrophobic portion (Phe177, Leu218, Ala278, Phe300, Phe158, Phe157, Pro309, Phe310, Phe311) allows the ligand incorporation into the cavity, reducing the exposure to the external environment. This favors the formation of two hydrogen bonds between the OH at C-2 and C-3 and Asp349, while the B-ring establishes an π-cation interaction with Arg312. Similar considerations are related to α-Amy. The ligand **35** seems to be incorporated into the cavity so that the A-ring changes its orientation, favoring the formation of two hydrogen bonds: the OH at C-2 with His299 and the OH at C-3 with Glu233. The most active compounds toward the inhibition of α-Glu are **47** and **48**, according to the in vitro assay results. Docking analyses corroborated these results as indicated by calculated ΔG_{bind} (**47**: -5.34; **48**: -5.37 Kcal/mol). The ligand **47** interacts with the catalytic pocket only through the A-ring, establishing a hydrogen bond between the OH at C-3 and Asp349, whereas the B-ring does not stabilize the complex being more exposed to the external environment. However, the introduction of bromine on B-ring, as in the ligand **48**, allows the formation of a π-cation and a π-π interaction with the close Arg312 and Phe157, thus justifying the higher inhibitory activity with respect to **47**. The simultaneous presence of the thioether and bromine groups makes the interaction with the enzyme more stable; consequently, the inhibition effect obtained is higher than with obovatol (**3**). The **48** ligand is also efficient in stabilizing the complex with α-Amy (-5.50 Kcal/mol). The A-ring mimics the obovatol maintaining the same interactions but being more incorporated and less exposed to the external environment. The B-ring is better accommodated and

surrounded by a hydrophobic portion (Tyr151, Ile215, Ala198, Leu162, Leu165, Tyr62, Trp59) of the biological target that contributes to stabilizing the complex altogether. These observations perfectly agree with its IC50 value (6.2 μM) and allow us to consider **48** a potent α-Amy inhibitor.

Ligands **36** and **37** maintain the B-ring of obovatol (**3**), whereas the substitution on the A-ring differs from **3** (one OH/OMe at C-2 and the allylic chain at C-4 instead of C-5). The outcomes obtained for both enzymes highlight as the lack of OH at the C-3 position worsens the stability of the complex (α-Glu ΔG_{bind} -2.84 and -3.02 Kcal/mol; α-Amy ΔG_{bind} -3.30 and -2.70 Kcal/mol) and therefore providing a weaker inhibition. These data confirm the crucial role of the A-ring for the expected biological activity and simultaneously reveal the secondary function of the B-ring of obovatol (**3**), which does not participate in the stabilization. The structural modifications on the A-ring of ligands **39** (carboxymethyl group at C-2) and **41** (carboxyl group at C-4) seem to have no significant effect on the stabilization of correspondent complexes with α-Glu. Consequently, they have comparable inhibitory activity to that of **3**. Different consideration concerns α-Amy. Indeed, both ligands are well accommodated within the hydrophobic pocket with a ΔG_{bind} of -5.09 and -5.02 Kcal/mol, respectively, suggesting the stability of the complexes with the biological target. Compound **39** can establish a hydrogen bond between the carbonyl oxygen of the carboxymethyl group, and Gln63.

Moreover, the same ring establishes two π-π stacking interactions with Trp58 and Trp59. Ligand **41** has a different orientation into the hydrophobic pocket compared to **39**, establishing two hydrogen bonds between the two oxygens of the carboxyl group in position C-4 and the amino acids Lys200 and Ile235; moreover, the A ring is involved in a π-π interaction with His201. In both ligands, the B-ring does not participate in the interaction with the biological counterpart and appears to be more exposed to the external environment. Finally, the formyl group on the A-ring of ligand **44** is involved in the formation of a hydrogen bond

with His239 of α-Glu hydrophobic pocket; consequently, a good stabilization energy of -4.66 Kcal/mol was observed. Analogously, a hydrogen bond between the carbonyl group and Ile235 and a π-π stacking interaction between the A-ring and His201 occur with the α-Amy catalytic site. In both cases, no stabilization effect was due to the B-ring maintained as in **3**.

Considering the above, the most important outcome is that OH groups at C-2 and mostly at C-3 of the obovatol scaffold are relevant for interacting with α-Glu and α-Amy. In particular, the OH group in position C-3 would seem to have a critical role in stabilizing the complex; when it is involved in forming hydrogen bonds with the biological counterpart, the complex is more stable, and consequently, the inhibitory effect is stronger. Compounds **35**, **47,** and **48** are among the most active ligands for α-Glu: they establish a hydrogen bond between the OH at C-3 and Asp349, which is part of the catalytic triad of α-Glu and would seem to have a key role precisely in the stabilization of the transition state of the substrate [196]. Analogously, ligands **35** and **48** establish a hydrogen bond between the OH at C-3 with Glu233, part of the catalytic triad [196]. In this context, when this substitution pattern on the A-ring is retained, the B-ring seems to have only a supporting role. The 2D interaction diagrams are reported in **Figures 23** and **24**.

Table 12. Binding Energies (ΔG_{bind}) and list of molecular interaction and interacting residues of obovatol and derivatives with the α-Glu catalytic site.

Ligands	[a] Glide calcd ΔG_{bind}	Interacting residues	Interaction	Binding Glide distance (Å)
3				
B-ring	-3.69	Phe300	π - π	-
A-ring		Arg312	π-cation	-
OH (C-3)		Asp408	H-donor	2.1
30				
B-ring	-5.52	Phe177	π - π	-
A-ring		Phe300	π - π	-
34				
OH (C-2)	-3.35	Glu304	H-donor	1.9
A-ring		Arg312	π-cation	-
35				
OH (C-2)	-5.04	Asp349	H-donor	1.7
OH (C-3)		Asp349	H-donor	1.9
B-ring		Arg212	π-cation	-
36				
B-ring	-3.02	Phe300	π - π	-
B-ring		Phe157	π - π	-
37				
OH (C-2)	-2.84	Glu304	H-donor	1.8
A-ring		Phe157	π - π	-
A-ring		Arg312	π-cation	-
39				
OCH_3 (C-5)	-4.61	Asn241	H-acceptor	2.0
COO^- (C-2)		Lys155	salt bridge	-
COO^- (C-2)		Arg312	H-acceptor	1.9
B-ring		Arg312	π-cation	-
41				
COO^- (C-4)	-4.14	Lys155	salt bridge	-
COO^- (C-4)		Arg312	H-acceptor	2.1
44				
CHO (C-3)	-4.66	Hie239	H-acceptor	2.1
47				
OH (C-2)	-5.34	Asp349	H-donor	1.9
OH (C-3)		Asp349	H-donor	1.6
48				
OH (C-2)	-5.37	Asp349	H-donor	1.9
OH (C-3)		Asp349	H-donor	1.6
B-ring		Phe157	π - π	-
B-ring		Arg312	π-cation	-
acarbose				
	-7.09	Glu304, Thr307, Ser308, Arg312, Phe157, Asp408, Asp349	-	-

[a] The ΔG_{bind} values were calculated with Glide and are expressed as Kcal/mol.

Table 13. Binding Energies (ΔG_{bind}) and list of molecular interaction and interacting residues of obovatol and derivatives with the α-Amy catalytic site.

Ligands	[a] Glide calcd ΔG_{bind}	Interacting residues	Interaction	Binding Glide distance (Å)
3				
OH (C-3)	-4.48	Glu233	H-donor	1.6
OH (C-2)		Asp197	H-donor	1.7
30				
A-ring	-4.64	Trp59	π - π	-
34				
OCH_3 (C-3)	-3.22	Gln63	H-acceptor	2.4
OH (C-2)		Tyr62	H-donor	2.7
35				
OH (C-3)	-4.83	Glu233	H-donor	1.6
OH (C-2)		Hie299	H-acceptor	2.7
36				
A-ring	-2.70	Trp59	π - π	-
37				
OH (C-2)	-3.30	Asp197	H-donor	1.8
39				
A-ring	-5.09	Trp58	π - π	-
A-ring		Trp59	π - π	-
COO^- (C-2)		Gln63	H-acceptor	2.0
41				
A-ring	-5.02	His201	π - π	-
COO^- (C-4)		Lys200	H-acceptor	2.5
COO^- (C-4)		Ile235	H-acceptor	1.9
44				
CHO (C-3)	-5.60	Ile235	H-acceptor	2.1
A-ring		His201	π - π	-
47				
B-ring	-4.99	His201	π - π	-
OH (C-2)		Glu233	H-donor	1.8
OH (C-3)		Glu233	H-donor	1.8
48				
OH (C-3)	-5.50	Glu233	H-donor	1.6
OH (C-2)		Asp197	H-donor	1.9
acarbose				
	-8.33	Glu240, Glu233, Trp59, GLN63, His201, Lys200		

[a] The ΔG_{bind} values were calculated with Glide and are expressed as Kcal/mol.

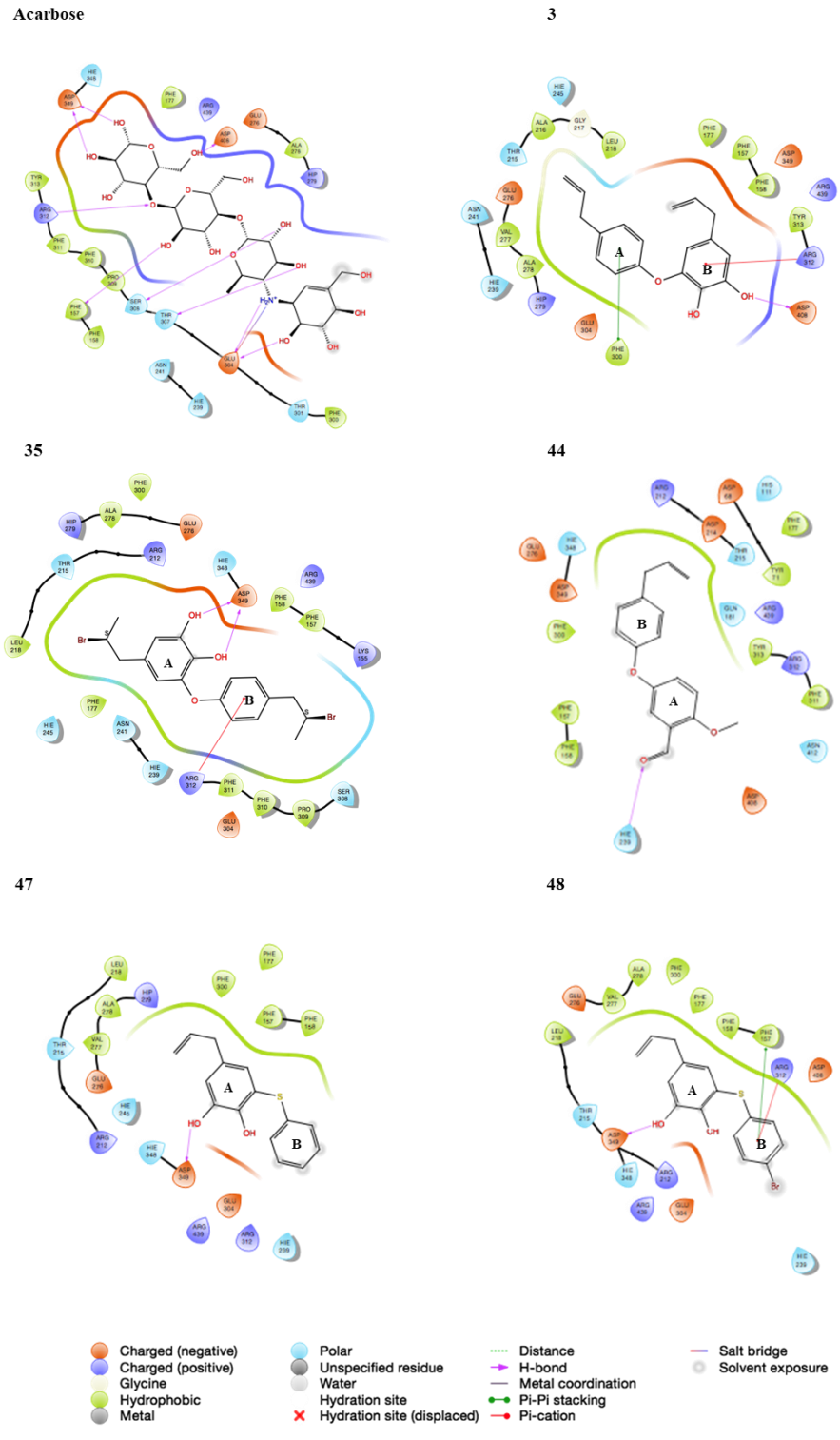

Figure 23. 2D interaction diagrams of **acarbose**, **3**, **35**, **44**, **47** and **48** with α-Glu.

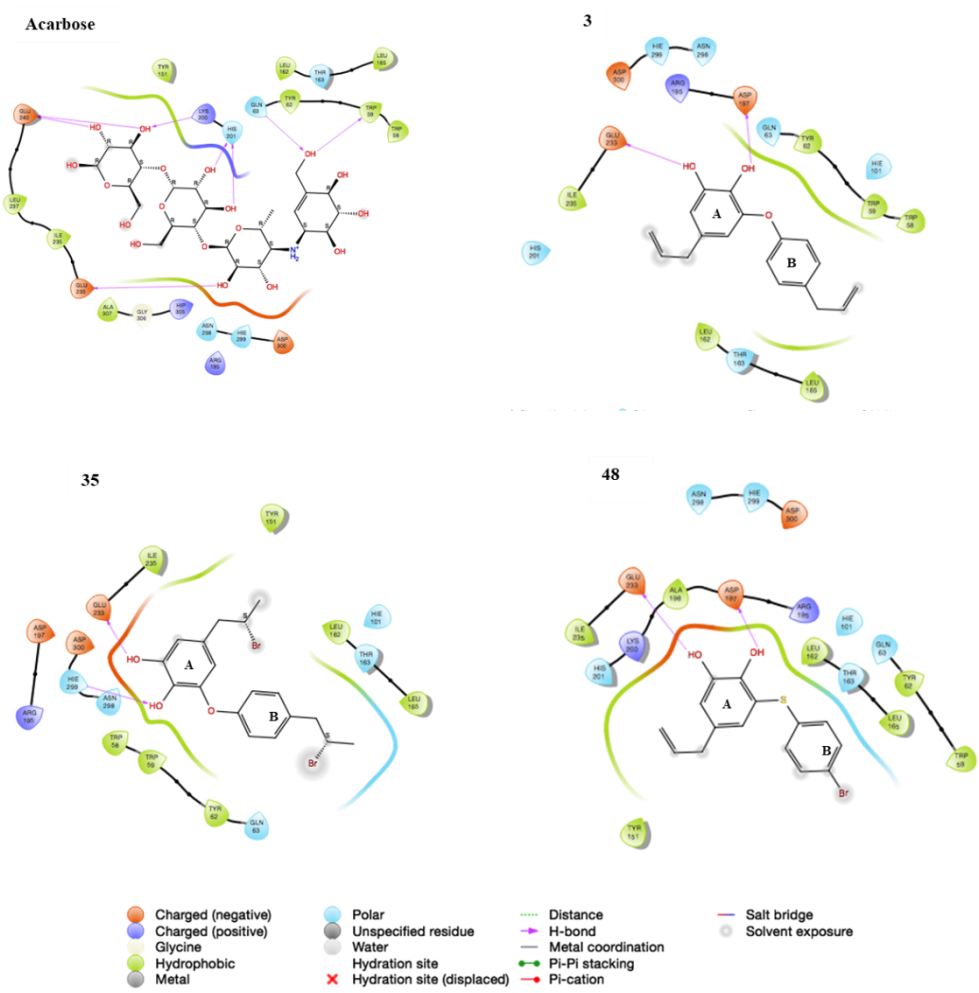

Figure 24. 2D interaction diagrams of **acarbose**, **3**, **35** and **48** with α-Amy.

Kinetic of inhibition

The inhibition of obovatol (**3**) and its promising analogues targeting α-glucosidase (**35**, **44**, **47**, and **48**) and α-amylase (**35** and **48**) was explored. The mode of inhibition on α-Glu and α-Amy was determined through the Lineweaver-Burk (L-B) graph by plotting the reciprocal of initial velocity (v_0) and the reciprocal of the concentration of substrate (NPG for α-Glu and CNPG3 for α-Amy. The details are reported in the **Chapter 5** (**Paragraph 5.9 - 5.10**), while the kinetic results are reported in **Table 14**. The mode of inhibition of obovatol (**3**) was investigated as well.

Obovatol was a non-competitive inhibitor toward α-glucosidase, as the lines in the L-B plot cross the x-axis, and a competitive inhibitor toward α-amylase. The L-B plot of α-Glu and α-Amy inhibition in the presence of **3** are reported in **Figure 25.**

The L-B plots of α-Glu and α-Amy inhibition in the presence of **3** are reported in **Figure 25.**

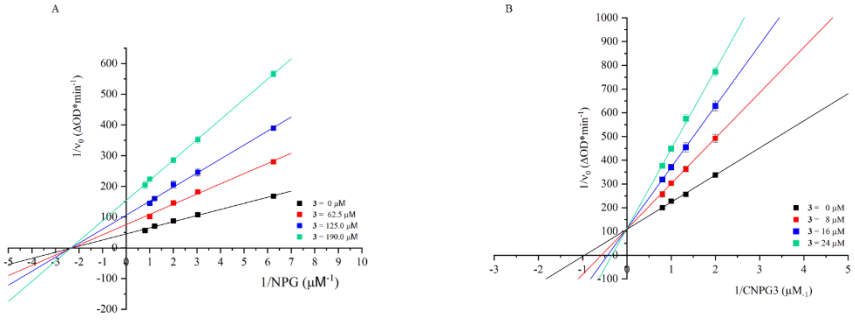

Figure 25. Lineweaver-Burk plots of A) α-glucosidase and B) α-amylase inhibition in the presence of **3**.

The K_i values, calculated by plotting the slope of the L-B plot line and the concentration of the inhibitor, resulted in 79.1 μM and 12.7 μM respectively, for

α-Glu and α-Amy. The secondary plots are reported in Supplementary materials (**Figure S178 - 179**) at the following link: https://drive.google.com/file/d/1OxXuw5qQ0mIGLRJQivSZsiDnba253SV7/view?usp=sharing

The Lineweaver-Burk plots for obovatol analogues (**35**, **44**, **47**, and **48**) are reported in **Figures 26** for α-Glu and **27** for α-Amy. The kinetic parameters are summarized in **Table 14,** while the secondary plots to determine kinetic constants are depicted in Supplementary materials (**Figure S179 - 180**) at the following link:

https://drive.google.com/file/d/1OxXuw5qQ0mIGLRJQivSZsiDnba253SV7/view?usp=sharing

Compounds **35** and **47** showed a similar α-glucosidase inhibitory mechanism observed for obovatol (non-competitive inhibition mode), yielding K_i values of 146.2 μM and 125 μM, respectively. Conversely, the L-B plots for **44** and **48** suggested a mixed-type inhibition, an intermediate mechanism between non-competitive and uncompetitive inhibition [147]. The K_i values for the EI complex were respectively 234.2 μM for **44** and 42.0 μM for **48**, while the K'_i values for the ESI complex were 44.2 μM for **44** and 4.9 μM for **48**. The kinetic results agreed with the lowest IC_{50} value observed in the inhibitory assay, thus suggesting a strong capability of **48** to interact with the enzyme to the ES complex.

To explain the α-Glu mixed-type inhibition of **44** and **48,** other potential binding sites were in silico examined, four obtained by sitemap and another recently proposed in the literature [197]. The molecular interaction with both molecules was studied for each binding site [197], and the calculated ΔG_{bind} energies are reported in **Table S1** (see supporting). The best interaction was collected in the allosteric site composed of the following residues (**Table S2**, line 2): Thr287, Ala289, Ala290, Tyr292, Glu293, Val294, Ser295, His258. Arg259, Met261, Lys262, Asn263, Val265, Gly268, Arg269, Glu270, Ile271, Met272,

Thr273 Lys12 with a calculated ΔG_{bind} of -5.97 and -6.21 kcal/mol for molecules **44** and **48**, respectively. Both values are lower than those obtained for the interaction with the catalytic site. Compound **44** interacts into the allosteric binding site with His258, establishing a π-π stacking interaction; compound **48** interacts with the cavity through a H-bond interaction between the OH at C-3 and Arg269, whereas the B-ring is involved in a π-cation interaction with Lys12 and a π-π interaction with His258 (**Figure S177)**. No other significant interactions were found with other reported allosteric sites for both molecules, for which binding energies <5 (from -2.78 to 4.76 kcal/mol) were registered, suggesting that both molecules interact only with the first reported allosteric site.

The analysis of the kinetic data for α-amylase inhibition reported a competitive inhibition mode for **35** and **48** as well as the obovatol. The K_i values of **3** (12.7 μM) **35** (29.9 μM), **48** (8.5 μM) agree with the experimental IC_{50} values and docking outcomes with **48** being the most effective inhibitor toward the two enzymes.

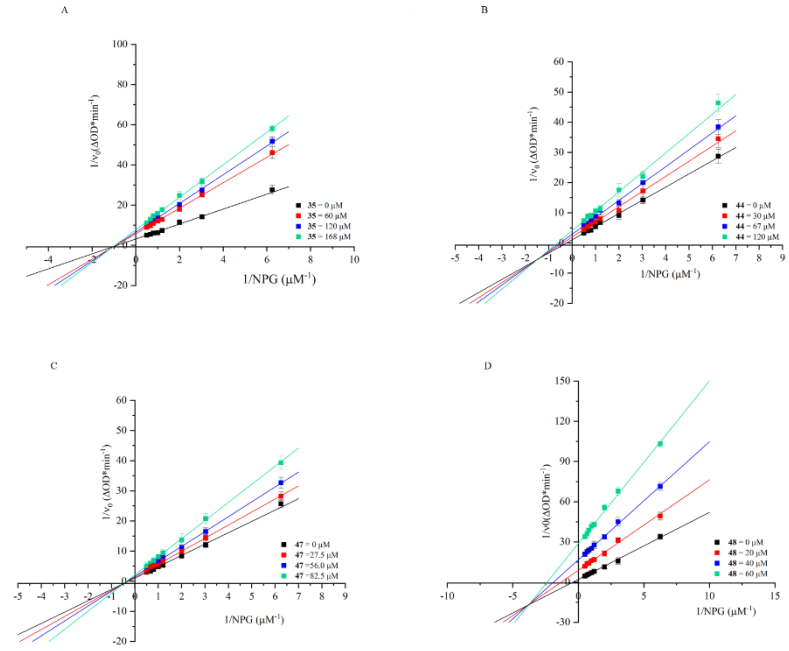

Figure 26. Lineweaver-Burk plots of A) **35**, B) **44**, C) **47**, D) and **48** with α-Glu.

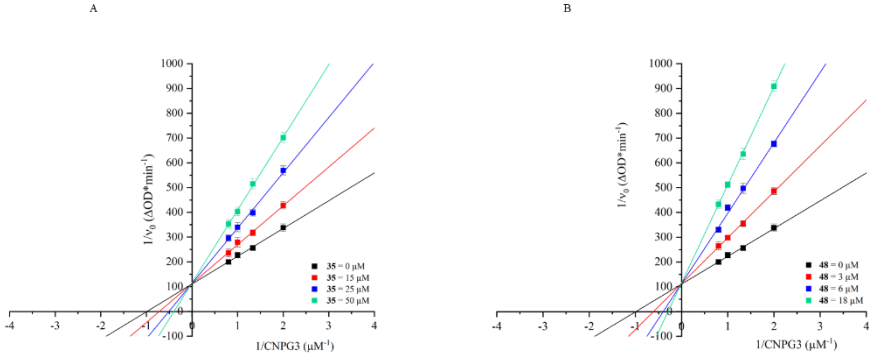

Figure 27. Lineweaver-Burk plots of A) **35** and B) **48** with α-Amy.

Table 14. Kinetic parameters for α-glucosidase and α-amylase inhibition with **3**, **35**, **44**, **47** and **48**.[a]

ID	α-Glu			α-Amy	
	Type of inhibition	**K_i = ± SD (μM)**	**K'_i= ± SD (μM)**	**Type of inhibition**	**K_i = ± SD (μM)**
3	non-competitive	79.1 ± 2.0	-	competitive	12.7 ± 3.0
35	non-competitive	146.2 ± 5.7	-	competitive	29.9 ± 2.4
44	mixed-type	234.2 ± 7.2	44.2 ± 5.4	-	-
47	non-competitive	125.0 ± 5.1	-	-	-
48	mixed-type	42.0 ± 2.3	4.9 ± 0.2	competitive	8.5 ± 0.9

[a] K_i refers to the constants for the formation EI complex; K'_i refers to the constants for the formation ESI complex.

Fluorescence measurements

The affinity of **3** for α-Glu and α-Amy was determined spectroscopically by fluorometric titration. Tryptophan (Tyr) possesses chromophore groups responsible for the endogenous fluorescence of several proteins, including α-glucosidase and α-amylase [198]. The interaction between enzyme and substrate alters the microenvironment surrounding Trp residues resulting in a decrease in fluorescence. To elaborate on the results, α-Glu exhibited an intrinsic fluorescence emission peak at around 340 nm when excited at 295 nm. In comparison, α-Amy showed an emission peak near 345 nm under the same excitation. Obovatol did not exhibit fluorescence when it was irradiated at 295 nm, and the fluorescence spectra are reported in Supplementary materials (**Figure S181**) at the following link:

https://drive.google.com/file/d/1OxXuw5qQ0mIGLRJQivSZsiDnba253SV7/view?usp=sharing

The fluorescence spectra of α-glucosidase and α-amylase in the presence of increasing concentrations of compound **3** are depicted in **Figure 28**. These analyses were performed at three different temperatures, 298.15, 303.15, and

310.15 K, to provide information on the nature of the interaction. The addition of the neolignan reduced the fluorescence intensity of α-Glu and α-Amy, and the data obtained were elaborated following the equation (Eq. 4) detailed in **Chapter 5** (**paragraph 5.11**). The linear correlation observed in the Stern-Volmer plots, reported in **Figure 29,** indicated a singular quenching mode for both enzymes. According to the equation and from the plots, it was possible to determine the dissociation constant K_{sv} and the bimolecular quenching constant K_q. The results are collected in **Table 15**. As the studied temperature increased, the collisions increased, thus leading to higher K_{sv} values.

Consequently, the fluorescence quenching occurred through a dynamic mechanism with the consequent raising of K_{sv} values [182, 199]. The determination of the number of binding sites (n) and the binding constant (K_a) for the interaction of **3** with both enzymes were calculated using the equation (Eq. 5) reported in **Chapter 5** (**Paragraph 5.11**). The resulting values are reported in **Table 15,** and the number of sites was close to 1 in the temperature range studied, suggesting the establishment of a one-to-one complex between the fluorophore and the quencher.

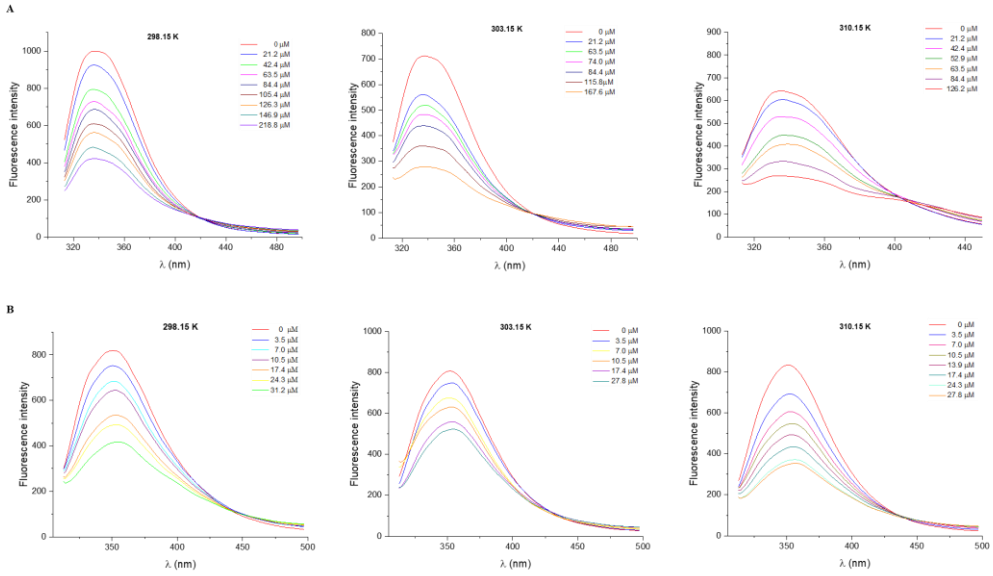

Figure 28. Changes in the intrinsic A) α-Glu and B) α-Amy fluorescence at different concentrations of **3** at different temperatures (pH 6.9, λex = 295 nm).

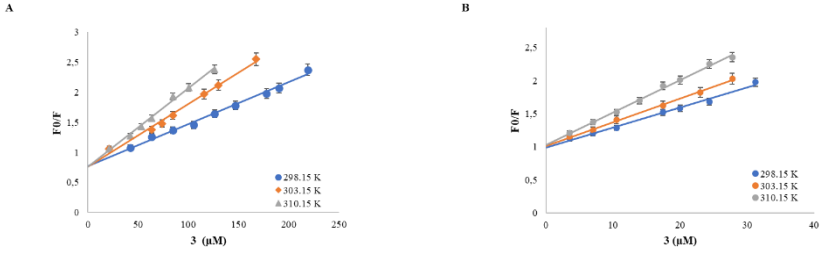

Figure 29. Stern-Volmer plots for the quenching effects of A) α-Glu and B) α-Amy with **3**.

The affinity of the inhibitor **35**, **44**, **47,** and **48** for α-Glu and **35** and **48** α-Amy was determined spectroscopically by fluorometric titration. The fluorescence spectra of α-glucosidase and α-amylase in the presence of increasing concentrations of selected analogues are depicted in **Figure 30 - 31**. The addition of the neolignans reduced the fluorescence intensity of α-glucosidase and α-amylase enzymes, and the data obtained were elaborated following the equation (Eq.4) detailed in **Chapter 5** (**paragraph 5.11**). Compound **44** exhibited an

intrinsic fluorescence in the region at 405 nm when irradiated at 295 nm (**Figure S180** supporting materials). In contrast, the other compounds didn't possess an intrinsic fluorescence in the same range. The linear correlation observed in the Stern-Volmer plots, reported in **Figure 32** – **33,** indicated a similar quenching mode for both enzymes. The dissociation constant K_{sv} and the bimolecular quenching constant K_q are collected in **Table 15**. As for obovatol, the fluorescence quenching occurred through a dynamic mechanism. The resulting values are reported in **Table 15**.

Table 15. Quenching constants K_{SV}, quenching rate constants K_q, and binding constants K_a of the interaction of obovatol and analogues (**35**, **44**, **47** and **48**) with the proper enzyme.

	T (K)	K_{sv} (× 10^4 L/mol)	K_q (× 10^{12} L/mol)	R^2	K_a (× 10^4 L/mol)	n	R^2
			α-Glu				
	298.15	0.70 ± 0.02	0.70 ± 0.02	0.9905	0.95 ± 0.04	1.11	0.9954
3	303.15	1.04 ± 0.15	1.04 ± 0.15	0.9902	1.79 ± 0.23	0.76	0.9936
	310.15	1.30 ± 0.18	1.30 ± 0.18	0.9935	2.20 ± 0.32	1.35	0.9994
	298.15	0.54 ± 0.02	0.54 ± 0.02	0.9942	0.20 ± 0.14	1.18	0.9933
35	303.15	0.70 ± 0.03	0.70 ± 0.03	0.9931	0.24 ± 0.04	1.14	0.9951
	310.15	0.84 ± 0.04	0.84 ± 0.04	0.9980	0.52 ± 0.05	1.20	0.9935
	298.15	0.81 ± 0.02	0.81 ± 0.02	0.9908	0.20 ± 0.02	1.36	0.9902
44	303.15	1.27 ± 0.45	1.27 ± 0.45	0.9929	0.35 ± 0.08	1.28	0.9902
	310.15	1.64 ± 0.38	1.64 ± 0.38	0.9989	0.50 ± 0.04	1.30	0.9926
	298.15	2.61 ± 0.25	2.61 ± 0.25	0.9976	0.99 ± 0.13	1.23	0.9965
47	303.15	2.96 ± 0.15	2.96 ± 0.15	0.9973	1.84 ± 0.24	1.11	0.9978
	310.15	3.33 ± 0.18	3.33 ± 0.18	0.9925	2.18 ± 0.31	1.11	0.9972
	298.15	1.81 ± 0.34	1.81 ± 0.34	0.9940	2.09 ± 0.44	0.96	0.9932
48	303.15	2.42 ± 0.18	2.42 ± 0.18	0.9912	3.54 ± 0.57	0.96	0.9908
	310.15	3.18 ± 0.21	3.18 ± 0.21	0.9965	3.87 ± 0.62	0.83	0.9919
			α-Amy				
	298.15	3.03 ± 0.40	3.03 ± 0.40	0.9902	3.49 ± 0.70	0.95	0.9944
3	303.15	3.62 ± 0.14	3.62 ± 0.14	0.9978	4.53 ± 0.54	0.93	0.9930
	310.15	4.89 ± 0.21	4.89 ± 0.21	0.9962	6.30 ± 0.54	0.92	0.9966
	298.15	2.95 ± 0.29	2.95 ± 0.29	0.9934	1.70± 0.12	1.14	0.9929
35	303.15	4.89 ± 0.32	4.89 ± 0.32	0.9913	2.25 ± 0.04	0.90	0.9994
	310.15	6.32 ± 0.13	6.32 ± 0.13	0.9907	6.10 ± 0.37	1.00	0.9924
	298.15	4.25 ± 0.04	4.25 ± 0.04	0.9985	3.10 ± 0.22	1.11	0.9926
48	303.15	5.75 ± 0.36	5.75 ± 0.36	0.9941	4.78 ± 0.54	1.07	0.9923
	310.15	7.20 ± 0.23	7.20 ± 0.23	0.9904	7.60 ± 0.07	0.97	0.9942

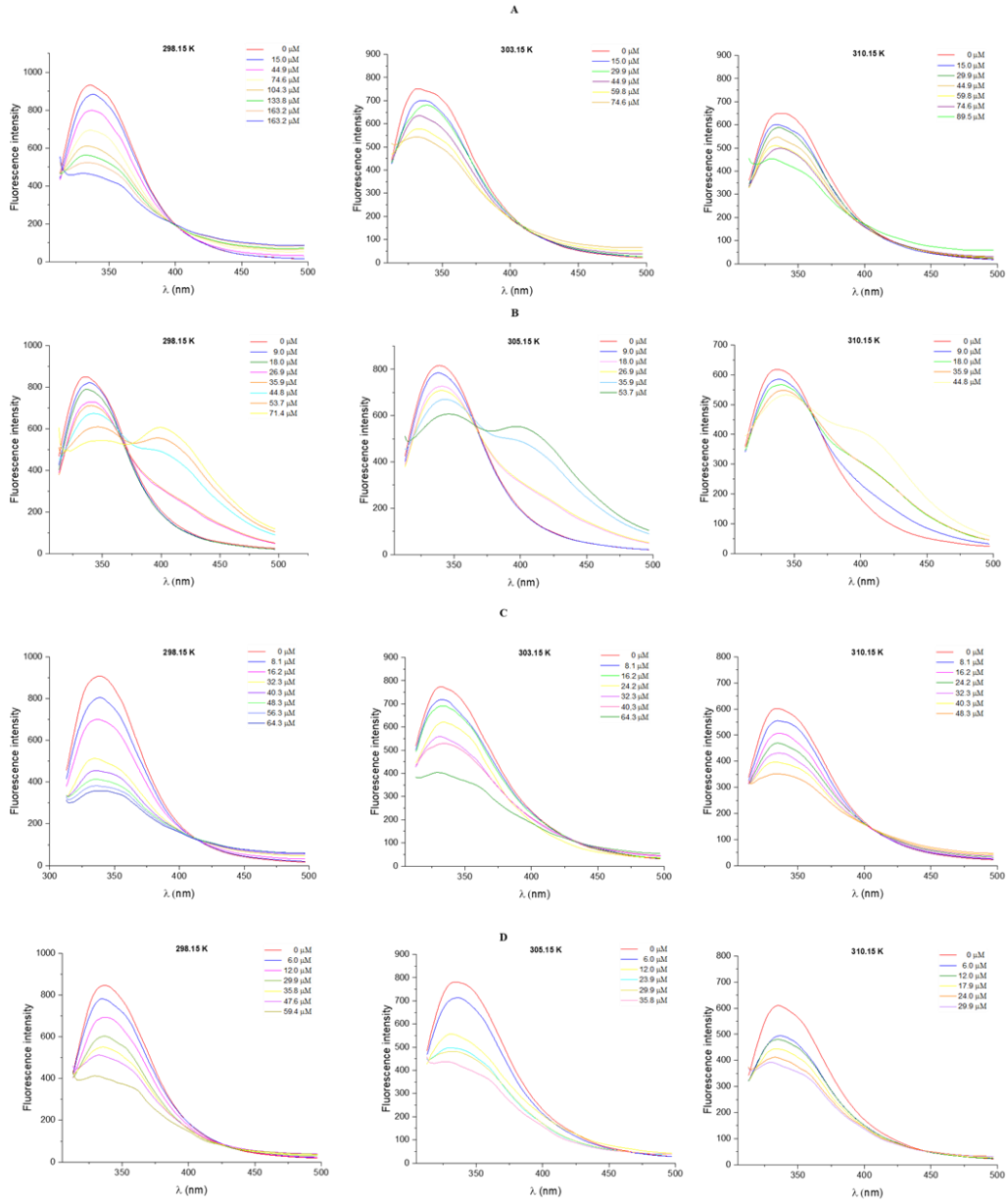

Figure 30. Changes in the intrinsic α-Glu fluorescence at different concentrations of A) **35**, B) **44**, C) **47** and D) **48** at different temperatures (pH 6.9, λ_{EXC} = 295 nm).

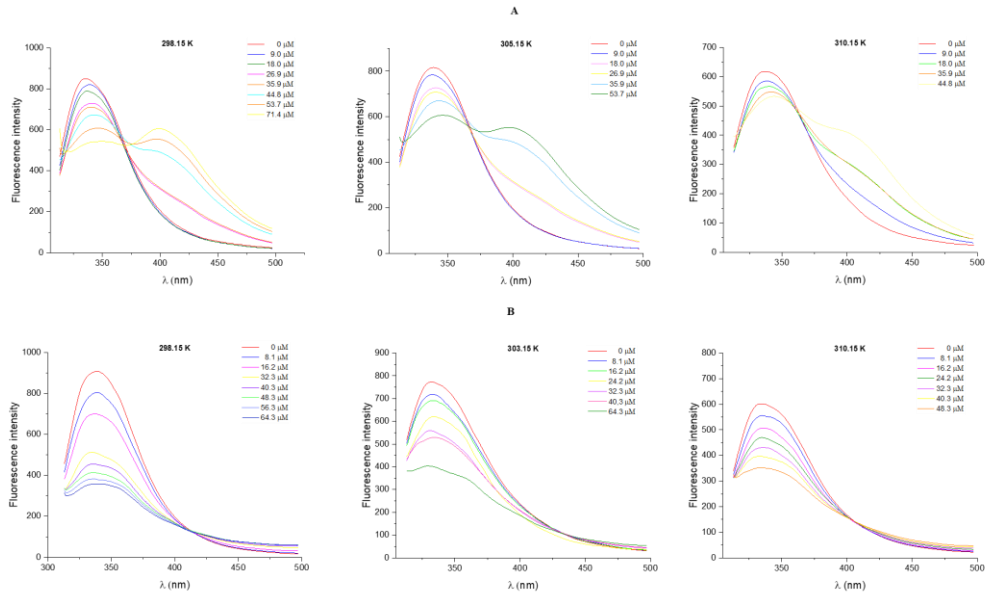

Figure 31. Changes in the intrinsic α-Amy fluorescence at different concentrations of A) **35** and B) **48** at different temperatures (pH 6.9, λ_{EXC} = 295 nm).

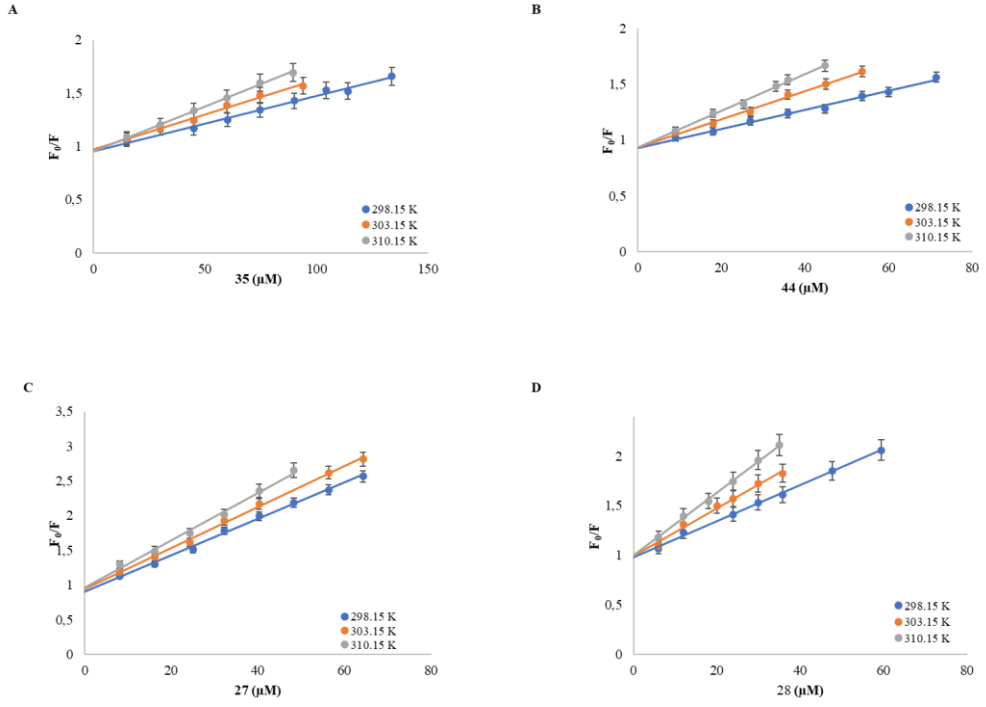

Figure 32. Stern-Volmer plots for the quenching effects of α-Glu with selected compounds A) **35**, B) **44**, C) **47**, and D) **48**.

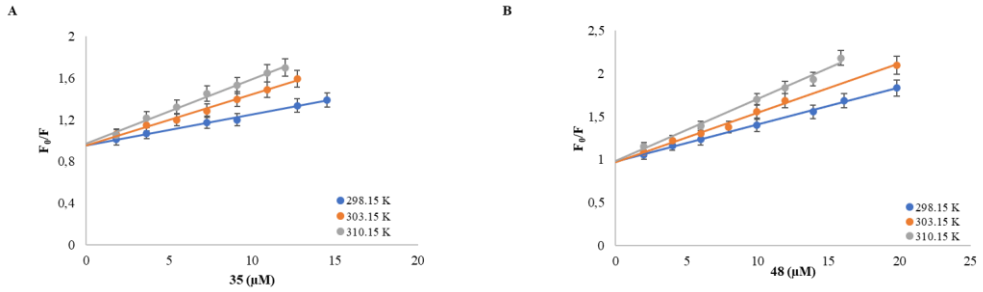

Figure 33. Stern-Volmer plots for the quenching effects of α-Amy with selected compounds A) **35** and B) **48**.

Circular dichroism

Circular dichroism (CD) spectroscopy was conducted thanks to a collaboration with Prof. Alessandro D'Urso and Dr. Gabriele Travagliante of the Department of Chemical Sciences of the University of Catania.

Circular dichroism (CD) spectroscopy is mainly used to monitor the secondary structure (α-helix, β-sheet, β-turn, and random coil) changes of proteins in solution and, more specifically, the conformational changes of a given protein in the presence of selected ligands [200, 201]. CD measurements were carried out to confirm further the interaction of **3** and the most promising analogues **35**, **44**, **47,** and **48** towards α-glucosidase, thus providing details and valuable information regarding the inhibition process. Reliable results using α-amylase have been not obtained due to the experimental conditions not being suitable for CD measures. The CD measurement of α-Glu has been carried out in the absence and presence of different aliquots of the selected compounds. ECD spectra were acquired in the 200-260 nm range and are reported in **Figure 34**.

The α-Glu seem to be arranged in α-helix structures exhibiting two negative bands (210 and 222 nm) attributable to n → π* transition for the peptide adopting the α-helix structures as reported in the literature [182, 202]. The ECD spectra of the selected compound in a buffer solution in the absence of the enzyme

were also acquired, and all compounds did not show any CD signal in the absorption region (see **Figure 34** orange line). Then, ECD spectra of the α-Glu solution with increasing amounts of neolignans were recorded (1:0; 1:1; 1:2, 1:4, 1:6). In detail, the intensity of both bands observed in the ECD spectrum of α-Glu decreases showing the loss of part of the α-helix structures as a result of the interaction between enzyme and ligands. **Figure 34** also reports the ECD difference spectra to visualize the conformational changes of α-Glu induced by the interaction with neolignans. In particular, all difference spectra show two bands: a negative band below 210 nm and a positive band centered around 225 nm (inset in **Figure 34**). These spectroscopic features are characteristic of the random coil conformation that shows a positive contribution at about 220 nm, a negative at 200 nm, a cross-over point at 210 nm. However, the positive contribution at 225 nm is also attributed to the β- turns, together with a positive signal in the 200 nm region, and the broad positive feature of the difference spectra suggests that the content of random coil and β-turns may increase after the interaction with neolignans.

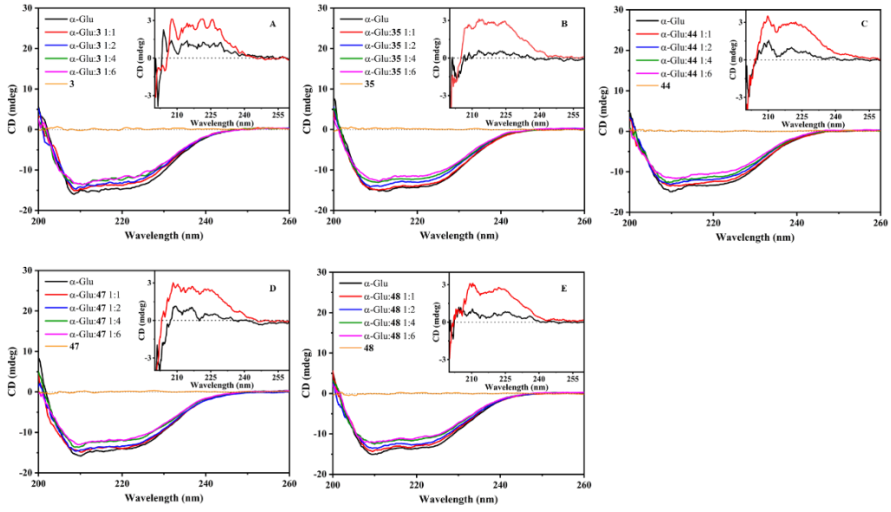

Figure 34. ECD spectra of α-Glucosidase [0.5 μM] in the presence of increasing amounts of A) **3**, B) **35**, C) **44**, D) **47** and E) **48**. Inset: ECD difference between the spectra of α-Glu:compound 1:1 minus that of α-Glu alone (black line) and α-Glu:compound 1:6 minus that of α-Glu alone (red line).

CD data were further estimated with the secondary Structure Estimation software included in the JASCO Spectra Manager software to quantify the changes in the secondary structure and the results are reported in **Table 16**.

Table 16. The secondary structure content of α-glucosidase influenced by **3**, **35**, **44**, **47** and **48**.[a]

3 (μM)	**α-helix (%)**	**β-sheet (%)**	**β-turn (%)**	**random (%)**
0	37.9	3.6	27.0	31.5
0.5	33.7	4.5	28.4	33.4
3.0	31.0	8.3	27.6	33.1
35 (μM)	**α-helix (%)**	**β-sheet (%)**	**β-turn (%)**	**random (%)**
0	38.7	9.3	22.9	29.1
0.5	34.1	9.3	24.4	32.3
3.0	31.2	13.9	22.1	32.8
44 (μM)	**α-helix (%)**	**β-sheet (%)**	**β-turn (%)**	**random (%)**
0	34.1	8.4	25.5	31.9
0.5	32.5	11.8	22.3	33.4
3.0	27.0	15.0	23.2	34.8
47 (μM)	**α-helix (%)**	**β-sheet (%)**	**β-turn (%)**	**random (%)**
0	37.7	11.7	22.5	28.1
0.5	32.7	14.7	19.7	32.9
3.0	28.9	10.1	25.6	35.4
48 (μM)	**α-helix (%)**	**β-sheet (%)**	**β-turn (%)**	**random (%)**
0	34.6	9.6	24.5	31.4
0.5	33.9	12.2	23.0	30.8
3.0	30.3	11.1	25.8	32.8

[a] ECD spectra data were elaborated with the JASCO Spectra Manager software.

According to the CD data, the interaction between the enzyme and the tested neolignans caused:

- a significant decrease of the α-helix content (from 38.7% to 27%) as increasing concentrations of inhibitors.
- an increase in random coil content (from 29.1 to 35.4%) at the highest concentrations of inhibitors.

-**3**, **35**, and **44** caused an increase in β-sheet content with the increase of the complex's ratio, while compounds **47** and **48** led to an initial increase at 1:1 ratio and a decrease at ratio 1:6.

-the β-turn content exhibited a slight increase when compounds **3**, **47,** and **48** were added, while the content showed a reduction with compounds **35** and **44**.

3.7 Inhibitory activity of oligomeric compounds towards metabolic enzymes

In the light of the IC_{50} values reported for magnolol and honokiol (**Paragraph 3.4**), the three synthesized oligomeric compounds (**52** – **54**; **Paragraph 3.3**) have been investigated for their potential metabolic enzyme inhibitory activity through *in vitro* assays, kinetic analysis, and *in silico* study. The fluorescence measurements were not carried out due to the presence of the biphenyl scaffold.

In vitro inhibitory activity

The inhibition of the pancreatic lipase, α-glucosidase, and α-amylase was assessed using established spectrophotometric methodologies previously described in **Paragraph 3.4**. The obtained IC_{50} values are reported in **Table 17**. The results were compared to the IC_{50} values of the hypoglycemic drug acarbose for α-Glu and α-Amy enzyme used as a positive control and of anti-obesity drug orlistat for PL enzyme. The inhibition results were also compared to the IC_{50} values of **1** and **2**. According to the inhibition results, the synthesized dimers showed higher IC_{50} values than the related parent compounds, being more effective inhibitors than the hypoglycemic drug (248.3 μM for α-Glu and 34.6 μM for α-Amy). In detail, the honokiol dimer **52** exhibited a significant inhibitory α-Amy inhibitory activity (10.3 μM), while its inhibition effect on PL and α-Glu was relatively moderate (respectively 65.0 μM and 80.8 μM).

Conversely, the magnolol dimer **53** displayed a strong inhibitory activity towards α-Amy and moderate activity toward α-Glu; it was also three times more active against PL (52.9 μM) than magnolol (158.7 μM). Interestingly, the mixed honokiol-magnolol dimer **54** demonstrated potent α-Amy inhibition similar to compounds **52** and **53**, but limited lipase inhibition as to **52.** The oligomer **54** was

less active (83.4 μM) against α-Glu compared to magnolol (47.1 μM) while displaying moderate activity compared to honokiol (121.2 μM).

Based on the above-obtained results, the magnolol dimer **53** was a more effective inhibitor for all three enzymes than the corresponding natural product and the related synthesized oligomers. For this reason, it was selected for additional investigation of its inhibitory activity effects through docking studies and kinetic analysis.

Table 17. Inhibitory activity (IC_{50}) of **1**, **2** and synthesized dimers towards PL, α-Amy and α-Glu.

ID	PL [a] IC_{50} ± SD	α-Amy [a] IC_{50} ± SD	α-Glu [a] IC_{50} ± SD
1	158.7 ± 5.1	24.0 ± 2.7	47.1 ± 2.9
2	115.5 ± 9.0	44.3 ± 3.9	121.3 ± 5.5
52	65.0 ± 2.0	10.3 ± 1.6	80.8 ± 1.2
53	52.9 ± 3.0	8.0 ± 0.6	33.4 ± 1.9
54	85.8 ± 1.4	9.1 ± 0.4	83.4 ± 9.2
orlistat	0.9 ± 0.1	-	-
acarbose	-	34.6 ± 0.9	248.3 ± 2.3

[a] Results are expressed in μM. IC_{50} is the concentration required to inhibit 50% of enzyme activity. The IC_{50} values are mean ± SD (n = 3).

The dimers **52**, **53,** and **54** were also subjected to ADME evaluation on the [186]. The results are reported in Supplementary materials (**Figure S202 - 204**) at the following link:

https://drive.google.com/file/d/1OxXuw5qQ0mIGLRJQivSZsiDnba253SV7/view?usp=sharing

The three dimers exhibited a computational TPSA of less than 140 Angstroms squared [$Å^2$] (80.92 $Å^2$), thus showing computational moderate skin permeation and cytochrome P450 1A2 and 2D6 inhibition.

Molecular docking analysis

The molecular docking studies were conducted thanks to a collaboration with Dr. Luana Pulvirenti of the ICB-CNR of Catania.

The key interacting residues in the binding site of PL were previously reported in **Paragraph 3.5** [181]. All the ligands were well accommodated into the binding pocket, occupying almost the same spatial portion. The calculated binding energies (Kcal/mol) listed in **Table 18** suggest a good affinity for inhibitors. All the synthetic analogues (**52**, **53,** and **54**) showed good binding energies toward the pancreatic lipase catalytic site (from -6.02 to -7.35 Kcal/mol) than the two natural products (**1**: -5.72; **2**: -6.69). The magnolol dimer **53**, exhibited the most significant binding energy (-7.35 Kcal/mol), in good agreement with the *in vitro* inhibition results (**Paragraph 3.7**). The list of molecular interactions for each analysed compound, obtained by the visual inspection of docked conformation, is reported in **Table 18**.

Table 18. Binding Energies (ΔG_{bind}) and list of molecular interaction and interacting residues of magnolol (**1**), honokiol (**2**), and derivatives **52** – **54** with PL Catalytic Site.

Ligands	[a] Glide calcd ΔG_{bind}	Interacting residues	Interaction	Binding Glide distance (Å)
1				
OH (ring A)	-5.72	Phe77	H - bond	-
B-ring		Phe77	π - π stacking	-
OH (B-ring)		His151	Salt bridge	-
2				
OH (ring A)	-6.69	Phe77	H - bond	-
B-ring		Phe77	π - π stacking	-
52				
A ring	-6.02	Tyr114	π - π stacking	-
OH (D ring)		Asp79	H - bond	-
53				
A ring	-7.35	Tyr114	π - π stacking	-
OH (D ring)		Asp79	H - bond	-
54				
OH (D ring)	-6.18	Asp79	H - bond	-
orlistat				
	-3.45	His263	H-acceptor	2.6

[a] The ΔG_{bind} values were calculated with Glide and are expressed as Kcal/mol.

The docking analysis of **1** and **2** showed a stabilization into the hydrophobic pocket of PL originated by the formation of a hydrogen bond between the hydroxyl group of ring A and Phe77, and a π-π interaction between the B-ring and Phe77. The magnolol also appeared to be stabilized by a salt bridge between the hydroxyl group of ring B and His151. Similar to the natural products, the dimeric compounds **52** – **54** were stabilized in the PL pocket thanks to the formation of hydrogen bonds between the OH present in the ring D and Asp79. A π-π interaction between the B-ring and Tyr114 also stabilized the ligands **53** and **54**. Furthermore, the dimers would appear to be stabilized by a hydrophobic portion (Tyr114, Pro180, Ala178, Ile209, Phe215, Leu213, and Leu153) near the allylic chain of the A-ring. The 2D interaction diagrams of the anti-obesity drug (**orlistat**), magnolol (**1**) and the promising magnolol dimer **53** are reported in **Figure 35.** The 3D interaction of dimer **53** are reported in Supplementary materials (**Figure S208**).

The composition of the α-Glu and α-Amy binding sites were previously reported in **Paragraph 3.6** [195]. The *in silico* data for α-Glu and α-Amy are listed in **Tables 19** and **20**. The results obtained for α-Glu highlighted the higher binding energy values of the synthesized oligomeric compounds (from -6.03 to 6.79 Kcal/mol) than the natural neolignans **1** (-5.02 Kcal/mol) and **2** (-5.48 Kcal/mol). The binding energies of dimers were also lower than the hypoglycemic drug acarbose (-7.09 Kcal/mol). The *in silico* data for α-Amy enzyme showed **53** (-6.10 Kcal/mol) as the most active compound according to the in vitro assay results. The dimer **52** exhibited less binding energy (-5.43 Kcal/mol) than the related natural product **1** (-5.46 Kcal/mol). In comparison, **53** had moderate binding energy (-5.19 Kcal/mol) than the related parent compounds **1** (-5.46 Kcal/mol and **2** (-5.44 Kcal/mol). The synthetic dimer and the natural products were less active than acarbose (-8.33 Kcal/mol). The list of molecular interactions for each analyzed compound, obtained by visually inspecting docked conformation, is reported in **Tables 19** and **20**.

The analysis of the docked poses showed the main interacting residues that can stabilize the complex between each neolignan and the two enzymes. Non-covalent interactions were established with Pro309, Glu 304, Asp349, Arg312, Thr307, Asp408, Ser239 and Glu304 for α-Glu, while the interactions for α-Amy were established with Thr163, Gln63, Asp 300, Glu233, Tyr62, Trp59 and Asp300.

The docking analysis of neolignans also showed a stabilization into the binding pocket of α-Glu, originated by the formation of a π-π interaction and π-cation interaction. In detail, **52** was stabilized by the π-π interaction between Phe157 and A-ring, Hie239 and C-ring, Phe231 and D-ring and by π-cation interaction between Hip279 and C-rings. The honokiol dimer was also stabilized by a hydrophobic portion (Ala278, Pro309, Phe310, and Phe231) near the allylic chain of the C-ring. Magnolol dimer **53** appeared to be stabilized thanks to the π-π interaction between Phe300 and A-ring and π-cation interaction of Arg312 and

B- ring. The polar portion of the enzyme (Tyr215, Hie245, Asn241, Hie239, Ser308 and Thr307) was also important to stabilize the dimers near the allylic chain of the A and D-ring. The oligomer **54** was stabilized by the π-cation and π-π interaction of A-ring and Arg312, Hie239 and B- rings, respectively. As honokiol dimer, compound **54** was more stable thanks to the hydrophobic portion (Ala278, Leu218, Phe300, and Phe77) near the allylic chain of the A-ring.

The docking analysis of neolignans also showed a stabilization into the binding pocket of α-Amy, originating by the formation of a π-π interaction and π-cation interaction. In details, **52** was stabilized by the interaction between the Trp59 and B-ring, while the π-π interaction between Hip305 and D-ring stabilized **53**. All synthesized dimers also seemed to be stabilized by a hydrophobic portion near the allylic chain of the aromatic ring (**52**: Tyr151 and A-ring; **53**: Tyr62, Leu162, Trp28, Trp59, and C-ring; **54**: Tyr151, Leu237, Ile235, Val234 with B and C-ring). The 2D interaction diagrams of **acarbose**, magnolol (**1**), and the promising magnolol dimer **53** are reported in **Figures 36** and **37.**

Table 19. Binding Energies (ΔG_{bind}) and list of molecular interaction and interacting residues of magnolol (**1**), honokiol (**2**), and derivatives **52** – **54** with the α-Glu catalytic site.

Ligands	[a] Glide calcd ΔG_{bind}	Interacting residues	Interaction	Binding Glide distance (Å))
1				
OH (A-ring)	-5.02	Glu304	H - bond	-
A-ring		Arg312	π - cation	-
B-ring		Phe300	π - π stacking	-
B-ring		Phe157	π - π stacking	-
2				
OH (A-ring)	-5.48	Asp349	H - bond	-
A-ring		Phe157	π - π stacking	-
A-ring		Phe300	π - π stacking	-
OH (B-ring)		Asp408	H - bond	-
B-ring		312	π - cation	-
52				
A-ring	-6.79	Phe157	π - π stacking	-
OH (B-ring)		Pro309	H - bond	-
OH (C-ring)		Glu304	H - bond	-
C-ring		Hip279	π - cation	-
C-ring		Hie239	π - π stacking	-
OH (D-ring)		Pro309	H - bond	-
D-ring		Phe231	π - π stacking	-
53				
OH (A-ring)	-6.03	Asp349	H - bond	-
A-ring		Phe300	π - π stacking	-
B-ring		Arg312	π - cation	-
OH (C-ring)		Arg312	H - bond	-
OH (D-ring)		Thr307	H - bond	-
54				
OH (A-ring)	-6.33	Asp408	H - bond	-
A-ring		Arg312	π - cation	-
B-ring		Hie239	π - π stacking	-
OH (C-ring)		Thr307	H - bond	-
OH (D-ring)		Ser239	H - bond	-
acarbose				
	-7.09	Glu304		-
		Thr307		
		Ser308		
		Arg312		
		Phe157		
		Asp408		
		Asp349		

[a] The ΔG_{bind} values were calculated with Glide and are expressed as Kcal/mol.

Table 20. Binding Energies (ΔG_{bind}) and list of molecular interaction and interacting residues of magnolol (**1**), honokiol (**2**), and derivatives **52** – **54** with the α-Amy catalytic site.

Ligands	[a] Glide calcd ΔG_{bind}	Interacting residues	Interaction	Binding Glide distance (Å)
1				
OH (A-ring)	-5.46	Trp59	H - bond	
B-ring		Trp59	π - π stacking	
2				
OH (ring A)	-5.44	Asp300	H - bond	
A-ring		Trp59	π - π stacking	
OH (B-ring)		Glu233	H - bond	
B-ring		Tyr62	π - π stacking	
52				
OH (A ring)	-5.43	Thr163	H - bond	
B ring		Trp59	π - π stacking	-
OH (C ring)		Gln63	H - bond	
OH (D ring)		Asp300	H - bond	
53				
OH (A ring)	-6.10	Thr163	H - bond	
D ring		Hip305	π - π stacking	-
54				
OH (B ring)	-5.19	Glu233	H - bond	
OH (D ring)		Tyr62	H - bond	-
acarbose				
	-8.33	Glu240		
		Glu233		
		Trp59		
		Gln63		
		His201		
		Lys200		

[a] The ΔG_{bind} values were calculated with Glide and are expressed as Kcal/mol.

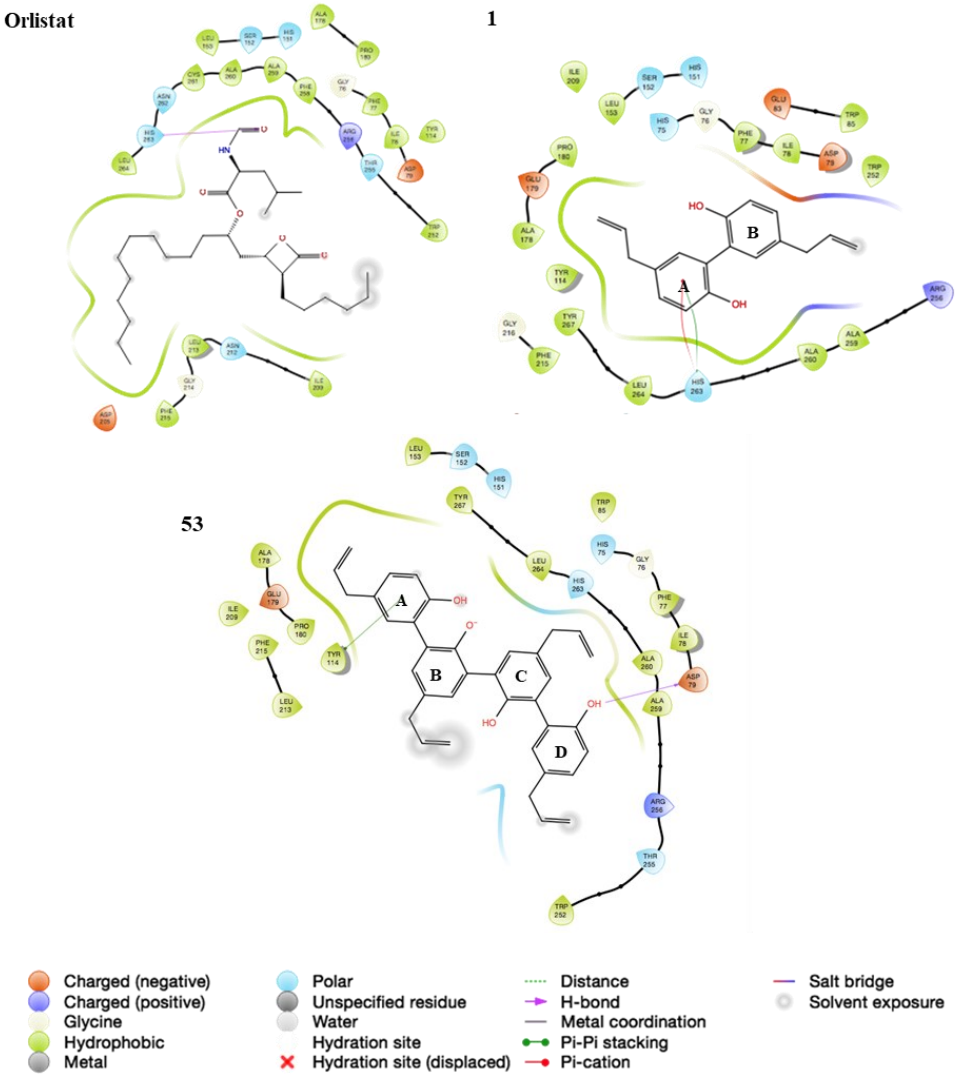

Figure 35. 2D interaction diagrams of **orlistat**, **1**, and **53** with PL.

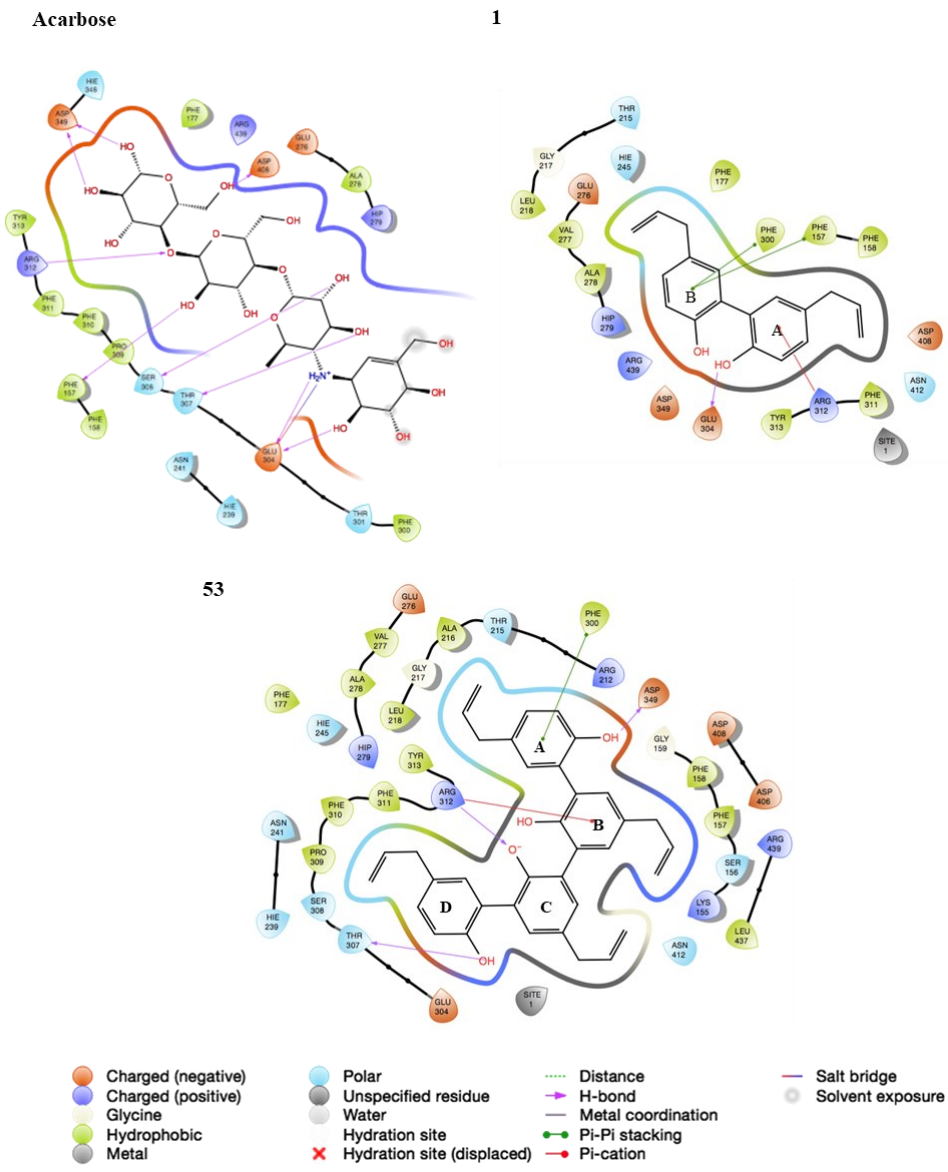

Figure 36. 2D interaction diagrams of **acarbose**, **1**, and **53** with α-Glu.

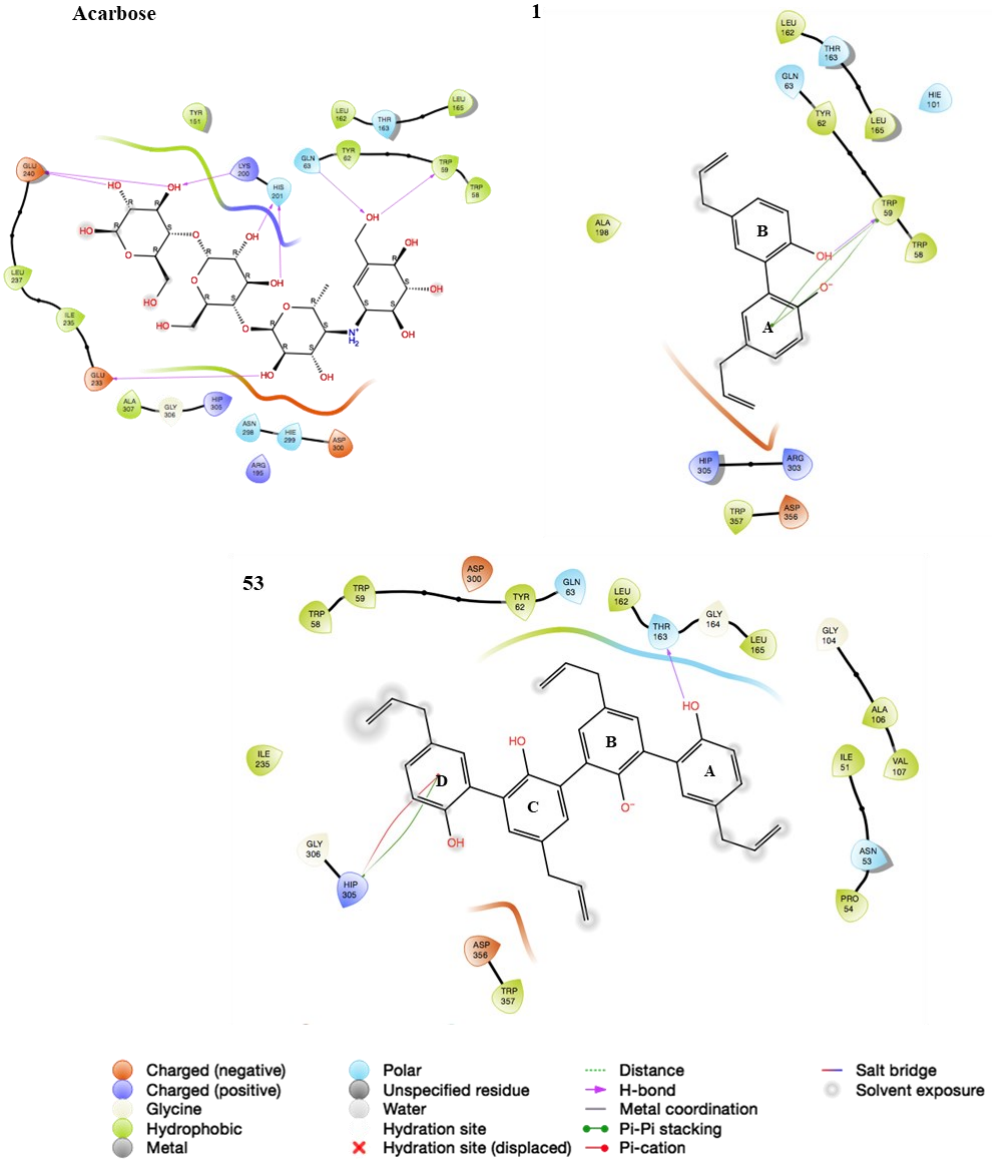

Figure 37. 2D interaction diagrams of **acarbose**, **1**, and **53** with α-Amy.

Kinetic of inhibition

The mode of inhibition of the magnolol dimer **53**, the most promising oligomer targeting pancreatic lipase, α-glucosidase, and α-amylase was explored using UV spectroscopy, and the kinetic data were elaborated as described before. The kinetic results are reported in **Tables 21**. The mode of α-Glu inhibition of magnolol has already been reported in the literature, exhibiting a mixed-type inhibition [185]. On the other hand, the mode of α-Amy inhibition of **1** is not reported and thus, it was also investigated. In contrast, the PL of inhibition mechanisms of **1** has already been investigated in **Paragraph 3.5** (mixed-type inhibition).

In detail, **1** exhibited a competitive mode of inhibition toward α-Amy with the K_i values of 11.6 μM (**Table 21**). The L-B plot of α-Amy inhibition in the presence of **1** is reported in **Figure 38,** while dimer **53** acted as a non-competitive α-amylase inhibitor (**Figure 39**) with K_i values of 21.6 μM (**Table 21**). The secondary plots of the L-B plot are reported in Supplementary materials (**Figure S209)** at the following link:
https://drive.google.com/file/d/1OxXuw5qQ0mIGLRJQivSZsiDnba253SV7/view?usp=sharing

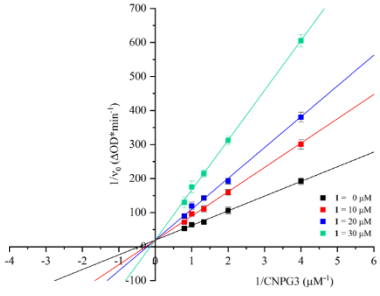

Figure 38. Lineweaver-Burk plots of **1** with α-Amy

Unlike magnolol**, 53** acted as PL uncompetitive inhibitor, binding not the free enzyme but the enzyme-substrate complex. The inhibitor does not compete with the substrate for the same binding site, and the value of both K_m and V_{max} result altered, but a distinctive kinetic pattern emerges under steady-state conditions. The L-B plot for an uncompetitive inhibitor produces a line parallel to the original enzymes-substrate plot but with a higher y-intercept rather than intersecting lines.

Conversely, **53** exhibited a competitive α-glucosidase inhibition mode with K_i values of 17.0 μM. The L-B plots of the three enzymes in the presence of **53** are reported in **Figure 39**, while the secondary plots of the L-B plot are reported in Supplementary materials (**Figure S210)** at the following link: https://drive.google.com/file/d/1OxXuw5qQ0mIGLRJQivSZsiDnba253SV7/view?usp=sharing

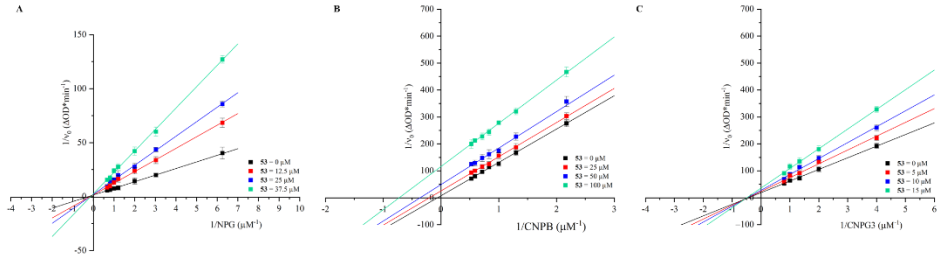

Figure 39. Lineweaver-Burk plots of A) **53** with α-Glu, B) with PL, and C) with α-Amy.

Table 21. Kinetic parameters for lipase, α-glucosidase and α-amylase inhibition with **1** and **53**.[a]

ID	PL			α-Glu		α-Amy	
	Type of inhibition	**K_i ± SD (μM)**	**K_i' ±SD (μM)**	**Type of inhibition**	**K_i ± SD (μM)**	**Type of inhibition**	**K_i ± SD (μM)**
1	mixed-type	614.3 ± 19.1	140.9 ± 8.6			competitive	11.6 ± 0.35
53	uncompetitive	10.9 ± 1.1		competitive	17.0 ± 0.9	non-competitive	21.6 ± 2.0

[a]K_i refers to the constants for the formation EI complex; K'_i refers to the constants for the formation ESI complex.

3.8 Additional screening

This Ph.D. project evaluated the inhibition of metabolic enzymes of new synthesized compounds. However, as highlighted in the Introduction, natural compounds and their analogues, could potentially exhibit many biological effects. For this reason, these compounds are under evaluation for other possible biological activities through ongoing collaboration.

The synthesized compounds are under evaluation in the frame of an agreement with EU-OPENSCREEN ERIC, a globally operating non-profit research infrastructure based in Berlin (Germany). The compounds will be profiled in a panel of about twenty assays, delivering extensive information on physical-chemical, cellular toxicity, and antimicrobial properties.

In addition, they will be studied as potential herbicides, fungicides, and insecticides in the frame of an agreement with the Open Innovation Platform Agro by BASF-SE (Ludwigshafen, Germany).

Moreover, the three libraries of new compounds will be evaluated in the frame of the COST Action CA21145, the European network for diagnosis and treatment of antibiotic-resistant bacterial infections (EURESTOP), a funding agency for research and innovation networks, for antibiotic-resistant bacterial infections.

Chapter 4

Conclusion and perspective

Natural products have long been considered a source of inspiration for developing new drugs thanks to their biological and therapeutical properties. In recent years, there has been renewed attention towards natural compounds, leading to the discovery of new lead compounds and related bioinspired molecules obtained through chemical modification or a total chemical synthesis.

My research project was developed within this scenario to discover new bioinspired enzymatic inhibitors of pancreatic lipase and α-glucosidase and α-amylase as potential anti-obesity or hypoglycaemic scaffolds starting from natural polyphenols. During my Ph.D. research project, I focused my activity on a specific class of polyphenolic compounds, namely neolignan. Mainly, my attention was dedicated to three natural compounds, magnolol (**1**), honokiol (**2**), and obovatol (**3**) (**Figure 7**, **Chapter 1**). Magnolol and honokiol are two bisphenolic neolignans extensively investigated for their wide range of biological effects, while obovatol, which features a biphenyl ether linkage, has received much less attention.

4.1 Nitrogenated analogues inspired by magnolol and honokiol as pancreatic lipase inhibitors

The first group of polyphenols included in these studies was related to the neolignans magnolol (**1**) and honokiol (**2**), naturally occurred from *Magnolia* species and cited mainly in the literature for a wide range of biological activities as well as antitumoral, antioxidant, anti-obesity and antidiabetic properties. Numerous works have demonstrated how the chemical modification of **1** and **2** can lead to synthesizing new molecules with biological activity higher than the natural leads. The above-cited biological features prompted us to synthesize new

honokiol and magnolol analogues, particularly nitrogenated analogues as potential pancreatic lipase inhibitors.

The project's initial phase was dedicated to the chemical synthesis of twenty-one nitrogenated analogues following an efficient synthetic strategy based on four steps. Specifically, the first step involved the borylation of phenol to synthesize arylboronate, giving two pinacol boronic esters (**4a** and **4b**) with 98% yield. The second step was dedicated to optimizing Suzuki-Miyaura reaction conditions varying catalyst, ligand, solvent, and reaction temperature (see **Chapter 3**, **Paragraph 3.1**). SM cross-coupling reaction was employed between pinacol boronic ester and aryl bromide containing amine or nitro group (**5a** – **5c**) to afford new diphenyl compounds (**6** – **9**) and **10** with a yield between 70 – 97%. The subsequent two steps were an allylation reaction to insert the allyl chain onto the biphenyl core, obtaining *O* and/or *N*-allyl derivatives (**11a** – **15**) with 9.2 – 82.6%yield, followed by a Claisen rearrangement to give the *ortho*-allyl derivatives (**16a** – **18c**) with 25 – 72%yield.

According to the inhibition results on other nitrogenated compounds reported in the literature, the synthesized nitrogenated analogues (**6** – **18c**) inspired by magnolol and honokiol have been evaluated for their inhibitory activity towards PL. This research describes a detailed investigation of the PL inhibitory activity of honokiol considered a suitable candidate for the treatment of obesity but lacking a deep *in vitro* analysis of the inhibition mechanism. The study was consequently extended to magnolol in light of their structural similarity.

The studies on the natural compounds and their analogues were conducted through *in vitro* assays, kinetic, and molecular docking analyses. Due to the peculiar structure of the biphenyls structure, fluorescence quenching measurements were not obtained.

According to the inhibition results, it is interesting to underline how the structure modification might affect the inhibitory activity. All synthesized biphenyls (**6** – **10**) were inactive or weak pancreatic lipase inhibitors. In contrast,

adding allyl chains increased the PL inhibitory activity from biphenyl to the corresponding *O*-allyl derivative with free NH_2 and the *C*-allyl derivative with free OH and NH_2. Neolignans **16b**, **17,** and **18b** were the most promising PL inhibitors with IC_{50} value <45 μM. These compounds possess free OH groups and the allyl chain in the *ortho* position to a phenolic group, a typical structural feature of honokiol (**2**).

Thanks to a collaboration, molecular docking analyses were also carried out to define the affinity for the PL catalytic site of **1**, **2,** and the new nitrogenated analogues. The docking results showed that all ligands are well located in the binding pocket, occupying almost the same spatial portion. The analysis of docked poses highlighted the main interacting residues that can stabilize the complex between each compound and the enzyme. Moreover, the allyl chain in *ortho* to the OH seemed necessary. Thus, this study suggested that biphenyl **16b**, **17,** and **18b** were among the most active ligands for PL. These biphenyls were selected for a deeper investigation of their PL inhibitors activity together with **1** and **2**.

As reported in Lineweaver-Burk plots, the neolignans showed different modes of PL inhibition despite their similar structure: **1**, **16b,** and **17** were mixed-type inhibitors, while **2** and **18b** were competitive inhibitors. The kinetic results were also in agreement with the inhibition data.

The above results highlighted how the proposed structures share promising structural features for developing new pancreatic lipase inhibitors.

The importance of this work lies in the high-yield synthetic strategy employed to achieve new biphenyls. Optimizing SM cross-coupling conditions to find high-yielding biphenyl structures inspired by natural products is one of the key topics for organic synthetic chemistry. For this reason, this approach can be of reference value for addressing this challenge. Moreover, up to date, few structures containing nitrogen atoms have been reported with a biphenyl core despite their biological properties.

4.2 Obovatol and its analogues as α-glucosidase and α-amylase inhibitors

The second group of neolignans included in these studies was related to the obovatol (**3**), a biaryl ether compound extracted from the *Magnolia obovata* trees. Previous studies have shown different biological properties of obovatol, including antioxidant, neuroprotective, antibacterial, and anti-inflammatory activities. This part of my Ph.D. project aimed to establish an efficient synthetic approach to synthesize obovatol and a small library of its analogues as new potential α-glucosidase and α-amylase inhibitors.

Several attempts to obtain **3** were carried out. The synthetic strategy employed to achieve the desired product was based on five steps starting from the commercially available phenol (**25**): i) allylation reaction to insert the allyl chain, ii) Claisen-Cope rearrangement to give the *para*-allyl derivative; iii) methylation reaction to protect both hydroxyl group; iv) Ullmann coupling and v) subsequent demethylation. Thanks to this strategy, it was possible to synthesize the natural product **3** with an overall of 15%. Other synthetic attempts have been employed to increase the reaction yield and decrease the number of steps and the waste amount. Unfortunately, a more sustainable and cost-effective synthetic route has been studied to achieve the synthesis of obovatol in *one-pot* strategy without any results (see **Chapter 3**, **Paragraph 3.2**). However, *one-pot* synthesis was exploited to synthesize two new thioether obovatol analogues (**47** – **48**) with 35 – 45% yield. Two new analogues (**34** and **35**) were obtained, modifying the reaction condition of the demethylation reaction, respectively with 18% and 10% yield overall. The synthetic strategy used for obtaining **3** also contributed to synthesizing a variety of obovatol analogues. Significantly, five new compounds (**36**, **37**, **39**, **41**, **44**) have been achieved by modifying the starting reagents of Ullmann condensation with a reaction yield between 20 – 94%.

A total of ten analogues (**30**, **34** – **37**, **39**, **41**, **44**, **47**, **48**) have been synthesized, exhibiting a wide range of functional groups (methoxy, bromine, carboxyl and formyl group) and moiety (thioether derivatives). In light of the previous finding reported in the literature, obovatol and its analogues have been evaluated as α-glucosidase and α-amylase inhibitors. The studies were conducted through *in vitro* assays, kinetic and molecular docking analyses, fluorescence quenching measurements, and circular dichroism studies. For the first time, a detailed evaluation of α-Glu and α-Amy activity was reported for the obovatol, and according to the inhibition data, it was twice active as an α-Glu inhibitor (124.6 μM) and a slightly better α-Amy inhibitor (24.6 μM) than acarbose (248.3 μM and 34.6 μM, respectively). Moreover, an investigation on the obovatol analogues showed that most of the new neolignans were more active toward the inhibition of α-Glu (39.6 – 97.7 μM) and of α-Amy (6.2 – 17.6 μM) than **1** and far more potent than acarbose. Among these, **35**, **44**, **47,** and **48** were more effective inhibitors of α-Glu, while **35** and **48** were potential inhibitors of α-Amy.

To rationalize the results of the enzymatic inhibition, **3** and the newly synthesized analogues were *in silico* evaluated for their affinity for the α-Glu or α-Amy catalytic sites through a molecular docking analysis. The *in silico* data for the α-Glu or α-Amy suggested a good interaction of obovatol and its analogues with both biological counterparts, and the results agreed with the *in vitro* inhibition results. Significantly, the most active compounds toward the inhibition of α-Glu were **35**, **47,** and **28**. In contrast, the most effective compounds toward the inhibition of α-Amy were **35** and **28,** according to the in vitro assay results. These biaryl ether compounds were selected for a deeper investigation of their α-Glu and α-Amy inhibitors activity together with **3**.

As reported in Lineweaver-Burk plots (**Chapter 3**, **Paragraph 3.6**), the neolignans showed different modes of α-Glu inhibition despite having very similar scaffolds: **3**, **35,** and **47** were non-competitive inhibitors, while **44** and **48** were mixed-type inhibitors. The kinetic results were also in agreement with the

inhibition data. The α-amylase inhibition occurred with a competitive inhibition mode for each compound.

Fluorescence experiments also investigated the interaction between the selected compound and α-Glu or α-Amy. The obovatol and the promising molecules did not exhibit fluorescence when irradiated at 295 nm. As reported in the fluorescence spectra (**Chapter 3**, **Paragraph 3.6**), the fluorescence intensity decreased as the inhibitor concentration increased, confirming the interaction. The fluorescence quenching occurred through a dynamic mechanism, and the number of the binding sites was near one concerning the two enzymes. The fluorescence results were also in good agreement with the inhibition data.

Finally, circular dichroism spectroscopy was carried out to confirm further the interaction of **3** and the most promising analogues **35**, **44**, **47,** and **48** towards α-glucosidase. The ECD spectra of the α-Glu solution with increasing amounts of neolignans suggested the conformational changes (α-helix, β- turns, and random coil content) of α-Glu induced by the interaction with neolignans.

The above results highlighted how the proposed structures could be considered interesting candidates for future studies to develop more effective α-glucosidase and α-amylase inhibitors.

This thesis reports an efficient synthetic strategy based on the Ullman coupling reaction to obtain obovatol and a small library of novel neolignans. For the first time, a detailed evaluation of α-glucosidase and α-amylase activity was reported here for the obovatol. These studies showed that the obovatol and the new analogues synthesized **35**, **44**, **47,** and **48** have promising structural features as acarbose-like potential drugs for developing hypoglycaemic agents. *In silico* studies highlighted how the free hydroxyl groups' combined effect and bromine's presence contribute to enhancing the ether neolignan's inhibitory activity and the thioether derivative. Conversely, the presence of allyl chains on biphenyl structure seems not relevant for inhibitory activity.

The value of this work lies in the efficient synthesis of obovatol involving the construction of the basic skeleton of the target molecule by a coupling reaction. Moreover, evaluating new structures inspired by natural products is one of the main subjects for synthetic organic chemistry in light of developing new scaffolds for managing type-2 diabetes.

4.3 Dimeric compounds as metabolic enzyme inhibitors

The phytochemical studies of the *Magnolia* content also provided different oligomeric compounds linked through aromatic rings. These compounds were isolated from various *Magnolia* trees (roots, bark, and leaves), though their extraction yields are pretty low (< 0.1%) and require several purification steps. As a result, a limited number of studies have been focused on their biological studies, with a few showing their anti-inflammatory, antioxidant, and antitumor activity. Consequently, the last part of my Ph.D. research project was devoted to the synthesis of honokiol dimer known as houpulin B and its evaluation of the inhibition towards metabolic enzymes. In addition, two new oligomers not naturally occurring, a magnolol dimer and a mixture of a honokiol-magnolol dimer, were also synthesized and evaluated.

Several attempts were conducted to synthesize the desired product. At first, the synthesis was carried out using a chemical catalyst and non-green reaction conditions. The Ag_2O-mediated reaction gave the desired product **52** with 32% yield. Additional synthetic attempts have increased the reaction yield and minimized waste. Significantly, the new reactions were performed by modifying the reaction condition by using an enzyme as a catalyst, solvent (organic solvent, or in biphasic solvent reactions, or aqueous solvents), and chemical mediator (see **Chapter 3**, **Paragraph 3.3**). The desired product was obtained using only an aqueous solvent without the employment of any mediator and organic solvent, however, resulting in a lower reaction yield (13.4 %). The optimized reaction

conditions were also employed to synthesize two oligomers that do not naturally occur: magnolol dimer **53** and a mixture of honokiol-magnolol dimer **54**. The new oligomers **53** and **54** have been achieved, respectively, with 33% and 30% reaction yield using the Ag_2O-mediated reaction with 13% and 10% yield using the enzymatic reaction. The two biomimetic reactions gave the natural product **52** and two new dimeric compounds **53** and **54**.

An investigation on the inhibitory activity of the oligomeric product (**52** – **54**) showed that each compound exhibited higher inhibitory activity (IC_{50} values of 33.4 – 83.4 μM for α-Glu; 8.0 – 10.3 μM for α-Amy) than the related natural lead **1** and **2** and far more potent than the hypoglycemic acarbose (248.3 μM for α-Glu and 34.6 μM for α-Amy). The dimer **52** and **53** were also twice active lipase inhibitors (respectively 52.9 μM and 65.0 μM) than the magnolol (158.7 μM) and honokiol (115.5 μM), while **54** exhibited a moderate PL activity (85.8 μM).

A collaboration for molecular docking analysis was also carried out to define the affinity for the PL, α- Glu, and α-Amy catalytic sites of **1**, **2**, and the oligomers **52** – **54**. The docking analysis of neolignans also showed a stabilization into the binding pocket of PL, α- Glu, and α-Amy, originating from the formation of a hydrogen bond, π-π interaction, and π-cation interaction. All synthesized dimers also seemed to stabilize by a hydrophobic portion near the allylic chain of the aromatic ring. The docking results agreed with the inhibition data, so **53** was selected for additional investigation of its inhibitory activity effects kinetic analysis.

The mode of enzymatic inhibition of **53** occurred with different mechanisms: uncompetitive for PL inhibition, competitive for α- Glu, and non-competitive for α-Amy inhibition. The kinetic data also confirmed the previous data and showed how these oligomeric compounds could enhance the natural lead's inhibition properties.

This work has enabled the synthesis of the natural compound houpulin B with improved yields, and the biological studies related to it. Notably, the

inhibitory activity of this natural product towards pancreatic lipase, α-glucosidase and α-amylase was assessed for the first time. Through the optimized biomimetic reactions, two novel non-natural dimers, magnolol-magnolol (**53**) and magnolol-honokiol (**54**), were obtained and evaluated as potential metabolic enzyme inhibitors. The synthesis of magnolol-magnolol dimer (**53**), exhibiting a promising inhibitory activity against the three enzymes, could be of interest in controlling post-prandial hyperglycemia and hyperlipidemia, thus managing type 2 diabetes and obesity. This research contributes to the development of new metabolic enzyme inhibitors, considering these compounds as interesting scaffolds for future studies.

Final comments

In conclusion, this thesis reports on the biological evaluation of pancreatic lipase, α-glucosidase and α-amylase inhibition of the three natural products, magnolol, honokiol, and obovatol, (**1** – **3**) and their bioinspired compounds (nitrogenated analogues, biaryl or thiol ether compounds, and oligomeric products).

The results highlighted the natural products as potential "*natural leads*", and their structural optimization might enhance their biological effects towards the selected enzymes. Based on the data, the proposed scaffolds could be considered interesting candidates for future studies to afford new potential structures for inhibiting the enzymes targeted for type 2 diabetes and obesity management.

Chapter 5

Experimental section

5.1 Materials and methods

All reactions were carried out under nitrogen or argon atmosphere using dry solvents under anhydrous conditions unless otherwise noted. Solvents for chromatographic purification (ethyl acetate, cyclohexane, *n*-hexane, acetone, dichloromethane, methanol) were purchases at the highest commercial quality. Reagents were purchased at the highest commercial quality and used without further purification, unless otherwise noted. Evaporations were conducted under reduced pressure at 35°C unless otherwise noted. Yields refer to chromatographically and spectroscopically (^{1}H NMR) homogeneous materials unless otherwise noted. Reactions were monitored by thin-layer chromatography (TLC) carried out using pre-coated Merck silica gel plates (60F-254). Merck silica gel (60, particle size 40-63 μm) was used for column chromatography. The visualization of the reaction components was obtained under UV light at wavelengths of 254 nm.

NMR spectra were recorded using a Varian Unity Inova spectrometer operating at 300 or 500 MHz (^{1}H) and 75 or 125 MHz (^{13}C) or Bruker Avance 300 MHz and were calibrated using residual undeuterated solvent as an internal reference [$CDCl_3$ (^{1}H): δ = 7.26 ppm; $CDCl_3$ (^{13}C): δ = 77.0 ppm; CD_3OD (^{1}H): δ = 3.31 ppm; CD_3OD (^{13}C): δ = 49.0 ppm; $(CD_3)_2CO$ (^{1}H): δ = 2.05 ppm; $(CD_3)_2CO$ (^{13}C): δ = 29.84 ppm]. All NMR experiments, including two-dimensional spectra, i.e., g-COSY, g-HSQCAD, and g-HMBCAD, were performed using software supplied by the manufacturer, and acquired at constant temperature (300 K). g-HMBCAD experiments were optimized for a long-range ^{13}C^{1}H coupling constant of 8.0 Hz. The following abbreviations were used to describe the multiplicities: s for singlet, d for doublet, t for triplet, q for quartet, dd for double doublet, ddd for

double double doublet, ddt for double double triplet, dq for double quartet, dddt for double double double triplet, bs for broad singlet, m for multiplet.

High-performance liquid chromatography (HPLC) was carried out using an Agilent 1100 Series with auto-sampler and pump and an Agilent UV detector. Preparative liquid chromatography (LC) was performed on silica gel (63-200 μm, Merck, Darmstadt, Germany), or Sephadex-LH20 (Sigma-Aldrich, Milan, Italy), or RP-18 (Merck, Darmstadt, Germany) using different mixtures of solvents, as reported for each compound. Thin layer Chromatography (TLC) was carried out using pre-coated silica gel F254 plates (Macherey-Nagel).

High-resolution mass spectra were acquired with a Q Exactive Orbitrap mass spectrometer (Thermo Fisher Scientific, Bremen, Germany) equipped with an ESI ion source operating in positive or negative mode and with a Q Exactive-Thermo mass spectrometer (Centre d'Etude Structurale et d'Analyse des Molécules Organiques (CESAMO) at the Institut des Sciences Moléculaires (ISM, CNR-UMR 5255, Talence), France). Samples were dissolved at $1E^{-5}$M concentration in 50:50 (MeOH/H_2O+1%). IR spectra were recorded between 4000 and 450 cm^{-1} on a Bruker IFS55 (OPUS/IR 3.0.2) FT-IR spectrometer.

The lipase (LIP), α-glucosidase (α-Glu) and α-amylase (α-Amy) inhibition assays were performed on a 96-well microplate, Intrinsic fluorescence experiments were performed on an Agilent Cary Eclipse spectrometer. The fluorescence spectrum was acquired after 1 min from each addition setting the instrument (Varian Cary Eclipse Spectrophotometer) with the following parameters: λEXC at 280 nm and excitation and emission slits of 5 nm, acquisition from 300 to 500 nm for pancreatic lipase; λEXC = 295 nm; slit 10 nm; acquisition from 310 to 500 nm for α-glucosidase and α-amylase. Experiments were carried out at 300.15, 305.15, and 310.15 K for pancreatic lipase 298.15, 303.15, and 310.15 K for α-glucosidase and α-amylase.

Natural products **1** and **2** and selected nitrogenated neolignans **16b**, **17** and **18b** were analyzed by HPLC-UV using Chiralcel OD column (4.6 mm x 250 mm,

5 µm, Daicel, Japan), eluted in isocratic mode (*n*- hexane: propan – 2- ol 80:20) at 0.7 mL/min at two different temperatures 283.15 K and 300.15 K. The chromatograms were acquired at 254 nm and reported in **Figures S133 – 134** in Supplementary materials.

5.2 General procedure for the synthesis of nitrogenated analogues

Synthesis of boronic acid pinacol ester.

Aminophenol (3.66 mmol) was weighed and moved to an amber vessel, and then it was solubilized with methanol (7.2 ml). Cool the reaction mixture at 0 °C and stir vigorously. Then, HCl 3M (3.6 ml) and H_2O (3.6 ml) were added to the reaction mixture and stirred for two minutes. Lastly, a solution of $NaNO_2$ and H_2O (1 eq in 1.8 ml) was added, and the reaction mixture was stirred for 40 min. In the next step, the reaction mixture was placed at room temperature, and a solution of bis(pinacolato)diboron (pin_2B_2) and H_2O (1.5 eq in 3.6 ml) was added, and the reaction mixture was stirred for 1 h and 15 min. The crude of reaction was diluted with H_2O and partitioned with CH_2Cl_2. The combined organic layer was washed dried over anhydrous Na_2SO_4, filtered, and taken to dryness.

Synthesis of 4 -(4,4,5,5-tetramethyl-1,3,2-dioxaborolan-2-yl) phenol (4a).

According to the general procedure, the reaction of 4- Aminophenol (400 mg, 3.66 mmol) with bis(pinacolate) diboron (1.37 g, 5.4 mmol) afforded compound **4a** with 100%yield, after silica gel column chromatography (cyclohexane: acetone 93:7). Compound **4a** is known in literature and HRESIMS (-) and ^{1}H NMR spectrum is only reported. HRESIMS *m/z* 219.1221 $[M-H]^-$ calcd for $C_{12}H_{17}BO_3$ *m/z* 219.127.

Synthesis of 2 -(4,4,5,5-tetramethyl-1,3,2-dioxaborolan-2-yl) phenol (4b).

According to the general procedure, the reaction of 2- Aminophenol (400 mg, 3.66 mmol) with bis(pinacolate) diboron (1.37 g, 5.4 mmol) afforded compound **4b** with 80%yield, after silica gel column chromatography (petroleum ether→

petroleum ether: ethyl acetate 98:2). Compound **4b** is known in literature and HRESIMS (-) and ^{1}H NMR spectrum is only reported. HRESIMS *m/z* 219.1218 $[M-H]^-$ calcd for $C_{12}H_{17}BO_3$ *m/z* 219.1271.

Preliminary reaction for the synthesis of 4-amino-3-methyl- [1,1'-biphenyl]-4'-ol (6).

Preliminary experiments for SM reaction were performed employing 4-bromo-2-methylaniline **5a** (10.0 mg; 54 μmol) and **4a** (11.2 mg, 81 μmol) as starting reagents. The catalyst-ligand system, solvent, and temperature were varied as reported in **Table 22** and the reaction yield was determined after quantification with HPLC-UV using a reversed-phase column (RP-18) and the following gradient of of CH_3CN/H^+ (99:1 v/v; B) in H_2O/H^+ (99:1 v/v; A) at 1 mL/min: t_0 min B = 10%, t_{20} min B = 100%. The diode array detector was set at 254, 280, and 305 nm. The quantification occurred at 280 nm.

Table 22. Preliminary experiments of SM cross-coupling reaction of **4a** with **5a**.

entry	Catalyst	mg, %mol	Ligand	mg, %mol	Solvent (µL)	Base (mmol)	T (°C)	Time (h)
1	$Pd(PPh_3)_4$	(4.6, 8%)	-		THF (800)	NaOH (0.11)	67	24
2	$Pd(OAc)_2$	(0.6, 5%)	dppf	(4.5, 15%)	THF:H_2O (800:80)	K_2CO_3 (0.27)	67	24
3	$Pd(OAc)_2$	(1.2, 10%)	dppf	(9.0, 30%)	THF:H_2O (800:80)	K_2CO_3 (0.27)	67	24
4	$Pd(OAc)_2$	(0.12, 1%)	SPhos	(0.5, 2%)	dry toluene (100)	K_2CO_3 (0.11)	80	22
5	$Pd(OAc)_2$	(0.12, 1%)	SPhos	(0.5, 2%)	THF (100)	K_2CO_3 (0.11)	67	22
6	$Pd(OAc)_2$	(1.3, 10%)	SPhos	(4.9, 20%)	dry toluene (100)	K_2CO_3 (0.11)	80	22
7	$Pd(OAc)_2$	(1.3, 10%),	SPhos	(4.9, 20%)	THF (100)	K_2CO_3 (0.11)	67	22
8	$Pd(OAc)_2$	(1.3, 10%),	SPhos	(4.9, 20%)	THF:H_2O (100:10)	K_2CO_3 (0.11)	67	3
9	$Pd(OAc)_2$	(0.12, 1%)	SPhos	(0.5, 2%)	THF:H_2O (100:10)	K_2CO_3 (0.11)	67	24
10	$Pd(OAc)_2$	(0.6, 5%)	SPhos	(2.3, 10%)	THF:H_2O (100:10)	K_2CO_3 (0.11)	67	5

Optimized procedure for preparation of biphenyls neolignane (6 − 10).

Aryl bromide (1.0 mmol, if solid), boronic acid pinacol ester (1.5 mmol), Pd $(OAc)_2$ (1.0 mol%), SPhos (2.0 mol%), and K_2CO_3 (2.0 mmol) were weighted and moved to a flask. The reaction flask was evacuated and backfilled with Ar (this procedure was repeated thrice). A mixture of THF: H_2O 10:1 (2 ml and 0.2 mL, respectively) was added with a syringe. The reaction mixture was heated at 67 °C and stirred vigorously for 24 h. The crude of the reaction mixture was filtered

through celite plug. The mixture was diluted with water (5 ml) and partitioned with EtOAc (3x5ml). The combined organic layer was washed, dried over anhydrous Na_2SO_4, filtered, and taken to dryness. The expected compound was recovered after column chromatography. When the aryl bromide was a liquid (1.0 mmol) it was added together with the solvents with a syringe.

Synthesis of 4-Amino-3-methyl-(1,1'-biphenyl)-4'-ol (6).

According to the general procedure, the reaction of **5a** (100.0 mg; 0.54 mmol) with **4a**; (178.2 mg; 0.81 mmol), afforded compound **6** (85.0 mg, 79%yield), after purification on silica gel column chromatography (dichloromethane → dichloromethane: methanol 98:2). White amorphous solid. ^{1}H NMR (500 MHz, CD_3OD- $CDCl_3$): δ 7.38 (d, J = 7.9 Hz, 2H, H-2'/H-6'), 7.24 (s, 1H, H-2), 7.22 (d, J = 8.2 Hz, 1H, H-6), 6.86 (d, J = 7.3 Hz, 2H, H-3'/H5'), 6.75 (d, J = 8.1 Hz, 1H, H-5), 2.23 (s, 3H, CH_3-3). ^{13}C NMR (125 MHz, CD_3OD- $CDCl_3$): δ 155.6 (C, C-4'), 143.1 (C, C-4), 133.1 (C, C-1'), 132.1 (C, C-1), 128.7 (CH, C-2), 127.5 (CH, C-2'/C-6'), 125.1 (CH, C-6), 123.1 (C, C-3), 115.7 (CH, C-3'/C-5'), 115.5 (CH, C-5), 17.4 (CH_3-3). HRESIMS *m/z* 200.1091 $[M + H]^+$, calcd for $C_{13}H_{14}NO$ *m/z* 200.0997.

Synthesis of 2-Amino-5-methyl-(1,1'-biphenyl)-4'-ol *(7)*.

The reaction of 2- bromo-4-methylaniline **5b** (75.0 mg; 0.40 mmol) with **4a** (82.7 mg; 0.60 mmol), afforded compound **7** (60.0 mg, 76 % yield), after purification on silica gel column chromatography (*n*-hexane: acetone 90:10 → 87:13). White amorphous solid. ^{1} H NMR. (500 MHz, CDCl3): δ 7.27 (d, J = 8.0 Hz, 2H, H-2' / H-6'), 6.96 (d, J = 8.1 Hz, 1H, H-4), 6.93 (s, 1H, H6), 6.88 (d, J = 7.9 Hz, 2H, H-3'/H-5'), 6.74 (d, J = 8.0 Hz, H-3), 2.20 (s, 3H, CH3). ^{13}C NMR (125 MHz, $CDCl_3$): δ 155.1 (C, C-4'), 139.8 (C, C-2), 131.4 (C, C-1'), 131.1 (CH, C-6), 130.3 (CH, C-2'/C-6'), 128.9 (C, C-5), 128.7 (CH, C-4), 128.3 (C, C-1), 116.4 (CH, C-3), 115.8 (CH, C-3'/C-5'), 20.4 (CH_3). HRESIMS m/z 200.1088 $[M + H]^+$, calcd for $C_{13}H_{14}NO$ m/z 200.1075.

Synthesis of 5-Nitro-(1,1'-biphenyl)-2,4'-diol (8).

According to the general procedure, the reaction of 2-bromo-4-nitrophenol **5c** (186.0 mg; 0.85 mmol) with **4a** (263.8 mg; 1.30 mmol), afforded compound **8** (138.6 mg, 70 % yield), after purification on a silica gel column chromatography (*n*-hexane: acetone 90:10 → 88:12). Yellow amorphous solid. ^{1} H NMR (500 MHz, CD_3OD-$CDCl_3$): δ 8.13 (d, *J* = 2.8 Hz, 1H, H-6), 8.00 (dd, *J* = 8.9 Hz,2.8 Hz, 1H, H-4), 7.41 (d, *J* = 8.5 Hz, 2H, H-2'/H-6'), 6.92 (d, *J* = 8.5 Hz, 1H, H-3), 6.86 (d, *J* = 8.5 Hz, 2H, H-3′ /H-5′). ^{13}C NMR (125 MHz, CD_3OD-$CDCl_3$): δ 160.9 (C, C-2), 157.0 (C, C-4'), 140.8 (C, C-5), 130.7 (CH, C-2'/C-6'), 129.5 (C, C-1'), 128.0 (C, C-1), 126.6 (CH, C-6), 124.3 (CH, C-4), 116.1 (CH, C-3), 115.5 (CH, C-3′ /C-5′). HRESIMS m/z 230.0482 $[M- H]^-$, calcd for $C_{12}H_8NO_4$ m/z 230.0453.

Synthesis of 4'-Amino-3'-methyl-(1,1'-biphenyl)-2-ol (9).

According to the general procedure, the reaction of **5a** (150.0 mg; 0.80 mmol) with **4b** (263.8 mg; 1.20 mmol) afforded compound **9** (160.0 mg, 97 % yield), after purification on a silica gel column chromatography (dichloromethane → dichloromethane: methanol 90:10). White amorphous solid. ^{1} H NMR (500 MHz, $CDCl_3$): δ 7.22 (s,1H, H-2'), 7.19 (d, *J* = 7.9 Hz, 1H, H-6'),7.17 (d, *J* = 7.2 Hz, 1H, H-6), 7.06 (t, *J* = 7.7 Hz, 1H, H-4), 6.84 (t, *J* = 7.2 Hz, 1H, H-5), 6.84 (t, *J* = 7.2 Hz, 1H, H-3) 6.75 (d, *J* = 8.1 Hz, 1H, H-5'), 2.19 (s, 3H, CH_3). ^{13}C NMR (125 MHz, $CDCl_3$): δ 154.9 (C, C2), 145.0 (C, C-4′), 132.1 (CH, C-2'), 131.3 (CH, C-6'), 130.2 (C, C-1), 130.2 (C, C-1), 128.7 (C, C-6), 128.4 (C, C-4), 123.5 (C, C-3′), 120.6 (CH, C-5), 116.7 (CH, C-3), 116.2 (CH, C-5'), 17.6 (CH_3). HRESIMS m/z 200.1089 $[M + H]^+$, calcd for C13H14NO m/z 200.1075.

Synthesis of 2'-Amino-5'-methyl-(1,1'-biphenyl)-2-ol (10).

According to the general procedure, the reaction of **5b** (186.0 mg; 1 mmol) with **4b** (330.0 mg; 1.50 mmol) afforded compound 9 (139.3 mg, 70 % yield) after purification on a silica gel column chromatography (*n*-hexane → *n*-

hexane:acetone 80:20). White amorphous solid. Spectroscopic data agreed with those previously reported. [29] HRESIMS m/z 200.1075 $[M + H]^+$, calcd for $C_{13}H_{14}NO$ m/z 200.1075.

Synthesis of O-allyl and N-allyl derivatives

Synthesis of N-Allyl-4'-(allyloxy)-3-methyl-(1,1'-biphenyl)-4-amine (11a).

A solution of compound **6** (25.0 mg; 0.12 mmol) in dry acetone (2 mL) was mixed in K_2CO_3 (33.2 mg; 0.24 mmol) for 10 min, then, allyl bromide (29.0 mg; 0.24 mmol) was added, and the mixture was refluxed for 6 h. The mixture was filtered, and the expected compound **11a** (17.0 mg, 50 % yield) was recovered after purification on silica gel column chromatography (cyclohexane → cyclohexane: acetone 99:1). Yellow oil. ^{1} H NMR (500 MHz, $CDCl_3$): δ 7.47 (d, *J* = 8.8 Hz, 2H, H-2'/H-6'), 7.33 (d, *J* = 8.3 Hz, 1H, H-6), 7.30 (s, 1H, H-2), 6.97 (d, *J* = 8.8 Hz, 2H, H-3'/H-5'), 6.68 (d, *J* = 8.3 Hz, 1H, H-5), 6.09 (m, 2H, H-8/H-8'), 5.45 (dd, *J* = 17.3, 1.5 Hz, 1H, H_a-9'), 5.34 (dd, *J* = 14.8, 1.4 Hz, 1H, H_a-9), 5.32 (dd, *J* = 8.4, 1.5 Hz, 1H, Hb-9'), 5.20 (dd, *J* = 10.4,1.4 Hz, 1H, H_b-9), 4.57 (d, *J* = 5.4 Hz, 2H, H-7'), 3.88 (d, *J* = 5.4 Hz, 2H, H-7), 2.24 (s, 3H, CH_3). ^{13}C NMR (125 MHz, $CDCl_3$): δ 157.3 (C, C-4'), 145.0 (C, C-4), 135.5 (CH, C-8), 134.3 (C, C-1'), 133.5 (CH, C-8'), 129.8 (CH, C-1), 128.5 (CH, C-2), 127.3 (CH, C-2'/C-6'), 125.3 (CH, C-6), 122.3 (C, C-3), 117.6 (CH2, C9'), 116.3 (CH2, C-9), 114.9 (CH, C-3'/C-5'), 110.3 (CH, C-5), 68.9 (CH_2, C-7'), 46.6 (CH_2,C-7), 17.6 (CH_3). HRESIMS m/z 280.1732 $[M + H]^+$, calcd for $C_{19}H_{22}NO$ m/z 280.1703.

Synthesis of 4'-(allyloxy)-3-methyl-(1,1'-biphenyl)-4-amine (11b).

A solution of compound **6** (25.0 mg; 0.12 mmol) in dry acetone (2 mL) was mixed in K_2CO_3 (33.2 mg; 0.24 mmol) for 10 min, then, allyl bromide (29.0 mg; 0.24 mmol) was added, and the mixture was refluxed for 6 h. The mixture was filtered, and the expected compound **11b** (13.0 mg, 45 % yield) was recovered after purification on silica gel column chromatography (cyclohexane → cyclohexane: acetone 99:1), further purified on Sephadex LH-20 (eluted in chloroform).

Colourless oil. ^{1} H NMR (500 MHz, $CDCl_3$): δ 7.46 (d, *J* = 8.7 Hz, 2H, H-2'/H-6'), 7.27 (s, 1H, H-2), 7.25 (d, *J* = 8.2 Hz, 1H, H-6), 6.96 (d, *J* = 8.7 Hz, 2H, H-3'/H-5'), 6.74 (d, *J* = 8.1, 1H, H-5), 6.10 (m, 1H, H-7'), 5.45 (dd, *J* = 17.2, 1.4 Hz, 1H, H_a-9'), 5.31 (dd, *J* = 10.5, 1.2 Hz, 1H, H_b-9'), 4.58 (d, *J* = 5.3 Hz, 2H, H-8'), 2.24 (s, 3H, CH_3). ^{13}C NMR (125 MHz, $CDCl_3$): δ 157.5(C, C-4'), 143.7 (C, C-4), 134.4 (C, C-1'), 133.6 (CH, C-8'), 131.6 (CH, C-1), 129.0 (CH, C-2), 127.5 (CH, C-2'/C-6'), 125.3 (CH, C-6), 122.7 (C, C-3), 117.7 (CH2, C-9'), 115.4 (C-5), 115.1 (CH, C-3'/C-5'), 69.0 (CH_2, C-7′), 17.7 (CH_3). HRESIMS m/z 240.1412 $[M + H]^+$, calcd for $C_{16}H_{18}NO$ *m/z* 240.1388.

Synthesis of 4-(Allylamino)-3-methyl-(1,1'-biphenyl)-4'-ol (11c).

A solution of compound **6** (25.0 mg; 0.12 mmol) in dry acetone (2 mL) was mixed in K_2CO_3 (41.5 mg; 0.30 mmol) for 10 min, then, allyl bromide (36.3; 0.30 mmol) was added, and the mixture was refluxed for 6 h. The mixture was filtered, and silica gel column chromatography (cyclohexane → cyclohexane: acetone 90:10). **11c**: 3.0 mg, 11% yield, colourless oil. ^{1} H NMR (500 MHz, $CDCl_3$): δ 7.41 (d, *J* = 8.3 Hz, 2H, H-2'/H-6'), 7.30 (d, *J* = 7.7 Hz, H-6), 7.26 (s,1H, H-2), 6.85 (d, *J* = 8.3, 2H, H-3'/H-5'), 6.66 (d, *J* = 7.9 Hz, H-5), 6.02 (m, 1H, H-8), 5.32 (d, *J* = 18.2 Hz, 1H, H_a-9), 5.20 (d, *J* = 10.2 Hz,1H, H_b-9), 3.87 (d, *J* = 4.9 Hz, 2H, H-7), 2.22 (s, 3H, CH_3). ^{13}C NMR (125 MHz, $CDCl_3$): δ 154.3 (C, C-4'), 145.1 (C, C- 4), 135.6 (CH, C-8), 134.5 (C, C-1'), 129.9 (C, C-1), 128.7 (CH, C-2), 127.7 (CH, C-2'/C-6'), 125.4 (CH, C-6), 122.4 (C, C-3), 116.4 (CH2, C-9), 115.6 (CH, C-3' /C-5'), 110.5 (CH, C-5), 46.6 (CH2, C-7), 17.7 (CH_3). HRESIMS m/z 240.1411 $[M + H]^+$, calcd for $C_{16}H_{18}NO$ m/z 240.1388.

Synthesis of 4'- (diallylamino)-3-methyl-(1,1'-biphenyl)-4'-ol (11d).

A solution of compound **6** (25.0 mg; 0.12 mmol) in dry acetone (2 mL) was mixed in K_2CO_3 (41.5 mg; 0.30 mmol) for 10 min, then, allyl bromide (36.3; 0.30 mmol) was added, and the mixture was refluxed for 6 h. The mixture was filtered, and silica gel column chromatography (cyclohexane → cyclohexane: acetone 90:10).

11d: 3.3 mg, 9.2 % yield, yellowish oil. ^{1} H NMR (500 MHz, $CDCl_3$): δ 7.46 (d, *J* = 8.5 Hz, 2H, H-2'/H-6'), 7.37 (s, 1H, H-2), 7.30 (d, *J* = 8.3 Hz, 1H, H-6), 7.05 (d, *J* = 8.3 Hz, 1H, H-5), 6.88 (d, *J* = 8.5 Hz, H-3'/H-5'), 5.83 (m, 2H, H-8/H-11), 5.20 (d, *J* = 17.1 Hz, 2H, H_a-9/H_a-12), 5.13 (d, *J* = 10.2, 2H, H_b-9/H_b-12), 3.62 (d, *J* = 6.0, 4H, H-7/H-10), 2.38 (s, CH_3). ^{13}C NMR (125 MHz, $CDCl_3$): δ 154.6 (C, C-4'), 148.8 (C, C-4), 135.3 (CH, C-8/C-11), 133.9 (C, C-1/C-1'/C-3), 129.4 (CH, C-2), 128.0 (CH, C-2'/C-6'), 124.1 (CH, C-6), 122.1 (CH, C-5), 117.0 (CH_2, C-9/ C-12), 115.5 (CH, C-3'/C-5'), 55.6 (CH2, C-7/C-10), 18.5 (CH_3). HRESIMS m/z 280.174 [M + H]+, calcd for $C_{19}H_{22}NO$ m/z 280.1701.

Synthesis of 4'-(Allyloxy)-5-methyl-(1,1'-biphenyl)-2-amine (12).

A solution of compound **7** (20.0 mg; 0.10 mmol) in dry acetone (2 mL) was mixed in K_2CO_3 (55.3 mg; 0.40 mmol) for 10 min, then, allyl bromide (60.5 mg; 0.50 mmol) was added, and the mixture was refluxed for 6 h. The mixture was filtered, and the expected compound (8.9 mg, 37 % yield) was recovered after purification on silica gel column chromatography (cyclohexane: acetone 95:5 → cyclohexane: acetone 90:10). Amorphous white solid. ^{1} H NMR (500 MHz, $CDCl_3$): δ 7.37 (d, *J* = 8.4 Hz, 2H, H-2'/ H-6'), 6.99 (d, *J* = 8.2 Hz, 2H, H-3'/H-5'), 6.93 (s, 1H, H-6), 6.89 (m, 1H, H-4), 6.68 (d; *J* = 7.9 Hz,1H, H-3), 6.09 (m, 1H, H-8'), 5.45 (d, *J* = 17.2 Hz, 1H, H_a-9), 5.31 (d, *J* = 10.3 Hz, 1H, H_b-9), 4.58 (d, *J* = 5.3 Hz, H-7'), 2.27 (s, 3H, CH_3). ^{13}C NMR (125 MHz, $CDCl_3$): δ 157.9 (C, C-4'), 141.2 (C, C-2), 133.4 (CH, C-8'), 132.2 (C, C-1'), 131.1 (CH, C-6), 130.3 (CH, C-2'/C-6'), 128.8 (CH, C-4), 128.0 (C, C-5), 127.6 (C, C-1), 117.9 (CH2, C-9'), 115.8 (CH, C-3), 115.1 (CH, C-3'/C-5'), 69.0 (CH2, C-7'), 20.6 (CH_3). HRESIMS m/z 240.1407 $[M + H]^+$, calcd for $C_{16}H_{18}NO$ *m/z* 240.1389.

Synthesis of 2,4'-Bis(allyloxy)-5-nitro-1,1'-biphenyl (13).

A solution of compound **8** (16.9 mg; 0.07 mmol) in dry acetone (1 mL) was mixed in K_2CO_3 (40.4 mg; 0.30 mmol) for 10 min, then, allyl bromide (47.2 mg; 0.39 mmol) was added, and the mixture was refluxed for 6 h. The mixture was filtered,

and the expected compound (18.8 mg, 82.6 % yield) was recovered after purification on silica gel column chromatography (cyclohexane: acetone 90:10). Yellow solid. ^{1} H NMR (500 MHz, $CDCl_3$): δ 8.22 (dd, *J* = 2.9,1.0 Hz, 1H, H-6), 8.17 (dd, *J* = 2.9,0.9 Hz, H-4), 7.50 (d, *J* = 8.8 Hz, 2H, H-2'/H-6'), 7.00 (d, *J* = 8.8 Hz, 2H, H-3'/H-5'), 7.00 (d, *J* = 3.0 Hz, 1H, H-3), 6.09 (m, 1H, H-8'), 5.99 (m, 1H, H-8), 5.45 (d, *J* = 17.3 Hz, 1H, H_a-9'), 5.37 (d, *J* = 17.4 Hz, 1H, H_a-9), 5.32 (d, *J* = 10.5 Hz, 1H, H_b-9'), 5.29 (d, *J* = 10.5, 1H, H_b-9), 4.67 (d, *J* = 4.5 Hz, 2H, H-7), 4.59 (d, *J* = 5.8 Hz, 2H, H-7'). ^{13}C NMR (125 MHz, $CDCl_3$): δ 160.5 (C, C-1), 158.6 (C, C-4'), 141.7 (C, C-5), 133.2 (CH, C8'), 132.0 (CH, C-8),131.4 (C, C-1'), 130.8 (CH, C-2'/C-6'), 128.7 (C, C-1), 126.3 (CH, C-6), 124.3 (CH, C-4), 118.0 (CH2, C-9'), 117.9 (CH_2, C-9), 114.6 (CH, C-3'/C-5'), 112.0 (CH, C-3), 69.7 (C, C-7), 69.0(C, C-7'). HRESIMS m/z 312.1275 $[M + H]^+$, calcd for $C_{18}H_{18}NO_4$ m/z 312.1236.

Synthesis of N-Allyl-2-(allyloxy)-3'-methyl-(1,1'-biphenyl)-4'-amine (14a).

A solution of compound **9** (25.0 mg; 0.12 mmol) in dry acetone (2 mL) was mixed in K_2CO_3 (66.3 mg; 0.48 mmol) for 10 min, then, allyl bromide (72.6 mg; 0.60 mmol) was added and the mixture was refluxed for 7 h. The mixture was filtered, and the expected compound **14a** (10.0 mg, 30 % yield) was recovered after purification on silica gel column chromatography (petroleum ether → petroleum: dichloromethane 35:65). Yellowish oil.^{1} H NMR (500 MHz, $CDCl_3$): δ 7.37 (d, *J* = 8.3 Hz, 1H, H-6'), 7.34 (d, *J* = 7.8 Hz, 1H, H-6), 7.33 (s, 1H, H-2'), 7.22 (t, *J* = 7.8 Hz, 1H, H-4), 7.01(t, *J* = 7.4 Hz, 1H, H-5), 6.95 (d, *J* = 8.2 Hz, 1H, H-3), 6.67 (d, *J* = 8.3 Hz, 1H, H-5'), 6.00 (m, 2H, H-8/H-8'), 5.36 (ddt, *J* = 17.6, 16.1, 1.6, 2H, H_a-9'/H_a-9), 5.22 (ddt, *J* = 10.3, 2.6, 1.4 Hz, H_b-9'/H_b-9), 4.55 (d, *J* = 4.7 Hz, 2H, H-7), 3.88 (d, *J* = 3.9 Hz, 2H, H-7'), 2.21 (s, 3H, CH_3). ^{13}C NMR (125 MHz, $CDCl_3$): δ 155.4 (C, C-2), 144.9 (C, C-4'), 135.6 (CH, C-8'), 133.6 (CH, C-8), 131.4 (CH, C-2'), 131.3 (C, C-1), 130.6 (CH, C-6), 128.2 (CH, C-6'), 127.4 (CH, C-4), 127.1 (C, C-1'), 121.4 (C, C-3'), 121.1 (CH, C-5), 116.6 (CH2, C-9), 116.3 (CH2, C-9'), 113.0 (CH, C-3), 109.6 (C, C-5'), 69.1 (CH_2, C-7), 46.6 (CH2, C-7'),

17.6 (CH_3). HRESIMS m/z 280.1730 $[M + H]^+$, calcd for $C_{19}H_{22}NO$ m/z 280.1701.

Synthesis of 2-(allyloxy)-3'-methyl-(1,1'-biphenyl)-4'-amine (14b).

A solution of compound **9** (25.0 mg; 0.12 mmol) in dry acetone (2 mL) was mixed in K_2CO_3 (66.3 mg; 0.48 mmol) for 10 min, then, allyl bromide (72.6 mg; 0.60 mmol) was added and the mixture was refluxed for 7 h. The mixture was filtered, and silica gel column chromatography (cyclohexane → cyclohexane: acetone 90:10). **14b**: 5.7 mg, 20 % yield. Colourless oil. ^{1}H NMR (500 MHz, CD_3OD): δ 7.22 (t, *J* = 7.8 Hz, 1H, H-4), 7.20 (s, 1H, H-2'), 7.16 (t, *J* = 7.8 Hz, 1H, H-6), 7.15 (d, *J* = 8.1 Hz, 1H, H-6'), 7.00 (t, *J* = 7.4 Hz, 1H, H-5), 6.95 (d, *J* = 7.4 Hz, 1H, H-3), 6.75 (d, *J* = 8.1 Hz, 1H, H-5'), 5.99 (m, 1H, H-8), 5.35 (d, *J* = 17.3 Hz, 1H, H_a-9), 5.20 (d, *J* = 16.6 Hz, 1H, H_b-9), 4.54 (d, *J* = 4.6 Hz, 2H, H-7), 2.12 (s, 3H, CH_3). ^{13}C NMR (125 MHz, CD_3OD): δ 156.8(C, C-2), 145.4 (C, C-4), 135.0 (CH, C-8), 133.0 (C, C-1'), 132.4 (CH, C-2′), 131.4 (CH, C-6'), 130.2 (C, C-1), 129.0 (CH, C-6), 128.5 (HC, C-4), 123.4 (CH, C-5), 122.2 (C, C-2'), 116.7 (CH_2, C-9), 116.0 (CH, C5'), 114.5 (CH, C-3), 70.2 (CH_2, C-7), 17.6 (CH_3). HRESIMS m/z 240.1407 $[M + H]^+$, calcd for $C_{16}H_{18}NO$ *m/z* 240.1388.

Synthesis of N,N-diallyl-2-(allyloxy)-3'-methyl-(1,1'-biphenyl)-4'-amine(14c).

A solution of compound **9** (25.0 mg; 0.12 mmol) in dry acetone (2 mL) was mixed in K_2CO_3 (66.3 mg; 0.48 mmol) for 10 min, then, allyl bromide (72.6 mg; 0.60 mmol) was added and the mixture was refluxed for 7 h. The mixture was filtered, and silica gel column chromatography (cyclohexane → cyclohexane: acetone 90:10). **14c**: 5.5 mg, 14 % yield. Yellowish oil. ^{1}H NMR (500 MHz, $CDCl_3$): δ 7.39 (d, *J* = 1.7 Hz, 1H, H-2'), 7.33 (d, *J* = 1.7 Hz, 1H, H-6'), 7.32 (d, *J* = 7.6 Hz, 1H, H-6), 7.23 (d, *J* = 1.3 Hz, 1H, H-5'), 7.02 (t, *J* = 7.5, Hz, 1H, H-4/H-5), 6.95 (d, *J* = 8.1 Hz, 1H, H-3), 5.93 (m, 1H, H-8), 5.76 (m, 2H, H-8'/ H-11'), 5.27(dd, *J* = 17.3, 1.7 Hz, 1H, H_a-9), 5.12 (dd, *J* = 9.1, 1.5 Hz, 2H, H_a-9'/H_a−12'), 5.05 (dd, *J* = 10.2, 1.3 Hz,2H, H_b-9/H_b-9'), 4.46 (d, *J* = 4.7 Hz, 2H, H-7), 3.55 (d, *J* = 6.1

Hz, 4H, H-7'/ H-10'), 2.28 (s,3H, CH_3). ^{13}C NMR (125 MHz, $CDCl_3$): δ 155.5 (C, C-2), 148.9 (C, C-2″), 135.5(CH, C-8'/ C-11'), 133.4 (CH, C-8), 132.9 (C, C-1), 132.8 (CH, C-2'), 132.3(C, C-1'), 131.0 (C, C-3'), 130.8 (CH, C-5), 127.9 (CH, C-5'), 127.1 (CH, C-6'), 121.2 (CH, C-4), 121.1 (CH, C-5), 116.9 (CH_2, C-9'/ C-12'), 116.6 (CH_2, C-9), 113.0 (CH, C-3), 69.0 (CH_2, C-7), 55.3 (CH_2, C-7'/ C-10'), 18.4 (CH_3). HRESIMS m/z 320.2044 $[M + H]^+$, calcd for $C_{22}H_{26}NO$ m/z 320.2014.

Synthesis of N,N-Diallyl-2-(allyloxy)-3'-methyl-(1,1'-biphenyl)-6'-amine (15)

A solution of compound **11** (50.0 mg; 0.25 mmol) in dry acetone (3.5 mL) was mixed in K_2CO_3 (103.7 mg; 0.75 mmol) for 10 min, then allyl bromide (90.7 mg; 0.75 mmol) and the mixture was refluxed for 24 h. The mixture was filtered, and the expected compound (12.0 mg, 15 % yield) was recovered after reversed-phase C18 column chromatography (water-acetonitrile 60:40 → acetonitrile. Brownish oil.[1] H NMR. (500 MHz, $CDCl_3$): δ 7.24 (d, *J* = 7.5 Hz, 1H, H-6), 7.24 (t, *J* = 7.4 Hz, 1H, H4), 7.03 (s, 1H, H-2'), 7.04 (d, *J* = 8.2 Hz, 1H, H-5'), 6.97 (t, *J* = 7.4 Hz, 1H, H-5), 6.93 (dd, *J* = 8.1, 2.3 Hz, 1H, H-3/H-4'), 6.92 (d, *J* = 2.5 Hz, 1H, H-3), 5.91(m, 1H, H-8), 5.52 (m, 2H, H-8'/ H-11'), 5.21 (dd, *J* = 17.3, 1.5 Hz, 1H, H_a-9), 5.13 (dd, *J* = 17.3, 1.2 Hz, 2H, H_a-9'/ H_a-12'), 5.00 (dd, *J* = 10.1, 1.5 Hz, 1H, H_b-9), 4.96 (dd, *J* = 10.3, 1.2 Hz, 2H, H_b-9'/ H_b-12'), 4.50 (d, *J* = 4.7 Hz, 2H, H-7'), 3.39 (d, *J* = 6.2, 2H, H-7'/H10'), 2.29 (s, 3H, CH_3). ^{13}C NMR (125 MHz, $CDCl_3$): δ 155.7 (C, C-2), 147.3 (C, C-6'), 135.9 (CH, C-8'/ C-11'), 133.7 (CH, C-8), 133.7 (C, C-1'), 132.8 (CH, C-5'), 131.9 (C,C-6), 131.1 (C, C-3'), 130.9 (C, C-1), 128.1 (CH, C-2'), 128.0 (CH, C-4), 121.1 (CH, C-4'), 120.5 (CH, C-5), 116.6 (CH2, C-9'/C-12'), 116.6 (CH_2, C-9), 112.5 (CH, C-3), 68.7 (CH_2, C-7), 55.4 (CH2, C-7'/C-10'), 21.0 (CH_3). HRESIMS m/z 320.2055 $[M + H]^+$, calcd for $C_{22}H_{26}NO$ m/z 320.2014.

General procedure for the synthesis of Claisen products.

A 1 M Et_2AlCl solution (in n-hexane; 100 µL) was added dropwise to allyl derivatives **11a**–**15** in dry CH_2Cl_2 (1 mL). The mixture was stirred at room

temperature for 2–3 h, and then the reaction was quenched by adding 2 N HCl solution (2 mL) at 0 ◦C temperature. The mixture was partitioned with CH_2Cl_2 (2 × 5 mL); the combined organic phases were washed with water, dried over anhydrous Na_2SO_4, filtered and taken to dryness. The expected compound was recovered after column chromatography, affording the pure products.

Synthesis of 3'-Allyl-4-(allylamino)-3-methyl-(1,1'-biphenyl)-4'-ol (16a).

According to the general procedure, compound **16a** (5.0 mg, 51 % yield) was recovered after a Sephadex LH-20 column chromatography (dichloromethane). Yellowish oil. ^{1} H NMR (500 MHz, $CDCl_3$): δ 7.32 (d, *J* = 8.2 Hz, 1H, H-2'/H-6), 7.28 (s, 1H, H-6'/H-2), 6.85 (d, *J* = 8.1 Hz, 1H, H-3'), 6.67 (d, *J* = 8.1 Hz, 1H, H-5), 6.05 (m, 2H, H-8/H-8'), 5.33 (dd, *J* = 17.2,1.4 Hz, 1H, H_a-9), 5.21 (m, 3H, H_b-9b / H_a-9'/ H_b-9'), 3.88 (d, *J* = 5.3 Hz, 2H, H-7), 3.48 (d, *J* = 6.3 Hz, 2H, H-7'), 2.23 (s, 3H, CH_3). ^{13}C NMR (125 MHz, $CDCl_3$): δ 153.2 (C, C-4'), 145.4 (C, C-4), 136.9 (CH, C-8'), 135.9 (CH, C-8), 134.9 (C, C-1'), 130.3 (C, C-1), 129.0 (CH, C-2), 128.9 (CH, C-6'), 126.2 (CH, C-6), 125.7 (CH, C-2'), 125.7 (C, C-5), 122.7 (C, C-3), 116.9 (CH_2, C-9'), 116.7 (CH_2, C-9), 116.5 (CH, C-3'), 110.8 (CH, C-5), 47.0 (CH_2, C-7), 35.8 (CH_2, C-7'), 18.0 (CH_3). HRESIMS m/z 280.1680 $[M + H]^+$, calcd for $C_{19}H_{22}NO$ m/z 280.1702.

Synthesis of 3'-Allyl-4-amino-3-methyl-(1,1'-biphenyl)-4'-ol (16b).

According to the general procedure, compound **16b** was achieved without further purification (3.6 mg, 60 % yield). Colorless oil. ^{1} H NMR (500 MHz, $CDCl_3$): δ 7.29 (d, *J* = 8.3 Hz, 1H, H-6'), 7.28 (s,1H, H-2'), 7.25 (s, 1H, H-2), 7.23 (d, *J* = 8.3 Hz, 1H, H6), 6.84 (d, *J* = 8.1 Hz, 1H, H-5'), 6.72 (d, *J* = 8.0 Hz, 1H, H-5), 6.05 (m, 1H, H-7'), 5.20 (d, *J* = 17.3 Hz, 1H, H_a-9'), 5.17 (d, *J* = 10.1 Hz, 1H, H_b-9'), 3.46 (d, *J* = 6.1 Hz, 2H), 2.22 (s,3H, CH_3). ^{13}C NMR (125 MHz, $CDCl_3$): δ 153.0 (C, C-4'), 143.7 (C, C-4), 136.6 (CH_2, C-8'), 134.5 (C, C1'), 131.7 (C, C-1), 131.6 (C, C-3'), 129.0 (CH, C-2), 128.7 (CH, C-2'), 125.9 (CH, C-6'), 125.5 (C, C-3), 125.4 (CH, C-6), 116.7 (CH_2, C-9'), 116.2 (CH, C-5'), 115.4 (CH, C-5), 35.4

(CH_2, C-7'), 17.7 (CH_3). HRESIMS m/z 240.1352 $[M + H]^+$, calcd for $C_{16}H_{18}NO$ m/z 240.1388.

Synthesis of 3'-Allyl-2-amino-5-methyl-(1,1'-biphenyl)-4'-ol (17).

According to the general procedure, the expected compound **16** (8.0 mg, 50 % yield) was recovered after silica gel column chromatography (cyclohexane → cyclohexane: acetone 100 → 50:50). Amorphous white solid. ^{1}H NMR (500 MHz, $CDCl_3$): δ 7.21 (s, 1H, H-2'), 7.20 (d, *J* = 7.8 Hz, 1H, H-6'), 6.94 (d, *J* = 8.3 Hz, 1H, H-4), 6.92 (s, 1H, H-6), 6.86 (d, *J* = 7.8 Hz, 1H, H-5'), 6.68 (d, *J* = 7.9 Hz, 1H, H-3), 6.04 (ddt, *J* = 16.6, 10.1, 6.4 Hz, 1H, H-8'), 5.19 (d, *J* = 17.4 Hz, 1H, H_a-9'), 5.16 (d, *J* = 10.1 Hz, 1H, Hb-9'), 3.44 (d, *J* = 6.2 Hz, 2H, H-7'), 2.26 (s, 3H, CH_3). ^{13}C NMR (125 MHz, $CDCl_3$): δ 153.4 (C, C-4'), 141.1 (C, C-2),136.4 (CH_2, C-8'), 132.3 (C, C-5), 131.2 (CH, C-6), 131.1 (CH, C-2'), 128.8 (CH, C-4), 128.6 (CH, C-6'), 128.1 (C, C-1'), 125.8 (CH, C-3'), 116.7 (CH_2, C-9'), 116.2 (CH, C-5'), 115.9 (CH, C-3), 35.3 (CH_2, C-7'), 20.6 (CH_3). HRESIMS m/z 240.1403 $[M + H]^+$, calcd for $C_{16}H_{18}NO$ m/z 240.1388.

Synthesis of 3-Allyl-4'-(allylamino)-3'-methyl-(1,1'-biphenyl)-2-ol (18a).

According to the general procedure, compound **18a** (5.6 mg, 25 % yield) was recovered after silica gel column chromatography (petroleum ether: dichloromethane 95:5 → 90:10). Yellowish oil. ^{1}H NMR (500 MHz, $CDCl_3$): δ 7.20 (dd, *J* = 8.2,1.8 Hz, 1H, H-6'), 7.15(s, 1H, H-2'), 7.08 (d, *J* = 7.6 Hz, 2H, H-4/H-6), 6.89 (t, *J* = 7.5 Hz, 1H, H-5), 6.70 (d, *J* = 8.2 Hz, 1H, H-5'), 6.05 (m, 2H, H-8/ H-8'), 5.33(dd, *J* = 17.3, 1.3 Hz, 1H, H_a-9'), 5.22 (dd, *J* = 10.3, 1.1 Hz, 1H, H_b-9'), 5.13 (dd, *J* = 17.1, 1.6 Hz, 1H, H_a-9), 5.09 (dd, *J* = 10.0, 1.1 Hz, 1H, H_b-9), 3.88(d, *J* = 5.2 Hz, 2H, H-7'), 3.46 (d, *J* = 6.5 Hz, 2H, H-7), 2.21 (s, 3H, CH_3). ^{13}C NMR (125 MHz, $CDCl_3$): δ 150.7 (C, C-2), 145.8 (C, C-4'), 137.1 (CH, C-8), 135.4 (CH, C-8'), 131.0 (CH, C-2'), 128.9 (CH, C-4), 128.5 (C,C-1), 128.3 (CH, C-6), 127.9 (CH,C-6'), 126.3 (C, C-3), 125.4 (C, C-1'), 123.0 (C, C-3'), 120.3 (CH, C-5), 116.6 (CH2, C-9'), 115.7 (CH_2, C-9), 110.7 (CH, C-5'), 46.6 (CH_2, C-7'),

34.9 (CH_2, C-7), 17.6 (CH_3). HRESIMS m/z 280.1685 $[M + H]^+$, calcd for $C_{19}H_{22}NO$ m/z 280.1701.

Synthesis of 3-Allyl-4'-amino-3'-methyl-(1,1'-biphenyl)-2-ol (18b).

According to the general procedure, expected compound **18b** (3.1 mg) was achieved with 72 % yield after liquid–liquid partition. ^{1} H NMR (500 MHz, $CDCl_3$): δ 7.17 (s, 1H, H-2'), 7.13 (d, *J* = 8.1 Hz, 1H, H-6'), 7.08 (t, *J* = 8.5 Hz, 1H, H-5), 7.09 (d, *J* = 8.9 Hz, 1H, H-6), 6.90 (d, *J* = 7.9 Hz, 1H, H-4), 6.87 (d, *J* = 7.9 Hz, 1H, H-5'), 6.03 (m, 1H, H-8), 5.13 (d, *J* = 17.1 Hz, 1H, H_a-9), 5.09 (d, *J* = 10.0 Hz, 1H, H_b-9), 3.45 (d, *J* = 6.3 Hz, 2H, H-7), 2.26 (s, 3H, CH_3). ^{13}C NMR (125 MHz, $CDCl_3$): δ 150.5 (C, C-2), 142.8 (C, C-4'), 136.8 (CH_2, C-9), 131.3 (CH, C-2'), 129.1 (CH, C-5), 128.2 (CH, C-6), 128.2 (C, C-1), 127.8 (CH, C-6'), 126.2 (C, C-3), 124.1 (C, C-1'/C-3'), 120.2 (CH, C-4), 116.4 (CH, C-5'), 115.7 (CH_2, C-8), 34.8 (CH_2, C-7), 17.5 (CH_3). HRESIMS m/z 240.1357 $[M + H]^+$, calcd for $C_{16}H_{18}NO$ m/z 240.1388.

Synthesis of 3-Allyl-4'-(diallylamino)-3'-methyl-(1,1'-biphenyl)-2-ol (18c)

According to the general procedure, the expected compound **18c** (6.7 mg, 50 % yield) was recovered after silica gel column chromatography (petroleum ether 100%). Brownish oil. ^{1} H NMR (500 MHz, $CDCl_3$): δ 7.26 (s, 1H, H-2′), 7.20 (d, *J* = 6.4 Hz, 1H, H-6'), 7.10 (m, 3H, H-4/H-6/H-5'), 6.91 (t, *J* = 7.5 Hz, 1H, H-5), 6.06 (ddt, *J* = 16.7, 10.6, 6.6 Hz, 1H, H-8), 5.82 (ddt, *J* = 16.4, 10.4, 6.1 Hz, 2H, H-8'/H-11'), 5.21 (dd, *J* = 17.2, 1.2 Hz, 2H, H_a-9'/H_a-12'), 5.14 (d, *J* = 11.7 Hz, 2H, H_b-9'/H_b-12'), 5.13 (d, *J* = 16.2 Hz, 1H, H_a-9), 5.10 (d, *J* = 10.1 Hz, 1H, H_b-9), 3.63 (d, *J* = 6.0 Hz, 4H, H-7'), 3.46 (d, *J* = 6.8 Hz, 2H, H-7), 2.36 (s, 3H, CH3). ^{13}C NMR (125 MHz, $CDCl_3$): δ 150.6 (C, C-2), 149.9 (C, C-4'), 137.0 (CH, C-8), 135.3 (CH, C-8'/ C-11'), 134.6 (C, C-3'), 132.0 (CH, C-2'), 131.5 (C, C-1'), 129.4 (CH, C-4), 128.4 (CH, C-6), 128.2 (C, C-1), 126.8 (CH, C-6'), 126.4 (C, C-3), 122.6 (CH, C-5'), 120.4 (CH, C-5), 117.4 (CH_2, C-9'/C-12'), 115.8 (CH_2, C-9),

55.6 (CH_2, C-7'/C-10'), 34.9 (CH_2, C-7), 18.7 (CH_3). HRESIMS m/z 320.1985 [M + H]$^+$, calcd for $C_{16}H_{18}NO$ m/z 320.2014.

Preliminary reaction for Aza-Cope rearrangement

Synthesis of 3-allyl-4-amino-5-methyl-[1,1'-biphenyl]-4'-ol (16c).

Preliminary experiments for Aza-Cope rearrangement reaction were performed employing *N*-allyl derivative **11c** (10.0 mg; 0.041 mmol) as starting reagent. The reaction conditions are varied as follow and monitored by TLC (95:5 $CHCl_3$: MeOH).

a) **11c** was solubilized in 0.35 mL of dry CH_2Cl_2 and 1 equivalent or 2 equivalents, respectively of 1 M Et_2AlCl (in n-hexane, 10 or 20 µL) were added. The reaction mixture was stirred at room temperature for 24 h.

b) **11c** was solubilized in 0.35 mL of dry CH_2Cl_2 and 2 equivalents of 1 M Et_2AlCl (in n-hexane, 20 µL) were added. The reaction mixture was stirred at 40°C for 24 h.

c) **11c** was solubilized in 0.2 mL of xylene and 1 equivalent of BF3 * $O(Et)_2$ (≥46.5%, 10 µL) was added. The reaction mixture was refluxed for 24h.

d) **11c** (0.041 mmol) and 15 mg of $H_3PMo_{12}O_{40}$ (20% mol) were solubilized in 2 mL of different organic solvent (dry THF, or dry CH_3CN or dry CH_2Cl_2). The reaction mixture was stirred at room temperature for 24 h.

5.3 General procedure for the synthesis of obovatol and its analogues

***Preliminary reaction for the synthesis of 2-(allyloxy) benzene-1,3-diol* (20)**.

Initial experiments for allylation reaction were performed employing pyrogallol **19** (10.0 mg; 0.79 mmol) as starting material in dry acetone (8 mL) at 56°. The base K_2CO_3 and allyl bromide were varied as reported in **Table 23**.

Table 23. Preliminary experiments of allylation reaction of **20**.

entry	K_2CO_3 (mg, mmol)	Allyl bromide (mg, mmol)	T (°C)	Time(h)
1	(219.2, 1.58)	(95.9, 0.79)	56	3
2	(109.2, 0.79)	(95.9, 0.79)	56	2
3	(109.2, 0.79)	(95.9, 0.79) *	56	4
4	(109.2, 0.79)	(119.5, 1.10)	56	6
5	(109.2, 0.79)	(133.8, 1.39)	56	6

*****The second addition of base was carried out after 2h

Synthesis of 2-(allyloxy) benzene-1,3-diol (20).

A solution of **19** (100.0 mg; 0.79 mmol) in dry acetone (8 mL) was mixed in K_2CO_3 (109.2 mg; 0.79 mmol) for 10 min, then, allyl bromide (133.8 mg; 1.39 mmol) was added, and the mixture was refluxed for 6h and afforded compound **20** (85.3 mg, 65%yield), after purification on silica gel column chromatography (*n*-hexane → *n*-hexane: ethyl acetate 98:2). yellowish oil. ^{1}H NMR (300 MHz, $CDCl_3$): δ 6.88 (t, J = 8.3 Hz, 1H, H-5), 6.50 (d, J = 8.3 Hz, 2H, H-4/H6), 6.11 (dd, J = 17.1, 10.3 Hz, 1H, H-8), 5.58 (m, 2H, h-9), 4.52 (m, 1H, H-7). ^{13}C NMR (75 MHz, $CDCl_3$): δ 149.3 (C, C-1/C-3), 144.2 (C, C-2), 133.3 (CH, C-8), 124.9 (CH, C-5), 119.8 (CH_2, C-9), 108.3 (CH, C-4/C-6), 74.5(CH_2, C-7). Spectroscopic data were in agreement with those previously reported [203].

Synthesis of 2-(allyloxy)-3-bromophenol (26).

A solution of 3-bromobenezene-1,2 diol **25** (300.0 mg; 1.58 mmol) in dry acetone (12 mL) was mixed in K_2CO_3 (219.4 mg; 1.59 mmol) for 10 min, then, allyl bromide (268.8 mg; 2.22 mmol) was added, and the mixture was refluxed for 2h

and afforded compound **26** (224.7 mg, 62%yield) after purification on silica gel column chromatography (*n*-hexane → *n*-hexane: ethyl acetate 98:2). Yellowish oil. ^{1}H NMR (300 MHz, $CDCl_3$): δ 7.09 (dd, *J* = 6.4, 3.2 Hz, 1H, H-5), 6.94-6.88 (m, 2H, H-4/H-6), 6.22-5.98 (m, 1H, H-8), 5.47 (dq, *J* = 17.1, 1.5 Hz, 1H, H_a-9), 5.36 (dq, *J* = 10.3, 1.5 Hz, 1H, H_b-9), 4.60 (dt, *J* = 6.0, 1.2 Hz, 2H, H-7). ^{13}C NMR (75 MHz, $CDCl_3$): δ 150.4 (C, C-2), 143.3 (C, C-1), 132.8 (CH, C-8), 126.0 (CH, C-4), 124.6 (CH, C-5), 119.7 (CH_2, C-9), 116.1 (C, C-3), 114.9 (CH, C-6), 74.6 (CH_2, C-7).

Synthesis of Claisen - Cope derivatives

Synthesis of 5-allylbenzene-1,2,3-triol (21).

A 1 M Et_2AlCl solution (in n-hexane; 2 eq.) was added dropwise to a solution of *O*-allyl derivative **20** (1 eq.) in dry CH_2Cl_2 (1 mL). The mixture was stirred at room temperature for 2 h and then the reaction was quenched adding 2 N HCl solution (2 mL) at 0°C temperature. The mixture was partitioned with CH_2Cl_2 (2 × 5 mL); the combined organic phases were washed with water, dried over anhydrous Na_2SO_4, filtered and taken to dryness. The expected compound was recovered after a silica gel column chromatography (*n*-hexane → *n*-hexane: ethyl acetate 98:2)., affording the pure products (68.24 mg, 80 % yield) Yellowish oil. ^{1}H NMR (300 MHz, $CDCl_3$): δ 6.33 (s, 2H, H-4/ H-6), 5.90 (ddt, *J* = 16.9, 10.1, 6.7 Hz, 1H, H-8), 5.28 (s, 2H, OH), 5.19 (s, 1H, OH), 5.05 (m, 2H, H-9), 3.22 (d, *J* =7.4 Hz, 2H, H-7). Spectroscopic data were in agreement with those previously reported [204].

5-allyl-3-bromobenzene-1,2-diol (27).

A 1 M Et_2AlCl solution (in *n*-hexane; 2 eq.) was added dropwise to a solution of allyl derivative **26** (1 eq.) in dry CH_2Cl_2 (1 mL). The mixture was stirred at room temperature for 3 h and then the reaction was quenched adding 2 N HCl solution (2 mL) at 0°C temperature. The mixture was partitioned with CH_2Cl_2 (2 × 5 mL); the combined organic phases were washed with water, dried oved anhydrous

Na_2SO_4, filtered and taken to dryness. The expected compound **27** (179.6 mg, 80% yield) was recovered after a flash column chromatography, eluting with cyclohexane → cyclohexane: acetone 85:15. Brownish oil. ^{1}H NMR (300 MHz, $CDCl_3$): δ 6.97 (d, *J* = 2.1 Hz, 1H, H-4), 6.67 (d, *J* = 2.0 Hz, 1H, H-6), 5.95 (m, 1H, H-8), 5.14-5.03 (m, 2H, H-9), 3.31 (dt, *J* = 7.4, 1.3 Hz, 2H, H-7). ^{13}C NMR (75 MHz, $CDCl_3$): δ 144.3 (C, C-1) 142.0 (C, C-2), 136.9 (CH, C-8),134.3 (C, C-5), 123.2 (CH, C-4), 116.3 (CH_2, C-9), 115.4 (CH, C-6), 113.8 (C, C-3), 39.3 (CH_2, C-7).

General procedure for the synthesis of methylated derivatives.

To a solution of Claisen-Cope product **21** or **27** or compound **42** (1 equiv.) in DMF was added potassium carbonate (2 equiv.). After stirring for 30 min, methyl iodide (3 equiv. per OH group) was added. The resulting solution was stirred for 4 h at room temperature. The reaction mixture was quenched by the addition of saturated aqueous NH_4Cl solution and diluted with diethyl ether. The mixture was extracted with diethyl ether, and the combined organic layers were washed with brine, dried over anhydrous Na_2SO_4, filtered, and evaporated.

Synthesis of 5-allyl -2-methoxybenzene-1,3 diol (22).

According to the general procedure, the reaction of **21** (65.0 mg; 0.39 mmol) with potassium carbonate (107.9 mg; 0.78 mmol) and methyl iodide (83.8 mg; 0.59 mmol) afforded compound **22** (49.2 mg, 70% yield) was recovered after a silica gel column chromatography, eluting with cyclohexane: acetone 90:10 → cyclohexane: acetone 80:20. Yellowish oil. ^{1}H NMR (300 MHz, $CDCl_3$): δ 6.35 (s, 2H, H-4/ H-6), 6.01-5.81 (m, 1H, H-8), 5.15-5.00 (m, 2H, H-9), 3.85 (s, 3H, CH_3), 3.24 (d, *J* = 5.4 Hz, 2H, H-7).

Synthesis of 5-allyl-1-bromo-2,3-dimethoxybenzene (28).

According to the general procedure, the reaction of **27** (112.3 mg; 0.49 mmol) with potassium carbonate (135.6 mg; 0.98 mmol) and methyl iodide (208.7 mg; 1.47 mmol) afforded compound **22** (88.2 mg, 70% yield) after a flash column

chromatography, eluting with *n*-hexane → *n*-hexane: acetone 98:2. Yellowish oil. ^{1}H NMR (300 MHz, $CDCl_3$): δ 6.97 (d, *J* = 1.9 Hz, 1H, H-4), 6.67 (d, *J* = 1.9 Hz, 1H, H-6), 6.04-5.83 (m, 1H, H-8), 5.16-5.05(m, 2H, H-9), 3.85 (s, 3H, CH_3), 3.83 (s, 3H, CH_3), 3.31 (dt, *J* = 6.7, 1.4 Hz, 2H, H-7). ^{13}C NMR (75 MHz, $CDCl_3$): δ 153.6 (C, C-3), 144.7 (C, C-2), 137.3 (CH, C-8), 136.6 (C, C-5), 124.5 (CH, C-6), 117.5 (CH, C-4), 116.5(CH_2, C-9), 112.1(C, C-1), 60.6 (CH_3), 56.0 (CH_3), 39.7 (CH_2, C-7).

5-bromo-2-methoxybenzaldehyde (43).

According to the general procedure, the reaction of 5-bromo-2-hydroxybenzaldehyde **42** (130.0 mg; 0.75 mmol) with potassium carbonate (207.5 mg; 1.5 mmol) and methyl iodide (320.0 mg; 2.25 mmol) afforded compound **20** (155.4 mg, 97% yield). Yellow solid. ^{1}H NMR (300 MHz, $CDCl_3$): δ 10.38 (s, 1H, H-7), 7.92 (d, *J* =2.6 Hz, 1H, H-6), 7.63 (dd, *J* =8.9, 2.6 Hz, 1H, H-2), 6.90 (d, *J* = 8.9 Hz, 1H, H-3), 3.90 (s, 3H, CH_3). Spectroscopic data were in agreement with those previously reported [177].

***Preliminary reaction for the synthesis of 5-allyl-3(4-allylphenoxy)-2-methoxyphenol* (24)**.

Preliminary experiments for Ullmann coupling reaction were performed employing 1-allyl-1-bromobenzene **23** (50 mg, 0.25 mmol) as starting material in the presence of methylated compound **22** (68.5 mg, 0.38 mmol) cesium carbonate (162.9 mg, 0.50 mmol) as base, copper(I) iodide as catalyst and *N,N*-Dimethylglycine hydrochloride as ligand. The solvent, temperature, ligand, and catalyst were varied, as reported in **Table 24.**

Table 24. Preliminary experiments of Ullmann coupling reaction of **22** with **23**.

entry	Catalyst mg, %mol	Ligand mg, %mol	Solvent (mL)	T (°C)	Time (h)
1	(2.4, 5%)	(5.3, 15%)	DMA (1.5)	90	48
2	(0.7, 1.5%)	(1.7, 5%)	DMF (1.5)	135	24
3	(4.8, 10%)	(10.5, 30%)	Dioxane (1.5)	90	48
4	(9.5, 20%)	(20.9, 60%)	Dioxane (1.5)	90	48

General procedure for Ullmann coupling condensation.

A mixture of bromide (1 equiv.), p-allyl-phenol (1.5 equiv.), Cs_2CO_3(2 equiv.), CuI (10% mol.) and *N*,*N*-dimethylglycine hydrochloride (30% mol.) in dioxane in a sealed tube was heated at 90°C under nitrogen atmosphere for 48 h. The cooled mixture was partitioned between ethyl acetate and water. The organic layer was separated, and the aqueous layer was extracted with ethyl acetate (3 x 15 mL). The combined organic layers were washed with brine, dried over Na_2SO_4, filtered and evaporated.

Synthesis of 5-allyl-1-(4'-allylphenoxy)-2,3-dimethoxybenzene (30).

According to the general procedure, the reaction of **28** (65.0 mg; 0.25 mmol) with **29** (50 mg; 0.38 mmol) afforded compound **30** (38.8 mg, 52% yield) after a flash column chromatography, eluting with *n*-hexane → *n*-hexane: acetone 98:2. Yellowish oil. ^{1}H NMR (300 MHz, $CDCl_3$): δ 7.11 (d, *J* = 8.7 Hz, 2H, H-2'/H-6'), 6.90 (d, *J* = 8.7 Hz, 2H, H-3'/H-5'), 6.54 (d, *J* = 2.0 Hz, 1H, H-6), 6.42 (d, *J* = 2.0 Hz, 1H, H-4), 5.92 (dddt, *J* = 17.5, 16.1, 10.7, 6.7 Hz, 2H, H-8 /H-8'), 5.17-4.96 (m, 4H, H-9/H-9'), 3.88 (s, 3H, CH_3), 3.81 (s, 3H, CH_3), 3.35 (d, *J* = 6.7 Hz, 2H, H-7), 3.27 (d, *J* = 6.7 Hz, 2H, H-7'). ^{13}C NMR (75 MHz, $CDCl_3$): δ 156.2 (C, C-1'), 153.8 (C, C-3), 149.6 (C, C-1), 139.2 (C, C-2), 137.7(CH, C-8'), 137.1 (CH, C-8), 136.0 (CH, C-5'), 134.3(C, C-5), 129.7 (CH, C-3'/C-5'), 117.5 (CH, C-2'/C-6'), 116.1 (CH_2, C-9'), 115.7 (CH_2,C-9), 113.4 (CH, C-4), 108.2 (CH, C-6), 61.1 (CH_3), 56.2 (CH_3), 40.1 (CH_2, C-7), 39.5 (CH_2, C-7'). HRESIMS m/z 311.1630

$[M+H]^+$,calcd for $C_{20}H_{23}O_3$ 311.1647. IR (NaCl): 2920, 2848, 1508, 1426, 1234, 1094 cm^{-1}.

Synthesis of 4-allyl-1-(4'-allylphenoxy)-2-methoxybenzene (36).

According to the general procedure, the reaction of **23** (50.0 mg; 0.25 mmol) with **33** (61.8 mg; 0.38 mmol) afforded compound **36** (64.4 mg, 94% yield) after a flash column chromatography, eluting with cyclohexane → cyclohexane: ethyl acetate 98:2. Colourless oil. ^{1}H NMR (300 MHz, $CDCl_3$): δ 7.12 (d, *J* = 8.7 Hz, 2H, H-2'/H-6'), 6.93-6.87 (m, 3H, H-3'/H-5', H-6), 6.85 (d, *J* = 2.1 Hz, 1H, H-3), 6.75 (dd, *J* = 8.1, 2.1 Hz, 1H, H-5), 6.00 (dddt, *J* = 17.1, 10.3, 8.6, 6.7 Hz, 2H, H-8/H-8'), 5.20-5.04 (m, 4H. H-9/H-9'), 3.85 (s, 3H, CH_3), 3.41 (dt, *J* = 6.7, 1.5 Hz, 2H, H-7), 3.37 (dt, *J* = 6.7, 1.5 Hz, 2H, H-7').^{13}C NMR (75 MHz, $CDCl_3$): δ 156.5 (C, C-1'), 151.3 (C, C-2), 143.5 (C, C-1), 137.7 (CH, C-8'), 137.3 (CH, C-8), 136.7 (C, C-4'), 133.9 (C, C-4), 129.6 (CH, C-3'/C-5'), 121.0 (CH, C-5), 120.8 (CH, C-6), 117.2 (CH, C-2'/C-6'), 116.0 (CH_2, C-9'), 115.7 (CH_2, C-9), 113.2 (CH, C-3), 56.0 (CH_3), 40.0 (CH_2,C-7), 39.5 (CH_2, C-7'). HRESIMMS m/z 303.1345$[M+Na]^+$, calcd for $C_{19}H_{20}O_2Na$ 303.1361. IR (NaCl): 3077, 2977, 2836, 1638, 1613, 1597, 1503, 1463, 1417, 1271, 1225, 1151, 1036 cm^{-1}.

Synthesis of 2-(2-(4'-allyl-2'-methoxyphenoxy)-4-methoxyphenyl) acetic acid (39).

According to the general procedure, the reaction of **38** (170.0 mg; 0.70 mmol) with **33** (172.4 mg; 1.05 mmol) afforded compound **39** (90.0 mg, 40% yield) after a flash column chromatography, eluting with cyclohexane: ethyl acetate 95:5 → cyclohexane: ethyl acetate 70:30. Colourless oil. ^{1}H NMR (300 MHz, $CDCl_3$): δ 7.17 (d, *J* = 8.3 Hz, 1H, H-6), 6.88 (d, *J* = 8.1 Hz, 1H, H-6'), 6.79 (d, *J* = 2.0 Hz, 1H, H-4'), 6.72 (dd, *J* = 8.1, 2.0 Hz, 1H, H-5'), 6.56 (dd, *J* = 8.3, 2.5 Hz, 1H, H-5), 6.24 (d, *J* = 2.5 Hz, 1H, H-3), 6.08 – 5.88 (m, 1H, H-8'), 5.18 – 5.02 (m, 2H, H-9'), 3.77 (s, 3H, CH_3), 3.75 (s, 2H, H-6), 3.69 (s, 3H, CH3), 3.37 (dt, *J* = 6.7, 1.5 Hz, 2H, H-6'). ^{13}C NMR (75 MHz, $CDCl_3$): δ 176.9 (C, C-8), 160.1 (C, C-4),

157.1 (C, C-2'), 151.2 (C, C-2), 142.7 (C, C-1'), 137.3 (CH_2, C-9'), 137.2 (C, C-4'), 131.6 (CH, C-6), 121.3 (C, C-1), 121.0 (CH, C-5'), 116.0 (CH, C-8'), 115.7 (CH, C-6'), 113.2 (CH, C-3'), 107.1 (CH, C-5), 102.8 (CH, C-3), 55.9 (CH_3), 55.4 (CH_3), 40.7 (CH_2, C-7'), 35.1(CH_2, C-7). HRESIMS 327.1236 $[M+H]^-$, calcd for $C_{19}H_{19}O_5$ 327.12332. IR (NaCl): 2993, 1765, 1379.07, 1244, 1056, 750 cm^{-1}.

Synthesis of 4-(4'-allyl-2'-methoxyphenoxy)-benzoic acid (41).

According to the general procedure, the reaction of **40** (100.0 mg; 0.46 mmol) with **33** (113.3 mg; 0.69 mmol) afforded compound **41** (20 mg; 20%yield) after a flash column chromatography, eluting with cyclohexane: ethyl acetate 95:5. Orange solid. ^1H NMR (300 MHz, $CDCl_3$): δ 8.03 (d, *J* = 9.1 Hz, 2H, H-2/H-6), 7.01 (d, *J* = 8.0 Hz, 1H, H-6'), 6.92 (d, *J* = 9.0 Hz, 2H, H-3/H-5), 6.85 (d, *J* = 2.0 Hz, 1H, H-3'), 6.81 (dd, *J* = 8.0, 2.0 Hz, 1H, H-5'), 6.00 (ddt, *J* = 17.0, 10.3, 6.7 Hz, 1H, H-8'), 5.24-5.08 (m, 2H, H-9'), 3.78 (s, 3H, CH_3), 3.42 (dd, *J* = 6.7, 1.5 Hz, 2H, H-7'). ^{13}C NMR (75 MHz, $CDCl_3$): δ 171.6 (C, C-7), 163.2 (C, C-4), 151.5 (C, C-2'), 141.3 (C, C-1'), 138.5 (CH, C-8'), 137.1(C, C-4'), 132.3 (CH, C-2/C-6), 122.8 (C, C-1), 122.3 (CH, C-5'), 121.2 (CH, C-6'), 116.3 (CH_2, C-9'), 115.7 (CH, C-3/C-5), 113.3 (CH, C-3'), 55.9 (CH_3), 40.1 (CH_2, C-7'). HRESIMS 283.0969 $[M+H]^-$, calcd for $C_{17}H_{15}O_4$ 283.0970, . IR (NaCl): 2924, 2854, 1685, 1610, 1597, 1504, 1463, 1423, 1273, 1232, 1161, 1122, 1035 cm^{-1}.

Synthesis of 5-(4'-allylphenoxy)-2-methoxybenzaldehyde (44).

According to the general procedure, the reaction of **43** (155.4 mg; 0.72 mmol) with **29** (145.0 mg; 1.08 mmol) afforded compound **44** (110.0 mg; 52 %yield) after a flash column chromatography, eluting with dichloromethane. Orange oil. ^1H NMR (300 MHz, $CDCl_3$): δ 10.40 (s, 1H, H-7), 7.43 (d, *J* = 3.1 Hz, 1H, H-6), 7.22 (dd, *J* = 9.0, 3.2 Hz, 1H, H-4), 7.11 (d, *J* = 8.7 Hz, 2H, H-2'/H-6'), 6.94 (d, *J* = 9.0 Hz, 1H), 6.86 (d, *J* = 8.6 Hz, 2H, H-3'/H-5'), 5.94 (ddt, *J* = 16.0, 10.7, 6.7 Hz, 1H, H-8'), 5.18 – 5.03 (m, 2H, H-9'), 3.89 (s, 3H, CH_3), 3.34 (dt, *J* = 6.8, 1.6 Hz, 2H, H-7'). ^{13}C NMR (75 MHz, $CDCl_3$): δ 189.4 (C, C-8), 158.1 (C, C-2), 155.8 (C, C-1'),

151.1 (C, C-5), 137.5 (CH, C-8'), 135.1 (CH, C-4'), 130.0 (CH, C3'/C-5'), 127.0 (CH, C-5'), 125.5 (CH, C-4), 118.4 (CH, C-2'/C-6'), 118.0 (CH, C-6), 115.9 (CH_2, C-9'), 113.2 (C, C-3), 56.2 (CH_3), 39.5 (CH_2, C-7'). HRESIMS 291.0980 $[M+Na]^+$, calcd for $C_{17}H_{16}O_3Na$ 291.0997. IR (NaCl):3360, 3076, 2922, 2852., 1683,1639, 1613, 1505, 1488, 1425, 1393, 1266, 1219, 1151, 1025, 819 cm^{-1}

General procedure for demethylation reaction.

To a solution of Ullman coupling product (1.0 equiv.) in dry CH_2Cl_2 at -78°C was added BBr_3 (solution 1M in DCM, 1.0 or 2.0 equiv.), and the reaction mixture was stirred for 2h. The reaction mixture was quenched by an addition of methanol and diluted with ethyl acetate. The mixture was extracted with ethyl acetate, and the combined organic layers were washed with brine, dried over Na_2SO_4, filtered, and evaporated.

Synthesis of 5-allyl-3-(4'-allylphenoxy)-benzene-1,2-diol (3).

According to the general procedure, the reaction of **30** (65.0 mg; 0.21 mmol) with BBr_3 (solution 1M in DCM, 0.44 mmol) afforded compound **3** (50 mg, 84% yield) was recovered after a flash column chromatography, eluting with dichloromethane. Yellowish oil. ^1H NMR (300 MHz, $CDCl_3$): δ 7.18 (d, *J* = 8.6 Hz, 2H, H-2'/H-6'), 6.97 (d, *J* = 8.6 Hz, 2H, H-3'/H-6'), 6.60 (d, *J* = 1.9 Hz, 1H, H-6), 6.31 (d, *J* = 1.9 Hz, 1H, H-4), 6.01-5.77 (m, 2H, H-7/H-7'), 5.35 (brs, 1H, OH), 5.30 (brs, 1H, OH), 5.22-4.92 (m, 4H, H-9/H-9'), 3.40 (dt, *J* = 6.8, 1.5 Hz, 2H, H-7), 3.23 (d, *J* = 6.7, 1.6 Hz, 2H, H-7'). ^{13}C NMR (75 MHz, $CDCl_3$): δ 155.0 (C, C-1'), 144.8 (C, C-3), 143.7 (C, C-1), 137.4 (CH, C-8), 137.2 (CH, C-8'), 135.3 (C, C-4'), 132.9 (C, C-2), 132.5 (C, C-5), 129.9 (CH, C-3'/C-5'), 117.9(CH, C-2'/C-6'), 115.9 (CH_2, C-9), 115.8 (CH_2, C-9'), 111.1 (CH, C-6), 110.6 (CH, C-4), 39.7 (CH_2, C-7), 39.4 (CH_2, C-7'). HRESIMS 281.1176 $[M+H]^-$, calcd for $C_{18}H_{17}O_3^-$281.1178. IR (NaCl): 3450, 2924, 2853, 1639, 1602, 1504, 1444, 1360, 1214, 1168, 1022 cm^{-1}.

Synthesis of 4-allyl-2-(4'-allylphenoxy)-6-methoxyphenol (34).

According to the general procedure, the reaction of **30** (30.0 mg; 0.10 mmol) with BBr_3 (solution 1M in DCM, 0.1 mmol) afforded compound **34** (30 mg, 100%yield). Brownish oil. ^{1}H NMR (300 MHz, $CDCl_3$): δ 7.12 (d, *J* = 8.5 Hz, 2H, H-2'/H-6'), 6.92 (d, *J* = 8.6 Hz, 2H, H-3'/H-5'), 6.53 (d, *J* = 1.9 Hz, 1H, H-3), 6.44 (d, *J* = 1.8 Hz, 1H, H-5), 6.10-5.80 (m, 2H, H-8/H-8'), 5.14-4.99 (m, 4H, H-9/H-9'), 3.91 (s, 3H, CH_3), 3.36 (dt, *J* = 6.5, 1.6 Hz, 2H, H-7), 3.26 (dt, *J* = 6.6, 1.5 Hz, 2H, H-7').^{13}C NMR (75 MHz, $CDCl_3$): δ 155.8 (C, C-1'), 147.9 (C, C-6), 143.3 (C, C-2), 137.6 (CH, C-8'), 137.3 (CH, C-8), 135.6 (C, C-4'), 134.5 (C, C-4), 131.5 (C, C-1), 129.7(CH, C-3'/C-5'), 117.3 (CH, C-2'/C-6'), 115.9 (CH_2, C-9), 115.7 (CH_2, C-9'), 113.0 (CH, C-3), 107.3 (CH, C-5), 56.3(CH_3), 39.9 (CH_2, C-7), 39.5 (CH_2, C-7'). HRESIMS 319.1302 $[M+Na]^+$, calcd for $C_{19}H_{21}O_3$ 319.1310 . IR (NaCl): 2923, 2853, 1504, 1452, 1433, 1222, 1084. cm^{-1}.

Synthesis of 5-(8-bromopropyl)-3[4'-(8'-bromopropyl) phenoxy)]benzene-1,2-diol (35).

To a solution of Ullmann coupling **30** (30.0 mg, 0.10 mmol) in dry CH_2Cl_2 (0.2 mL) at -78°C was added BBr_3 (solution 1M in DCM, 0.1 mmol). After stirring for 30 min at the same temperature, the reaction mixture was allowed to warm to room temperature and stirred for 2h. Compound **32** (22.5 mg, 50% yield) was recovered after a flash column chromatography, eluting with cyclohexane: acetone 90:10 → cyclohexane: acetone 80:20. Brownish oil. ^{1}H NMR (300 MHz, $CDCl_3$): δ 7.18 (d, *J* = 8.4 Hz, 2H, H-2'/H-6'), 6.97 (d, *J* = 8.4 Hz, 2H, H-3'/H-5'), 6.59 (d, *J* = 1.9 Hz, 1H, H-6), 6.33 (d, *J* = 1.8 Hz, 1H, H-4), 4.45-3.94 (m, 2H, H-8/H-8'), 3.29-2.76 (m, 4H, H-7/H-7'), 1.68 (dd, *J* = 19.6, 6.6 Hz, 6H, CH_3). ^{13}C NMR (75 MHz, $CDCl_3$): δ 155.6 (C, C-1'), 144.9 (C, C-1), 143.3 (C, C-3), 133.8 (C, C-2), 133.7 (C, C-5), 131.0 (C, C-4'), 130.7 (CH, C-2'/C-6'), 117.7 (CH, C-3'/C-6'), 111.9 (CH, C-4), 111.6 (CH, C-6), 46.9 (CH_2, C-7), 46.6 (CH_2, C-7'), 43.6 (CH_2, C-8), 43.6 (CH_2, C-8'), 25.7 (CH_3), 25.6 (CH_3). HRESIMS 442. 9681 $[M+H]^-$, calcd for $C_{18}H_{19}Br_2O_3$ 442.9857. IR (NaCl): 3425, 2923, 1505, 1219, 1170, 601. cm^{-1}.

Synthesis of 5-allyl-2-(4'-allylphenoxy) phenol (37).

According to the general procedure, the reaction of **36** (30.0 mg; 0.11 mmol) with BBr_3 (solution 1M in DCM, 0.11 mmol) afforded compound **37** (30 mg, 100%yield). Brownish oil. ^1H NMR (300 MHz, $CDCl_3$): δ 7.17(d, *J* = 8.6 Hz, 2H, H-2'/H-6'), 6.97 (d, *J* = 8.6 Hz, 2H, H-3'/H-5'), 6.92 (d, *J* = 2.1 Hz, 1H, H-6), 6.83(d, *J* = 8.3 Hz, 1H, H-3), 6.69 (dd, *J* = 8.3, 2.1 Hz, 1H, H-4), 6.26-5.74 (m, 2H, H-8/H-8'), 5.34-4.91 (m, 4H, H-9/H-9'), 3.38 (ddd, *J* = 8.6, 6.8, 1.6 Hz, 4H, H-7/H-7'). ^{13}C NMR (75 MHz, $CDCl_3$): δ 155.3 (C, C-1'), 147.3 (C, C-1), 141.8 (C, C-2), 137.4 (C, C-5), 137.3 (C, C-4'), 136.9 (CH, C-8), 135.2 (CH, C-8'), 129.9(CH, C-3'/C-5'), 120.6 (CH, C-2'/C-6'), 118.7 (CH, C-4), 117.8 (CH, C-3), 116.2(CH_2, C-9), 116.0 (CH_2, C-9'), 115.9 (CH, C-6), 39.7 (CH_2, C-7), 39.4 (CH_2, C-7'). HRESIMS 265.1233 $[M+H]^-$, calcd for $C_{18}H_{17}O_2$ 265.1229. IR (NaCl): 3520, 3077, 2923, 2853, 1637, 1598, 1502, 1452, 1432, 1270, 1223, 1163, 1111 cm^{-1}.

General procedure for phenol oxidation and Michael type addition.

To a stirred suspension of SIBX (2.15 equiv.) in dry THF (ca. 0.05M) was added phenol (1.0 equiv.). After stirring in the dark at room temperature for 16 h, thiophenol (3.0 equiv.) was added and the reaction mixture was stirred at room temperature for 2h. The white suspension was filtered out from the resulting solution. The filter cake was washed with CH_2Cl_2 (20 mL), and the combined filtrate and washings were poured into water (30 mL). After separation, the aqueous layer was further extracted with CH_2Cl_2 (30 mL). the combined organic layers were washed with saturated aqueous $NaHCO_3$ (4 x 15 mL) and treated with an aqueous solution (2 mL) of $Na_2S_2O_4$ for 10 min with vigorous under nitrogen in the dark. The resulting solution was washed with water (10 mL), brine (10 mL), dried over Na_2SO_4, filtered and evaporated.

Synthesis of 5-allyl-3-(phenylthio)- benzene-1,2-diol (47)

According to the general procedure, the reaction of **33** (50.0 mg; 0.30 mmol) with **45** (99.2 mg; 0.90mmol) afforded compound **47** (30 mg, 44%yield) after flash

column chromatography, eluting with cyclohexane → cyclohexane: ethyl acetate 80:20. Colourless oil. ^{1}H NMR (300 MHz, $CDCl_3$): δ 7.33 (d, *J* = 8.4 Hz, 2H, H-3'/H-5'), 7.28-7.24 (m, 1H, H-4'), 7.19 (dd, *J* = 8.3, 1.4 Hz, 2H, H-2'/H-6'), 7.00 (d, *J* = 2.0 Hz, 1H, H-4), 6.97 (d, *J* = 2.0 Hz, 1H, H-6), 6.21-5.79 (m, 1H, H-8), 5.28-5.05 (m, 2H, H-9), 3.38 (dt, *J* = 6.7, 1.5 Hz, 2H, H-7). ^{13}C NMR (75 MHz, $CDCl_3$): δ 144.2 (C, C-1), 142.8 (C, C-2), 137.1 (CH, C-7), 135.8 (C, C-1'), 133.5 (C, C-5), 129.3 (CH, C-2'/C-6'), 127.3 (CH, C-4'), 126.9 (CH, C-3'/C-5'), 126.2 (CH, C-4), 118.0 (CH_2, C-9), 116.1 (CH, C-6), 115.9 (C, C-3), 39.4 (CH_2, H-7). HRESIMS (257.0639 $[M+H]^-$, calcd for $C_{15}H_{13}O_2S$ 257.0636. IR (NaCl):3422, 3073.72, 2923, 2853, 1581.91, 1638.35, 1581, 1478, 1438, 1265, 1168, 1122, 988, 737, 688 cm^{-1}.

***Synthesis of 5-allyl-3-((4'-bromophenyl) thio)-benzene-1,2-diol (48*).**

According to the general procedure, the reaction of **33** (100.0 mg; 0.60 mmol) with **46** (346.0 mg; 1.80 mmol) afforded compound **48** (30 mg, 44%yield) after flash column chromatography, eluting with cyclohexane → cyclohexane: ethyl acetate 95:5. Colourless oil. ^{1}H NMR (300 MHz, $CDCl_3$): δ 7.35 (d, *J* = 8.7 Hz, 2H, H-3'/H-5'), 6.94 (d, *J* = 8.7 Hz, 2H, H-2'/H-6'), 6.88 (d, *J* = 1.8 Hz, 1H, H-6), 6.19 (d, *J* = 1.8 Hz, 1H, H-4), 6.03-5.79 (m, 1H, H-8), 5.16-5.00 (m, 1H, H-9), 3.29 (dt, *J* = 6.7,1.5 Hz, 2H, H-7). ^{13}C NMR (75 MHz, $CDCl_3$): δ 144.4 (C, C-1), 142.9 (C, C-2), 137.1 (CH, C-8), 135.2 (C, C-1'), 133.8 (CH, C-4), 132.4 (CH, C-3'/C-5'), 128.5 (CH, C-2'/C-6'), 127.3 (C, C-5), 120.0 (C, C-4'), 118.3 (CH_2, C-9), 116.3 (CH, C-6), 115.5 (C, C-3), 39.4 (CH_2, C-7). HRESIMS 336.9718 $[M+H]^+$,calcd for $C_{15}H_{14}BrO_2S$ 336.9798 . IR (NaCl): 3420., 2923, 2853, 1715, 1471, 1267, 668 cm^{-1}.

Preliminary experiments for the synthesis of 5-allyl-3-((4'-allylphenyl)thio)benzene-1,2-diol (50).

Preliminary experiment for SM reaction were performed employing thioether analogues **48** (10.0 mg; 0.03 mmol) and allyl boronic acid pinacol ester **49** (7.6

mg, 0.045 μmol) as starting reagents heating at 67°C. The catalyst-ligand system, solvent and temperature were varied as reported in **Table 25.**

Table 25. Preliminary experiments of SM cross-coupling reaction of **48** with **49.**

entry	$Pd(OAc)_2$ (mg, %mol)	Ligand (mg, %mol)	Solvent (μL)	K_2CO_3 (mg, mmol)	Time (h)
1	(0.7, 10%)	Dppf (5.0, 30%)	THF:H_2O (800:80)	K_2CO_3 (20.7, 0.15)	24
2	(0.1, 1%)	SPhos (0.3, 2%)	THF:H_2O (100:10)	K_2CO_3 (8.3, 0.06)	24

5.4 General procedure for the synthesis of oligomeric compounds

Preliminary reaction for the synthesis of houpulin B (52).

Preliminary experiments for dimerization reaction were performed employing honokiol **2** (10.0 mg; 0.04 mmol) as starting reagent. The catalyst, solvent and temperature, were varied as reported in **Table 26** and the reaction yield was determined after quantification with HPLC-UV using a reversed-phase column (RP-18) and the following gradient of of CH_3CN/H^+ (99:1 v/v; B) in H_2O/H^+ (99:1 v/v; A) at 1 mL/min: t_0 min B = 40%, t_{15} min B = 100%. The diode array detector was set at 254, 280, and 305 nm. The quantification occurred at 280 nm.

Table 26. Preliminary experiments of dimerization reaction of **52**.

Entry	Catalyst	mg, µmol	Solvent	mL	T (°C)	T (h)
1	$FeCl_2$ [b]	0.1, 8	Buffer phosphate 0.1 M pH = 6	0.8	25	24
2	$FeCl_2$ [b]	0.1, 8	Buffer phosphate 0.1 M pH = 6	0.8	25_b	24[d]
3	Ag_2O	9.26, 40	$CHCl_3$	0.5	25	5

[a] reaction in presence of H_2O_2; [b]using ultrasounds.

General procedure for Ag_2O-mediated reaction.

A solution of honokiol **2** (0.094 mmol) in $CHCl_3$ (5 mL) was combined with Ag_2O (0.094 mmol). The resulting reaction mixture was stirred at room temperature in the dark for 5 h. The mixture was filtered, and the solvent was evaporated under reduced pressure. The expected compound was recovered after column chromatography.

Preliminary reaction for the enzymatic synthesis of houpulin B.

Preliminary experiment for dimerization reaction were performed employing honokiol **2** (10.0 mg; 0.04 mmol) as the starting reagent. The catalyst, solvent, and temperature, were varied, as reported in **Table 27** the reaction yield was determined after quantification with HPLC-UV using a reversed-phase column (RP-18) and the following gradient of of CH_3CN/H^+ (99:1 v/v; B) in H_2O/H^+ (99:1

v/v; A) at 1 mL/min: t_0 min B = 40%, t_{15} min B = 100%. The diode array detector was set at 254, 280, and 305 nm. The quantification occurred at 280 nm.

Table 27. Preliminary experiments of enzymatic dimerization reaction of **52**.

Entry	Enzyme (mg)	Mediator (mg, µmol)	Solvent (mL)	Buffer (mL)	T(°C)	Time
1	HRP[a]	-	Acetone	Acetate[b]	25	24 h
	(0.32)	-	(2.4)	(1.2)		
2	HRP[a]	-	Methanol	Acetate[b]	25	24 h
	(0.32)	-	(2.4)	(1.2)		
3	HRP[a]	-	Acetone	Acetate[b]	37	24 h
	(0.32)	-	(2.4)	(1.2)		
4	HRP[a]	-	-	Phospate[c]	25	24 h
	(0.32)	-		(1.2)		
5	LTV	-	-	Acetate[b]	25	4 gg
	(24.0)	-		(15.0)		
6	LTV	-	Dioxane	Acetate[b]	25	4 gg
	(24.0)	-	(3)	(12.0)		
7	LTV	TEMPO	-	Acetate[b]	25	4 gg
	(24.0)	(4.13, 26.4)		(15.0)		
8	LTV	TEMPO	Dioxane	Acetate[b]	25	4 gg
	(24.0)	(4.13, 26.4)	(3)	(12.0)		
9	LTV	ABTS	-	Acetate[b]	25	4 gg
	(24.0)	(6.0, 12.0)		(15.0)		
10	LTV	ABTS	Dioxane	Acetate[b]	25	4 gg
	(24.0)	(6.0, 12.0)	(3)	(12.0)		
12	LTV	TEMPO	-	Phosphate[c]	25	4 gg
	(24.0)	(4.13, 26.4)		(15.0)		
11	LTV	TEMPO	Dioxane	Phosphate[c]	25	4 gg
	(24.0)	(4.13, 26.4)	(3)	(12.0)		
13	LTV	ABTS	-	Phosphate[c]	25	4 gg
	(24.0)	(6.0, 12.0)		(15.0)		
14	LTV	ABTS	Dioxane	Phosphate[c]	25	4 gg
	(24.0)	(6.0, 12.0)	(3)	(12.0)		
15	LTV	-	Dioxane	Phosphate[c]	25	4 gg
	(24.0)		(3)	(12.0)		
16	LTV	-	-	Phosphate[c]	25	4 gg
	(24.0)			(15.0)		

[a] reaction in presence of H_2O_2 ;[b] acetate buffer 0.1 M pH = 5; [c] phosphate buffer 0.1 M pH = 6; HRP: horseradish peroxidase; LTV: laccase from *Trametes versicolor;* TEMPO: (2,2,6,6-Tetramethylpiperidin-1-yl)oxyl; ABTS: acid 2,2'-azino-bis(3-etilbenzotiazolin-6-solfonico

General procedure for enzymatic reaction

Honokiol **2** (0.11 mmol) was solubilized in phosphate buffer 0.1 M pH = 6 (50 mL) and subjected to ultrasonication. Subsequently, laccase mixture (74 mg)

was added to the solution The reaction was then incubated at 25 °C under agitation (150-200 rpm) for four days. The mixture was partitioned with EtOAc (3x25ml). The combined organic layer was washed, dried over anhydrous Na_2SO_4, filtered, and taken to dryness. The expected compound was recovered after column chromatography.

Synthesis of 5,5',5'',5'''-tetraallyl-[1,1':3',1'':3'',1'''-quaterphenyl]-2,2''',4',6''-tetraol (52).

According to the Ag_2O-mediated dimerization reactions, the desired product **52** (15 mg, 31.3%) was achieved after flash column chromatography eluting with cyclohexane: ethyl acetate 95:5→ cyclohexane: ethyl acetate 60:40. Brownish oil. According to the LTV-mediated dimerization reactions, the desired product **52** (3.5 mg, 12%) was achieved after flash column chromatography eluting with cyclohexane: ethyl acetate 95:5→ cyclohexane: ethyl acetate 60:40. Brownish oil. The spectroscopic data were in agreement with those previously reported in the literature [91].

^{1}H NMR (500 MHz, $(CD_3)_2CO$): δ 7.37 (s, 4H, H-2'/H-6'/ H-2''/H-6''), 7.13 (dd, *J* = 2.4 Hz, 2H, H-6/H-6'''), 6.97 (dd, *J* = 8.2, 2.4 Hz, 2H, H-3, H-4'''), 6.88 (d, *J* = 8.2, Hz, 2H, H-4/ H-2'''), 5.04 (m, 4 H, H-8/ H-8'/ H-8''/H-8'''), 5.08 (m, 8 H, H-9/ H-9'/ H-9''/H-9'''), 3.52 (d, *J* = 7.1, Hz, 4H, H-7/H-7''') 3.33 (*J* = 6.7, Hz, 4H. H-7'/H-7'').^{13}C NMR (125 MHz, $(CD_3)_2CO$): δ 152.4 (C, C-2/C-2'''), 150.8 (C,C-4'/C-6''), 138.4 (CH, C-8/C-8''), 137.1 (CH, C-8'/C-8''), 131.2 (C, C-5), 131.0 (C, C-1'/C-3''), 130.5 (C, C-2'/C-2''), 130.4 (CH, C-6), 130.4 (CH, C-6'/C-6''),129.6 (C, C-1/C-1''') 128.1 (C, C-5'), 128.0 (C, C-5''), 128.0 (CH, C-3/C-4'''), 127.6 (C, C-3'') 125.5 (C, C-1'), 116.0 (CH, C-4/ C-2'''), 115.1 (CH_2, C-9/C-9'''), 114.6 (CH_2, C-9'/C-9''), 39.1 (CH_2, C-7'/C-7''), 34.6 (CH_2, C-7/C-7'''). HRESIMS 553.2370 $[M+Na]^+$,calcd for $C_{36}H_{34}NaO_4$ 553.2355.

Synthesis of 5,5',5'',5'''-tetraallyl-[1,1':3',1'':3'',1'''-quaterphenyl]-2,2',2'',2'''-tetraol (53).

According to the Ag_2O-mediated dimerization reactions, the desired product **53** (16.4 mg, 33%) was achieved after flash column chromatography eluting with cyclohexane: ethyl acetate 95:5→ cyclohexane: ethyl acetate 60:40. White amorphous solid.

According to the LTV-mediated dimerization reactions, the desired product **53** (3.9 mg, 13.4%) was achieved after flash column chromatography eluting with cyclohexane: ethyl acetate 95:5→ cyclohexane: ethyl acetate 60:40. White amorphous solid.

^{1}H NMR (500 MHz, $(CD_3)_2CO$): δ 7.31 (d, *J* = 2.2 Hz, 1H, H-6'), 7.2 (d, *J* = 2.2 Hz, 1H, H-4''), 7.23 (d, *J* = 2.9 Hz, 1H, H-4'), 7.20 (d, *J* = 2.9 Hz, 1H, H-6''), 7.17 (d, *J* = 2.3 Hz, 2H, H-6/ H-6'''), 7.01 (d, *J* = 8.2 Hz, 2H, H-4/H-4'''), 6.91 (d, *J* = 8.2 Hz, 1H, H-3'''), 6.89 (d, *J* = 8.2 Hz, 1H, H-3), 6.04 (m, 4H, H-9/H-9'/H-9''/H-9'''), 5.04 (m, 8H, , H-8/H-8'/H-8''/H-8'''), 3.43 (d, 4H, *J* = 7.2 Hz, , H_a-7/ H_a -7'/ H_a -7''/ H_a -7'''), 3.43 (d, 4H, *J* = 7.2 Hz, , H_b -7/ H_b -7'/ H_b -7''/ H_b -7'''). ^{13}C NMR (125 MHz, $(CD_3)_2CO$): δ 155.1 (C, C-2/C-2'''), 151.1 (C, C-2'/C-2'')), 138.4 (CH, C-8/C-8'/C-8''/C-8'''), 131.5 (C, C-5/C-5'''), 131.3 (C, C-5'/C-5''),131.1 (CH, C-6/C-6'), 130.8 (CH, C-4'/C-6'/ C-4''/C-6''), 130.6 (CH, C-6/C-6'''), 129.6 (C, C-1'/C-3'/C-1''/C-3''), 128.7 (C, C-1'/C-1'''), 128.3 (CH, C-6/C-6'''), 117.6 (CH, C-3), 116.6 (CH, C-3'''), 114.6 (CH_2, C-9/C-9'/C-9''/C-9'''), 39.5 (CH_2, C-7/-7'''), 39.2(CH_2, C-7'/-7''). HRESIMS 553.2369 $[M+Na]^+$,calcd for $C_{36}H_{34}NaO_4$ 553.2355.

Synthesis of 5,5',5'',5'''-tetraallyl-[1,1':3',1'':3'',1'''-quaterphenyl]-2,2',2''',6''-tetraol (54).

According to the Ag_2O-mediated dimerization reactions, the desired product **54** (14.9 mg, 30%) was achieved after flash column chromatography eluting with cyclohexane: ethyl acetate 95:5→ cyclohexane: ethyl acetate 60:40. Brownish oil.

According to the LTV-mediated dimerization reactions, the desired product **54** (2.9 mg, 10.0%) was achieved after flash column chromatography eluting with cyclohexane: ethyl acetate 95:5→ cyclohexane: ethyl acetate 60:40. Brownish oil. ^{1}H NMR (500 MHz, $(CD_3)_2CO$): δ 7.38 (s, 2H, H-2''/H-4''), 7.24 (s, 2H, H-6/H-6'''), 7.14 (m, 2H, H-4'/H-6'), 7.05 (d, *J* = 8.3 Hz, 2H, H-4/H-4'''), 6.91 (d, *J* = 8.2 Hz, 2H, H-3/H-3'''), 6.07 (m, 4H, H-9/H-9'/H-9''/H-9'''), 5.02 (m, 8H, , H-8/H-8'/H-8''/H-8'''), 3.39 (d, *J* = 7.2 Hz, , H-7/H-7'/H-7''/H-7'''). ^{13}C NMR (125 MHz, $(CD_3)_2CO$): δ 152.5 (C, C-2/C-2'), 150.6 (C, C-6''), 148.9 (C, C-2'), 138.3 (CH, C-8/C-8'/C-8''/C-8'''), 131.6 (C-5, C-5'/C-5'''), 131.5 (C-5''),131.1 (CH, C-6/C-6'), 130.8 (CH, C-2''/C-4''), 130.6 (CH, C-4'/C-6'), 129.6 (CH, C-4, C-4'''), 128.5 (C, C-1''/C-3''), 128.1 (C, C-1''/C-1'''), 128.0 (C, C-1'), 127.2 (C, C-3'), 116.5 (CH, C-3/C-3'''), 116.1 (CH_2, C-9/C-9'/C-9''/C-9'''), 39.1 (CH_2, C-7/C-97'/C-7''/C-7''). HRESIMS 553.2370 $[M+Na]^+$,calcd for $C_{36}H_{34}NaO_4$ 553.2355.

5.5 Measurements of pancreatic lipase (PL) inhibition

The inhibition of pancreatic lipase from porcine pancreas [EC 3.1.1.3; triacylglycerol acyl hydrolase] was performed using 4-nitrophenyl butyrate as a substrate.[36] In a 96-well microplate, 150 µL of phosphate buffer (50 mM, pH = 7.2), the enzyme solution (5 mg/mL in phosphate buffer; 15 µL), and different aliquots (4, 6, 8, 10, and 15 µL) of tested compounds (stock solutions were prepared in MeOH ranging from 1.79 mM to 0.94 mM) or of orlistat (6.7 µM in buffer) were mixed. The reactions were incubated at 37 °C for 10 min. Then, the substrate (3.2 mM in H_2O: DMF 70:30, 10 µL) was added, and the microplate was incubated at 37 °C for 30 min under moderate shaking. The plate measurements were acquired at 405 nm. Orlistat was used as a positive reference. The following equation gave the inhibition percentage of enzyme activity and was employed to elaborate the data for both PL.

$$\%\ inhibition = \frac{OD_{control} - OD_{sample}}{OD_{control}} * 100 \qquad (Eq.1)$$

Here, $OD_{control}$ represents the measured optical density for *Eq* the enzyme-substrate mixture in the absence of an inhibitor, and OD_{sample} represents the optical density of the reaction mixture in the presence of the inhibitor. The *in vitro* assay results are reported as IC_{50} values.

5.6 Measurements of α - glucosidase(α-Glu) inhibition

The α-glucosidase inhibition assay was performed employing the conditions previously reported. Briefly, in a 96-well microplate, the enzyme solution (0.25 U/ml in 50 mM phosphate buffer, pH 6.8; 100 µL) was mixed with different aliquots (2, 4, 6, 8 µL) of tested compounds (stock solutions in methanol ranging from 3.22 mM to 0.4 mM). Then, the substrate *p*-nitro-phenyl-α-glucoside (NPG 78 µM; 100 µL) was added and the microplate was incubated at 37 °C for 30 min under shaking. The reaction was stopped by adding 1 M Na_2CO_3 solution (10 µL) and the absorbance of *p*-nitrophenol was measured at 405 nm with the Synergy H1 microplate reader (BioTek, Bad Friedrichshall, Germany). Acarbose was used as a reference standard. The assays were performed in triplicate with different concentrations for each compound. The amount of methanol used in the experiment did not affect the glucosidase inhibitory activity. The inhibition percentage was calculated by the following equation (*Eq.1*), and the inhibition results are reported as IC_{50} values.

5.7 Measurements of α - amylase(α-Amy) inhibition

The inhibition of the porcine pancreatic α-amylase (EC3.2.1.1, Type VI-B, α-Amy) was performed using the previously reported. The reactions were

carried out in test tubes by mixing 50 µL of the enzyme solution (6 U/ml in 20 mM phosphate buffer containing 6.7 mM NaCl) with tested compounds (2, 4, 6, 8 of 3.87 – 0.50 mM solutions). The reactions were incubated at 37 °C for 10 min, then, a starch solution (0.5% in phosphate buffer; 50 µL), previously stirred at 90 °C for 20 min, was added in the test tubes, and the mixtures were incubated again at 37 °C for 15 min. Lastly, 100 µL of a 96 mM 3,5-dinitrosalicylic acid solution (containing 30% sodium potassium tartrate in 2 N NaOH) were added, and the test tubes were heated at 80 °C for 10 min. Each mixture was diluted with water (final volume 540 µL), and the solutions were moved into a 96-well microplate, and the OD at 540 nm was acquired. Acarbose was used as a positive reference. The inhibition percentage was calculated by solving *Eq. (1)* and the inhibition results the as reported ad IC_{50} value.

5.8 Kinetic of pancreatic lipase inhibition

The mode of inhibition of PL in the presence of selected neolignans was determined spectroscopically. The experiments were performed in 96-well plates employing the enzyme (120 U/mL in phosphate buffer; 10 µL), the selected molecules, and the increasing concentrations of *p* - nitrophenyl butyrate (from 0.3 to 1.9 mM) in a final volume of 200 µL. The concentration of tested neolignans was chosen based on the IC_{50} values. The absorbance was read at 405 nm every 1 min for 45 min at 37 °C. The inhibition constants were calculated from the equations:

$$v_0 = \frac{v_{max} S}{K_m\left(1+\frac{I}{K_i}\right)+S} \qquad \textit{(Eq.2)}$$

$$v_0 = \frac{v_{max} S}{K_m\left(1+\frac{I}{K_i}\right)+S\left(1+\frac{I}{K\prime_i}\right)} \qquad \textit{(Eq.3)}$$

here v_0 is the initial velocity in the absence and presence of the inhibitor, S and I are the concentrations of substrate and inhibitor, respectively, v_{max} is the maximum velocity, K_m is the Michaelis-Menten constant, K_i is the competitive inhibition constant, and K'_i is the uncompetitive inhibition constant. The graphs of slope and y-intercept of Lineweaver-Burk plots versus the inhibitor concentration gave a straight line, whose intercept corresponds to K_i and K'_i values, respectively.

5.9 Kinetic of α - glucosidase inhibition

The mode of inhibition of α – Glu in the presence of selected neolignans was determined spectroscopically. The experiments were performed in 96-well plates employing. Precisely, mixtures containing α-Glu (5 μL of a 31 μM solution), the inhibitors (concentration chosen based on IC_{50} value) and *p*-nitro-phenyl-α-glucoside at different concentration (2.00, 1.50, 1.25, 0.83, 0.50, 0.33 and 0.15 mM) were incubated at 37 °C and the optical density was read at 405 nm every 1 min for 30 min with the Synergy H1. The initial velocity (*v*) was determined as the slope of the OD changes at 405 nm during the linear course of the reaction. The data acquired were elaborated according to the Lineweaver-Burk equations (*Eq.2-3*).

5.10 Kinetic of α - amylase inhibition

The mode of inhibition of α—Amy in the presence of selected neolignans were determined according to a procedure previously described with some modifications. The assay was performed in 96-well microplates (final volume of 200 μL). In a typical set of experiments were added 10 μL of enzyme solution (4.0 U/mL in 0.1 mM phosphate buffer containing 0.02% NaN_3; pH 6.8) and the inhibitor at different concentrations chosen based on IC_{50} values. The plate was incubated at 37 °C for 10 min, and the reaction was started by addition of different

aliquots of 10 mM 2-chloro-4-nitrophenyl-α-maltotrioside (1.25, 1.00, 0.75, 0.50, 0.25 mM), the OD was measured at 405 nm every minute for 30 min, maintaining the plate at 37 °C. The initial velocity (v) was determined as the slope of the OD changes at 405 nm during the linear course of the reaction. The inhibition constants were calculated from the Lineweaver-Burk equations *Eq.2* and *Eq.3*.

5.11 Fluorescence measurement

Fluorescence experiments were performed as previously reported. A solution of α-Glu (0.03 mg/mL in 0.1 M phosphate buffer containing 0.1 M NaCl, pH 6.9; 2 mL) or α-Amy (0.4 mg/mL in 0.1 M phosphate buffer containing 0.1 M NaCl, pH 6.9; 2 mL) was titrated by consecutive additions (2 or 4 μL) respectively of the natural product **3** or its synthesized analogues **35**, **44**, **47** or **48** for α-glucosidase while **3**, **35**, or **48** for α-amylase. The concentration of the starting solution of the tested compounds was chosen based on the IC_{50} values. Each titration was replicated at three different temperature 298.15, 303.15, and 310.15 K. The fluorescence spectrum was acquired after 1 min from each addition setting the instrument (Varian Cary Eclipse Spectrophotometer) with the following parameters: λ_{EXC} = 295 nm; slit 10 nm; acquisition from 310 to 500 nm).
The fluorescence at the maximum intensity was employed to obtain the Stern-Volmer plots using the equation:

$$\frac{F_0}{F} = 1 + K_{SV}[Q] = 1 + K_q\tau_0[Q] \qquad (Eq.4)$$

F_0 and F represent the fluorescence intensities of the enzyme before and after the addition of the inhibitor, respectively. [Q] represents the concentration of the compounds studied; τ_0, the average lifetime of the fluorophore in the absence of quencher protein (approximately 10^{-8} s for α-Glu and α-Amy), K_{sv} represents the Stern-Volmer quenching constant. K_q is the biomolecule quenching rate and (K_a)

is the binding constant and n is the number of binding sites. K_a and n were calculated with the following equation:

$$log\frac{F_0 - F}{F} = logK_a + nlog[Q] \quad (Eq.5)$$

5.12 Molecular docking analysis

The 3D structure of pancreatic lipase (PDB ID: 1LPB) was downloaded from Protein Data Bank (RCSB Protein Data Bank: https://www.rcsb.org/structure/ 1lpb accessed April 2020). The lipase is cocrystallised with colipase in the presence of methoxy undecyl phosphonic acid (MUP) as an inhibitor and β-octylglucoside (BOG) as a surfactant. Protein was prepared with Protein wizard, MUP, and BOG, and H_2O molecules were removed; then, the .pdb file obtained was processed with Autodock Tools 1.5.6 and converted in.pdbqt file, merging nonpolar hydrogens and adding Gasteiger charges. The molecular docking studies were conducted using Glide Ligand Docking software integrated with Schrödinger Suite and Autodock Vina software 1.5.6. [205, 206] Autogrid4 (4.2.6 version) was used to generate the gridmaps used in the Vina calculations. The grid box was centred in the protein's binding site, with grid coordinates of 50 × 40 × 50 Å3 for x, y, and z, respectively. The spacing between the grid coordinates was 0.708 Å. The grid centre was set to 7.500, 26.042, and 47.696 Å. Receptor grid generation interfaced with Schrödinger Suite was used to generate the gridmaps for the Glide calculations. The grid box was centred in the protein's binding site, with the grid centre set to 6.52, 22.27 and 43.85 Å. The minimized geometries were converted into.pdbqt files by Autodock Tools (1.5.6). The.sdf files of anti-obesity drug orlistat, and the natural products **1** and **2** were downloaded from PubChem (https://pubchem.ncbi.nlm.nih.gov/, I.D. cod respectively: 3034010, 72300, 72303). Meanwhile, the synthesized

nitrogenated analogues biphenyls **6**–**18c**, were drawn by Chemdraw and saved in.sdf files. The 3D models were geometrically minimised with optimised potential liquid simulation (OPLS3) force fields considering the protonation state at pH of 7.0 ± 1 and processed using LigPrep interfaced with Schrödinger Suite (Version 11) of Schroedinger suite. For the docking experiments carried out with AD4, the Lamarckian Genetic Algorithm was chosen to search for the best conformers. During the docking process, a maximum of 10 conformers was considered for each ligand. In Docking calculation, ligands were treated as flexible while protein was treated as rigid. Autodock Vina and Glide were compiled and run in O.S.X. Yosemite (10.10.5) environment. The analysis of docking outcomes was carried out by Schrödinger Suite (Version 11), and figures of 3D models were generated by Pymol (2.3.5).

Due to the absence of the related solved structure of α-Glu in the Protein Data Bank, it would have been necessary to proceed with the construction of a homology model [207]. After 2022, the AphaFold protein structure database (https://alphafold.ebi.ac.uk) provides 3D protein models with high-accuracy counting more than 200 million entries, between which also α-Glu, provides broad coverage of UniProt (the standard repository of protein sequences and annotations) freely available for the scientific community [208, 209]. Therefore, the α-Glu from *S. cerevisiae* (AF-P53341-F1-model_v4) was downloaded from the above-cited AlphaFold data bank, whereas the α-Amy (PDB ID: 4W93) from the Protein Data Bank (https://alphafold.ebi.ac.uk). Glide Ligand Docking was employed to acquire the computational experiments. The model was first prepared and minimized by Protein preparation wizard. The putative binding site was identified through SiteMap software, that allowed to generate a ranking of five possible druggable binding pockets based on the site score output and the best-one was then used for the molecular docking calculation. Specifically starting from site 1 the following coordinates were obtained by Grid generation experiment: 14.61 (x), 2.13 (y), 1.91 (z), 10 x 10 x 10 as innerbox, and 36.76 x 36.76 x 36.76 as outerbox.

The .pdb file of human pancreatic α-amylase (PDB ID: 4W93) was downloaded from Protein Data Bank. The α-amylase is cocrystallized with montbretin A as specific inhibitor. The grid box was centred in the binding site of protein, with grid centre set to -7.28 (x), 7.43 (y) and -18.44 (z), 10 x 10 x 10 as innerbox, and 30 x 30 x 30 as outerbox. The .sdf file of hypoglycemic drug acarbose was downloaded from Pubchem (https://pubchem.ncbi.nlm.nih.gov ID code: 41774), while the natural lead **3** and the synthesized analogues **30**, **34** – **37**, **39**, **41**, **44** and **47** – **48** were drawn by ChemDraw and saved in .sdf file. Then the library was prepared by LigPrep software, generating all the possible tautomers and protonation states (pH = 7.4 ± 1.0) for each compound. The obtained structures were minimized by OPLS3. The molecular docking studies were performed using Glide interfaced with Schrödinger Suite. In docking calculation, the protein was treated as rigid and ligands as flexible. Glide were compiled and run in OSX Yosemite (10.10.5) environment. The analysis of docking outcomes was carried out by Schrödinger Suite (Version 11), and figures of 3D models were generated by Pymol (2.3.5). The same procedures were employed to analyze the dimers **52** – **54**. The synthesized compounds were drawn by ChemDraw and saved in .sdf file.

5.13 Circular dichroism analysis

CD spectra were recorded using a Jasco J715 spectropolarimeter equipped with a single-position Peltier temperature control set at 37 °C. A quartz cuvette with a 1 cm path length was employed for all ECD experiments. The CD measurements were performed in the range 200–260 nm in the presence or absence of the tested compounds (**3**, **35**, **44**, **47** and **48**). The experimental parameters were as follows: scanning rate 50 nm/min, data pitch 0.2 nm, digital integration time (D.I.T) 4s, band width 2.0 nm. Each ECD spectrum was an average of at least five scans. For each experiment the α-glucosidase (0.5 µM in 10 mM phosphate buffer, pH 7.2) was titrated with increasing aliquots of natural lead or synthesized

obovatol analogues, thus the concentration of tested compounds was increased from a ratio of 0:1 to 6:1 respectively. The CD spectra were collected after each addition and corrected by subtracting the blank signal (100 mM phosphate buffer). Additionally, CD spectra of selected compounds, at the highest concentration tested, were acquired under the same conditions. To assess the changes of secondary structures of α-glucosidase, the secondary Structure Estimation software included in the JASCO Spectra Manager software were employed.

5.14 Assessment of the presence of atropisomerism for compounds 1, 2 16b, 17 and 18b

The 3D models of all the compounds were geometrically minimised OPLS3 force fields considering the protonation state at pH of 7.0 ± 1 and processed using LigPrep interfaced with Schrödinger Suite (Version 11). LigPrep can also generate and sample alternative chiralities, including tautomers, ring conformations, and alternative chiralities. Regarding the inhibitors, the software furnished only a single structure for each molecule selected.

In addition to *in silico* studies, HPLC on a chiral column was performed to verify the possible presence of atropisomers. The results indicated that neither the natural products **1** and **2** nor the new analogues **16b**, **17,** and **18b** were present as atropisomers at room temperature; thus, they had not restricted rotation along C1-C1' linkage as usually occurred in many di-*ortho*-substituted compounds. Furthermore, natural products **1** and **2** and selected nitrogenated neolignans **16b**, **17** and **18b** were analyzed by HPLC-UV using Chiralcel OD column (4.6 mm x 250 mm, 5 μm, Daicel, Japan). According to HPLC run at 10 °C, the energy barrier between two possible atropisomers may be low, and the interconversion of atropisomers occurred both at room temperature and at 10 °C. Based on those results, it can be stated that **1**, **2**, **16b**, **17,** and **18b** had no atropisomerism behaviour in the condition applied for our experiments (**Figure S133 – 134**).

List of figures

List of tables

List of schemes

Scheme 22. Synthesis of analogues **36**, **37**, **39**, **41** and **44**. *a)* dioxane, Cs_2CO_3 (2 eq.), phenol (1.5 eq.), CuI (10 mol%), *N*, *N*-dimethylglycine HCl (30 mol%), 24h, 90 °C. *b)* dry CH_2Cl_2, BBr_3 (1M in DCM, 1 eq.), 3h, -78 °C. *c*) DMF, K_2CO_3 (3 eq.), CH_3I (3 eq.), overnight, room temperature.

Scheme 23. Synthesis of analogues **47** - **48**. *a)* dry THF, SIBX (2.15 eq.), 16h, room temperature. *b)* thiol (3 eq,), dry 1-2h, room temperature.

Scheme 24. Synthesis of analogues **50**. *a)* $Pd(OAc)_2$ (10%mol), dppf (30%mol), K_2CO_3 (5 eq), allyl boronic acid pinacol ester (1.5 eq.), THF:H_2O (10:1), 67°C, 24h.*b)* $Pd(OAc)_2$ (1%mol), SPhos(2%mol), K_2CO_3 (2 eq), allyl boronic acid pinacol ester (1.5 eq.), THF:H_2O (10:1), 67°C, 24h.

Scheme 25. Retrosynthetic analysis of houpulin B (**52**).

Scheme 26. Possible mechanism for the synthesis of **52**.

Scheme 27. Synthesis of oligomeric compounds **53**- **54**. *a)* $CHCl_3$, Ag_2O (catalyst, 1 eq.), 5h, room temperature. *b)* LTV (catalyst), phosphate buffer 0.1 M pH = 6, 4 days, room temperature.

Supplementary Materials

The following are available online at

https://drive.google.com/file/d/1OxXuw5qQ0mIGLRJQivSZsiDnba253SV7/view?usp=sharing

List of Supplementary Figures

Figure S1. HRESIMS (-) spectrum of **4a**.

Figure S2. ^{1}HNMR spectrum (500 MHz, $CDCl_3$) of **4a**.

Figure S3. HRESIMS (-) spectrum of **4b**.

Figure S4. ^{1}HNMR spectrum (500 MHz, $CDCl_3$) of **4b**.

Figure S5. HRESIMS (+) spectrum of **6**.

Figure S6. ^{1}HNMR spectrum (500 MHz, $CDCl_3$) of **6**.

Figure S7. ^{13}CNMR spectrum (125 MHz, CD_3OD- $CDCl_3$) of **6**.

Figure S8. gCOSY spectrum of **6**.

Figure S9. gHMBC spectrum of **6**.

Figure S10. gHSQC spectrum of **6**.

Figure S11. HRESIMS (+) spectrum of **7**.

Figure S12. ^{1}HNMR spectrum (500 MHz, $CDCl_3$) of **7**.

Figure S13. ^{13}CNMR spectrum (125 MHz, $CDCl_3$) of **7**.

Figure S14. gCOSY spectrum of **7**.

Figure S15. gHMBC spectrum of **7**.

Figure S16. gHSQC spectrum of **7**.

Figure S17. HRESIMS (-) spectrumof **8**.

Figure S18. ^{1}HNMR spectrum (500 MHz, CD_3OD-$CDCl_3$) of **8**.

Figure S19. ^{13}CNMR spectrum (125 MHz, CD_3OD-$CDCl_3$) of **8**.

Figure S20. gCOSY spectrum of **8**.

Figure S21. gHMBC spectrum of **8**.

Figure S22. gHSQC spectrum of **8**.

Figure S23. HRESIMS (+) spectrum of **9**.

Figure S24. ^{1}HNMR spectrum (500 MHz, $CDCl_3$) of **9**.

Figure S25. ^{13}CNMR spectrum (125 MHz, CD_3OD-$CDCl_3$) of **9**.

Figure S26. gCOSY spectrum of **9**.

List of supplementary Tables

Publications

- **C. Sciacca**, N. Cardullo, V. Muccilli. "*2,3-Bis((E)-4- hydroxybenzylidene)-N1,N4-bis(4- methylbenzyl)succinimide*". *Molbank*, **2023**.
- **C. Sciacca**, N. Cardullo, L. Pulvirenti, A. Di Francesco, V. Muccilli. "*Evaluation of honokiol, magnolol and of a library of new nitrogenated neolignans as pancreatic lipase inhibitors*". *Bioorganic Chemistry* 134 (**2023**) 106455.
- **C. Sciacca**, N. Cardullo, L. Pulvirenti, G. Travagliante, A. D'Urso, A. Cornu, D. Deffieux, L. Pouségu, S. Quideau, V. Muccilli." *Synthesis of obovatol and related neolignans as α- glucosidase and α-amylase inhibitors*". (Manuscript to be submitted to Bioorganic Chemistry)

Conference proceedings

- **C. Sciacca**, N. Cardullo, V. Muccilli, C. Tringali. "*Sintesi di analoghi azotati dell'honokiolo*" poster communication presented at Workshop della Sezione Sicilia 2020- Società Chimica Italiana. December 2020.
- **C. Sciacca**, N. Cardullo, V. Muccilli, C. Tringali. "*Synthesis and structural characterization of a library of nitrogen analogues derived from honokiol*" poster communication presented at European Chemical Biology Symposium 2021(ECBS). May 24th - 26th, 2021.
- **C. Sciacca**, N. Cardullo, V. Muccilli, C. Tringali. "*Nitrogenated analogues of honokiol as potential metabolic enzymes inhibitors*" poster communication presented at European School of Medicinal Chemistry (ESMEC). 28th May – 1st June 2021.
- **C. Sciacca**, N. Cardullo, V. Muccilli, C. Tringali. "*Synthesis and inhibitory activity towards metabolic enzymes of dimeric neolignans inspired by honokiol agents*" oral communication presented at International Summer School on Natural Products (ISSNP). July 6th – 8th, 2021.
- **C. Sciacca**, N. Cardullo, V. Muccilli, C. Tringali. "*Synthesis and inhibitory activity towards metabolic enzymes of dimeric neolignans inspired by honokiol agents*" oral communication presented at XXVII Congresso nazionale della Società Chimica Italiana. September 14th - 23 rd, 2021.
- V. Muccilli, **C. Sciacca**, N. Cardullo, C. Tringali. "*Natural polyphenols and synthetic analogues as potential hypoglycemic and antiobesity agents*" poster communication presented at XXVII Congresso nazionale della Società Chimica Italiana. September 14th – 23rd, 2021 (co-author).
- **C. Sciacca**, N. Cardullo, V. Muccilli, C. Tringali. "*Synthetic nitrogenated analogues inspired by honokiol as hypoglygemic and anti-obesity agents*" oral communication presented at Merk Young Chemists' Symposium 2021 (MYCS21). Rimini, Italy, November 22nd – 24th, 2021.

- **C. Sciacca**, N. Cardullo, V. Muccilli, C. Tringali. "*Synthesis and evaluation of α-amylase and lipase inhibitory activities of dimeric neolignans nitrogenated analogues inspired by honokiol as hypoglycemic and anti-obesity agents*" oral communication presented at SCI Conference2021- Section Sicily. December 2nd, 2021.
- N. Cardullo, **C. Sciacca**, V. Muccilli. "*Synthesis of gallic acid-resveratrol hybrid molecules as potential bioactive compounds*" poster communication presented at XL Convegno Nazionale della Divisione di Chimica Organica della Società Chimica Italiana. Palermo, Italy, September 11th - 15th 2022. (co-author)
- **C. Sciacca**, N. Cardullo, A. Cornu, D. Deffieux, L. Pouségu, V. Muccilli, S. Quideau. "*Chemical synthesis of bioactive neolignane obovatol and analogues*" poster communication presented at Ischia Advanced School of Organic Chemistry (IASOC). Ischia, Italy, September 23rd – 26th, 2022.
- **C. Sciacca**, N. Cardullo, A. Cornu, D. Deffieux, L. Pouségu, V. Muccilli, S. Quideau. "*Synthesis of neolignane obovatol and its analogues*" poster communication presented at 2nd Virtual Symposium for Young Organic Chemists of Società Chimica Italiana. October 20th – 27th, 2022.
- **C. Sciacca**, N. Cardullo, L. Pulvirenti, V. Muccilli. "*Lipase inhibitory analysis of magnolol, honokiol and three nitrogenated derivatives*" oral and poster communications presented at Merk Young Chemists' Symposium 2022 (MYCS22). Rimini, Italy, November 21st – 23rd, 2022.
- **C. Sciacca**, N. Cardullo, L. Pulvirenti, A. Cornu, D. Deffieux, L. Pouségu, S. Quideau, V. Muccilli. "*Synthesis of bioactive neolignane obovatol and analogues as hypoglycemic agents*" oral communication presented at International Summer School on Natural Products (ISSNP). Maratea, Italy, July 2nd – 7th, 2023.
- **C. Sciacca**, N. Cardullo, L. Pulvirenti, A. Cornu, D. Deffieux, L. Pouségu, S. Quideau, V. Muccilli. "*Evaluation of obovatol and of a small library of*

analogues as hypoglycemic agents" oral communication presented at XLI Convegno Nazionale della Divisione di Chimica Organica della Società Chimica Italiana. Roma, Italy, September 10th - 14th 2023.

- **C. Sciacca**, N. Cardullo, L. Pulvirenti, V. Muccilli. "*Bioactive neolignans magnolol, honokiol and obovatol and their synthetic analogues as digestive enzymes inhibitors*" oral communication presented at 31st International Symposium on the Chemistry of Natural Products and 11th International Congress on Biodiversity (ISCNP31&ICOB11). Napoli, Italy, October 15th - 19th, 2023.

Acknowledgments

I would like to express my deepest gratitude to all those who have supported and guided me throughout my PhD career. I am immensely grateful to my tutor Prof. Vera Muccilli for her supervision, teaching and mentoring and continuous support. Her unwavering encouragement and assistance have been invaluable in the completion of this doctoral thesis.

I am thankful to Dr. Nunzio Cardullo for his advice, immense availability to provide me suggestions and personal support. Special thanks to all the team of Laboratory of Bioactive Natural Products (LabCoNaBi) of the University of Catania. Thanks should also go to Prof. Stéphane Quideau and the group of the Institut of des Sciences Molécularеis for the infinity hospitality and kindness.

Lastly, I extend my sincere gratitude to my family for their unwavering love and support. To Federica, thank you for being a source of encouragement and for helping me stay grounded.

References

[1] M.M. Rahman, S. Bibi, M.S. Rahaman, F. Rahman, F. Islam, M.S. Khan, M.M. Hasan, A. Parvez, M.A. Hossain, S.K. Maeesa, M.R. Islam, A. Najda, H.S. Al-malky, H.R.H. Mohamed, H.I.M. AlGwaiz, A.A. Awaji, M.O. Germoush, O.A. Kensara, M.M. Abdel-Daim, M. Saeed, M.A. Kamal, Natural therapeutics and nutraceuticals for lung diseases: Traditional significance, phytochemistry, and pharmacology, Biomedicine & Pharmacotherapy 150 (2022) 113041.

[2] S. Kanba, K. Yamada, H. Mizushima, M. Asai, Use of herbal medicine for treating psychiatric disorders in Japan, Psychiatry and Clinical Neurosciences 52 (1998) S331-S333.

[3] M. Homma, K. Oka, H. Kobayashi, T. Niitsuma, S. Yamamoto, H. Itoh, N. Takahashi, Liquid-chromatographic determination of magnolol in urine collected from volunteers after a single-dose of saiboku-to, an oriental herbal medicine for bronchial-asthma, Journal of Pharmacy and Pharmacology 45(9) (1993) 839-841.

[4] M. Yuzurihara, Y. Ikarashi, A. Ishige, H. Sasaki, Y. Maruyama, Anxiolytic-like effect of saiboku-to, an oriental herbal medicine, on histaminergics-induced anxiety in mice, Pharmacology Biochemistry and Behavior 67(3) (2000) 489-495.

[5] J.L. Shen, K.M. Man, P.H. Huang, W.C. Chen, D.C. Chen, Y.W. Cheng, P.L. Liu, M.C. Chou, Y.H. Chen, Honokiol and Magnolol as Multifunctional Antioxidative Molecules for Dermatologic Disorders, Molecules 15(9) (2010) 6452-6465.

[6] A.C. D. Thirumurugan, S.S. Raja and R. Vijayakumar, An Introductory Charpter: secondary metabolites, (2018).

[7] B.M.T.a.M.N. Hasan, Bioactive secondary metabolites from plant sources: type, synthesis and their therapeutic uses, International Journal of Plant Biology 13(1) (2022) 4-14.

[8] E.S. J.N. Kabera, A.R. Mussa and X. He, Plant secondary metabolites: Biosynthesis, classification, function and pharmacological properties, Journal of Pharmacy and Pharmacology (2014) 377-392.
[9] P.M. Dewick, Chimica, Biosintesi e Bioattività delle sostanza naturali, 2001.
[10] T.F. Corrado Tringali Bioactive compounds from natural sources isolation,characterisation and biological properties, (2001).
[11] M. Feher, J.M. Schmidt, Property distributions: Differences between drugs, natural products, and molecules from combinatorial chemistry, Journal of Chemical Information and Computer Sciences 43(1) (2003) 218-227.
[12] D.J. Newman, G.M. Cragg, Natural products as sources of new drugs over the last 25 years, Journal of Natural Products 70(3) (2007) 461-477.
[13] R. Abu Khalaf, Exploring Natural Products as a Source for Antidiabetic Lead Compounds and Possible Lead Optimization, Current Topics in Medicinal Chemistry 16(23) (2016) 2549-2561.
[14] O.T. Ebob, S.B. Babiaka, F. Ntie-Kang, Natural Products as Potential Lead Compounds for Drug Discovery Against SARS-CoV-2, Natural Products and Bioprospecting 11(6) (2021) 611-628.
[15] D.J. Newman, G.M. Cragg, Natural Products as Sources of New Drugs over the Nearly Four Decades from 01/1981 to 09/2019, Journal of Natural Products 83(3) (2020) 770-803.
[16] D.J. Newman, G.M. Cragg, K.M. Snader, Natural products as sources of new drugs over the period 1981-2002, Journal of Natural Products 66(7) (2003) 1022-1037.
[17] E. Haslam, “Practical Polyphenolics: From Structure to Molecular Recognition and Physiological Action,” (1998) 52-60.
[18] K.D. A. Belščak-Cvitanović, A. Huđek, V. Bačun-Družina, D. Komes, Overview of polyphenols and their properties, (2018) 3-44.

[19] A. Durazzo, M. Lucarini, E.B. Souto, C. Cicala, E. Caiazzo, A.A. Izzo, E. Novellino, A. Santini, Polyphenols: A concise overview on the chemistry, occurrence, and human health, Phytotherapy Research 33(9) (2019) 2221-2243.
[20] S.C. Thomasset, D.P. Berry, G. Garcea, T. Marczylo, W.P. Steward, A.J. Gescher, Dietary polyphenolic phytochemicals - Promising cancer chemopreventive agents in humans? A review of their clinical properties, International Journal of Cancer 120(3) (2007) 451-458.
[21] S. Ramos, Cancer chemoprevention and chemotherapy: Dietary polyphenols and signalling pathways, Molecular Nutrition & Food Research 52(5) (2008) 507-526.
[22] S.N.A. Bukhari, Dietary Polyphenols as Therapeutic Intervention for Alzheimer's Disease: A Mechanistic Insight, Antioxidants 11(3) (2022) 554.
[23] R.B. Teponno, S. Kusari, M. Spiteller, Recent advances in research on lignans and neolignans, Natural Product Reports 33(9) (2016) 1044-1092.
[24] J. Zhang, J.J. Chen, Z.Z. Liang, C.Q. Zhao, New Lignans and Their Biological Activities, Chemistry & Biodiversity 11(1) (2014) 1-54.
[25] G.P. Moss, Nomenclature of lignans and neolignans (IUPAC Recommendations 2000), Pure and Applied Chemistry 72(8) (2000) 1493-1523.
[26] F. Zalesak, D. Bon, J. Pospisil, Lignans and Neolignans: Plant secondary metabolites as a reservoir of biologically active substances, Pharmacological Research 146 (2019) 104284.
[27] G. Lopes, E. Pinto, L. Salgueiro, Natural Products: An Alternative to Conventional Therapy for Dermatophytosis?, Mycopathologia 182(1) (2017) 143-167.
[28] Y.J. Lee, Y.M. Lee, C.K. Lee, J.K. Jung, S.B. Han, J.T. Hong, Therapeutic applications of compounds in the Magnolia family, Pharmacology & Therapeutics 130(2) (2011) 157-176.
[29] F. M., Profiles of effects of traditional oriental herbal medicines on central nervous systems in humans--assessment of saiboku-to and saiko-ka-ryukotsu-

borei-to using EEG and pharmacokinetics of herbal medicine-derived ingredients as indices, Seishin Shinkeigaku Zasshi 99(6) (1997) 355-69.
[30] I.H. Fujita M, Sashida Y., [Studies on the components of Magnolia obovata Thunb. 3. Occurrence of magnolol and hõnokiol in M. obovata and other allied plants], 93 (1973) 429-34.
[31] M.G.N. M.A. Kelm, A Brief Summary of Biologically Active Compounds from Magnolia spp., Studies in Natural Products Chemistry, Elsevier 24 (2000) 845-873.
[32] J.S. Kang, K.H. Lee, M.H. Han, H. Lee, J.M. Ahn, S.B. Han, G. Han, K. Lee, S.K. Park, H.M. Kim, Antiinflammatory activity of methanol extract isolated from stem bark of Magnolia kobus, Phytotherapy Research 22(7) (2008) 883-888.
[33] K.L. Xu, J. Ma, C.A. Li, C.J. Li, Y.D. Zang, X.Y. Sun, X.G. Chen, X.L. Wang, D.M. Zhang, Isolation and structural elucidation of bioactive obovatol dimeric neolignans from the bark of Magnolia officinalis var. biloba, Phytochemistry 194 (2022) 113020.
[34] J.J. Patočka J, Strunecká A, Expectations of biologically active compounds of the genus Magnolia in biomedicine, J Appl Biomed. 4 (2006) 171-178.
[35] W.H. Watanabe K, Goto Y, Yamaguchi M, Yamamoto N, Hagino K., Pharmacological properties of magnolol and honokiol extracted from Magnolia officinalis: central depressant effects, Planta Med 49 (1983) 103-8.
[36] W.W. Tao, Y.W. Hu, Z.Y. Chen, Y.X. Dai, Y. Hu, M.M. Qi, Magnolol attenuates depressive-like behaviors by polarizing microglia towards the M2 phenotype through the regulation of Nrf2/HO-1/NLRP3 signaling pathway, Phytomedicine 91 (2021) 153692.
[37] A.M. Ranaware, K. Banik, V. Deshpande, G. Padmavathi, N.K. Roy, G. Sethi, L. Fan, A.P. Kumar, A.B. Kunnumakkara, Magnolol: A Neolignan from the Magnolia Family for the Prevention and Treatment of Cancer, International Journal of Molecular Sciences 19(8) (2018) 2362.

[38] R. Amorati, J. Zotova, A. Baschieri, L. Valgimigli, Antioxidant Activity of Magnolol and Honokiol: Kinetic and Mechanistic Investigations of Their Reaction with Peroxyl Radicals, Journal of Organic Chemistry 80(21) (2015) 10651-10659.
[39] G.I.P. Cicalau, P.A. Babes, H. Calniceanu, A. Popa, G. Ciavoi, G.M. Iova, M. Ganea, I. Scrobota, Anti-Inflammatory and Antioxidant Properties of Carvacrol and Magnolol, in Periodontal Disease and Diabetes Mellitus, Molecules 26(22) (2021) 6899.
[40] Z.B. Liu, J. Xie, K. Lin, L.G. Qi, Influencing mechanism of magnolol on expression of BDNF and Bax in rats with cerebral ischemic stroke, Experimental and Therapeutic Medicine 16(6) (2018) 4423-4428.
[41] Y.F. Xian, C. Qu, Y. Liu, S.P. Ip, Q.J. Yuan, W. Yang, Z.X. Lin, Magnolol Ameliorates Behavioral Impairments and Neuropathology in a Transgenic Mouse Model of Alzheimer's Disease, Oxidative Medicine and Cellular Longevity 2020 (2020) 5920476.
[42] C.C. Weng, Z.A. Chen, K.T. Chao, T.W. Ee, K.J. Lin, M.H. Chan, I.T. Hsiao, T.C. Yen, M.P. Kung, C.H. Hsu, S.P. Wey, Quantitative analysis of the therapeutic effect of magnolol on MPTP-induced mouse model of Parkinson's disease using in vivo F-18-9fluoropropyl-(+)-dihydrotetrabenazine PET imaging, Plos One 12(3) (2017) e0173503.
[43] I. Usach, A. Alaimo, J. Fernandez, A. Ambrosini, S. Mocini, L. Ochiuz, J.E. Peris, Magnolol and Honokiol: Two Natural Compounds with Similar Chemical Structure but Different Physicochemical and Stability Properties, Pharmaceutics 13(2) (2021) 224.
[44] J.H. Chen, C.C. Wu, G. Hsiao, M.H. Yen, Magnolol induces apoptosis in vascular smooth muscle, Naunyn-Schmiedebergs Archives of Pharmacology 368(2) (2003) 127-133.
[45] Y.J. Kim, M.S. Choi, B.Y. Cha, J.T. Woo, Y.B. Park, S.R. Kim, U.J. Jung, Long-term supplementation of honokiol and magnolol ameliorates body fat

accumulation, insulin resistance, and adipose inflammation in high-fat fed mice, Molecular Nutrition & Food Research 57(11) (2013) 1988-1998.
[46] Y.P. Lin, Y.K. Li, Y.L. Zeng, B. Tian, X.L. Qu, Q.H. Yuan, Y. Song, Pharmacology, Toxicity, Bioavailability, and Formulation of Magnolol: An Update, Frontiers in Pharmacology 12 (2021) 632767.
[47] G. Pulivendala, S. Bale, C. Godugu, Honokiol: A polyphenol neolignan ameliorates pulmonary fibrosis by inhibiting TGF-beta/Smad signaling, matrix proteins and IL-6/CD44/STAT3 axis both in vitro and in vivo, Toxicology and Applied Pharmacology 391 (2020) 114913.
[48] X.Y. Liu, X.L. Chen, Y.J. Zhu, K.W. Wang, Y.Y. Wang, Effect of magnolol on cerebral injury and blood brain barrier dysfunction induced by ischemia-reperfusion in vivo and in vitro, Metabolic Brain Disease 32(4) (2017) 1109-1118.
[49] J.W. Lin, J.T. Chen, C.Y. Hong, Y.L. Lin, K.T. Wang, C.J. Yao, G.M. Lai, R.M. Chen, Honokiol traverses the blood-brain barrier and induces apoptosis of neuroblastoma cells via an intrinsic bax-mitochondrion-cytochrome c-caspase protease pathway, Neuro-Oncology 14(3) (2012) 302-314.
[50] Z.Y. Hu, X.L. Bian, X.Y. Liu, Y.J. Zhu, X.Y. Zhang, S.Z. Chen, K.W. Wang, Y.Y. Wang, Honokiol protects brain against ischemia-reperfusion injury in rats through disrupting PSD95-nNOS interaction, Brain Research 1491 (2013) 204-212.
[51] A. Kumar, U.K. Singh, A. Chaudhary, Honokiol analogs: a novel class of anticancer agents targeting cell signaling pathways and other bioactivities, Future Medicinal Chemistry 5(7) (2013) 809-829.
[52] W. Schuhly, A. Hufner, E.M. Pferschy-Wenzig, E. Prettner, M. Adams, A. Bodensieck, O. Kunert, A. Oluwemimo, E. Haslinger, R. Bauer, Design and synthesis of ten biphenyl-neolignan derivatives and their in vitro inhibitory potency against cyclooxygenase-1/2 activity and 5-lipoxygenase-mediated LTB4-formation, Bioorganic & Medicinal Chemistry 17(13) (2009) 4459-4465.

[53] C.H. Hsiao, C.J. Yao, G.M. Lai, L.M. Lee, J. Whang-Peng, P.H. Shih, Honokiol induces apoptotic cell death by oxidative burst and mitochondrial hyperpolarization of bladder cancer cells, Experimental and Therapeutic Medicine 17(5) (2019) 4213-4222.
[54] J.M. Lin, A.S.P. Gowda, A.K. Sharma, S. Amin, In vitro growth inhibition of human cancer cells by novel honokiol analogs, Bioorganic & Medicinal Chemistry 20(10) (2012) 3202-3211.
[55] S. Fujita, J. Taira, Biphenyl compounds are hydroxyl radical scavengers - their effective inhibition for uv-induced mutation in salmonella-typhimurium TA102, Free Radical Biology and Medicine 17(3) (1994) 273-277.
[56] H. Haraguchi, H. Ishikawa, N. Shirataki, A. Fukuda, Antiperoxidative activity of neolignans from Magnolia obovata, Journal of Pharmacy and Pharmacology 49(2) (1997) 209-212.
[57] A. Rauf, A. Olatunde, M. Imran, F.A. Alhumaydhi, A.S.M. Aljohani, S.A. Khan, M.S. Uddin, S. Mitra, T. Bin Emran, M. Khayrullin, M. Rebezov, M.A. Kamal, M.A. Shariati, Honokiol: A review of its pharmacological potential and therapeutic insights (vol 90, 153647, 2021), Phytomedicine 92 (2021) 153769.
[58] M. Poivre, P. Duez, Biological activity and toxicity of the Chinese herb Magnolia officinalis Rehder & E. Wilson (Houpo) and its constituents, Journal of Zhejiang University-Science B 18(3) (2017) 194-214.
[59] B. Zhang, P.P. Wang, K.L. Hu, L.N. Li, X. Yu, Y. Lu, H.S. Chang, Antidepressant-Like Effect and Mechanism of Action of Honokiol on the Mouse Lipopolysaccharide (LPS) Depression Model, Molecules 24(11) (2019) 2035.
[60] J.J. Seo, S.H. Lee, Y.S. Lee, B.M. Kwon, Y. Ma, B.Y. Hwang, J.T. Hong, K.W. Oh, Anxiolytic-like effects of obovatol isolated from Magnolia obovata: Involvement of GABA/benzodiazepine receptors complex, Progress in Neuro-Psychopharmacology & Biological Psychiatry 31(7) (2007) 1363-1369.

[61] N. Cardullo, V. Barresi, V. Muccilli, G. Spampinato, M. D'Amico, D.F. Condorelli, C. Tringali, Synthesis of Bisphenol Neolignans Inspired by Honokiol as Antiproliferative Agents, Molecules 25(3) (2020) 733.
[62] J. Ock, H.S. Han, S.H. Hong, S.Y. Lee, Y.M. Han, B.M. Kwon, K. Suk, Obovatol attenuates microglia-mediated neuroinflammation by modulating redox regulation, British Journal of Pharmacology 159(8) (2010) 1646-1662.
[63] Y. Lim, J.S. Kwon, D.W. Kim, S.H. Lee, R.K. Park, J.J. Lee, J.T. Hong, H.S. Yoo, B.M. Kwon, Y.P. Yun, Obovatol from Magnolia obovata inhibits vascular smooth muscle cell proliferation and intimal hyperplasia by inducing p21(Cip1), Atherosclerosis 210(2) (2010) 372-380.
[64] M.S. Lee, J.E. Yang, E.H. Choi, J.K. In, S.Y. Lee, H. Lee, J.T. Hong, H.W. Lee, Y.G. Suh, J.K. Jung, Synthesis of obovatol derivatives and their preliminary evaluation as antitumor agents, Bulletin of the Korean Chemical Society 28(9) (2007) 1601-1604.
[65] J.H. Oh, L.L. Kang, J.O. Ban, Y.H. Kim, K.H. Kim, S.B. Han, J.T. Hong, Anti-inflammatory effect of 4-O-methylhonokiol, a novel compound isolated from Magnolia officinalis through inhibition of NF-kappa B, Chemico-Biological Interactions 180(3) (2009) 506-514.
[66] W.S. Choi, T.H. Lee, S.J. Son, T.G. Kim, B.M. Kwon, H.U. Son, S.U. Kim, S.H. Lee, Inhibitory effect of obovatol from Magnolia obovata on the Salmonella type III secretion system, Journal of Antibiotics 70(11) (2017) 1065-1069.
[67] D.K. Choi, S. Koppula, K. Suk, Inhibitors of Microglial Neurotoxicity: Focus on Natural Products, Molecules 16(2) (2011) 1021-1043.
[68] M.S. Choi, S.H. Lee, H.S. Cho, Y. Kim, Y.P. Yun, H.Y. Jung, J.K. Jung, B.C. Lee, H.B. Pyo, J.T. Hong, Inhibitory effect of obovatol on nitric oxide production and activation of NF-kappa B/MAP kinases in lipopolysaccharide-treated RAW 264.7 cells, European Journal of Pharmacology 556(1-3) (2007) 181-189.
[69] E.S. Park, Y. Lim, S.H. Lee, B.M. Kwon, H.S. Yoo, J.T. Hong, Y.P. Yun, Antiplatelet Activity of Obovatol, a Biphenolic Component of Magnolia Obovata,

in Rat Arterial Thrombosis and Rabbit Platelet Aggregation, Journal of Atherosclerosis and Thrombosis 18(8) (2011) 659-669.
[70] F. Amblard, B. Govindarajan, B. Lefkove, K.L. Rapp, M. Detorio, J.L. Arbiser, R.F. Schinazi, Synthesis, cytotoxicity, and antiviral activities of new neolignans related to honokiol and magnolol, Bioorganic & Medicinal Chemistry Letters 17(16) (2007) 4428-4431.
[71] X.L. Sun, M.L. Zhu, Y.Q. Dai, H.M. Li, B.H. Li, H. Ma, C.H. Zhang, C.Z. Wu, Semi-Synthesis and In Vitro Anti-Cancer Evaluation of Magnolol Derivatives, Molecules 26(14) (2021) 4302.
[72] L. Pulvirenti, V. Muccilli, N. Cardullo, C. Spatafora, C. Tringali, Chemoenzymatic Synthesis and alpha-Glucosidase Inhibitory Activity of Dimeric Neolignans Inspired by Magnolol, Journal of Natural Products 80(5) (2017) 1648-1657.
[73] S. Jada, M.R. Doma, P.P. Singh, S. Kumar, F. Malik, A. Sharma, I.A. Khan, G.N. Qazi, H.M.S. Kumar, Design and synthesis of novel magnolol derivatives as potential antimicrobial and antiproliferative compounds, European Journal of Medicinal Chemistry 51 (2012) 35-41.
[74] B. Lee, J.H. Kwak, S.W. Huang, J.Y. Jang, S. Lim, Y.S. Kwak, K. Lee, H.S. Kim, S.B. Han, J.T. Hong, H. Lee, S. Song, S.Y. Seo, J.K. Jung, Design and synthesis of 4-O-methylhonokiol analogs as inhibitors of cyclooxygenase-2 (COX-2) and PGF(1) production, Bioorganic & Medicinal Chemistry 20(9) (2012) 2860-2868.
[75] L. Ma, J.Y. Chen, X.W. Wang, X.L. Liang, Y.F. Luo, W. Zhu, T.N. Wang, M. Peng, S.C. Li, S. Jie, A.H. Peng, Y.Q. Wei, L.J. Chen, Structural Modification of Honokiol, a Biphenyl Occurring in Magnolia officinalis: the Evaluation of Honokiol Analogues as Inhibitors of Angiogenesis and for Their Cytotoxicity and Structure-Activity Relationship, Journal of Medicinal Chemistry 54(19) (2011) 6469-6481.

[76] C. Yang, X.Y. Zhi, H. Xu, Semisynthesis and insecticidal activity of arylmethylamine derivatives of the neolignan honokiol against Mythimna separata Walker, Zeitschrift Fur Naturforschung Section C-a Journal of Biosciences 70(3-4) (2015) 65-69.
[77] B. Taferner, W. Schuehly, A. Huefner, I. Baburin, K. Wiesner, G.F. Ecker, S. Hering, Modulation of GABA(A)-Receptors by Honokiol and Derivatives: Subtype Selectivity and Structure-Activity Relationship, Journal of Medicinal Chemistry 54(15) (2011) 5349-5361.
[78] W.S.K. Chiang Chan E.W, Chan H.T, A short review on the chemistry, pharmacological properties and patents of obovatol and obovatol (neolignans) from *Magnolia obovata,* Natural Product Sciences 27(3) (2021) 141-150.
[79] E.J. Seo, N. Fischer, T. Efferth, Phytochemicals as inhibitors of NF-kappa B for treatment of Alzheimer's disease, Pharmacological Research 129 (2018) 262-273.
[80] S.Y. Lee, Y.S. Cho, S.M. Kim, D.J. Son, D.C. Moon, Y.P. Yuni, J.K. Jung, J.T. Hong, Obovatol enhances docetaxel resistant prostate and colon cancer cell death: Involvement of NF-kappa B inactivation, Journal of Pharmacological Sciences 111(2) (2009) 124-136.
[81] M.L. Duan, X.M. Du, G. Ren, Y.D. Zhang, Y. Zheng, S.P. Sun, J. Zhang, Obovatol inhibits the growth and aggressiveness of tongue squamous cell carcinoma through regulation of the EGF-mediated JAK-STAT signaling pathway, Molecular Medicine Reports 18(2) (2018) 1651-1659.
[82] J. Kim, H. Ahn, B.C. Han, H. Shin, J.C. Kim, E.M. Jung, H. Yang, J. Lee, S.G. Kang, S.H. Lee, G.S. Lee, Obovatol inhibits NLRP3, AIM2, and non-canonical inflammasome activation, Phytomedicine 63 (2019) 153019.
[83] H. Kim, E.A. Shin, C.G. Kim, D.Y. Lee, B. Kim, N.I. Baek, S.H. Kim, Obovatol Induces Apoptosis in Non-small Cell Lung Cancer Cells via C/EBP Homologous Protein Activation, Phytotherapy Research 30(11) (2016) 1841-1847.

[84] H.M. Li, S.R. Zhao, Q. Huo, T. Ma, H. Liu, J.K. Lee, Y.S. Hong, C.Z. Wu, A new dimeric neolignan from Magnolia grandiflora L. seeds, Archives of Pharmacal Research 38(6) (2015) 1066-1071.
[85] W. Schuehly, W. Voith, H. Teppner, O. Kunert, Substituted Dineolignans from Magnolia garrettii, Journal of Natural Products 73(8) (2010) 1381-1384.
[86] P.T. Ninh, C.T.T. Ha, T.H. Thai, N.P. Hanh, N.S. Khang, N.T. Dung, L.T.T. Hoai, T.V. Chien, T.V. Loc, V.T.Q. Nhu, N.T. Anh, T.Q. Hung, T.V. Sung, H.N. Anh, T.T.P. Thao, Chevalierinol A and B, two new neolignan sesquiterpenoids from Magnolia chevalieri, Natural Product Research 35(21) (2021) 3745-3751.
[87] V.T. Vu, X.J. Xu, K. Chen, M.T. Nguyen, B.N. Nguyen, G.N. Pham, L.Y. Kong, J.G. Luo, New oligomeric neolignans from the leaves of Magnolia officinalis var. biloba, Chinese Journal of Natural Medicines 19(7) (2021) 491-499.
[88] H.C. Shih, P.C. Kuo, S.J. Wu, T.L. Hwang, H.Y. Hung, D.Y. Shen, P.C. Shieh, Y.R. Liao, E.J. Lee, Q. Gu, K.H. Lee, T.S. Wu, Anti-inflammatory neolignans from the roots of Magnolia officinalis, Bioorganic & Medicinal Chemistry 24(7) (2016) 1439-1445.
[89] H.F. Ni, X.Y. Cai, X. Qiu, L. Liu, X. Ma, L. Wan, H.Y. Ye, L.J. Chen, Biphenyl-type neolignans from stem bark of Magnolia officinalis with potential anti-tumor activity, Fitoterapia 147 (2020) 104769.
[90] Y. He, X.B. Wang, B.Y. Fan, L.Y. Kong, Honokiol trimers and dimers via biotransformation catalyzed by Momordica charantia peroxidase: Novel and potent alpha-glucosidase inhibitors, Bioorganic & Medicinal Chemistry 22(2) (2014) 762-771.
[91] H.C. Shih, T.L. Hwang, H.C. Chen, P.C. Kuo, E.J. Lee, K.H. Lee, T.S. Wu, Honokiol Dimers and Magnolol Derivatives with New Carbon Skeletons from the Roots of Magnolia officinalis and Their Inhibitory Effects on Superoxide Anion Generation and Elastase Release, Plos One 8(5) (2013) e59502.

[92] H. Aldemir, R. Richarz, T.A.M. Gulder, The Biocatalytic Repertoire of Natural Biaryl Formation, Angewandte Chemie-International Edition 53(32) (2014) 8286-8293.
[93] B. Pickel, A. Schaller, Dirigent proteins: molecular characteristics and potential biotechnological applications, Applied Microbiology and Biotechnology 97(19) (2013) 8427-8438.
[94] K. Syrjanen, G. Brunow, Regioselectivity in lignin biosynthesis. The influence of dimerization and cross-coupling, Journal of the Chemical Society-Perkin Transactions 1 (2) (2000) 183-187.
[95] V. Dichiarante, M. Tagnoni, A. Albini, Metal-free synthesis of sterically crowded biphenyls by direct ar-h substitution in alkyl benzenes, Angewandte Chemie-International Edition 46(34) (2007) 6495-6498.
[96] A.I. Meyers, R.J. Himmelsbach, Enantioselective synthesis of 2,2',6-trisubstituted biphenyls, Journal of the American Chemical Society 107(3) (1985) 682-685.
[97] G. Pratsch, T. Wallaschkowski, M.R. Heinrich, The Gomberg-Bachmann Reaction for the Arylation of Anilines with Aryl Diazotates, Chemistry-a European Journal 18(37) (2012) 11555-11559.
[98] A.W. Effenberger F., Fischer P., Jogun K.H., Stezowski J.J., Daltrozzo E., Kollmannsberger- Von Nell G., Synthesis, structure and spectral behavior of donor-acceptor substituted biphenyls., 48 (1983) 4649-4658.
[99] R. Martin, S.L. Buchwald, Palladium-Catalyzed Suzuki-Miyaura Cross-Coupling Reactions Employing Dialkylbiaryl Phosphine Ligands, Accounts of Chemical Research 41(11) (2008) 1461-1473.
[100] D.G. Brow, J. Bostrom, Analysis of Past and Present Synthetic Methodologies on Medicinal Chemistry: Where Have All the New Reactions Gone?, Journal of Medicinal Chemistry 59(10) (2016) 4443-4458.
[101] C.M. Chen, Y.C. Liu, A concise synthesis of honokiol, Tetrahedron Letters 50(10) (2009) 1151-1152.

[102] C. Daquino, A. Rescifina, C. Spatafora, C. Tringali, Biomimetic Synthesis of Natural and "Unnatural" Lignans by Oxidative Coupling of Caffeic Esters, European Journal of Organic Chemistry 2009(36) (2009) 6289-6300.
[103] F. van de Velde, F. van Rantwijk, R.A. Sheldon, Improving the catalytic performance of peroxidases in organic synthesis, Trends in Biotechnology 19(2) (2001) 73-80.
[104] Q.S. Yan, X.G. Tang, B.J. Zhang, C.J. Wang, S. Deng, X.C. Ma, C. Wang, D.W. Li, S.S. Huang, P.P. Dong, Biocatalytic oxidation of flavone analogues mediated by general biocatalysts: horseradish peroxidase and laccase, Rsc Advances 9(23) (2019) 13325-13331.
[105] K. Piontek, M. Antorini, T. Choinowski, Crystal structure of a laccase from the fungus Trametes versicolor at 1.90-angstrom resolution containing a full complement of coppers, Journal of Biological Chemistry 277(40) (2002) 37663-37669.
[106] U. Guzik, K. Hupert-Kocurek, D. Wojcieszynska, Immobilization as a Strategy for Improving Enzyme Properties-Application to Oxidoreductases, Molecules 19(7) (2014) 8995-9018.
[107] N. Cardullo, V. Muccilli, C. Tringali, Laccase-mediated synthesis of bioactive natural products and their analogues, Rsc Chemical Biology 3(6) (2022) 614-647.
[108] M. Mogharabi, M.A. Faramarzi, Laccase and Laccase-Mediated Systems in the Synthesis of Organic Compounds, Advanced Synthesis & Catalysis 356(5) (2014) 897-927.
[109] J.R. Jeon, P. Baldrian, K. Murugesan, Y.S. Chang, Laccase-catalysed oxidations of naturally occurring phenols: from in vivo biosynthetic pathways to green synthetic applications, Microbial Biotechnology 5(3) (2012) 318-332.
[110] J.F. Hartwig, Carbon-heteroatom bond formation catalysed by organometallic complexes, Nature 455(7211) (2008) 314-322.

[111] T. Chen, H. Xiong, J.F. Yang, X.L. Zhu, R.Y. Qu, G.F. Yang, Diaryl Ether: A Privileged Scaffold for Drug and Agrochemical Discovery, Journal of Agricultural and Food Chemistry 68(37) (2020) 9839-9877.
[112] E.N. Pitsinos, V.P. Vidali, E.A. Couladouros, Diaryl Ether Formation in the Synthesis of Natural Products, European Journal of Organic Chemistry 2011(7) (2011) 1207-1222.
[113] Q. Wei, Z.P. Wang, X. Zhang, Y. Zou, Diaryl Ether Formation by a Versatile Thioesterase Domain, Journal of the American Chemical Society 144(22) (2022) 9554-9558.
[114] G. Evano, N. Blanchard, M. Toumi, Copper-mediated coupling reactions and their applications in natural products and designed biomolecules synthesis, Chemical Reviews 108(8) (2008) 3054-3131.
[115] R. Giri, A. Brusoe, K. Troshin, J.Y. Wang, M. Font, J.F. Hartwig, Mechanism of the Ullmann Biaryl Ether Synthesis Catalyzed by Complexes of Anionic Ligands: Evidence for the Reaction of Iodoarenes with Ligated Anionic Cu-I Intermediates, Journal of the American Chemical Society 140(2) (2018) 793-806.
[116] E. Sperotto, G.P.M. van Klink, G. van Koten, J.G. de Vries, The mechanism of the modified Ullmann reaction, Dalton Transactions 39(43) (2010) 10338-10351.
[117] M.M. Capdevielle P., Esters are effective co-catalyst in copper-catalyzed methanolysis of aryl bromides, Tetrahedron Letters 34(6) (1993) 1007-1010.
[118] J.F. Marcoux, S. Doye, S.L. Buchwald, A general copper-catalyzed synthesis of diaryl ethers, Journal of the American Chemical Society 119(43) (1997) 10539-10540.
[119] A. Ouali, J.F. Spindler, A. Jutand, M. Taillefer, Nitrogen ligands in copper-catalyzed arylation of phenols: Structure/activity relationships and applications, Advanced Synthesis & Catalysis 349(11-12) (2007) 1906-1916.

[120] S.V. Ley, A.W. Thomas, Modern synthetic methods for copper-mediated C(aryl)-O, C(aryl)-N, and C(aryl)-S bond formation, Angewandte Chemie-International Edition 42(44) (2003) 5400-5449.
[121] J.S. Sawyer, Recent advances in diaryl ether synthesis, Tetrahedron 56(29) (2000) 5045-5065.
[122] E.J. Abente, M. Subramanian, V. Ramachandran, S.H. Najafi-Shoushtari, MicroRNAs in obesity-associated disorders, Archives of Biochemistry and Biophysics 589 (2016) 108-119.
[123] J.J. Heindel, B. Blumberg, M. Cave, R. Machtinger, A. Mantovani, M.A. Mendez, A. Nadal, P. Palanza, G. Panzica, R. Sargis, L.N. Vandenberg, F.V. Saal, Metabolism disrupting chemicals and metabolic disorders, Reproductive Toxicology 68 (2017) 3-33.
[124] R. Padwal, S.K. Li, D.C.W. Lau, Long-term pharmacotherapy for overweight and obesity: a systematic review and meta-analysis of randomized controlled trials, International Journal of Obesity 27(12) (2003) 1437-1446.
[125] G. La Torre, R. Saulle, Obesity Epidemiology. from Aetiology to Public Health, 2nd edition, European Journal of Public Health 21(5) (2011) 676-676.
[126] P.G. Kopelman, Obesity as a medical problem, Nature 404(6778) (2000) 635-643.
[127] C. Martinussen, K.N. Bojsen-Moller, M.S. Svane, T.F. Dejgaard, S. Madsbad, Emerging drugs for the treatment of obesity, Expert Opinion on Emerging Drugs 22(1) (2017) 87-99.
[128] R.B. Birari, K.K. Bhutani, Pancreatic lipase inhibitors from natural sources: unexplored potential, Drug Discovery Today 12(19-20) (2007) 879-889.
[129] A. Ballinger, S.R. Peikin, Orlistat: its current status as an anti-obesity drug, European Journal of Pharmacology 440(2-3) (2002) 109-117.
[130] E.K. Weibel, P. Hadvary, E. Hochuli, E. Kupfer, H. Lengsfeld, Lipstatin, an inhibitor of pancreatic lipase, produced by streptomyces-toxytricini .1. producing

organism, Fermentation, isolation and biological-activity, Journal of Antibiotics 40(8) (1987) 1081-1085.
[131] E. Hochuli, E. Kupfer, R. Maurer, W. Meister, Y. Mercadal, K. Schmidt, Lipstatin, an inhibitor of pancreatic lipase, produced by streptomyces-toxytricini .2. chemistry and structure elucidation, Journal of Antibiotics 40(8) (1987) 1086-1091.
[132] G. Derosa, P. Maffioli, Anti-obesity drugs: a review about their effects and their safety, Expert Opinion on Drug Safety 11(3) (2012) 459-471.
[133] I. Conget, Diagnosis, classification and pathogenesis of diabetes mellitus, Revista Espanola De Cardiologia 55(5) (2002) 528-535.
[134] T. Jayalakshmi, A. Santhakumaran, I.C. Soc, A Novel Classification Method for Diagnosis of Diabetes Mellitus Using Artificial Neural Networks, Proceedings of the International Conference on Data Storage and Data Engineering (Dsde 2010) (2010) 159-163.
[135] H.W. Baynest, Classification, Pathophysiology, Diagnosis and Management of Diabetes Mellitus, Journal of Diabetes & Metabolism 6(5) (2015) 1-9.
[136] C.C. Thomas, L.H. Philipson, Update on Diabetes Classification, Medical Clinics of North America 99(1) (2015) 1-16.
[137] S. Canivell, R. Gomis, Diagnosis and classification of autoimmune diabetes mellitus, Autoimmunity Reviews 13(4-5) (2014) 403-407.
[138] M. Roden, Diabetes mellitus: definition, classification and diagnosis, Wiener Klinische Wochenschrift 128 (2016) S37-S40.
[139] L.X. Gong, D.N. Feng, T.X. Wang, Y.Q. Ren, Y.L. Liu, J. Wang, Inhibitors of alpha-amylase and alpha-glucosidase: Potential linkage for whole cereal foods on prevention of hyperglycemia, Food Science & Nutrition 8(12) (2020) 6320-6337.
[140] M. Marrelli, M.R. Loizzo, M. Nicoletti, F. Menichini, F. Conforti, Inhibition of Key Enzymes Linked to Obesity by Preparations From Mediterranean Dietary

Plants: Effects on alpha-Amylase and Pancreatic Lipase Activities, Plant Foods for Human Nutrition 68(4) (2013) 340-346.
[141] T. Fujisawa, H. Ikegami, K. Inoue, Y. Kawabata, T. Ogihara, Effect of two alpha-glucosidase inhibitors, voglibose and acarbose, on postprandial hyperglycemia correlates with subjective abdominal symptoms, Metabolism-Clinical and Experimental 54(3) (2005) 387-390.
[142] Y.S. Dong, L.P. Sui, F. Yang, X.X. Ren, Y. Xing, Z.L. Xiu, Reducing the intestinal side effects of acarbose by baicalein through the regulation of gut microbiota: An in vitro study, Food Chemistry 394 (2022) 133561.
[143] L. Rajan, D. Palaniswamy, S.K. Mohankumar, Targeting obesity with plant-derived pancreatic lipase inhibitors: A comprehensive review, Pharmacological Research 155 (2020) 104681.
[144] L.N. Xu, Y. Li, Y. Dai, J.Y. Peng, Natural products for the treatment of type 2 diabetes mellitus: Pharmacology and mechanisms, Pharmacological Research 130 (2018) 451-465.
[145] W.Y. Ma, L.G. Xiao, H.Y. Liu, X.J. Hao, Hypoglycemic natural products with in vivo activities and their mechanisms: a review, Food Science and Human Wellness 11(5) (2022) 1087-1100.
[146] O. Golovinskaia, C.K. Wang, The hypoglycemic potential of phenolics from functional foods and their mechanisms, Food Science and Human Wellness 12(4) (2023) 986-1007.
[147] N. Cardullo, G. Floresta, A. Rescifina, V. Muccilli, C. Tringali, Synthesis and in vitro evaluation of chlorogenic acid amides as potential hypoglycemic agents and their synergistic effect with acarbose, Bioorganic Chemistry 117 (2021) 105458.
[148] Z.J. Jain, P.S. Gide, R.S. Kankate, Biphenyls and their derivatives as synthetically and pharmacologically important aromatic structural moieties, Arabian Journal of Chemistry 10 (2017) S2051-S2066.

[149] C.M. Hu, W.J. Wang, Y.N. Ye, Y. Kang, J. Lin, P.P. Wu, D.L. Li, L.P. Bai, X.T. Xu, B.Q. Li, K. Zhang, Novel cinnamic acid magnolol derivatives as potent alpha-glucosidase and alpha-amylase inhibitors: Synthesis, in vitro and in silico studies, Bioorganic Chemistry 116 (2021) 105291.
[150] H.Q. Fei, M.X. Li, W.J. Liu, L. Sun, N. Li, L. Cao, Z.Q. Meng, W.Z. Huang, G. Ding, Z.Z. Wang, W. Xiao, Potential lipase inhibitors from Chinese medicinal herbs, Pharmaceutical Biology 54(12) (2016) 2845-2850.
[151] Hamdan, II, V.N. Kasabri, Y.M. Al-Hiari, D. El-Sabawi, H. Zalloum, Pancreatic lipase inhibitory activity of selected pharmaceutical agents, Acta Pharmaceutica 69(1) (2019) 1-16.
[152] N.H. Nguyen, N.M.A. Tran, T.H. Duong, G.V. Vo, a-Glucosidase inhibitory activities of flavonoid derivatives isolated from Bouea macrophylla: in vitro and in silico studies, Rsc Advances 13(12) (2023) 8190-8201.
[153] M. Nawaz, M. Taha, F. Qureshi, N. Ullah, M. Selvaraj, S. Shahzad, S. Chigurupati, A. Waheed, F.A. Almutairi, Structural elucidation, molecular docking, alpha-amylase and alpha-glucosidase inhibition studies of 5-amino-nicotinic acid derivatives, Bmc Chemistry 14(1) (2020) 43.
[154] S.M. Farid, M. Noori, M.N. Montazer, M.K. Ghomi, M. Mollazadeh, N. Dastyafteh, C. Irajie, K. Zomorodian, S.S. Mirfazli, S. Mojtabavi, M.A. Faramarzi, B. Larijani, A. Iraji, M. Mahdavi, Synthesis and structure-activity relationship studies of benzimidazole-thioquinoline derivatives as alpha-glucosidase inhibitors, Scientific Reports 13(1) (2023) 4392.
[155] H. Wali, A. Anwar, S. Shamim, K.M. Khan, M. Mahdavi, U. Salar, B. Larijani, S. Perveen, M. Taha, M.A. Faramarzi, Synthesis, in vitro, and in silico studies of newly functionalized quinazolinone analogs for the identification of potent alpha-glucosidase inhibitors, Journal of the Iranian Chemical Society 18(8) (2021) 2017-2034.
[156] A. Baschieri, L. Pulvirenti, V. Muccilli, R. Amorati, C. Tringali, Chain-breaking antioxidant activity of hydroxylated and methoxylated magnolol

derivatives: the role of H-bonds, Organic & Biomolecular Chemistry 15(29) (2017) 6177-6184.
[157] N. Cardullo, F. Monti, V. Muccilli, R. Amorati, A. Baschieri, Reaction with ROO center dot and HOO center dot Radicals of Honokiol-Related Neolignan Antioxidants, Molecules 28(2) (2023) 735.
[158] S. Di Micco, L. Pulvirenti, I. Bruno, S. Terracciano, A. Russo, M.C. Vaccaro, D. Ruggiero, V. Muccilli, N. Cardullo, C. Tringali, R. Riccio, G. Bifulco, Identification by Inverse Virtual Screening of magnolol-based scaffold as new tankyrase-2 inhibitors, Bioorganic & Medicinal Chemistry 26(14) (2018) 3953-3957.
[159] C.J. Zhao, D. Xue, Z.H. Jia, C. Wang, J.L. Xiao, Methanol-Promoted Borylation of Arylamines: A Simple and Green Synthetic Method to Arylboronic Acids and Arylboronates, Synlett 25(11) (2014) 1577-1584.
[160] K.W. Anderson, S.L. Buchwald, General catalysts for the Suzuki-Miyaura and Sonogashira coupling reactions of aryl chlorides and for the coupling of challenging substrate combinations in water, Angewandte Chemie-International Edition 44(38) (2005) 6173-6177.
[161] B.J. Reizman, Y.M. Wang, S.L. Buchwald, K.F. Jensen, Suzuki-Miyaura cross-coupling optimization enabled by automated feedback, Reaction Chemistry & Engineering 1(6) (2016) 658-666.
[162] R.A. Altman, S.L. Buchwald, Pd-catalyzed Suzuki-Miyaura reactions of aryl halides using bulky biarylmonophosphine ligands, Nature Protocols 2(12) (2007) 3115-3121.
[163] T.E. Barder, S.D. Walker, J.R. Martinelli, S.L. Buchwald, Catalysts for Suzuki-Miyaura coupling processes: Scope and studies of the effect of ligand structure, Journal of the American Chemical Society 127(13) (2005) 4685-4696.
[164] J.Y. Cho, G.B. Roh, E.J. Cho, Visible-Light-Promoted Synthesis of Dibenzofuran Derivatives, Journal of Organic Chemistry 83(2) (2018) 805-811.

[165] Z.L. Kong, S.C. Tzeng, Y.C. Liu, Cytotoxic neolignans: an SAR study, Bioorganic & Medicinal Chemistry Letters 15(1) (2005) 163-166.
[166] C. Zhao, Z.Q. Liu, Comparison of antioxidant abilities of magnolol and honokiol to scavenge radicals and to protect DNA, Biochimie 93(10) (2011) 1755-1760.
[167] M. Maioli, V. Basoli, P. Carta, D. Fabbri, M.A. Dettori, S. Cruciani, P.A. Serra, G. Delogu, Synthesis of magnolol and honokiol derivatives and their effect against hepatocarcinoma cells, Plos One 13(2) (2018) e0192178.
[168] M. Sanchez-Peris, J. Murga, E. Falomir, M. Carda, J.A. Marco, Synthesis of honokiol analogues and evaluation of their modulating action on VEGF protein secretion and telomerase-related gene expressions, Chemical Biology & Drug Design 89(4) (2017) 577-584.
[169] L.G. Beholz, J.R. Stille, Lewis acid-promoted 3-aza-cope rearrangement of n-alkyl-n-allylanilines, Journal of Organic Chemistry 58(19) (1993) 5095-5100.
[170] P. Mondal, L. Thander, S.K. Chattopadhyay, A new entry to the phenanthridine ring system, Tetrahedron Letters 53(11) (2012) 1328-1331.
[171] A. Chaskar, V. Padalkar, K. Phatangare, K. Patil, A. Bodkhe, B. Langi, Heteropoly acids as useful recyclable heterogeneous catalysts for the facile and highly efficient aza-cope rearrangement of N-allylanilines, Applied Catalysis a-General 359(1-2) (2009) 84-87.
[172] S. Tripathi, M.H. Chan, C.P. Chen, An expedient synthesis of honokiol and its analogues as potential neuropreventive agents, Bioorganic & Medicinal Chemistry Letters 22(1) (2012) 216-221.
[173] S. Horikoshi, T. Watanabe, M. Kamata, Y. Suzuki, N. Serpone, Microwave-assisted organic syntheses: microwave effect on intramolecular reactions - the Claisen rearrangement of allylphenyl ether and 1-allyloxy-4-methoxybenzene, Rsc Advances 5(110) (2015) 90272-90280.
[174] B.P. Bandgar, S.P. Kasture, Protection of phenols as t-butyl ethers under mild conditions, Journal of Chemical Research-S (5) (2000) 252-253.

[175] P. G.M.Wuts, Protection for phenols and cathecols. In Greene's protective groups in organic synthesis., 2014.
[176] A. Ozanne, L. Pouysegu, D. Depernet, B. Francois, S. Quideau, A stabilized formulation of IBX (SIBX) for safe oxidation reactions including a new oxidative demethylation of phenolic methyl aryl ethers, Organic Letters 5(16) (2003) 2903-2906.
[177] S.P. Henry, T.J. Fernandez, J.P. Anand, N.W. Griggs, J.R. Traynor, H.I. Mosberg, Structural Simplification of a Tetrahydroquinoline-Core Peptidomimetic mu-Opioid Receptor (MOR) Agonist/delta-Opioid Receptor (DOR) Antagonist Produces Improved Metabolic Stability, Journal of Medicinal Chemistry 62(8) (2019) 4142-4157.
[178] S.K. Bhangu, M. Ashokkumar, F. Cavalieri, A Simple One-Step Ultrasonic Route To Synthesize Antioxidant Molecules and Fluorescent Nanoparticles from Phenol and Phenol Like Molecules, Acs Sustainable Chemistry & Engineering 5(7) (2017) 6081-6089.
[179] N. Cardullo, L. Pulvirenti, C. Spatafora, N. Musso, V. Barresi, D.F. Condorelli, C. Tringalii, Dihydrobenzofuran Neolignanamides: Lactase-Mediated Biomimetic Synthesis and Antiproliferative Activity, Journal of Natural Products 79(8) (2016) 2122-2134.
[180] C. Zippilli, L. Botta, B.M. Bizzarri, M.C. Baratto, R. Pogni, R. Saladino, Biomimetic synthesis of galantamine via laccase/TEMPO mediated oxidative coupling, Rsc Advances 10(18) (2020) 10897-10903.
[181] N. Cardullo, V. Muccilli, L. Pulvirenti, C. Tringali, Natural Isoflavones and Semisynthetic Derivatives as Pancreatic Lipase Inhibitors, Journal of Natural Products 84(3) (2021) 654-665.
[182] N. Cardullo, V. Muccilli, L. Pulvirenti, A. Cornu, L. Pouysegu, D. Deffieux, S. Quideau, C. Tringali, C-glucosidic ellagitannins and galloylated glucoses as potential functional food ingredients with anti-diabetic properties: a study of

alpha-glucosidase and alpha-amylase inhibition, Food Chemistry 313 (2020) 126099.
[183] J.Y. Chu, R.G. Yang, W.Q. Cheng, L.P. Cui, H.C. Pan, J.F. Liu, Y. Guo, Semisynthesis, biological activities, and mechanism studies of Mannich base analogues of magnolol/honokiol as potential alpha-glucosidase inhibitors, Bioorganic & Medicinal Chemistry 75 (2022) 117070.
[184] T. Xu, J.R. Meng, W.Q. Cheng, J.Z. Liu, J.Y. Chu, Q. Zhang, N.N. Ma, L.P. Bai, Y. Guo, Discovery of honokiol thioethers containing 1,3,4-oxadiazole moieties as potential ?-glucosidase and SARS-CoV-2 entry inhibitors, Bioorganic & Medicinal Chemistry 67 (2022) 116838.
[185] F.M. Djeujo, E. Ragazzi, M. Urettini, B. Sauro, E. Cichero, M. Tonelli, G. Froldi, Magnolol and Luteolin Inhibition of alpha-Glucosidase Activity: Kinetics and Type of Interaction Detected by In Vitro and In Silico Studies, Pharmaceuticals 15(2) (2022) 205.
[186] A. Daina, O. Michielin, V. Zoete, SwissADME: a free web tool to evaluate pharmacokinetics, drug-likeness and medicinal chemistry friendliness of small molecules, Scientific Reports 7 (2017) 42717.
[187] Y.C. Martin, A bioavailability score, Journal of Medicinal Chemistry 48(9) (2005) 3164-3170.
[188] A. Daina, O. Michielin, V. Zoete, iLOGP: A Simple, Robust, and Efficient Description of n-Octanol/Water Partition Coefficient for Drug Design Using the GB/SA Approach, Journal of Chemical Information and Modeling 54(12) (2014) 3284-3301.
[189] D.J. Newman, G.M. Cragg, Natural Products as Sources of New Drugs from 1981 to 2014, Journal of Natural Products 79(3) (2016) 629-661.
[190] J.B. Baell, G.A. Holloway, New Substructure Filters for Removal of Pan Assay Interference Compounds (PAINS) from Screening Libraries and for Their Exclusion in Bioassays, Journal of Medicinal Chemistry 53(7) (2010) 2719-2740.

[191] C. Proenca, M. Freitas, D. Ribeiro, S.M. Tome, E.F.T. Oliveira, M.F. Viegas, A.N. Araujo, M.J. Ramos, A.M.S. Silva, P.A. Fernandes, E. Fernandes, Evaluation of a flavonoids library for inhibition of pancreatic alpha-amylase towards a structure-activity relationship, Journal of Enzyme Inhibition and Medicinal Chemistry 34(1) (2019) 577-588.
[192] N. Cardullo, G. Catinella, G. Floresta, V. Muccilli, S. Rosselli, A. Rescifina, M. Bruno, C. Tringali, Synthesis of Rosmarinic Acid Amides as Antioxidative and Hypoglycemic Agents, Journal of Natural Products 82(3) (2019) 573-582.
[193] T. Luthra, R. Agarwal, M. Estari, U. Adepally, S. Sen, A novel library of -arylketones as potential inhibitors of alpha-glucosidase: Their design, synthesis, in vitro and in vivo studies, Scientific Reports 7 (2017) 13246.
[194] D.X. Jin Lin, Li Lu, Bingwen Liang, Zhuang Xiong, Xuetao Xu,, New β-carboline derivatives as potential α-glucosidase inhibitor: Synthesis and biological activity evaluation, Journal of Molecular Structure 128 (2023) 135279.
[195] A. Kryshchyshyn-Dylevych, L. Radko, N. Finiuk, M. Garazd, N. Kashchak, A. Posyniak, K. Niemczuk, R. Stoika, R. Lesyk, Synthesis of novel indole-thiazolidinone hybrid structures as promising scaffold with anticancer potential, Bioorganic & Medicinal Chemistry 50 (2021) 116453.
[196] S.A. Halim, S. Jabeen, A. Khan, A. Al-Harrasi, Rational Design of Novel Inhibitors of alpha-Glucosidase: An Application of Quantitative Structure Activity Relationship and Structure-Based Virtual Screening, Pharmaceuticals 14(5) (2021) 482.
[197] N.U. Rehman, S.A. Halim, M. Al-Azri, M. Khan, A. Khan, K. Rafiq, A. Al-Rawahi, R. Csuk, A. Al-Harrasi, Triterpenic Acids as Non-Competitive alpha-Glucosidase Inhibitors from Boswellia elongata with Structure-Activity Relationship: In Vitro and In Silico Studies, Biomolecules 10(5) (2020) 751.
[198] Y.X. Zheng, W.H. Yang, W.X. Sun, S.G. Chen, D.H. Liu, X.L. Kong, J.H. Tian, X.Q. Ye, Inhibition of porcine pancreatic alpha-amylase activity by chlorogenic acid, Journal of Functional Foods 64 (2020) 103587.

[199] S. Scsukova, M. Jezova, J. Vranova, M. Tatara, J. Kolena, Fluorescence quenching studies of the rat ovarian LH/hCG receptor, General Physiology and Biophysics 15(6) (1996) 451-462.
[200] Z. Allahdad, M. Varidi, R. Zadmard, A.A. Saboury, Spectroscopic and docking studies on the interaction between caseins and beta-carotene, Food Chemistry 255 (2018) 187-196.
[201] A. Wen, Y.L. Chen, S.F. Yuan, H. Yu, Y.H. Guo, Y.L. Cheng, Y.F. Xie, H. Qian, W.R. Yao, Elucidation of the binding behavior between tetracycline and bovine casein by multi-spectroscopic and molecular simulation methods, Journal of Luminescence 260 (2023) 119879.
[202] X. Peng, G.W. Zhang, Y.J. Liao, D.M. Gong, Inhibitory kinetics and mechanism of kaempferol on alpha-glucosidase, Food Chemistry 190 (2016) 207-215.
[203] V. vanAxelCastelli, R. Cacciapaglia, G. Chiosis, F. vanVeggel, L. Mandolini, D.N. Reinhoudt, The uranyl unit as electrophilic catalyst of acyl transfer reactions, Inorganica Chimica Acta 246(1-2) (1996) 181-193.
[204] S. Tamura, A. Miyoshi, T. Kawano, T. Horii, S. Itagaki, N. Murakami, Structure-Activity Relationship of Anti-malarial Allylpyrocatechol Isolated from Piper betle, Chemical & Pharmaceutical Bulletin 68(8) (2020) 784-790.
[205] W.Z. Tang, J.T. Liu, Q. Hu, R.J. He, X.Q. Guan, G.B. Ge, H. Han, F. Yang, H.W. Lin, Pancreatic Lipase Inhibitory Cyclohexapeptides from the Marine Sponge-Derived Fungus Aspergillus sp. 151304, Journal of Natural Products 83(7) (2020) 2287-2293.
[206] H.M.T. Vu, D.D. Vu, V.D. Truong, T.V.P. Nguyen, T.D. Tran, Virtual Screening, oriented-synthesis and evaluation of lipase inhibitory Activity of benzyl Amino chalcone derivatives, Journal of medical and pharmaceutical research 1 (2017) 26-36.

[207] M.P. Jacobson, D.L. Pincus, C.S. Rapp, T.J.F. Day, B. Honig, D.E. Shaw, R.A. Friesner, A hierarchical approach to all-atom protein loop prediction, Proteins-Structure Function and Bioinformatics 55(2) (2004) 351-367.
[208] J. Jumper, R. Evans, A. Pritzel, T. Green, M. Figurnov, O. Ronneberger, K. Tunyasuvunakool, R. Bates, A. Zidek, A. Potapenko, A. Bridgland, C. Meyer, S.A.A. Kohl, A.J. Ballard, A. Cowie, B. Romera-Paredes, S. Nikolov, R. Jain, J. Adler, T. Back, S. Petersen, D. Reiman, E. Clancy, M. Zielinski, M. Steinegger, M. Pacholska, T. Berghammer, S. Bodenstein, D. Silver, O. Vinyals, A.W. Senior, K. Kavukcuoglu, P. Kohli, D. Hassabis, Highly accurate protein structure prediction with AlphaFold, Nature 596(7873) (2021) 583-589.
[209] M. Varadi, S. Anyango, M. Deshpande, S. Nair, C. Natassia, G. Yordanova, D. Yuan, O. Stroe, G. Wood, A. Laydon, A. Zidek, T. Green, K. Tunyasuvunakool, S. Petersen, J. Jumper, E. Clancy, R. Green, A. Vora, M. Lutfi, M. Figurnov, A. Cowie, N. Hobbs, P. Kohli, G. Kleywegt, E. Birney, D. Hassabis, S. Velankar, AlphaFold Protein Structure Database: massively expanding the structural coverage of protein-sequence space with high-accuracy models, Nucleic Acids Research 50(D1) (2022) D439-D444.